Dedicated to my wife Nasrin
and my two children Bayad and Bnar

THE ACCURATE MEASUREMENT OF LOSSES IN SMALL CAGE INDUCTION MOTORS USING A BALANCE CALORIMETRIC METHOD

Thesis submitted in accordance with the requirements of the University of Liverpoool for the degree of

Doctor in Philosophy

by

B.N.Shamsadeen

May, 1990

ACKNOWLEDGEMENT

The author is very grateful to his supervisor, Professor K.J.Binns, for his guidence and encouragement during the research and his help in the writing of this thesis.

The author is beholden to Mr D.R.Turner, for his invaluable advice and encouragement during the research and the writing of this thesis.

The author's thanks are also extended to Mr. D.F.Warne for his participation as industrial supervisor and his useful comments during the writing of this thesis.

The author acknowledges with gratitude the assistance offered by the technical staff of the department, in particular Mr K.Mealor.

Without the support of Mrs. N.Shamsadeen this thesis would not have been written. Thanks are due to her for her support and encuragement.

Finally the author would like to thank the SERC and Electromotors Ltd. for co-sponsoring this project and the University of Liverpool for providing laboratory facilities.

ABSTRACT

The accurate measurement of electrical machine losses using a calorimeter is described. The machine is contained within an insulated enclosure and the heat output is obtained from the temperature rise of the working fluid. For the 5.5kW TEFV induction motor tested air was used as the working fluid, the calorimeter differing significantly from that envisaged by IEC 34. It is shown how the problems associated with determining the specific heat, density and temperature of air can be overcome by employing a balance method of operation. Test results confirm that the method of loss measurement is accurate, repeatable and has a resolution of about 9W.

The calorimeter is used to investigate the variation of losses (excluding windage and friction losses) as the air gap and rotor cage skew are varied for a range of values of supply voltage and current. It is concluded that on no load the variations with voltage and air gap follow expected trends but that there is no correlation between losses and rotor cage skew. It is shown, however, that there is a dependence of losses on skew when the motor is loaded and that a skew of 1 SSP appears to produce the highest losses.

A theoretical treatment based only on the fundamental field is presented; calculations based on this model suggest that the losses will increase continuously with skew in the range considered (zero to 1.5 SSP). Comparison with the measured results which show a maximum at 1 SSP, suggests that harmonic fields and other effects must play a significant role in the dependence of losses on skew.

It is concluded that the balance calorimetric method of loss measurement is very accurate and may well make a substantial contribution to drive systems, especially those using non sinusoidal supply.

CONTENTS

CHAPTER ONE

INTRODUCTION

In many fields of engineering it would appear to be an almost natural progression for equipment to become smaller as it is redesigned and developed. Electrical machines are no exception to this and it is instructive to compare an early motor and its modern equivalent; the reduction in size is quite remarkable. In pursuing this path designers are of course constrained by a number of limiting factors, the properties of materials, magnetic saturation etc, but one of the most important is that imposed by the losses, indeed it is often the ability to handle a given level of power loss that fixes the size of the device. There are usually two conflicting aspects to this constraint, as the machine becomes smaller the cross sectional area of copper and iron are reduced and the working densities (current and flux) and consequently the losses, increased. On the other hand the reduction in volume of iron and copper reduces the thermal capacity and the surface area. For machines which do not have some form of forced internal cooling the effect of these changes has been to increase the internal temperatures. The reduction in size has been made possible by the introduction of new insulation materials operating at high temperatures and has been reflected by the evolution of international standards.

As this change has taken place it has become increasingly important for machine manufacturers to have an accurate knowledge of the losses and the way in which they will change as the design is altered. Whilst at the design stage it is the ability to predict the level of losses the current state of knowledge is such that this can not be done with complete certainity for all possible designs. Thus it is extremely important to the engineer that he is able to measure the losses accurately and it is with this aspect of machines technology that this thesis is concerned. Before considering further the question of loss or efficiency measurement, it can be noted that the losses in induction motors can be predicted by a number of calculation methods. Equivalent circuit and other mathematical methods are often used by the designers to predict the losses and to look at the behaviour of the machine before building. The finite element method is also used by the designers to look at the motor performance, it is normally used for the purpose of magnetic and thermal analysis.

The calculation of performance using equivalent circuits is a well known method, with standards organisations and learned societies such as the IEEE [1] recommending their use . Although reference 1 only uses one form of an equivalent circuit there have been many modifications suggested. One such was presented by Dell et al [2], where the goal was to accomodate non-sinusoidal supplies, transient performance and achieve a reduction in the number of parameters.

The use of an equivalent circuit of whatever form to determine the performance of the induction motor is simple and suitable for application in many situations, but there are always many approximations and it is very difficult to predict accurately the losses in the actual machine with different design parameters.

Finite element methods are widely used by engineers for examining the machine performance, mainly for magnetic field analysis. The name finite element comes from the use of a mesh of small elements (usually triangular for two dimensional work) to model the device. Equations relating the magnetic field to the properties of the material and the electric currents are solved within each element. Several thousand elements are normally required to model a machine accurately, this solution only being possible with the aid of the computer. In the FEM methods many assumptions are made, among them the following are tabulated :

1- The core material is isotropic and the BH-curve is homogeneous in all directions.

2- No flux leaks from the periphery of the stator core.

Despite the many advantages gained from using FEM methods in the design of the machines, it is currently not possible to predict accurately the total losses in induction motors, although work is progressing in this field [3].

The use of computers has enabled the engineers in industry to produce complex methods for designing motors and predicting the losses in induction motors, methods often based on empirical equations together with equivalent circuits [4]. In these methods the losses are calculated separately in different parts of the machine, i.e. iron losses in the back of the stator core and in the teeth, friction and windage loss , stator copper loss, rotor conductor loss, surface loss and other components of stray losses. These components are then summed to give the total losses.

The measurement of losses of induction motors as recommended by BS [5], and IEEE [1] can be performed in different ways: the input output method, separate measurement of losses,and the calorimetric method. The details of all these methods together, with other methods available [6][7][8][9][10], but not mentioned in the above two international references are discussed in more detail in chapter 2.

The input output and the loss separation methods are the most widely used methods for measuring the losses of induction motors. In the input output method the input power can normally be measured to an acceptable accuracy by using the standard instruments if it is supplied from a sinusoidal source, otherwise if the source is non-sinusoidal special instruments with better frequency response are required. The output power can be determined by means of

dynamometer, torque transducer with speed meter or calibrated machine (section 2.3). In the input output method, losses can be determined by subtracting the measured output from the measured input. The accuracy of this method depends to a large extent on the accuracy of the measuring instruments used, any small error in the measurement may cause significant error in the final result. For example, in a machine with 90% efficiency and 10kW input power, if the measurement was made by an instrument having an accuracy of 1% the total losses could be in error by up to 19% of the total losses , a value which is likely to be higher than some components of stray loss. Measurement of the output power is always more difficult than the input power, and the possibility of error is higher. In the case of dynamometer measurement, the output power is determined by multiplying two readings, each of them being subject to error. Use of a torque transducer and speed meter encounters the same problem.

The main difficulty in using the calibrated driving machine test is the calibrated machine itself. It is often of special design and manufacture (hence expensive) in order to control its own losses as far as possible and the need for these to be determined with the necessary accuracy . A calibrated machine of a particular size can only be used to test a limited range of machine ratings. These problems together with the difficulty in performing the test have made this method unpopular. While in case of back to back method the possibility of having two identical machines is almost rare and

operating them at exactly the same electromagnetic condition is impossible. Therfore it can be said that although the input output method is easy in concept, it is difficult to perform especially for large machines and it is difficult to achieve the required accuracy of loss measurement.

The determination of losses by loss separation method is less accurate than the input output method. In this method a series of tests (no load test, excitation test, load test, rotor removed test, reverse rotation test etc) are undertaken in order to estimate the total losses. Each one of these tests is subject to error and suffers from a variety of problems. Therefore with the time needed to complete all these tests they have made this method of loss determination unacceptable.

It is well known that all the losses dissipated within the electrical machine appear as heat, as a result of which the temperatures of various parts of the machine are increased. The measurement of the heat dissipated through the surface of the machine once it has reached thermal equilibrium is thus a direct measure of the losses.

The measurement of the heat output by the calorimetric method has been recognised by IEC [11], and a few authors have commented on it. Schwarz [12] said that it is not practicable owing to the great difficulty of obtaining measurements of sufficient accuracy particularly with large machines. Jimoh and Poloujadoff [13] have also described it as an inaccurate method saying that it is only possible for large machines and those in which cooling gas can be forced through specific passages.

The IEC standard [11] includes the statement that the method is primarily intended for large generators, but the principle can be used on other machines. The recommendation is based on the assumption that the majority of the heat generated by the machine is carried away by the liquid (water, oil) cooling circuit provided with the generator. The heat lost by conduction, radiation, convection and leakage which constitute a small part of the total losses can be ignored or estimated. It is also suggested in IEC [11] that the heat leakage can be reduced by the use of thermal lagging on the outside of the machine casing. The principle may be suitable for large machine but there are other machines, especially the smaller sizes, were this principle can not be applied; therfore a different approach has to be used.

Since the essential feature of the calorimetric method is that all the heat generated by the machine is to be measured, it is necessary to use a technique by which the maximum amount of the dissipated heat can be transported away. The best way of achieving this is to surround the machine totally on all sides by well insulated container to minimise the heat leakage to the lowest level possible and to provide a controlled heat removal mechanism . In this method it is essential that the condition under which the machine is tested should not differ from the normal operating conditions, therefore for machines without special cooling circuit (oil or water) the cooling medium must be air with sufficient flow rate to ensure that the temperature within the machine does not exceed the required limit. With these points in mind the obvious way to conduct away the maximum amount of the dissipated heat from the machine is to put the machine inside an insulated box either open figure(1.1), or closed figure(1.2). In both cases the heat generated from the machine can be determined from the measured temperature difference, the flow rate of the coolant and its properties; i.e the specific heat and the density. In the open type method obviously the coolant is air and the values of its specific heat and the density depend on the relative humidity and pressure. Therefore if this method is used it is necessary to have information about the air flow rate, relative humidity of the air, the barometric pressure and the temperature of the air at the inlet of the calorimeter. For the closed type in which the secondary fluid could be either water or oil, the specific heat and density are less variable and more easily measurable, but

the building of the secondary heat exchanger system adds complexity to the whole system and it is certainly more expensive. In the open type method, as noted by IEC [11] the generated heat can be measured indirectly by means of a calibration curve but as in case of direct method this method still requires a knowledge of the specific heat, humidity, temperature and flow rate .

As far as the author is aware , Binns and Wood [14] were the first to approach the calorimetric method in a different way to that suggested by IEC [11], but taking into consideration all the constraints mentioned above. In 1974 they built a calorimeter to test a ventilated, 45HP, 3-phase cage induction motor . The test motor was enclosed inside a well insulated container with inlet and outlet chimneys. Cooling air at a constant temperature and flow rate was drawn from another room by means of a constant speed centrifugal fan and forced into the container and passed through the machine and exhausted through the outlet chimney. The inlet and the outlet air temperatures were measured by means of thermistors installed inside the two chimneys. The test machine was left running at the required load until a steady state was achieved. Readings of the power input to the motor were taken together with the inlet and outlet temperatures. Subsequently the machine was disconnected from the supply, driven at the same speed by auxilary machine and the air flow rate kept constant whilst heat was supplied to the cooling medium (air) by means of an alterntive source of heat. This state was

maintained with appropriate adjustment of the input to the heater until the same temperature difference was obtained.Then the total losses (less friction and windage losses) are equal to the power delivered to the heater. Binns and Wood [14] concluded that the system and the method were suitable for measuring the losses of machines but that improvements could made in order to obtain better results.

A study of the work reported by Binns and Wood [14] showed that the significant difference between their method of operation and that recommended by IEC [11] was the use of the auxilary heater and the balance mode of operation, it also showed that the method could be extended to totally enclosed machines and improved by careful design of the calorimeter enclosure and auxilary system as made in this project. The improvements made on the system together with the details of the control and measuring system used in this project are discussed in chapters 3 and 4. In this project a TEFV squirrel cage induction motor rated 5.5kW has been used. The motor was tested at no load and at load with thirteen rotors of different skews and at different air gaps. Some of the tests were repeated using a double layer winding stator . The results obtained are discussed in detail in chapter 5. A theoretical study to predict the changes in losses and leakage reactance of induction motors due to skewing by modelling the skewed machine into a series of connected machines is discussed in chapter 6.

The calorimetric method for measuring total losses of small motors has also been used by R.Buccianti and two of his colleagues [10] in Italy in 1986. In their study a small induction motor of 3kW was tested at load and no load, it was found that the method is suitable for testing small machines of this kind and the probability of error in loss measurement by calorimetric method is less than that estimated from the direct input output method.

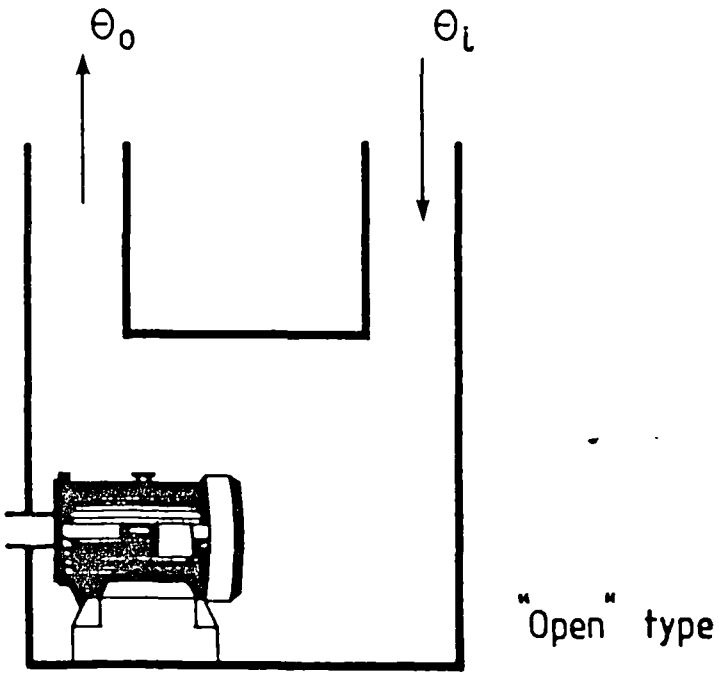
Θ_o
Θ_i
"Open" type

Fig.1.1

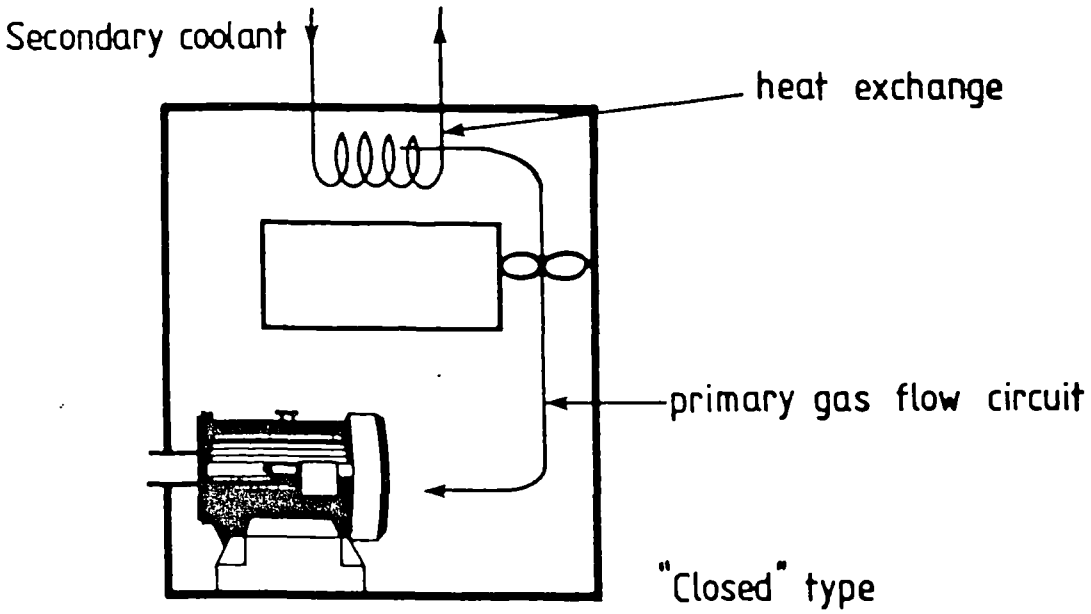
Secondary coolant
heat exchange
primary gas flow circuit
"Closed" type

Fig.1.2

CHAPTER TWO

LOSSES IN INDUCTION MOTORS

2.1 INTRODUCTION

The electromagnetic losses in electrical machines depend on the magnetic flux distribution, the current in the conductors and the speed of rotation. These losses appear as heat in the iron and copper and reduce the efficiency. An understanding of the losses, their nature and their origins in the machine is necessary in order to determine the efficiency of the machine .

In this chapter the nature of the losses in induction motors, their origins and methods of measurements are briefly described.

2.2 LOSSES IN INDUCTION MOTORS

Total losses are clearly the difference between the input and the output power of the machine. These losses can be divided into the following compnents:

1- Iron losses.

2- Stator copper losses.

3- Rotor I^2R losses due to fundamental current at slip frequency.

4- Friction and windage losses.

5- Stray losses.

2.2.1 IRON LOSSES

When the stator winding of a three phase induction motor is supplied from an ac source a rotating flux pattern is produced in the machine. This rotating flux gives rise to iron losses in both the stator and the rotor cores. Losses which appear as heat generated in both members. Iron losses have two components, hysteresis loss and eddy current loss.

2.2.1.1 HYSTERESIS LOSSES

When the rotating flux moves with respect to the stator and rotor iron, the domains in the iron are alternately magnetised first in one direction then in the other direction. During each cycle of magnetisation energy is required to achieve the magnetisation reversal, and this is called the hysteresis loss, this loss has a particular value for any one cycle, dependent upon the properties of the iron and the flux level. Therefore hysteresis loss can be defined as the amount of energy lost as a result of the cycling of the iron around its hysteresis loop; the magnitude of this loss being dependent upon the area of the loop and the frequency. There is no

mathmatical equation which fits the hysteresis loop due to the complexity in the arrangement of the domains [15]. However an empirical relation was found from tests which represents the loop area as function of flux density (B) and states that the area of the hysteresis loop is proportional to B^x, where x is a value in a range of (1.5 - 2.2),[15]. Since the energy loss per cycle is constant the total loss depends on the number of the cycles; therefore, the hysteresis loss is proportional to the frequency. For an induction motor the frequency of magnetisation in the stator is equal to the supply frequency but for the rotor it is variable and equal to the slip frequency. At normal operation of the motor when the slip frequency is very small the hysteresis loss in the rotor is negligible. An equation proposed by Steinmetz [16] for calculating hysteresis loss is:

$$W_h = \zeta \, v \, f \, B_m^{\,x} \qquad \ldots\ldots\ldots\ldots\ldots 2.1$$

Where : ζ = Stienmetz coefficient

v = Volume or weight depending on the value of ζ

f = Frequency (Hz)

B_m = Max flux density (Tesla)

In rotating machines the magnetic axis revolves due to the relative movement of the iron and the field axis and the hysteresis losses would be larger than that calculated by equation 2.1 [15].

2.2.1.2.EDDY CURRENT LOSSES

When a solid iron block, or any conducting material is subjected to to an alternating magnetic flux, e.m.f.s and hence circulating currents are set up in the iron in a direction tending to oppose the change of the flux. These circulating currents are called eddy currents; they are naturally alternating, occupying most of the exterior parts of the block and tend to force the magnetic field towards the outer surfaces. This phenomena is called skin effect and since the material is a conductor with resistance the flow of such currents produces heat and thus a loss.

It has been appreciated for many years that the eddy currents, hence the losses, can be significantly reduced by increasing the material resistance. This is difficult to achieve in a solid block without for example loosing some of the permeability; however, it can be affected by lamination of the core. Provided that the laminations are in the plane of the flux and a resistance is introduced between lamination, the resistance presented to the eddy currents is increased. In the majority of machines, this is achieved by the stacking of thin sheets of magnetic material. In high frequency applications, where eddy current loss is a major problem, increased resistance in more than one direction can be obtained by use of sintered materials. In a lamination core the energy loss due to eddy current can be expresed by:[16]

$$W_e = 1/6\rho \left(\pi \, d \, f \, B_m \right)^2 \quad (W.m^{-3}) \qquad \text{.....2.2}$$

Where: d = Thickness of the lamination (m)

f = Frequency of alternating flux (Hz)

B_m = Maximum value of the flux density (Tesla)

ρ = Resistivity of the laminated material (ohm.m)

The eddy current loss, as described by equation 2.2 varies as the square of the frequency and the lamination thickness and inversely as the resistivity of the iron. Although equation 2.2, gives a good idea of the variation of eddy curent loss with various parameters it does not give an accurate answer, because it is assumed that the flux density is uniform and not affected by eddy currents and that the permeability of the iron is constant throughout the cycle. This is not true because the iron is made up of domains and may operate in a non linear regime.

Although it is agreed that the division into these two components is a fundamental separation, it is not particularly helpful in the design or efficiency evaluation of a machine. Iron losses, as the sum of these two components, are always measured for given values of lamination thickness, frquency and flux density by the steel manufacturer, who provides tables and graphs of this information. Designers often use this information to estimate the losses in different parts of the machine, summing them to estimate

the total losses of the stator core. No account of iron losses in the rotor core is taken as they are negligible near synchronous speed.

Other workers in the same field have different approaches. Liwischitz Garik [17] classified iron losses into:

a - Iron losses due to the main flux.

b - Iron losses due to harmonic flux.

Spooner [16] gives the loss classification as :

a - Fundamental frequency losses in the stator core and the stator teeth.

b - Slip frequency losses in the rotor core and teeth.

c - High frequency losses in the stator and rotor dividing these two into:

1 - Surface losses.

2 - Tooth pulsation losses.

3 - Copper eddy current losses.

Chalmers [6] has proposed a resolution identifying the components of iron losses as :

1 - Core losses due to tangential flux.

2 - Core losses due to radial flux.

3 - Tooth losses due to radial flux.

4 - Surface losses.

5 - End ring losses.

6 - Additional losses due to industrial imperfections.

Recognising the difficulties in separating iron losses into hysteresis and eddy current losses and in measuring iron losses at different frequencies and at different parts of the machine in this project only the total losses are measured and segregated into their main components in chapter 5.

2.2.2 STATOR COPPER LOSSES

The copper losses in the stator winding of a three phase induction motor are produced as heat in the stator winding. They are equal to $3I^2R$, where I is the rms value of the per phase stator current and R is the stator winding resistance per phase at the test temperature.

The resistance of the stator winding is evaluated from the mean length of the turns, the number of turns, the wire size and the number of parallel circuits. The procedure for calculating the stator winding resistance is straight forward, needing no further discussion here. The dc winding resistance can be measured very

easily; the measured value then being used to determine the stator winding I^2R losses. Experimental results for the D132 S motor, used in this project, have shown that for this particular machine the stator winding resistance per phase varies from 3.1Ω for the motor at the ambient temperature of 20^o to 3.8Ω at the full load test temperature. The resistance of the winding is more than the ohmic value measured by a dc resistance method due to skin effect which forces the current to flow in the outer part of the conductor and results an increase in the resistance value. Liwschitz Garik [17] has estimated that in many cases the effective ac resistance can be taken to be 1.15 to 1.35 times the dc resistance. This factor may be true for large machines with large crossectional area of the conductors but for small machines with small diameter wires this factor may be nearer to one and the skin effects are often neglected. However supplied from an inverter these effects can become significant,[19].

2.2.3 ROTOR I^2R LOSSES

In a cage rotor the I^2R losses are produced as heat in the rotor due to the flow of the current through the rotor bars and end rings. Under normal operating condition the rotor I^2R losses comprise the following components:

1- Losses due to the slip frequency current induced by the fundamental flux.

2- Losses due to high frequency circulating currents induced by

the stator belt leakage flux.

3- Losses arising from the high frequency currents due to the permeance harmonics.

If the machine is supplied from a nonsinusoidal source some other components of I^2R losses are produced in the rotor winding, i.e, the losses due to time harmonics and other losses arising from the effects of space harmonic fluxes associated with each time harmonic component. Since the resistance of the rotor can not be measured directly the rotor I^2R losses are normally calculated by multiplying the power input to the rotor (P_i) by slip. The above method is simple and direct, otherwise the rotor I^2R loss have to be calculated from the currents and resistances of the bars and endrings. The effective rotor resistance can change significantly between starting and full load conditions as the frequency and the distribution of current across the conductor change. Designers make use of skin effect to control the shape of the torque speed curve by changes in the bar shape.

2.2.4 STRAY LOSSES

Stray losses are defined as the difference between the total losses actually occurring in a motor and the sum of calculated I^2R losses due to fundamental current, the no load iron losses and

friction and windage losses [20]. Some of these losses occur on no load and are due to the harmonics of the air gap flux caused by permeance variation,[12]. This part is measured at no load test and is difficult to separate from the fundamental iron losses. The other parts of stray losses occur under load condition and are caused by the mmf of the motor load current which divert some of the no load magnetic flux into leakage paths, creating additional losses in the laminations, the conductors and the adjacent parts,[20]. Stray losses of large magnitude would increase the motor heating , reduce the efficiency and impair the torque speed charecteristic. These losses can be reduced by the design and in the manufacturing of the motors. K. Oberretl [22] gives 13 rules to minimise the stray losses in induction motors. His rules are claimed to be supported by test results. In this section the theoretical background of stray losses is discussed briefly and classified into stray no load losses (Section 2.2.4.1) and stray load losses (Section 2.2.4.2).

2.2.4.1 STRAY NO LOAD LOSSES

Stray no load losses can be considered to have three main components; surface losses, tooth pulsation losses in the stator and the rotor teeth and tooth pulsation circulating current loss in the rotor. They are normally more serious in machines which have open stator slots. Despite numerous investigations [7][20][21][22][23][24] which have been carried out during the past few decades no reliable

method for computing stray no load losses would appear to be available.

2.2.4.2 STRAY LOAD LOSSES

These are the losses which are produced partly by the leakage fluxes, partly by the effect of the current distribution in the machine and partly by the effects of the self inductance of the windings [12]. Stray load losses can be classified according to their dependance on frequency into two main components: the fundamental and the high frequency components. The fundamental frequency losses are those losses which are produced by the penetration of the fundamental leakage flux into the conductors , end plates, end brackets and other adjacent metal parts of the machine. These losses are dependent on the load current, hence at no load they are very small, however when the load is increased the fundamental frequency losses also increase. High frequency losses are those losses which occur at frequencies higher than the fundamental frequency. They are caused mainly by the pulsation of the leakage fluxes and mainly due to the rotation of the rotor passing the stator slots. Like the no load stray losses they cannot be measured directly and they may vary from machine to machine due to manufacturing imperfections or difference between individual motors. The main components of stray load losses according to their dependence on frequency and leakage flux are classified into:

1- Additional losses due to slot leakage flux.

2- Losses due to end leakage flux.

3- Surface losses.

4- Tooth pulsation losses .

5- Losses due to phase belt leakage flux.

6- Skew leakage flux.

Among these six components skew leakage flux loss has been given importance and discussed in the next section and in chapter 5. Since the main objective of this study is to investigate the effect of skewing on losses.

2.2.4.3 SKEW LOSSES

Many induction motors have skewed slots usually on the rotor and some times on the stator. Skewed slots are used to reduce cogging tendency [25] and synchronous and asynchronous torques [26][27]. It also believed that it reduces the magnetic noise,[28].

In addition to the advantages mentioned above skewing has other undesirable effects on the performance of the induction motors. It leads to increase in leakage reactance of the machine [28] and gives rise to changes in the magnetic field distribution and associated losses [29]. The reasons for the changes in the magnetic field distribution are:

1-The axial phase displacement between the stator and the rotor m.m.f's.

2-The axial m.m.f. component (due to peripheral component of current) alternating in direction with movement peripherally round the air gap.

3-The change in reluctance of the flux paths, owing to the teeth on one side of the air gap overlaping the slots on the other side .

The displacement between the stator and the rotor m.m.f.'s can produce a steady increase in the air gap density from one end of the machine to the other, and the effect producing a load dependent axial force. Since the losses depend on B^2, the non-uniform distribution of the magnetic field results in extra losses.

In fact the changes in the flux distribution in motors due to the skewing is more complicated than the simple picture mentioned above, it involves variation in both the main flux and the harmonic leakage fluxes. In this study we are only concerned with the change in main flux and this is dealt with in detail in chapter 6.

Apart from the effect of the change in flux distribution on losses skewing has some other effects on the losses in cage rotors which are purely ohmic losses. If the insulation between the rotor

bars is insufficient the interbar currents can flow through the iron and another component of losses will be affected and increased by skewing. This is called the interbar losses[30][31][32]. In skewed rotors the I^2R losses produced by the stator m.m.f harmonics constitute a great proportion of total I^2R loss. Previous investigations undertaken by others on the same subject [33] have shown that the losses in uninsulated rotors due to crosspath currents reach as high as 33% of the fundamental losses.

Another component of losses which is affected by skewing is the rotor I^2R losses due to the relative changes in the length and cross-sectional area of the rotor bars. Although the effect of skewing on this component of loss has received little attention it is worthy of consideration in skewed rotors with a large skew angle. If a cage rotor is skewed by α , the increase in the rotor conductor losses due to skewing can be determined as follows.

Assuming that the length and the crossectional area of unskewed rotor bar are L and A respectively.

For the skewed rotor bar :

$$L^- = L / \cos \alpha \qquad \text{.....2.3}$$

$$A^- = A \cos \alpha \qquad \text{.....2.4}$$

Therefore the resistance of the skewed rotor bars is:

$$R^-_2 = \rho(1/\cos \alpha)^2 \, L/A \qquad \text{.....2.5}$$

But for unskewed rotor $R_2 = \rho \, L/A$ 2.6

Therefore $R^-_2 = (1 / \cos \alpha)^2 \, R_2$ 2.7

If it is assumed that the the ratio of the rotor bar resistance to the total rotor resistance is K_s, then the resistance of the skewed rotor can be given as : $R_2^- = (K_s R_2/\cos^2 \alpha) + (1 - K_s) R_2$ 2.8

ie $R_2^- = R_2 + K_s R_2 (1/\cos^2 \alpha - 1)$ 2.9

2.3 MEASUREMENT OF LOSSES

A variety of methods for measuring the losses of induction motors is available and during the past few decades new techniques have been proposed to increase the precision of loss determination. Many of these methods are fundamentally the same, differing only in detail. Most of these methods are discussed in BS [5] and its correspondent IEEE [1], and there are other methods proposed by other workers on the same subject,[13][34][35][36]. There are three main methods for measuring total losses in induction motors, the input output method, loss separation and the measurement of the effect of the losses. The first two methods are often used, while the third method has received scant attention because of the difficulties faced by those who have used it before.

The input output method is easy in concept but difficult in execution. In this method the machine is run at rated values of voltage and frequency and the load is adjusted according to demand (50%,75%,100% etc of rated current). The power input to the machine

is measured by using standard laboratory instruments, the mechanical output power can be determined from the shaft torque measured by means of dynamometer, calibrated machine or torque transducer together with the rotational speed. Thus the total losses can be determined by subtracting the output power from the input power. Here a very high degree of accuracy is required, any small error in measuring the values of input and output power could cause a significant error in the final result. Therefore for accurate measurement of losses, particularly if the machine is supplied from a non sinusoidal source, instruments with high degree of accuracy and better frequency responce are required to measure the input power. Measurement of mechanical output power is rather difficult. The cost of achieving measurements with high accuracy often carries a high price. In case of using dynamometer or torque transducer, the output power has to be determined by multiplying two or three values, the force by the distance by speed (for dynamometer) and the torque by speed (in case of torque transducer), in both cases the possibility of errors is high.

To determine the total losses by a calibrated machine, the test motor is connected mechanically to the calibrated machine and run at rated condition. The mechanical output of the test motor is determined from the electrical output of the calibrated machine. This method is easy in concept but raises the problems of testing the calibrated machine in the first instance and ensuring that its

losses do not vary with time and are known accurately over its total operation range. The calibrated machine has to be of a similar size to the test machine to ensure adequate accuracy and hence a wide range of units may be needed. These disadvantages have made the use of a calibrated machine unpopular.

The back to back test is another method by which one can measure the total losses of an induction motor. In this test, two identical machines have to be used and run at essentially the same rated condition, one of them is run as a motor and the other as a generator. In this test it is almost impossible to get two absolutely identical machines and it is also impossibile to operate them exactly at the same condition, hence their losses will be different, although their sum is accurately known.

Total losses can be segregated to their components, iron losses, friction and windage losses, rotor I^2R losses and stray losses by conducting a series of tests. Iron losses and the windage and friction losses can be determined by a no load test followed by excitation test at variable voltage, or by a no load test followed by a calibrated machine test, the latter has to be performed with the test motor disconnected from the supply. The iron losses measured by this method include the fundamental component and the high frequency component due to slot openings, but it is very difficult to separate

these two components from each other. The point often made against no load tests is that the flux condition during the no load test is not the same as at load condition. The test mentioned above in conjunction with other tests like the rotor removed test, reverse rotation test, differential dynamometer, mechanical differential [1] [6][9][13][21][37] can be used to determine components of losses including stray losses in induction motors.

The rotor removed test is a simple test to perform and it is used to determine the fundamental frequency stray losses which could be found by subtracting the I^2R losses from the power input. This method was first suggested by Koch [38] and later described by D.H.Ware [39] and said that the current, I,is the load component of primary current since the magnetising current is present on no load and only the additional losses due to load current are included in the stray load losses. D.H. Ware suggested that this loss has to be measured at current (I) where:

$$I^2 = I_1^2 - I_m^2 \qquad \text{.....2.10}$$

I_1 = Stator current.

I_m = Magnetising current

There are two points which must be noted about this test :

1- In the absence of rotor the end region losses are not the same as when the rotor is in.

2- The component of losses due to skew leakage is not includ ed in the losses measured by this test.

The reverse rotation test can be performed to measure the high frequency stray load losses [6]. In this test the machine is driven backwards at synchronous speed. While the stator is supplied by a low voltage supply to circulate full stator current. The stator power input P_i, and the shaft power input P_m are measured at the current I (as given by equation 2-10). With the stator power removed the mechanical power ($P_{f\&w}$) required to drive the rotor at synchronous speed in the same direction is measured.

Under this condition the slip s is equal to 2

The fund. electrical power input to rotor = $m(I_2^2 R_2)/2$. 2.11

Mechanical power input = $-mI_2^2 R_2/s(1-s)$ 2.12

for s = 2, Mechanical power input = $mI_2^2 R_2/2$ 2.13

Where m = No. of phases.

This shows that the double frequency losses occur in the rotor (P_{2f}) which is equal to $m I_2^2 R_2$ are supplied half from the stator and half from the mechanical shaft input.

Hence the stator input power $P_i = mI_1^2 R_1 + P_{ff} + 1/2\ P_{2f}$ 2.14

Where P_{ff} = fundamental frequency stray losses. If it is assumed that the high frequency stray load losses P_{hf} occuring under full load condition are supplied wholly by mechanical power input P_m, therefore:

$$P_m = P_{f\&w} + 1/2(P_{2f}) + P_{hf} \quad .....2.15$$

$$P_{hf} = (P_m - P_{f\&w}) - (P_1 - mI_1^2 R_1 - P_{ff}) \quad .....2.16$$

P_{hf} = mechanical input - (stator input - Stator loss)

Here again since the P_s(at 2f) is measured by the rotor removed test the problems associated with that test influence the results of

the reverse rotation test results.

Although none of these tests (rotor removed, reverse rotation ,mechanical differential, etc.)has gained world wide acceptance for measuring stray losses, they are used in some parts of the world especially in the USA. In the UK instead of using these tests they would appear to be a preference to assume a nominal value of 0.5% of the input power as approved by BS [5]. Alger has shown his concern about this figure [28], our work and others have shown that this assumption does not help the designer in any way in their prediction during the design and the development of induction motor.

Another method for measuring losses in induction motors is the calorimetric method which has been used in this project. The background of the test, its principle together with detailed construction and the results obtained from the tests using calorimetric mnethod are discussed in chapters 1,3,4,5.

CHAPTER THREE

THE CALORIMETRIC METHOD FOR MEASURING INDUCTION MOTOR LOSSES

3.1 INTRODUCTION

In the last chapter (section 2.3) various methods of measuring machine losses were discussed. Some of these methods are complex to perform and it is often difficult to obtain accurate results, both factors being a direct result of the relatively high efficiency of modern induction motors. However it is self evident that a method of loss measurement which is accurate, repeatable and inherently insensitive to external parameter variations would of great benefit in machine work.

By their nature the losses in all machines are dissipated as heat, normally causing an increase in machine temperature above the ambient level, the heat being transferred to the surroundings by the three processes of conduction, convection and radiation.

The technique of measuring the heat produced by an action using a calorimeter is well known in the physical sciences. Although BS [5] does not formally include calorimetric method of loss measurement it refers to IEC [11] in which two calorimetric methods are described.

In the first method, the fluid flow rate and appropriate parameters are measured; the heat transfer is determined from these and the measured temperature rise across the calorimeter. The second method is described as the calibrated method for which a calibration curve (obtained by appropriate means) is used to relate the heat transfer to the temperature rise.

The method of loss measurement described in this thesis can be considered to be a variant of the second method, in which the calibration is obtained for every test on the induction motor. This is achieved by *a second, balance test during* which the conditions of the induction motor test are carefully reproduced, but with alternative source of heat providing the energy input. Experimental results are presented to show that the loss measurement has a resolution of 9.4 W.

3.2 PRINCIPLE OF THE BALANCE METHOD OF CALORIMETRIC LOSS MEASUREMENT

In general a calorimeter consists of an enclosure of some form, usually insulated, and a working fluid to which the heat is passed from the device or a sample under test. A calorimeter can be of closed or open form, by which is meant that either a fixed predetermined amount of working fluid is used and is not changed during the course of the experiment, or there a continuous flow of

new working fluid through the calorimeter. When testing TEFV motors it is clearly not sensible to use a liquid as the working medium and air becomes the natural choice. Since the specific heat and density of air at normal pressure are relatively low it is clearly necessary to use an open form of calorimeter in which the motor is enclosed in a thermally insulated box and air is passed through the latter to extract the heat.

At first sight the easiest way of determining the rate of heat generation is to use the equation relating the temperature rise and material properties to flow rate and heat input.

$$P = Q \sigma C_p \Delta t \qquad \ldots\ldots\ldots\ldots\ldots 3.1$$

where: Q = volume flow rate (m^3/s)

σ = density (Kg/m^3)

C_p = specific heat (KJ/Kg K)

Δt = temperature difference in K

However this demands accurate, continuous measurement of all the terms on the right hand side of equation (3.1). Measurement of Δt is perhaps the simplest , even though care must be taken to ensure that the temperature distribution across inlet and outlet are known, however the measurements of flow rate, density and specific heat present greater difficulties.

If, however, after the temperature increase due to the induction motor losses has been determined, the experiment is repeated with a different source of heat (a simple resistance heater element) and the same temperature difference obtained, then providing certain conditions are met the energy into the heater is equal to the heat energy provided by the machine, and is therefore a direct measure of the losses of the motor.

It is clear from equation 3.1 that the first conditions that must be satisfied by such a test are the volume flow rate (Q), density (σ) and the specific heat (C_p) must be the same for both the induction motor and balance tests. Throughout this thesis the phrase 'induction motor test' will in general mean the running of the induction motor on no load or load within the calorimeter to determine the temperature rise, whilst the phrase 'balance test' implies that the alternative source of heat is energised.

Typical test results for a D132S, 4pole, 5.5kW induction motor show that the temperature of the motor components will rise experimentally towards the steady state value (for constant load)and the time needed to achieve the steady state value is about 3 hours. Since the material within the calorimeter enclosure does not change between the two tests, it follows that the time needed for the balance test to achieve the steady state will be of similar length,

and thus realistically only one loss measurement could be made on each day. Hence the condition that the air density and the specific heat must be the same for the two tests is equivalent to having a constant barometric pressure and a relative humidity over the 8 hour working day. Measurement of the relative humidity in the room from which the cooling air was drawn showed a maximum variation of 6% in one day.

Reference to the graphs of specific heat against temperature in BS [5] figure 3.9 shows that at a constant temperature of 20°C such variation are only likely to cause a change in specific heat of about 0.5%, a value which is sufficiently small to give confidence in the balance method.

Another graph of air density against temperature, figure 3.10 shows that at a temperature of 20°C and under a constant pressure a variation of 40% in humidity causes a change of only 0.26% in air density. Again this small change in the air density even if it happened within a day, does not produce significant errors in the measurement of loss.

The other condition that the flow rate should be constant, was checked by direct measurement of the pressure drop across a choke

by a water manometer, the reading of which was recorded and no measurable difference in the air flow rate was found.

This similarity in air flow rate,with the fact that the induction motor was rotated at the same speed and in the same direction in both parts of the test, means that the windage losses are likely to be the same in both parts. However during the balance test the torque and the power required by the induction motor friction and windage are provided by the dc machine, this power flow into the calorimeter must contribute towards the temperature difference between the inlet and the outlet. Similarly during the induction motor test the windage and friction losses, provided by the supply, must also cause a part of the measured temperature difference. Thus, if the friction and the windage losses are the same during both parts of the test, the power into the main heater is a measure of the machine losses excluding friction and windage losses. If the loss changes between the two tests then the measurement of the losses will be in error by the difference in the two sets of the friction and windage losses. Keeping the air flow rate and the shaft speed conditions the same provides the best means of achieving no changes.

3.2.1 THE MECHANISMS OF HEAT TRANSFER WITHIN THE CALORIMETER

The heat produced by the motor during the induction motor test and that produced by the heater during the balance test are transferred to the working fluid and the surrounding by convection, conduction and radiation. It can be estimated from typical test results that 96% of heat is removed by the forced convection of the working air flow, but clearly if there is to be confidence in the accuracy of the test it is necessary to consider and evaluate the importance of the other two mechanisms. Consider first the question of conduction through the machine mounting points. Inspection of figure 3.1 shows that the induction motor is not directly mounted on the thermally insulated base of the calorimeter but on a steel platform suspended 10cm above the base, effectively increasing the conduction path length, and increasing the area of metal exposed to the air flow through the calorimeter. Because it is in the air flow, the temperature of the support structure at the point of contact with the base is similar in both tests and hence the heat loss through the mounting bolts will be the same in both tests. The accuracy of loss measurement is therefore unaffected by this mechanism. The level of heat loss through the bolts is assessed quantitively in section 3.5, where it is estimated that some 18W of heat is conducted by this route. The difference between the two tests will be much smaller than this since the boundary temperatures are similar. The other more significant, conduction path is through the walls of the calorimeter. It is estimsted in section 3.5 that this heat loss is of the order of

40W on full load when the total machine losses are about 1600W. Because the balance heater and the induction motor are not located at the same point within the enclosure the internal temperature distribution will be different during the two tests. It is estimated section 3.5 that this difference will cause the conduction loss through the calorimeter walls to be 5W higher on the balance test than on the induction motor test, meaning that measurement of losses is likely to be high by this amount. For the purpose of comparing the losses in the machine when parameters such as skew or air gap are varied this error is not critical since it applies to all test results.

The third conduction loss is along the shaft of the induction motor, which it can be seen from figure 3.1 passes through the calorimeter wall and is connected to the DC motor by a coupling which incorporated a rubber torque transmission component. The coupling which represents a high thermal resistance is mounted very close to the calorimeter wall and thus any heat passing along the machine shaft is dissipated by forced convection from the driving part of the coupling. Although the rotor temperature will be very different between the two tests, hence producing a different temperature distribution along the shaft, it is estimated that the losses involved did not create any significant error in the measurements.

3.3 CALORIMETRIC STRUCTURE

The shape of the calorimeter is shown in the isometric sketch of figure 3.2 together with the general overall arrangement shown in figure 3.1. The shape and dimensions were chosen to give good mixing of the cooling air with minimum losses through the calorimeter walls. By increasing the size of the structure the latter could be reduced but at the expense of significant temperature gradients in the cooling air. It was considered that these should be kept to minimum to achieve maximum accuracy.

The calorimeter box was constructed from nine sandwich panels, each of which has outer layer of 4mm hard board glued to the main thermal insulator, 25mm thick expanded polystyrene sheets. The outer edges of each panel were made from 25mm x 25mm soft wood as shown in the cross section of a panel to panel joint, figure 3.3. It is clearly important that all air which enters through the inlet chimney leaves via the outlet chimney, thus the panel to panel joints must be draught tight. This was achieved by fitting a nylon brush draught excluder strip on the soft wood frame. When the panels were screwed together this draught excluder prevented air leakage through the inevitable gaps between the panels.

The base of the unit figure 3.4 was of the same construction with the exception of two strips of "monolux", an insulating material having sufficient mechanical strength, to take the weight of test machine.

It was recognised that there would be frequent changes in the test machine (different rotors) and the calorimeter was assembled in such a way that the bulk of it could lifted as shown in figure 3.2, leaving only the base and the lower part of the shaft side panel. Again these joints were sealed by means of the draught excluder design described above, with specially adapted wood screws (wings were added to facilitate turning) used to tighten the joints.

As can be seen from figure 3.1 the induction motor shaft passed through a hole formed by two semicircular recesses in the panel sections, and the air leakage was reduced to acceptable proportions by the use of sponge rubber "gland stuffing" around the shaft.

The main heater for the balance test was inserted near the base of the inlet chimney and consisted of four 1 kW cylindrical heating elements in electrical and mechanical parallel. Although the total losses were expected not to exceed 1.5 kW, four parallel elements were used to reduce the heater surface temperature and hence its radiated energy. To reduce the conduction losses through the calorimeter wall in the vicinity of the heater 10mm thick monolux

sheets were fastened to the inner walls. Two sheets of aluminum were attached to the inner surface of the inlet chimney, in order to direct the air onto the heater.

It was realised at an early stage that it was important that the inlet air should not be taken from the laboratory into which the outlet is exhausted. The inlet air was drawn from an adjacent unheated generator room whose temperature was found by measurement to change very slowly. The arrangement used to duct the air the 5 metres from the adjacent room to the top of the inlet chimney is shown in the general arrangement, figure 3.1. Further details of particular components of the inlet system are given in figures 3.5, 3.6, 3.7 and 3.8. It can be seen that the duct used was formed from two concentric flexible plastic hoses 130mm and 230mm in diameter with 50mm thick fibreglass insulation in the inter tube space figure 3.5. To keep the inlet air at constant temperature (20 ± 0.1^{o} C) a 1kW preheater was fitted in the duct some 2 metres from the entry of the calorimeter , figure 3.1. This heater operated under feedback control with the inlet temperature measuring device an integral part of the control system.

The air was driven through the unit by a centrifugal fan mounted in line with the flexible ducting near the entry point from the adjacent room, together with the three axial flow fans mounted at

the top of the outlet chimney. These fans gave an air flow rate of approximately $300m^3/hr$. A choke plate mounted just upstream of the calorimeter, figure 3.5, was used to keep a check on the air flow rate, a water manometer being used to measure the pressure drop across the choke plate.

It is mentioned above that the inlet air was kept at a constant temperature of 20^oC by the preheater, however it was found that the centrifugal fan raised the air temperature by approximately 3^oC. Hence for any temperature above 17^oC in the adjacent room the inlet temperature rose above 20^oC with no input from the heater. To provide some cooling a radiator carrying chilled water was fitted to the entry grill in the adjacent room, and this is shown in simplified form in figure 3.8. A temperature drop of 4 to 5^oC across the cooler was achieved and this was only needed in hot summer days. The inlet and the outlet temperatures were measured by platinum resistance thermometers located in the inlet and exit stream as shown in figure 3.1.

3.4 INITIAL TESTING OF THE CALORIMETER

The final form of the calorimeter has been described in the last section. However a number of modifications to the initial design were needed to bring it to this state. This section describes those

those modification in detail and can be omitted by those readers more interested in the results of the loss measurement. Briefly the changes made to the initial design were:

a. Increased air flow rate.
b. Increased thermal insulation between main heater and calorimeter walls.
c. Reduction of main heater surface temperature.
d. Relocation of pre-heater away from the inlet chimney.
e. Relocation of the inlet temperature measurement.

When the calorimeter was completed in its first form, three axial fans each having an unrestricted flow capacity of 160 m^3/hr were mounted above the inlet chimney and connected in parallel to draw air through the flexible duct and blow it into the calorimeter. Experimental results showed that air flow rate was much lower than required , the reason being that the air flow resistance was much higher than anticipated due to the relatively long length of ducting. A centrifugal fan (CSB single phase, capacity = $310m^3/hr$ at free discharge) was mounted at the inlet to the duct to increase the air flow rate, the three axial fans were later removed from their initial place and mounted above the outlet chimney. By so doing the air flow rate was increased to a level that was sufficent to ensure that the outlet temperature did not exceed 40^oC, hence complying with the appropriate requirement of BS [5]. For the initial tests the flexible inlet ducting consisted of only one flexible plastic hose 230mm in

diameter. Experience showed that at times when the room temperature was higher than the required inlet temperature, the inlet air temperature was increased by typically 2 to 3°C along the length of the ducting. To reduce this a 130mm diameter hose was inserted within the 230mm tube and the 50mm space between the two filled with glassfibre as an insulator. This new arrangement decreased the radial thermal conductivity.

As mentioned previously the motor losses were not expected to exceed 1.5kW and the first design of the main heater used only one element. During the initial tests it was noticed that the surface temperature of the heater was much higher than that of the motor and since the heater was much closer to the wall of the calorimeter, this caused additional heat to escape by conduction during the balance test. It was also noticed that the inlet air temperature measured by resistance thermometer at its position XX figure 3.12 rose by 0.1°C to 0.5°C when the main heater was switched on . It was thought that this was due to radiant energy from the main heater. These problems were cured by increasing the number of the heater elements to four in order to decrease their surface temperature and hence its radiated energy and by moving the main heater to the base of the inlet chimney. Furthermore by adding two sheets of insulation material (monolux) to the inner walls of the inlet chimney near the main heater conduction losses were reduced. The two sheets of the monolux were covered by aluminium foil to reflect the radiated heat from the

heater.

It was also realised that the platinum resistance inlet air thermometer initially mounted inside the inlet chimney at XX, was still affected by heat radiation from the pre-heater, which at first was located at ZZ figure 3.12, causing a false reading of the inlet air temperature. To overcome this problem the pre-heater was replaced by another heater positioned coaxially with the flexible ducting some two metres away from the inlet chimney. The platinum resistance thermometer was also moved from its first position to inside the inlet duct just above the inlet chimney. Test results with these arrangements showed that the inlet temperature was no longer affected by radiation. It should be noted that all the radiant energy emitted by the heater or the motor is absorbed by the walls of the calorimeter and removed by the air flow or lost by conduction through the calorimeter walls.

3.5 ESTIMATION OF HEAT LEAKAGE BY CONDUCTION

As described in section 3.2.1 there are two leakage paths for conducting heat from the machine to the outside of the calorimeter and the surroundings. One of these paths is through the walls of the calorimeter and the other paths is through the bolts which secure the steel platform on which the motor is mounted to the base frame. To

estimate the heat leakage by conduction through the walls of the calorimeter it is necessary to know something about the temperature distribution across the wall. The temperature difference across the polystyrene in one of the panels surrounding the outlet was measured by two mercury thermometers and found to be $10^{o}C$ at the end of a full load test. The total area (2.724m) of the polystyrene in the calorimeter was calculated from the dimensions and together with the polystyrene thermal conductivity of 0.03W/m.K the heat flow could be calculated from:

$$P_i = \frac{\lambda \, a \, \Delta t}{d} \qquad \ldots\ldots\ldots\ldots\ldots 3.2$$

Where : P_i = Heat leakage by conduction (W)

λ = Thermal conductivity of the polystyrene(W/m.K)

a = Area through which the heat could escape (m^2)

Δt = Temperature difference across the polystyrene (k)

d = Thickness of the polystyrene (m)

Note : The thickness of the polystyrene was taken to be 20mm, because of the comparatively large diameter of the bulbs of the mercury thermometer compared with the actual thickness of the polystyrene 25mm, substituting numerical values yields:

Pi = 0.03 x (2.724) x 10 / 0.02 = 40.86W

Since the balance heater and the test motor are not located at the same point inside the calorimeter, the temperature distribution

inside the enclosure will not be the same during the two tests. It was estimated that the conduction losses during the balance test will be 5W higher than the induction motor test.

The same formula could be used to estimate the amount of the heat leakage through the four bolts. For this calculation it was assumed that the temperature of the steel base frame on which the calorimeter was mounted was equal to the room temperature, i.e. of the order of $20^{o}C$ and the temperature of the contact point at the top of the bolts is equal to the temperature of the motor frame. This is certainly higher than the temperature of the coolant inside the calorimeter depending upon the type of the test carried out and this is likely to give a pessimistic estimate of the loss, knowing that :

Cross sectional area of such bolt = 78×10^{-6} m^2

Length of the bolt = 0.03m

Thermal conductivity of steel = 58W/K.m

Temperature difference across bolt= 30 K

The total heat leakage through the 4 bolts is equal to 18W and the change between the two tests of the order of 1 or 2W.

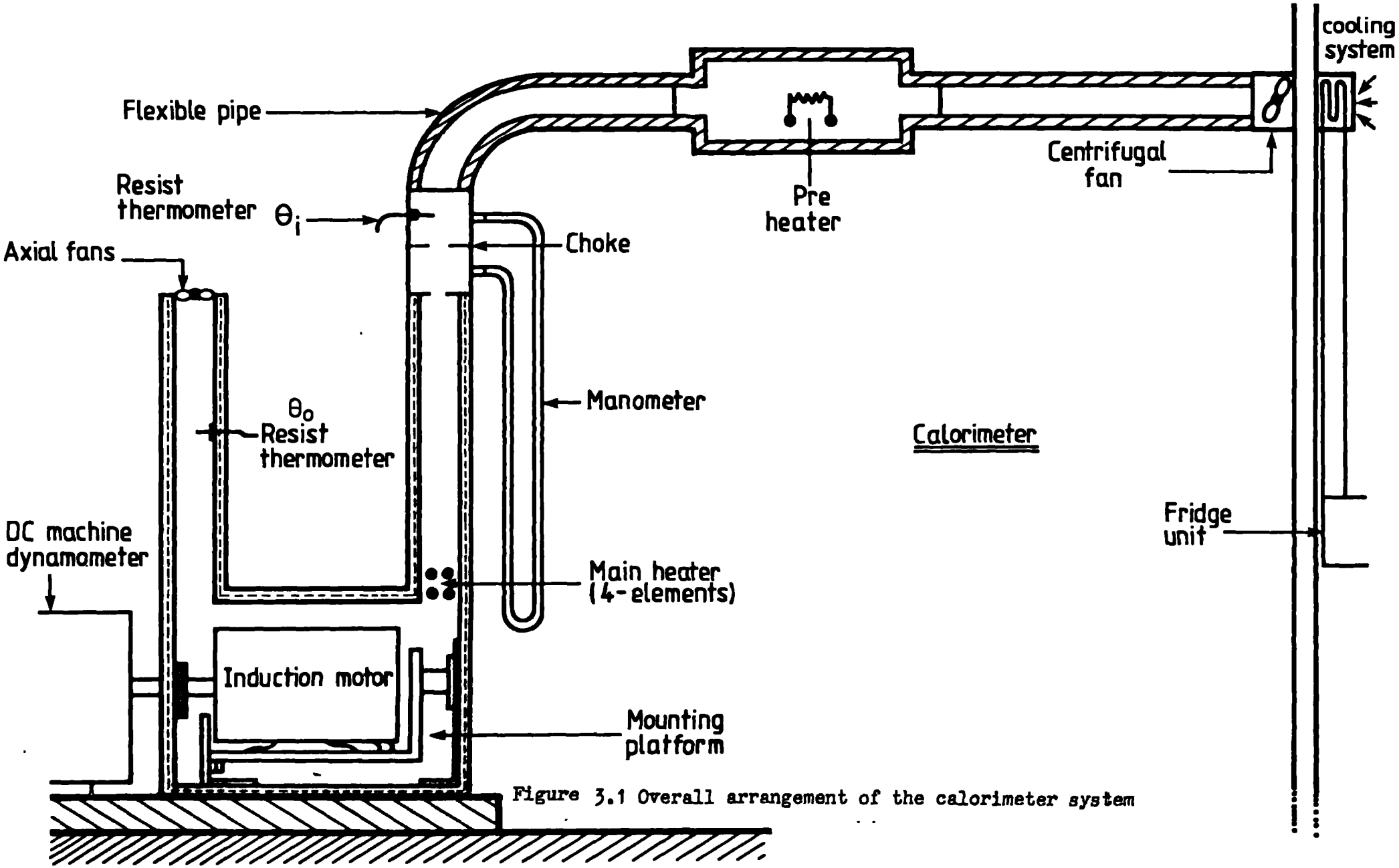

Figure 3.1 Overall arrangement of the calorimeter system

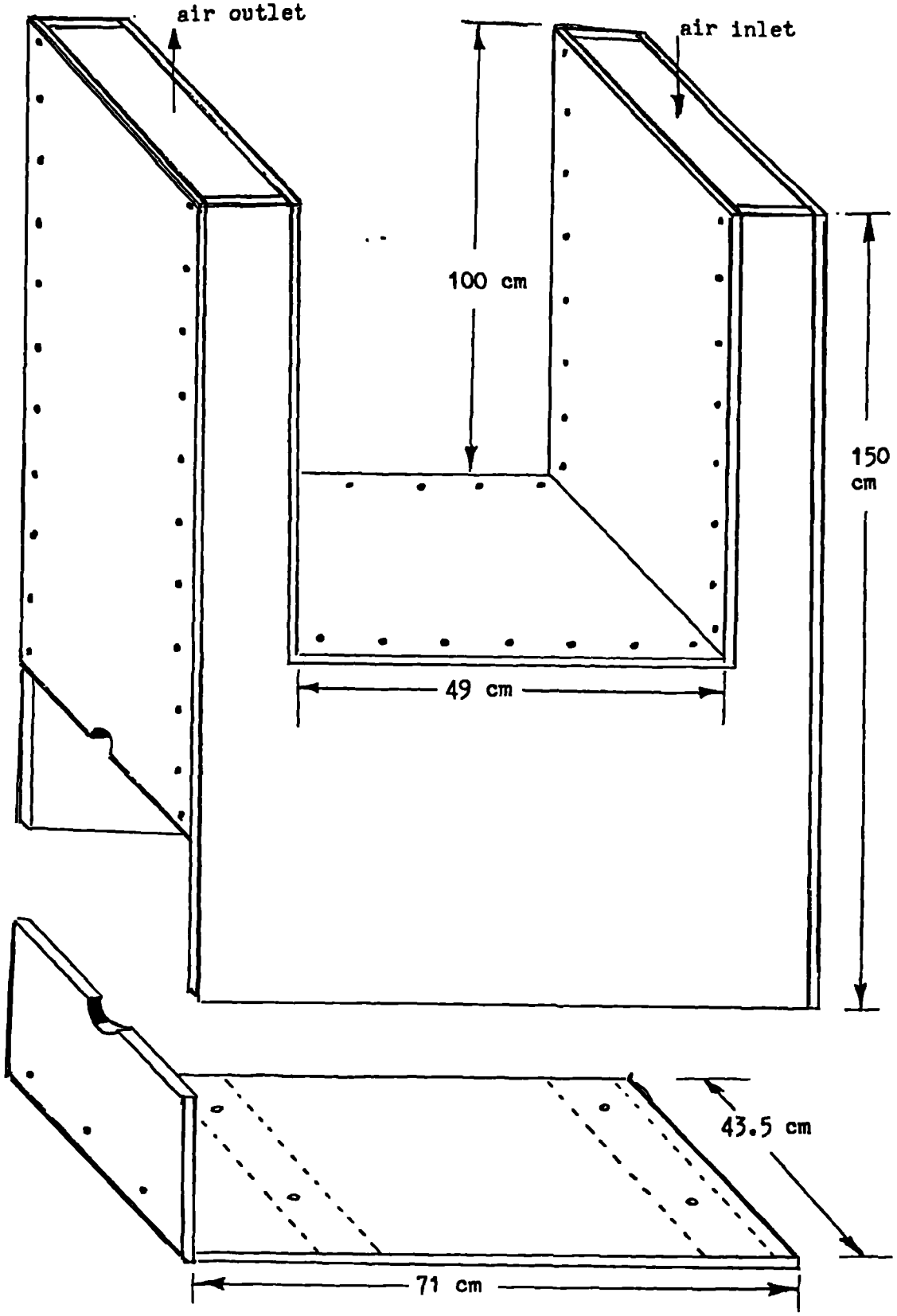

Figure 3.2 Isometric sketch of the calorimeter

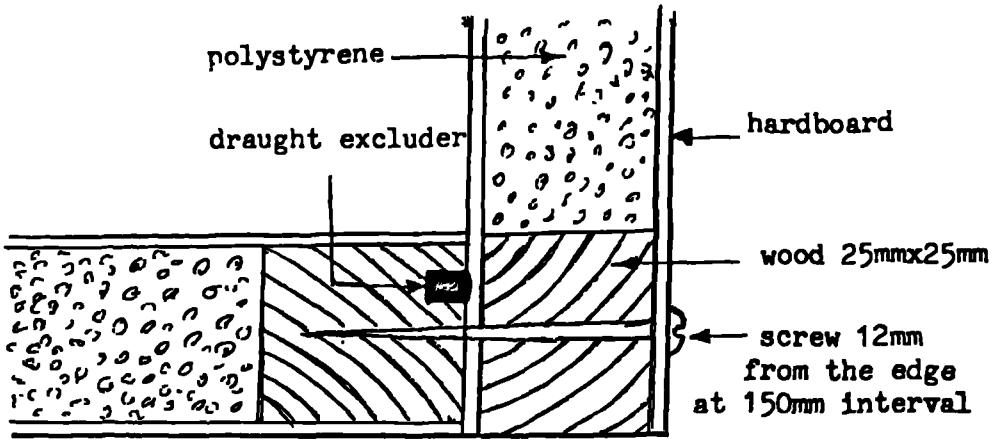

Figure 3.3 Panel junction

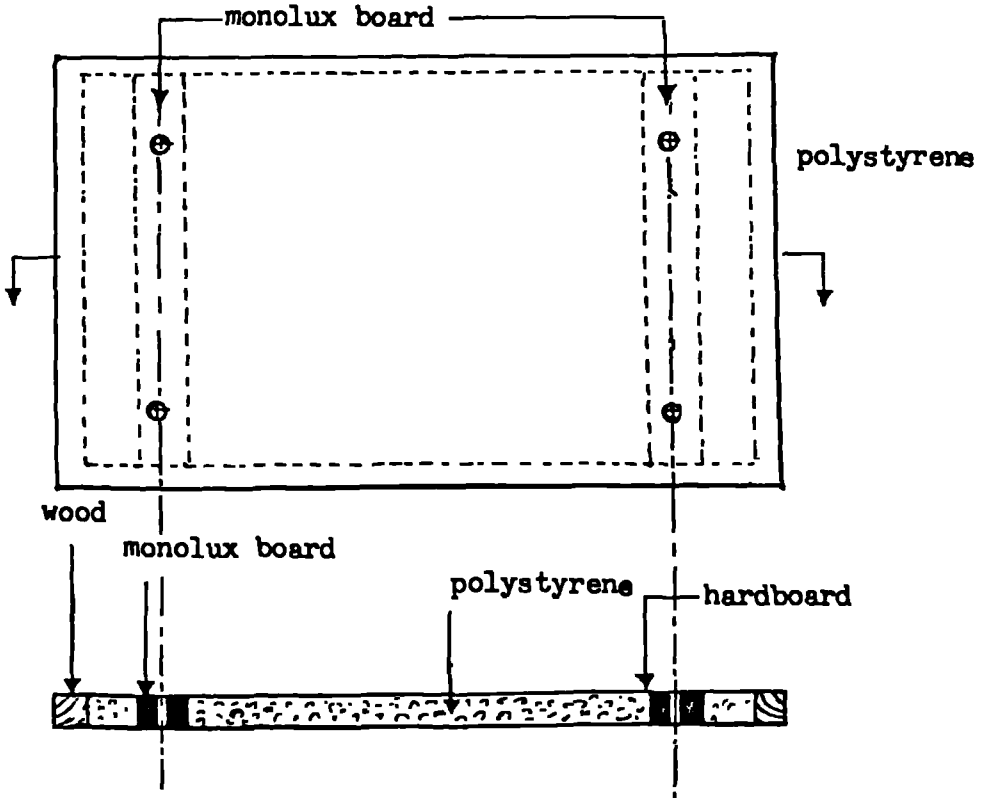

Figure 3.4 Base of the calorimeter

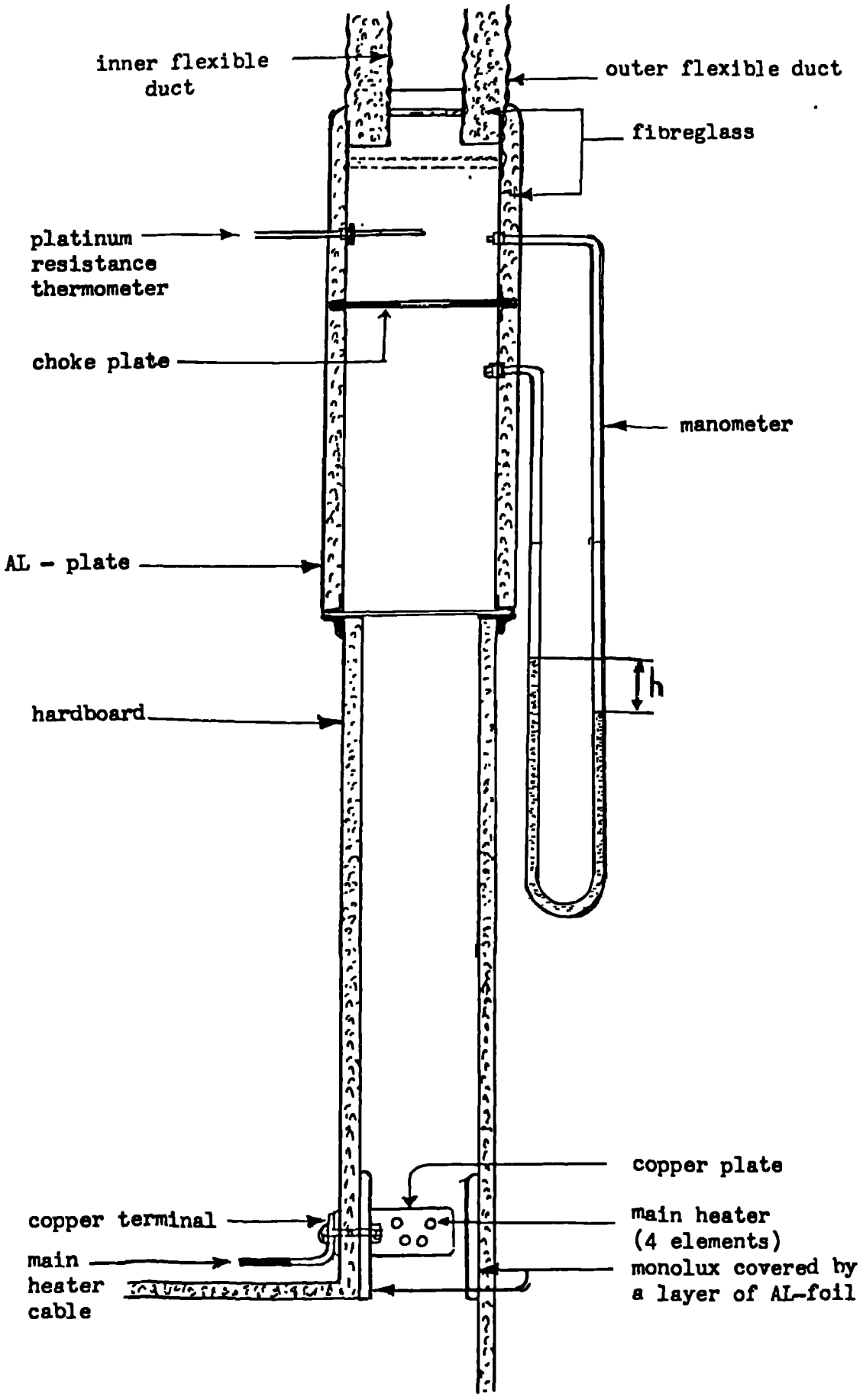

Figure 3.5 Vertical cross section of the inlet chimney

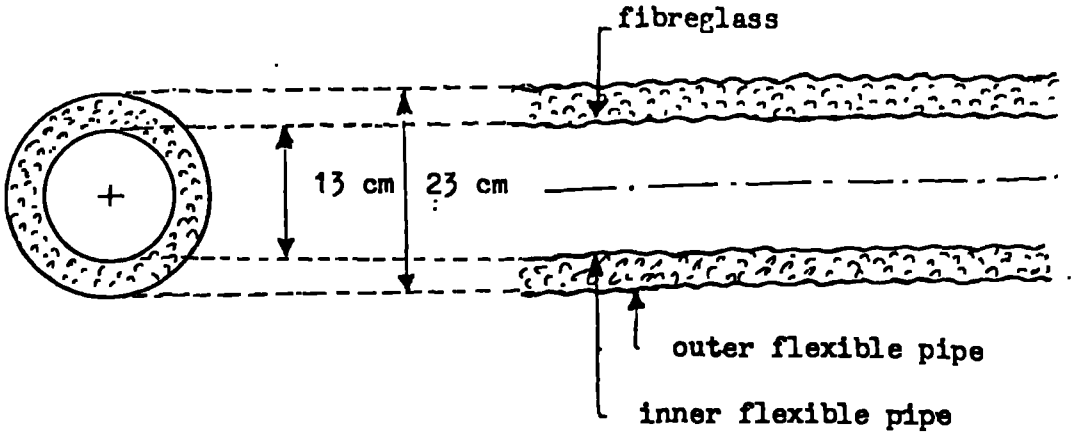

Figure 3.6 Longitudinal and crossectional view of the duct carrying air into the calorimeter

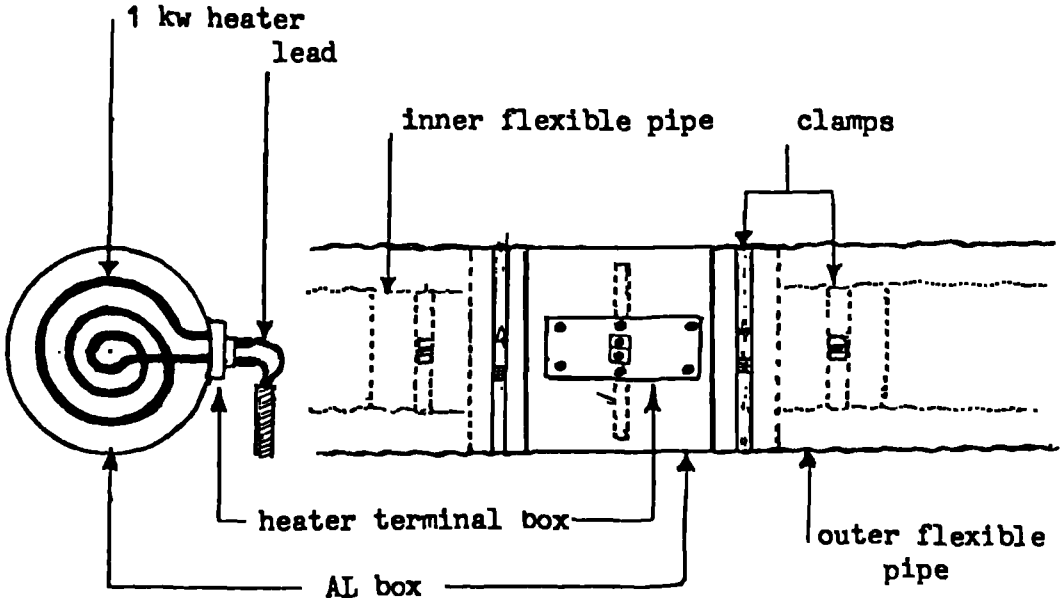

Figure 3.7 Preheater inside the AL - box

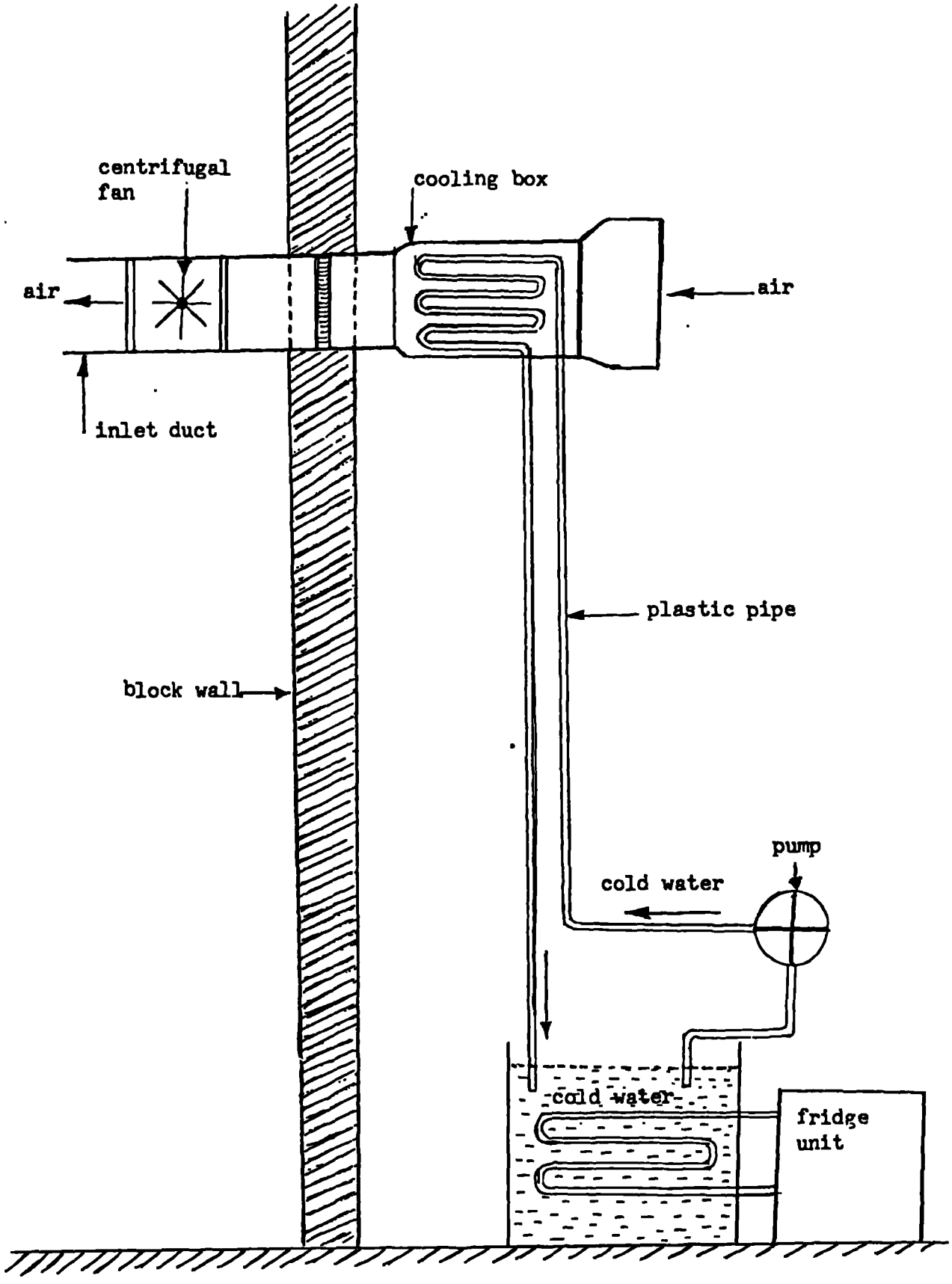

Figure 3.8 Cooling system

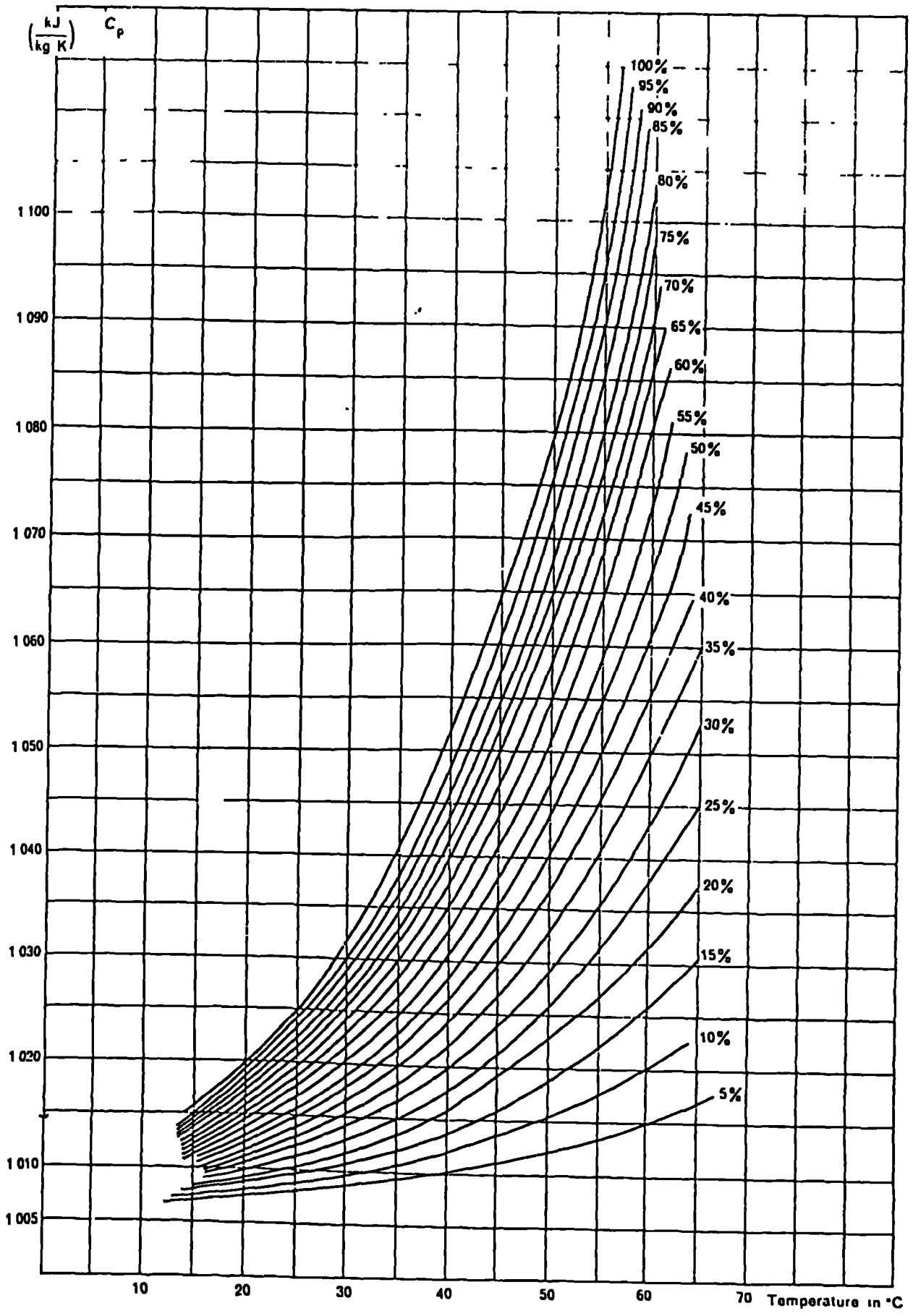

Figure 3.9— Specific heat capacity c_p of air for different values of humidity and temperature.

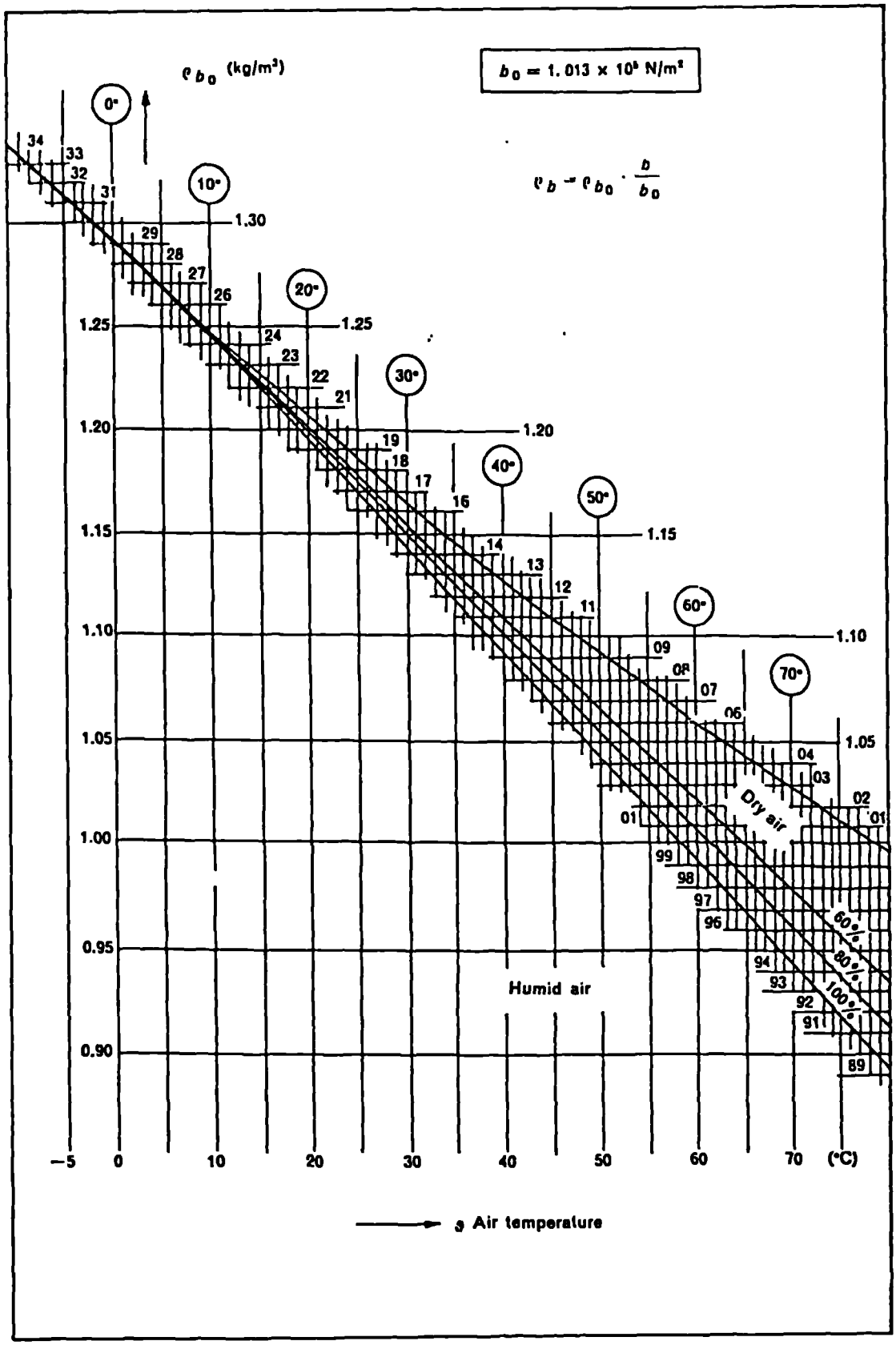

Figure 3.10- Air density depending on temperature and humidity.

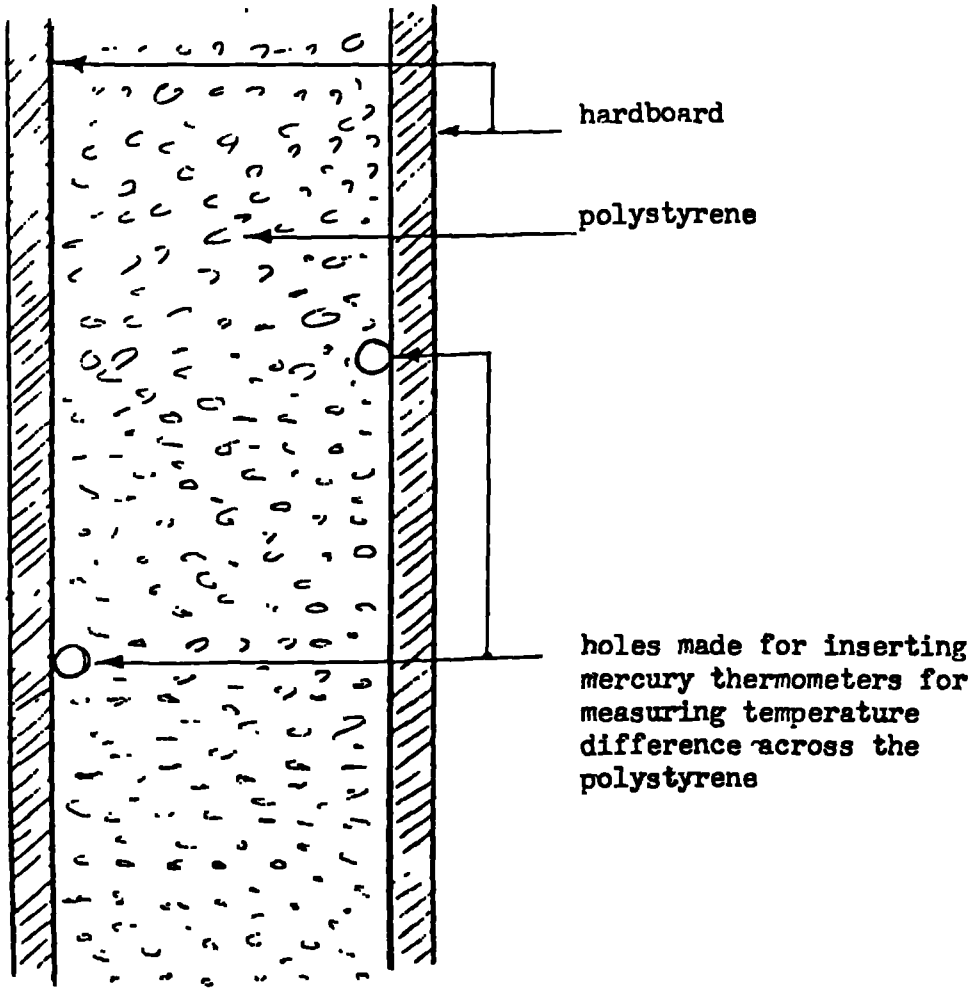

Figure 3.11 Temperature measurement across the width of polystyrene at the outlet chimeny.

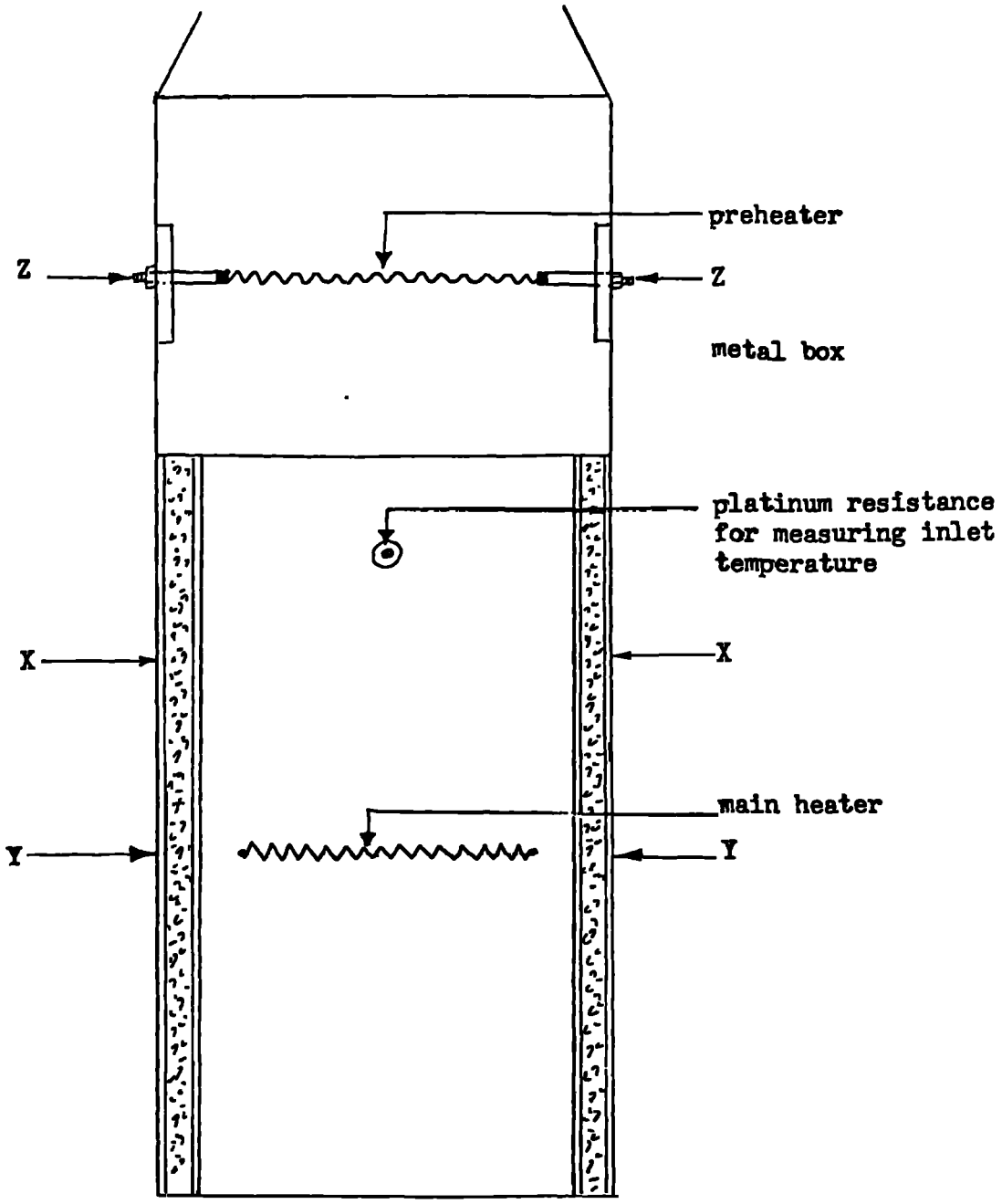

Figure 3.12 Position of the preheater and the main heater with the platinum resistance thermometer for measuring inlet temperature(initial design).

CHAPTER FOUR

MEASUREMENT AND CONTROL SYSTEM

4.1 INTRODUCTION

Since one of the objectives of this project was to measure the total losses of induction motors having different design parameters, accurate measuring instruments and reliable control and monitoring system were necessary in order to obtain repeatable results.

4.2 CONTROL AND MONITORING SYSTEM

4.2.1 VOLTAGE CONTROL SYSTEM

In order that the comparison of losses measured by the calorimeter should be valid it was considered essential to have a constant supply voltage. However when measurements over a working day were made it was found that the laboratory 415V supply (and the 200V supply which is derived by autotransformer from the 415V mains) varied quite significantly. This is illustrated in figure 4.1. A controlled voltage source was designed using an induction regulator and two buck- boost circuits to reduce inter-phase variations. Figure 4.2 shows the way in which the induction regulator was connected to the laboratory supplies, to give a variable voltage between 300 to 530V at the output terminals. Figure 4.3 shows the block diagram of

the system which was used to control the position of the regulator rotor in order to maintain the required red phase voltage. The yellow and blue phase voltages were maintained at the correct value by means of two buck-boost circuits, one of which is shown in figure 4.2. All three control systems were provided with switched set points (as reference voltages) which enabled the required voltage to be set at three phase values (216V, 240V and 264V). Following commissioning of this equipment measurements were taken of the controlled output voltage over a working day.Typical values are shown in figure 4.4. It can be seen that circuit has acheived the desired aim of keeping the phase voltages within $\pm$ 0.5 volt.

4.2.2 LOAD CONTROL SYSTEM

Since an important aspect of the project was to measure the losses at specific values of load current it was considered important, that load current variations should be reduced as far as possible during a given test. As mentioned previously the motor was loaded by a separately excited DC generator connected to fan cooled load resistors. To keep the load current constant during the test a feedback control system was developed. This is shown in a diagramatic form in figure 4.5, for which it is seen that the AC current in one phase of the supply to the motor is sensed and compared with a reference voltage. The error signal is amplified and used to control a thyristor bridge to supply the DC machine field. The comparator,

reference voltage , firing circuit and bridge rectifier were all part of commercial unit (FC Robinson: Field control unit type 822).This method of load control worked well in practice and allowed the tests, which typically lasted 3.5 to 4 hours, to be conducted under automatic control.

4.2.3 TEMPERATURE CONTROL UNIT

Stability of the inlet air temperature to the calorimeter was found to be an aid in producing repeatable results from the calorimeter. It was agreed that this temperature should be kept constant at 20°C and for that purpose a system was built to measure the inlet air temperature and use that measured value as the feed back value in a closed loop system to control the power supplied to the preliminary heater. Reference to figure 3.1 shows that the latter is installed inside the duct carrying air into the calorimeter. In this system the inlet air temperature is sensed by means of a platinum resistance thermometer placed inside the inlet chimney. The DRT2 thermometer unit provided a digital display of this temperature and an analog signal proportional to temperature which was used as a feed back signal. After amplification (x 25 gain) this signal was compared with a reference, and the error was used to drive a phase controlled thyristor firing unit. The complete circuit is shown in figure 4.6 from which it can be seen that the thyristors controlled the power to the preliminary heaters. This system proved succesful in

practice and controlled the inlet temperature to 20 $\pm$ 0.1^{o}C. When the ambient temperature rose above 20^{o}C this system provided no extra heating but the inlet temperature without cooling, exceeded the desired value. To bring the temperature down to the required value a small degree (typically 3 to 4^{o}C) of cooling was provided by a chilled water heater exchanger mounted at the inlet to the ducting as shown in figure 3.8. This cooling system was only needed on a few occasions at times when the ambient temperature was above 20^{o}C .

4.2.4 GENERAL DESCRIPTION OF MONITORING SYSTEM

The thermal time constant of the induction motor and calorimeter are such that, to achieve stable conditions, the two components of the test (induction motor excited and balance test) take 3 to 4 hours. Since there were many such tests to be done the necessity for the controlled voltage supply and load control described in previous sections is obvious. In order that the experiment could be left unattended it was also thought wise to provide a test condition monitoring system, whose purpose was to log the test conditions thus providing a check on the constancy of the test parameters. The monitor was based upon an INTEL SDK85 [40] single board microprocessor development system which has an 8085 processor, key board, EPROM, RAM and I/O facilities. The processor used its internal timing circuitry to control the sampling of 10 parameters every 2 minutes and record the data in RAM, giving 120

sets of readings for a 4 hour test. Following the completion of the test these readings could be inspected on a monitor or transfered to disc for storage if thought necessary. The accuracy of the values recorded by this system was not high since no special precautions were taken with operational amplifier or RMS/DC converters, however it was repeatable and proved to be a useful check on the history of the tests. Some examples of logged data are given in appendix A. The readings of current voltage and power which were taken for the purpose of loss measurement were taken from accurate electrodynamic indicating instruments as described in the following sections.

4.3 MEASURING SYSTEM

4.3.1 MEASUREMENT OF POWER, VOLTAGE AND CURRENT

A three wattmeter method was used for measuring the power input to the induction motor and for this purpose three Cambridge AC-test sets were connected as shown in figure 4.7, the total power input to the motor being the sum of the three wattmeter readings. The same instuments were also used for measuring the line currents and the line - to - neutral voltages. The Cambridge test sets were calibrated using an electronic power analyser as a reference, this process of calibration being repeated at regular interivals throught the testing. During calibration the Cambridge test sets were connected in an appropriate series/parallel way to demonstrate their self consistency.

4.3.2 SLIP MEASUREMENT

Measurement of the induction motor slip was achieved by a direct method based on counting a number of electrically generated, speed dependent, pulses and comparing the sum with supply frequency. For this purpose a slotted aluminum disc was fixed to the end of the dc motor shaft as shown in figure 4.8. The disc had 120 slots equally spaced around its periphery and a slotted opto-switch using a Ga infra-red LED coupled to a silicon photo transistor was fixed so that the disc to rotate freely through the slot. The rotation of the machine set generates 120 pulses per revolution or 60 pulses per supply cycle when the set runs at synchronus speed. An electronic circuit was designed to generate a square wave signal with a period equal to 16 supply cycles (320 ms at 50 Hz). This square wave was used to gate a timer counter which counted the pulses from the opto-detected circuit. For synchronous speed the counter recorded 960 pulses, hence at lower speed the slip was :

$$s = \frac{960 - N}{960}$$

This method of measurements gives a slip to an accuracy of one part in 960, although averaged over 8 revolutions of the machine. It was considered that the speed would not change significantly over this period for the steady state operation. The slip was also determined by the same method in the INTEL 8085 based data logging system described in (section 4.2.4.) After a test was completed this data logger contained a record of slip over the test, together with

various other measurements. These records were used to check that there were no unexpected variations in the test conditions over the duration of the test.

4.3.3 DC - RESISTANCE MEASUREMENT

Since the only loss which can be separated with some confidence is the stator copper loss it is clearly necessary to know accurately the winding resistance at its operating temperature. To achieve this the induction motor stator dc resistance was measured immediately after each test at a number of equally spaced time intervals. Using this well established technique the variation of the winding resistance with time after load disconnection can be determined by extrapolation figure 4.9. The measurement of dc resistance was achieved by the circuit shown diagramatically in figure 4.10 for which it can be seen that the SDK 85 monitor system controlled and recorded the measurements for subsequent print out and analysis. In order to avoid extra heating due to dc braking the low dc voltage was connected to the stator only after the motor had stopped, taking the time origin at this point the first measurement was taken at t=2 seconds and subsequent measurements every 30 seconds at t= 30, 60 .....etc to allow the transient to decay. The processor took a set of readings over a total time of 5 minutes (11-readings). Other measurements showed that the phase resistances were equal, within measurement errors, and for all the tests it was therefore

assumed that the required phase resistance was 1.5 x measurement.

4.3.4 TEMPERATURE MEASUREMENT

Temperature measurement of the air at the inlet and the outlet of the calorimeter together with the room temperature were measured by platinum resistance thermometers. The locations of the platinum resistance probes are illustrated in figure 3.1 . The thermometers and the indicating instruments (FARNEL DRT2) were calibrated at the begining of the research work in accordance with the procedures given in the instruction manual. The units offer a resolution of 0.1^{o}C over the range of 0 - 50^{o}C and display the measured temperature in centigrade.

4.3.5 AIR FLOW MEASUREMENT

The use of a balance mode of operation means that it was not necessary to measure the air flow rate in an absolute way, but it was essential to know that the flow rate remained constant. This important difference between reading a repeatable absolute measurement and a repeatable indication meant that a relatively simple uncalibrated system could be used. This was achieved by measuring the pressure difference across a choke plate placed in the air stream, the arrangement being shown in figure 3.12. Experience

showed that during the normal operation of the system the pressure difference between the two sections was 24 - 26 mm of water. This was used as an indication to show the air flow rate. Using the choke plate dimensions and approximate values for the characteristics of air, the air flow rate can be estimated from this pressure difference as shown below.

D_1 = 230 m

A_1 = 0.0415 m^2

D_2 = 0.075 m

A_2 = 0.004417 m^2

Speed of air in the duct can be expressed by the Bernoulli equation of:

$$V_1 = \frac{2 \rho_1 g h}{\rho_2 ((A_1/A_2) - 1)} \quad \ldots\ldots\ldots\ldots 4.1$$

Where ρ_1 = density of water = 1000 Kg/m^3

ρ_2 = density of air = 1.2 Kg/m^3

h = height of column of water in the manometer = 25 mm

g = 9.8 m/s^2

V_1 = 2.166 m/s

Then the volume of the air

$Q = V_1 \times A_1 = 2.166 \times 0.0415 \times 3600 = 323.6$ m^3/hr

The air flow rate can also be estimated from the calorimetric test results by plotting values of power input to the main heater against temperature difference between the inlet and the outlet air.

It should be noted that this graph corresponds to the calibration curve of IEC [11] and that the displacement of the points from straight line can be attributed to variations in climatic conditions. The air flow rate can then be estimated from the slope of the graph, assuming typical values of the air properties. Figure 4.11 shows a linear relationship between P_i and Δt taken from a number of calorimetric tests, together with the estimated air flow rate. It can be seen that the air flow rate calculated by this method is less than that calculated by the other method, but that they indicate an air flow rate of about 300 m^3/hr. The agreement between the two estimates is considered to be resonable in view of the assumptions made, particularly for the choke plate. However, as indicated earlier it is not the actual value of the air flow rate that is of interest, but the fact that it should remain constant throughout complete test. Experience showed that this was the case.

4.3.6 TORQUE MEASUREMENT

The relative centre heights of the dc load machine and the D132S induction motor meant that the latter would have to sit on some form of platform. This was used as an opportunity to design and test a simple torque measuring system, which is shown in sketch form in figure 4.12. The system went through only one development stage and the results were not essential to the main theme of this work but it represented a useful exercise. The basic concept relies upon the fact

that the torque on the rotor is opposed, by Newtons third law, with an equal reaction torque on the stator. The mechanical platform upon which the induction motor was mounted could twist about an axis coincident with the machine axis, the torque being balanced by stress in the torque tube. Four strain gauges mounted along and perpendicular to the major strain axis were arranged in a bridge network, the output of which was proportional to the tube strain. Figure 4.13 shows the strain gauge output against dc machine output power and it is seen that there is a linear relationship between the two. Calibration was made by means of a torque arm (which could be fitted to the induction mototr frame) and weights, and calibration tests also produced a linear output. Unfortunately this initial mechanical design suffered from hysterisis due, probably, to slight misalignement of the front support bearings and friction in those bearings. It was clear that the system could be developed to reduce this, but this was not done during the project. It is thought that it is a measurement method worth pursuing.

4.3.7 MEAN AIR GAP MEASUREMENT

Accurate measurement of the mean air gap between the stator bore and the rotor was achieved indirectly by measuring the diameters of the stator bore and the rotor. The stator bore diameter was measured accurately by means of an electronic device (CORDIMENT 1200,C.E.JOHANSON) in the metrology measurement laboratory at GEC

Blackheath. The rotor diameters were measured when delivered and after each machining operation by means of a dial snap gauge. For each rotor twelve measurements were taken at different places, and the average of those readings obtained, care was taken to try to keep these values within a tolerance of 0.025mm.

4.3.8 ROTOR ECCENTRICITY

The determination of the air gaps described in the last section is based upon an assumption of uniformity. It was clearly necessary that this assumption be checked, since it is known that variation in air gap can causes flux non uniformity which themselves causes changes in the machine performance, including reduction of output power, cogging torque and unbalanced magnetic pull [42]. Although in the standard production machine the design tolerance make it almost inevitable that variations in air gap will exist, for a research project such as this, measurements have to be taken to ensure uniform conditions throughout the test. To do this a set of long handled feeler gauges, 0.152mm to 0.355mm in steps of 0.025mm, was made and four equally spaced 25mm diameter holes were drilled in each end cap on a circle concentric with and equal to that of the stator bore. These holes were also tapped and eight brass plugs made to close the holes for normal operation. Insertion of the feeler gauges through these holes allowed the air gap to be estimated (note that accurate measurement by this method was not possible due to the curvature of

the components). For each access hole four estimates of the gap were recorded, each corresponding to four equally spaced rotor positions. Measurements of eccentricity of rotor No.8 with stator No.1 has been given as an example in figure 4.14. This method only gives a picture of eccentricity at the two ends of the rotor, but taken with the other instruments of the stator and rotor were considered sufficient to ensure acceptable conditions for tests.

D.E	0	90	180	270	360
A	0.20	0.20	0.22	0.22	0.20
B	0.22	0.20	0.22	0.22	0.22
C	0.22	0.22	0.20	0.20	0.22
D	0.20	0.22	0.22	0.20	0.20

NDE	0	90	180	270	360
A	0.20	0.20	0.20	0.20	0.20
B	0.20	0.20	0.20	0.22	0.20
C	0.15	0.15	0.15	0.15	0.15
D	0.20	0.20	0.20	0.20	0.20

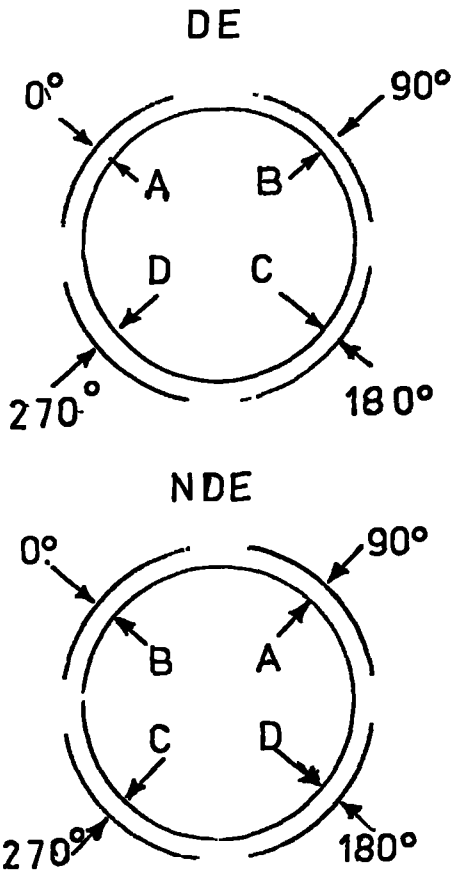

Note: All the measurements are in mm.

Fig 4.14 Measurement of eccentricity of rotor No.8 with stator No.1

4.3.9 SKEW MEASUREMENT

Since the major objective in this research was to investigate the effect of skewing on losses, it was necessary to find a method of measuring the skew of each of the rotors provided. As the rotor slots are of the closed form the location of the bars is not always apparent by visual inspection and if their position was to be found without destroying the rotor a method of bar location was needed. Searching with an AC supplied search coil was tried but found to be very imprecise, but the use of crack detection techniques proved to be quite acceptable. Initially a rotor was magnetised by means of a strong field and then sprayed with a magnetic ink (MANAFLUX 7HF). The latter clearly revealed the accumulation of the field around the slot bridges and this was quite adequate to determine the bar positions on the rotor. Subsequently it was found that the residual magnetisim (left from normal motor operation) was sufficient to cause the magnetic ink to reveal the bridge locations. Then the angle between the rotor bar line and the horizantal line is measured and expressed interms of stator slot angle.

4.3.10 BAR AND INTERBAR IMPEDANCE MEASUREMENT

The interbar impedance of two of the rotors, Nos. 2 and 8 which are skewed by 0.5 SSP and 1 SSP respectively were measured using the circuit shown in figure 4.15. The same circuit was used to measure the bar impedance of rotor No.2. The method of measurement is

described here and the results are presented in section 5.7.

In this method the endrings had been removed by machining, the exposed bar ends were drilled and copper contact pins driven into the holes. In order that the test current should be equally distributed between the two ends of each bar two special contact straps were made which connected with the pins in each end of the bars as shown in figure 4.15. Connection of these bars to the rest of the circuit was made by appropriate cables. An AC current between 20 and 80A (in steps of 20A) was used as the excitation and for each current the potential between bars (measured at each end) was determined. Special sharp ended probes were made for this purpose and were pressed (by hand) as hard as possible against the bar ends. Taking number of current and voltage readings for each pair of bars meant that the resistance value could be determined with resonable accuracy from the slope of the plotted VI line. The same equipment , without the current distribution straps, was used to measure individual bar impedance. During the machining process to remove the end rings it was noticed that the plane of the laminations was not perpendicular to the rotor axis and that aluminium had spread between the bars in the interlamination space. Fig 5.21 shows a photograph of one end of rotor No.2, showing clearly the interbar aluminium. Four laminations were removed and all exhibited this feature, but the extent thickness were quite different in the four cases.

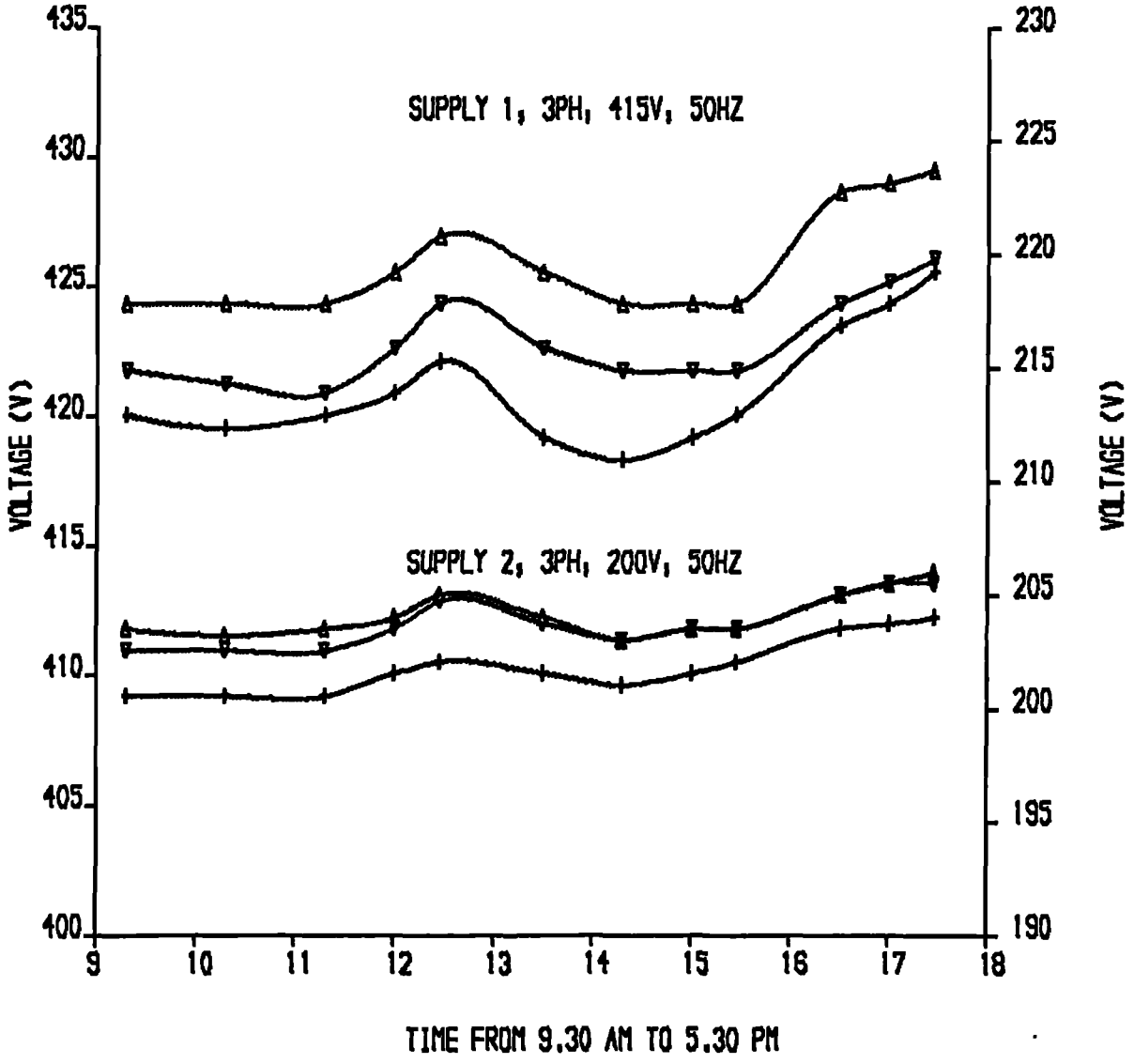

FIG. 4.1. LABORATORY MAINS VOLTAGE VARIATIONS

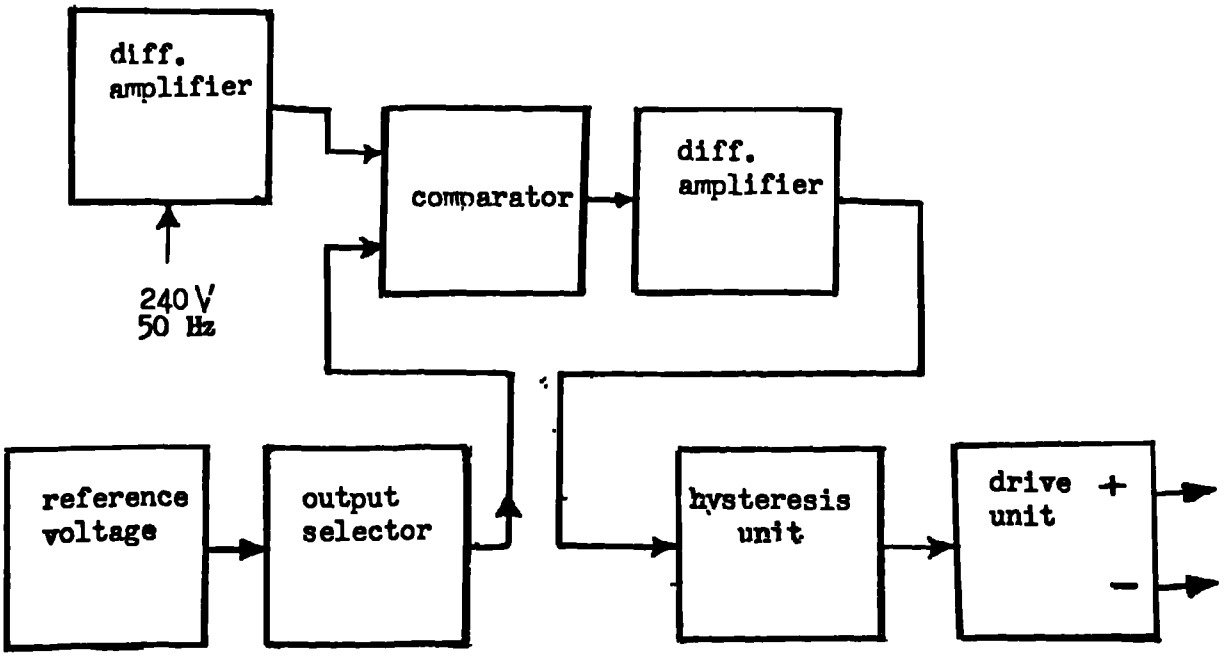

Figure 4.3 Block diagram of the voltage regulator

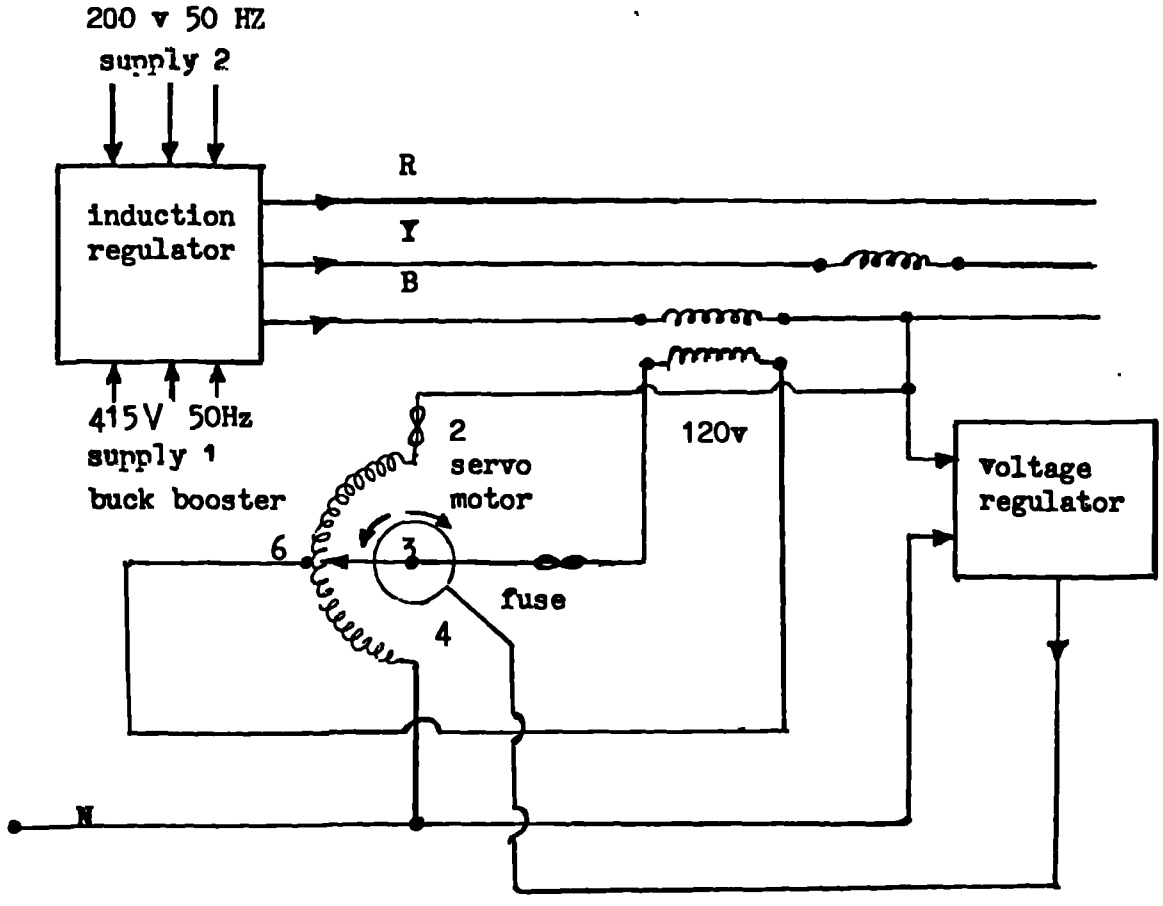

Figure 4.2 Connection diagram for the motorised buck boost system

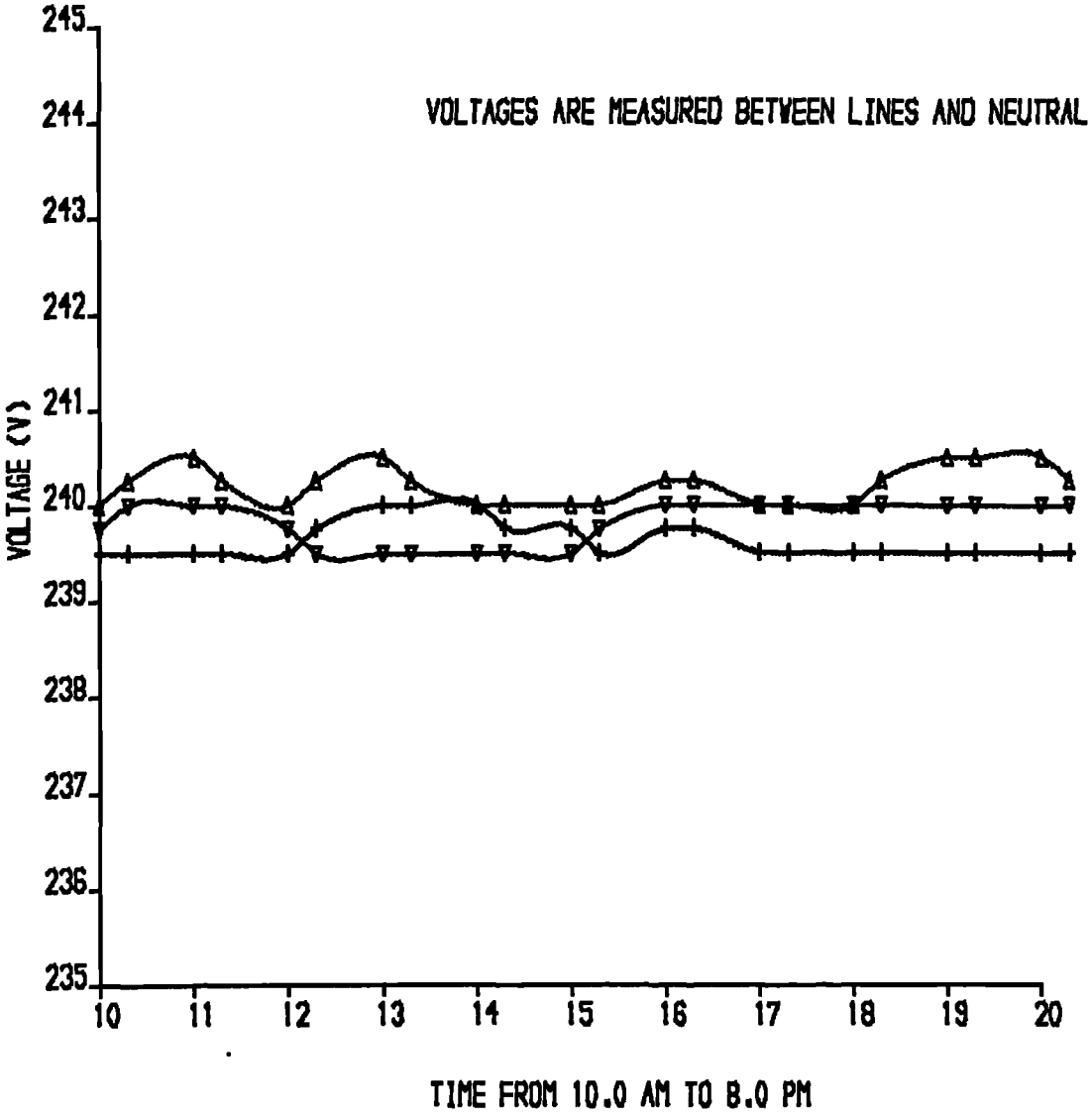

FIG. 4.4. VOLTAGE VARIATIONS AT THE TEST MOTOR TERMINALS AFTER VOLTAGE REGULATOR

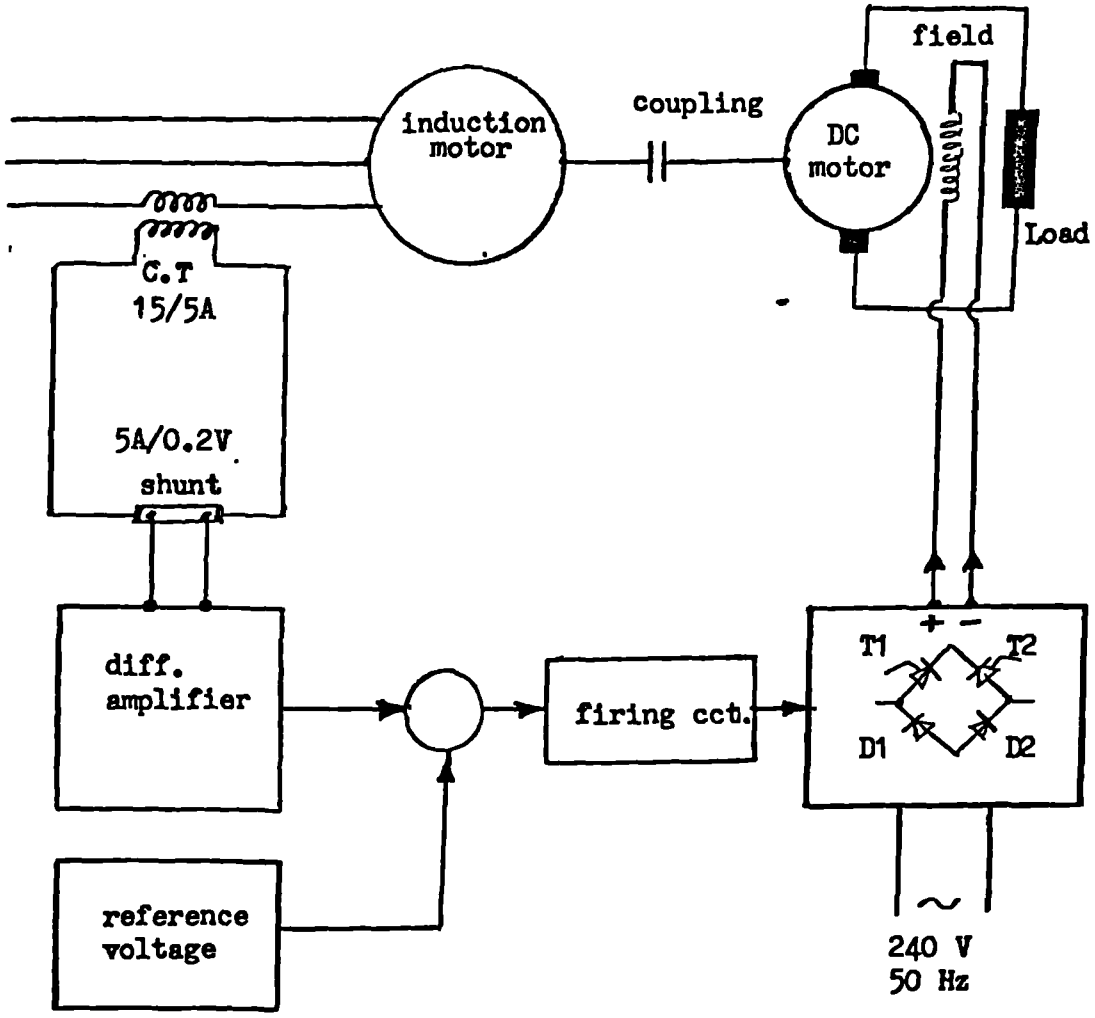

Figure 4.5 Schematic diagram of the load control unit.

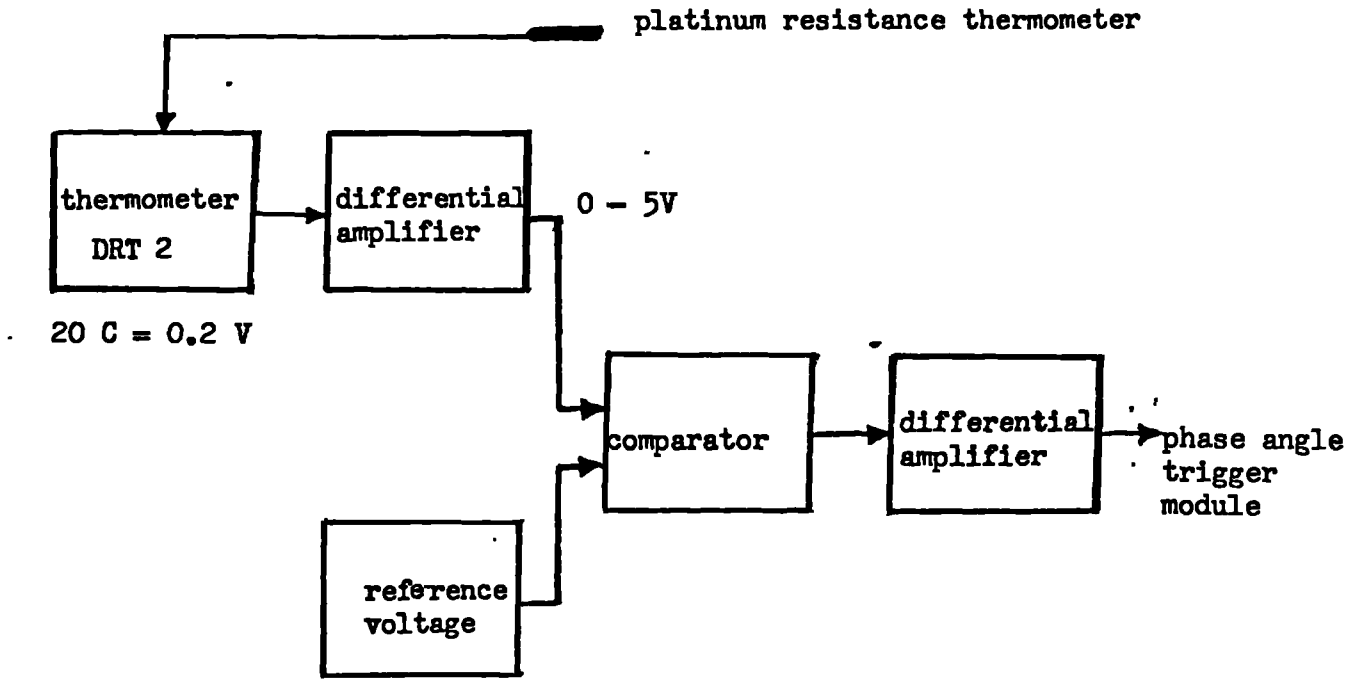

Figure 4.6 a

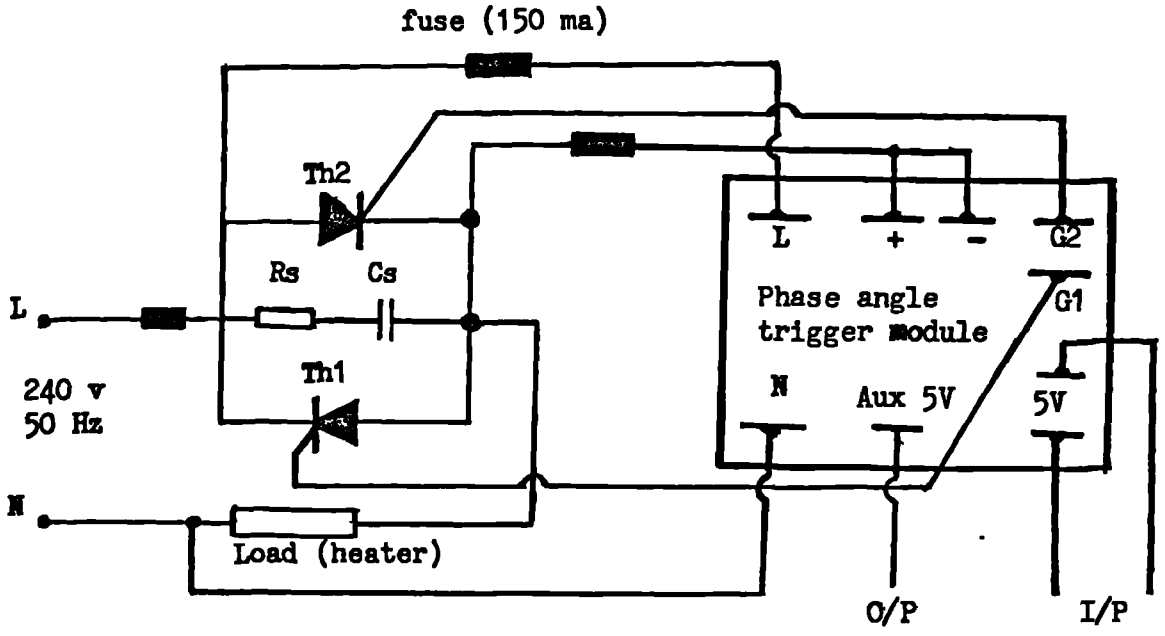

Figure 4.6 Inlet temperature control system.

(a) Block diagram of temperature monitoring unit.
(b) Circuit diagram showing the connection of phase angle trigger model, single phase thyristor control and load resistance.

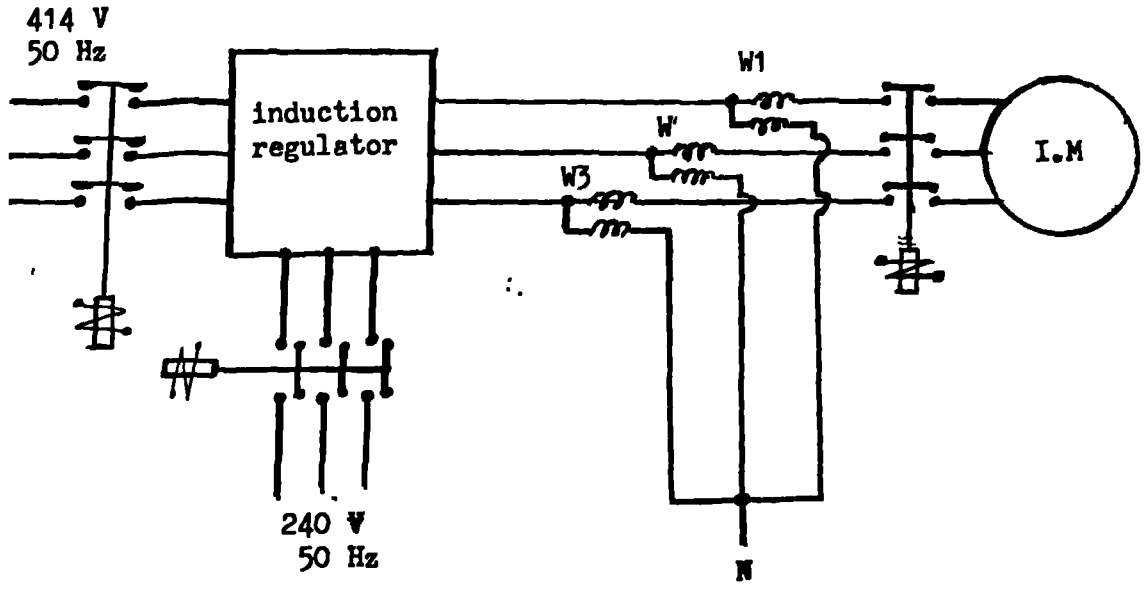

Figure 4.7 Connection diagram of the induction motor with the three watmeters and the induction regulator.

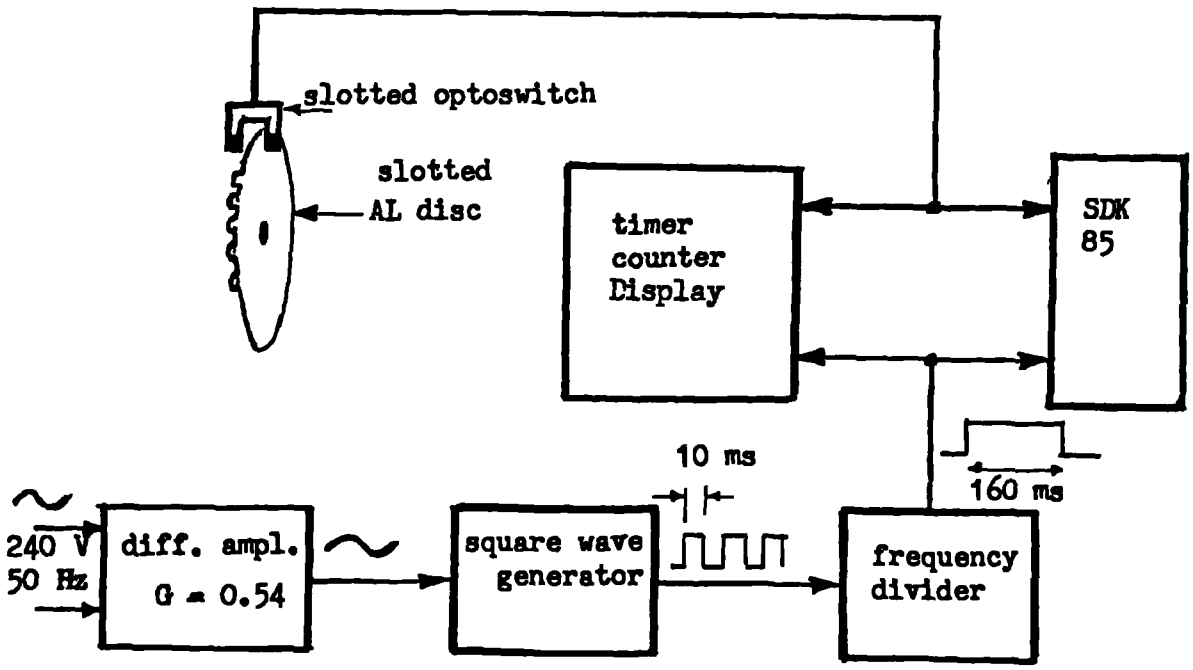

Figure 4.8 Slip measuring system

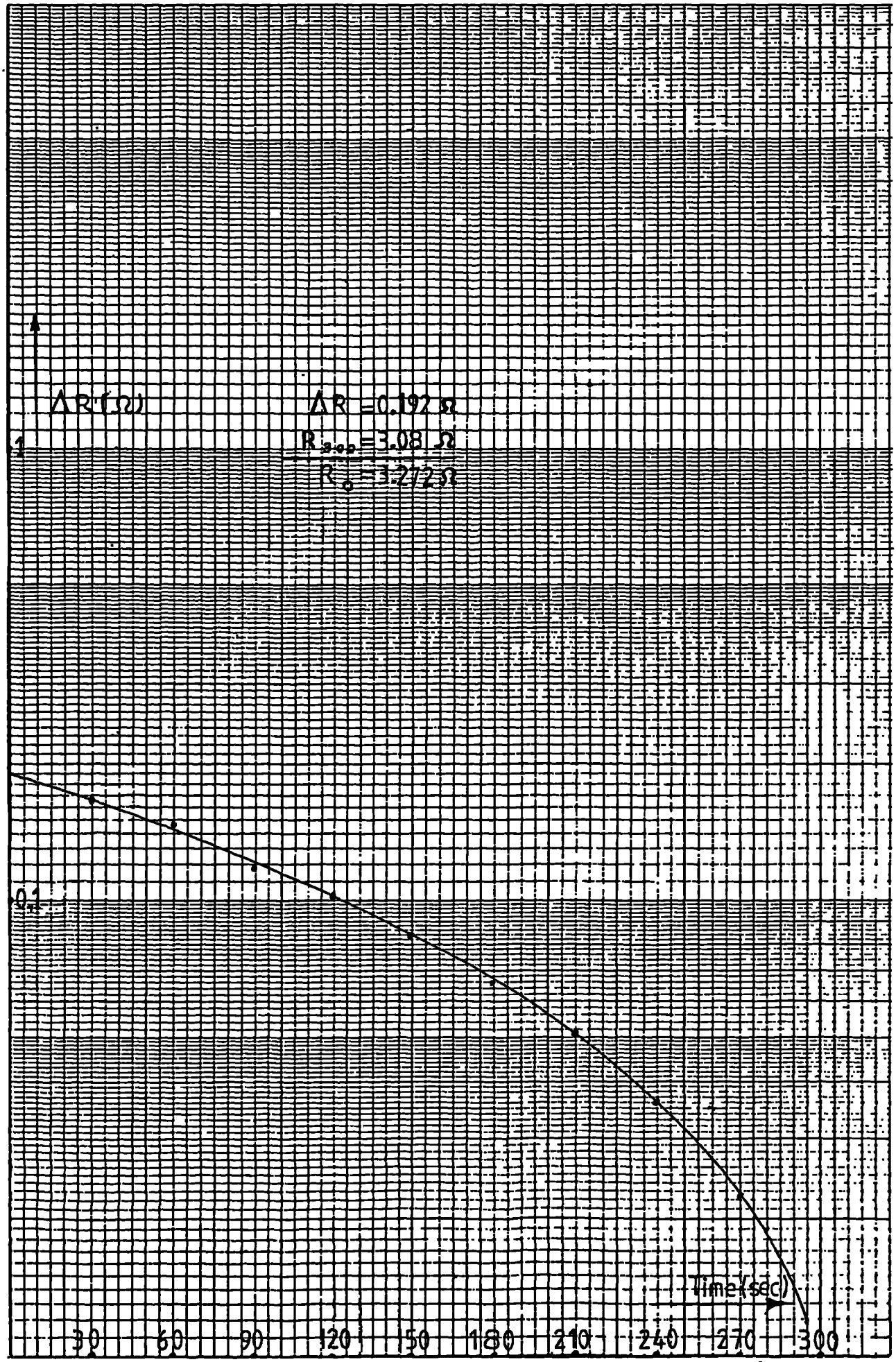

Figure 4.9 Measurement of stator winding resistance by extrapolation

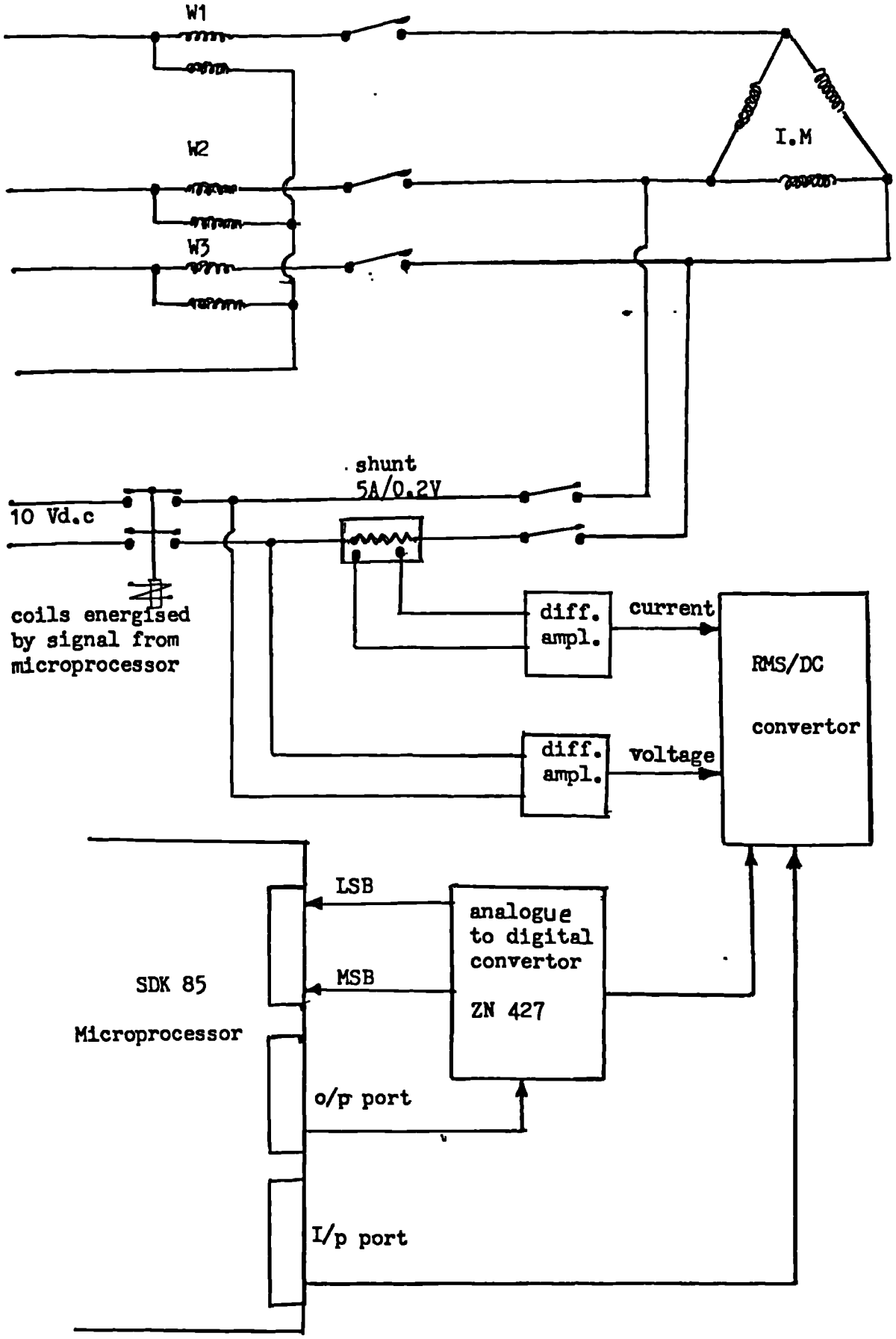

Figure 4.10 DC resistance measurement

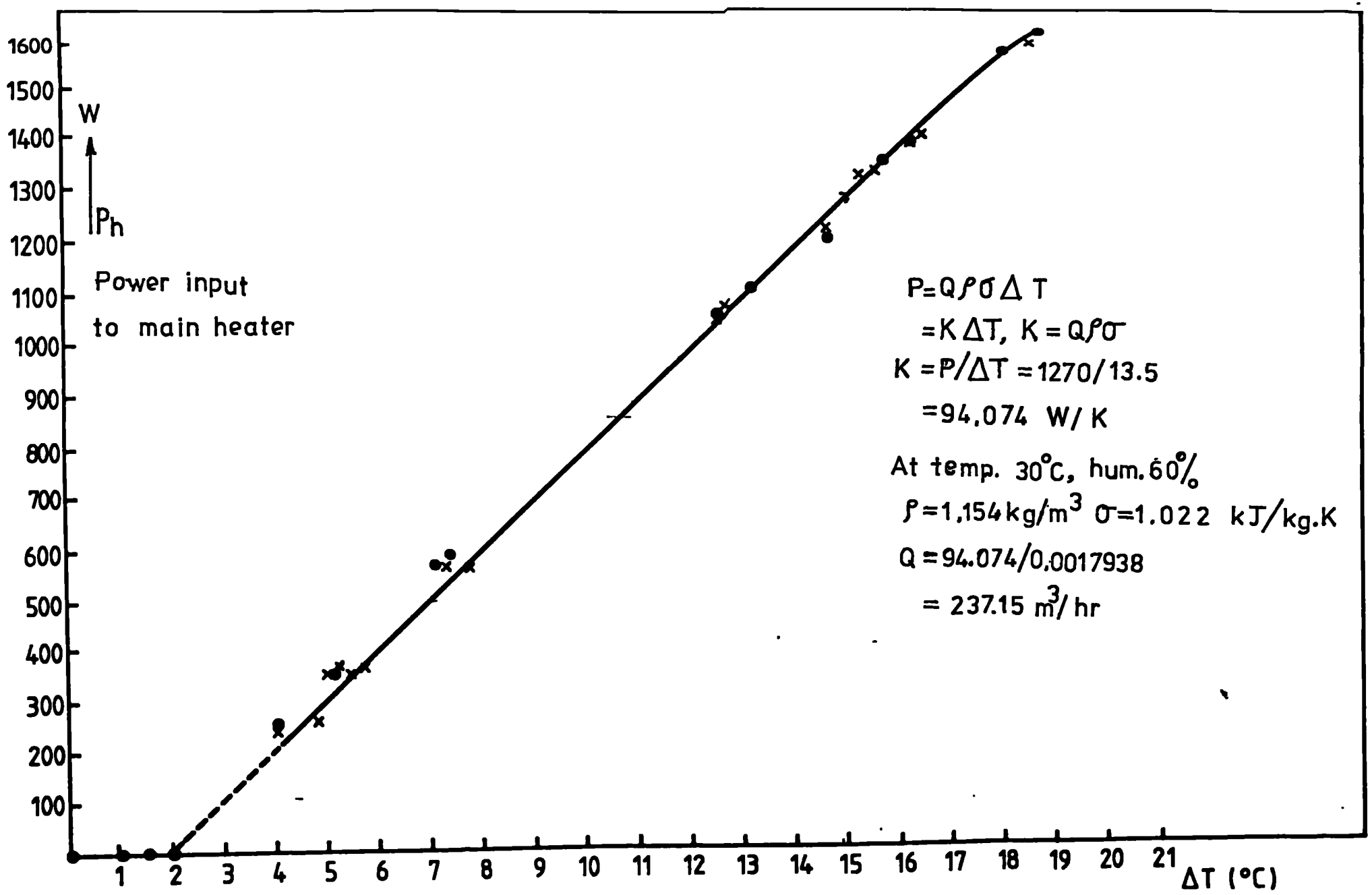

Figure 4.11 Relationship between the power input to the main heater (P_h) and teperature difference Δt

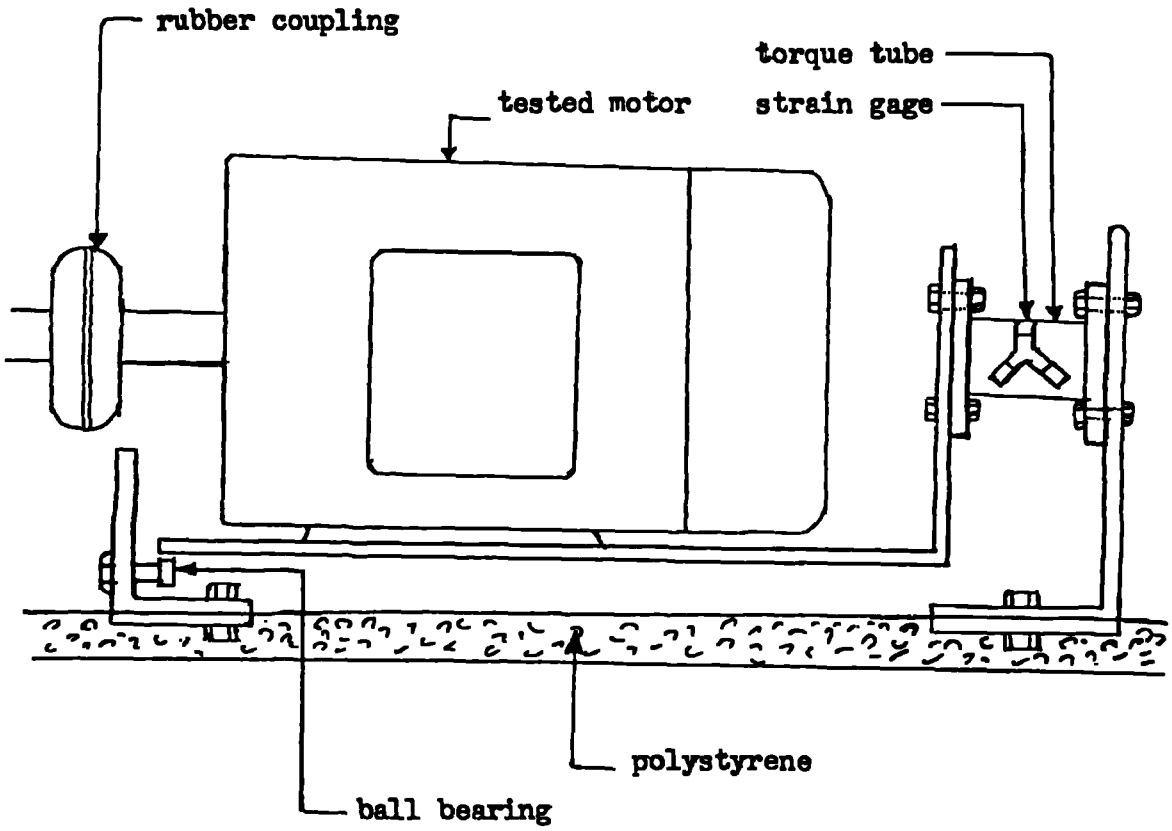

Figure 4.12 Torque measuring system

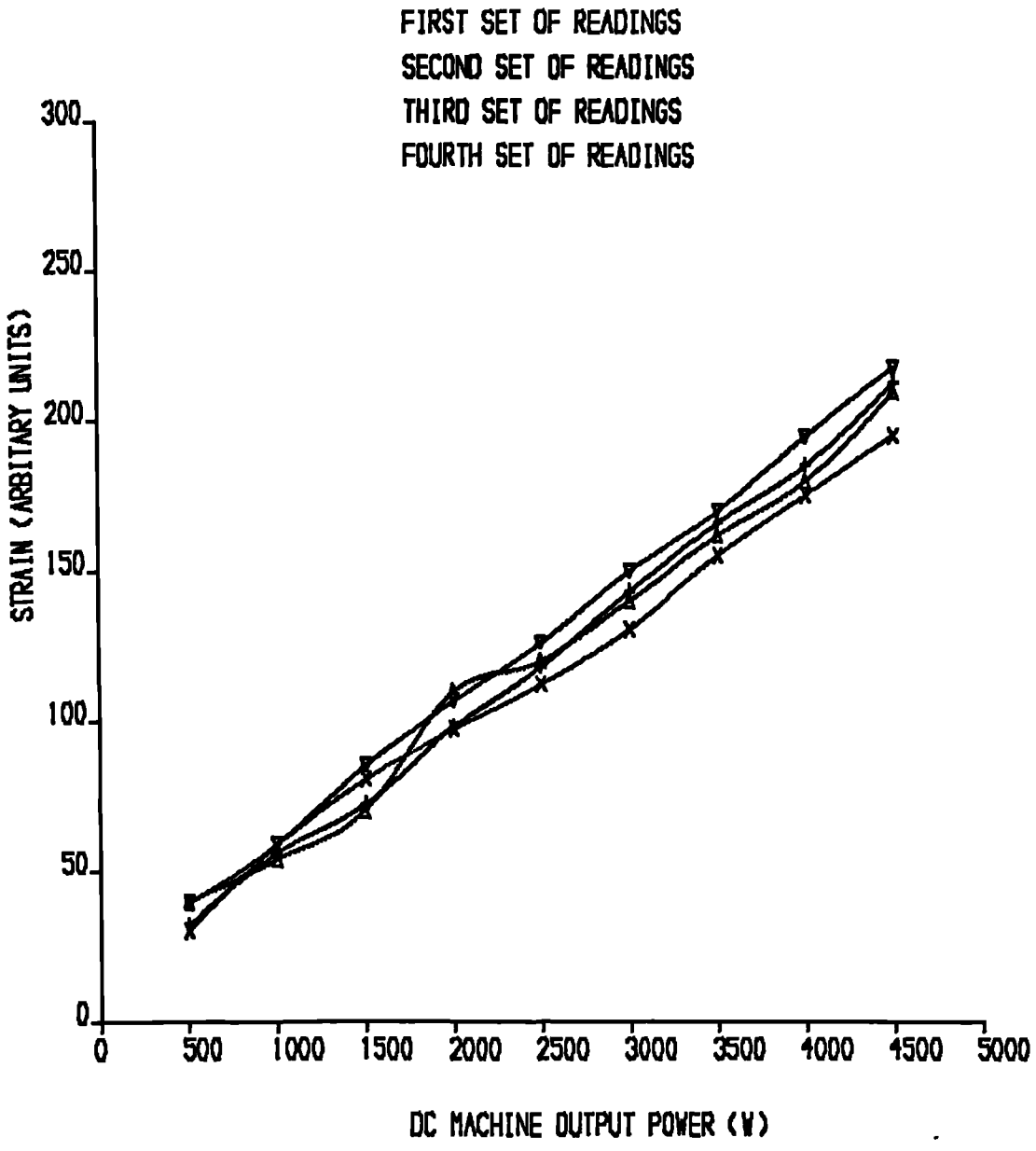

FIG. 4.13. CALIBRATION OF TORQUE MEASURING RIG

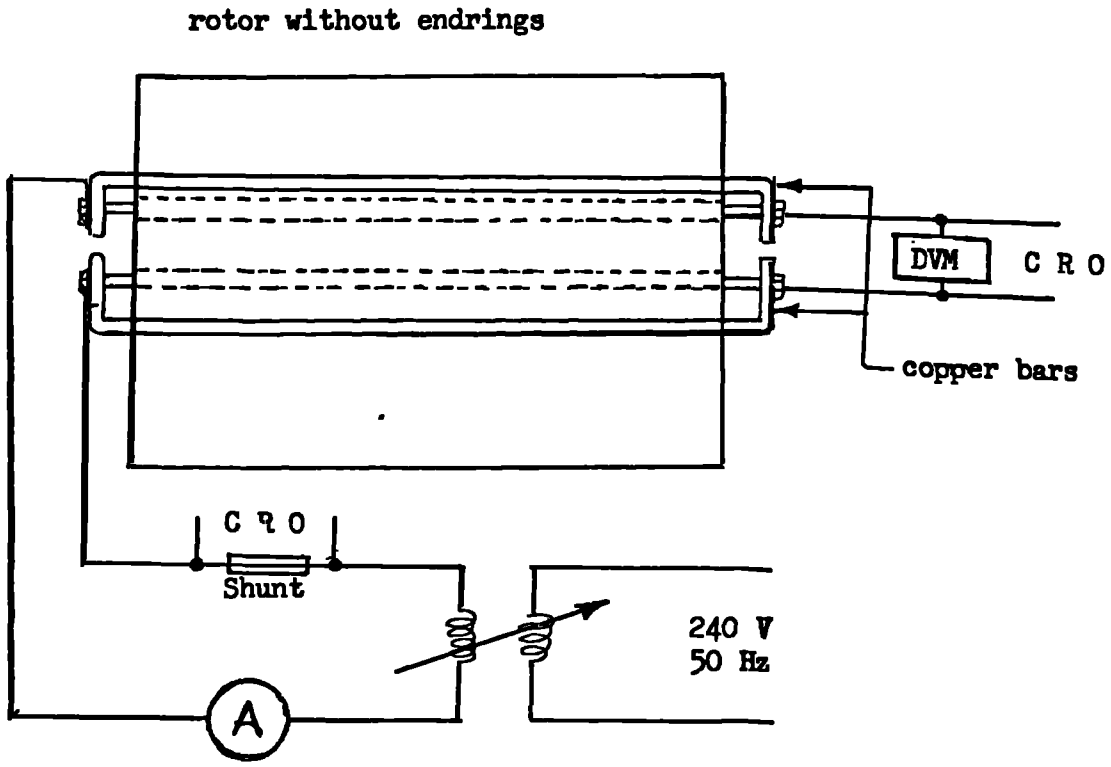

Figure 4.15 Rotor bar and interbar resistance measurement.

CHAPTER FIVE

ANALYSIS OF THE CALORIMETRIC NO LOAD AND LOAD RESULTS

5.1 CALORIMETRIC TEST PROCEDURE

A series of tests were performed to measure the total losses of a cage motor using the calorimeter to investigate the effect of a range of design parameters such as the air gap width,rotor bar skew angle and stator winding pitch, section 5.2. In the first part of the calorimetric test, called the induction motor test, section 3.2, the test machine was run at a defined voltage and load until a steady state had been achieved. The latter was considered to be achieved when no change in the outlet temperature of the calorimeter was recorded during the last hour of the test. The temperature difference between the outlet and the inlet of the calorimeter was recorded and readings of the motor power input , current, voltage and slip were taken. During the induction motor test the balance between the phases and the voltage supply were maintained constant using a closed loop system section 4.2.1 and the voltage were continuously monitored using data logging system, section 4.2.4. The desired machine load current was also controlled and maintained constant during the induction motor test using a closed loop system section 4.2.2. The data logging system was also used to monitor the load current in the three phases, the power input to the motor and the slip. Examples of logged data taken during the induction motor test are given in

appendix (A). These results show that the logged voltage values only change by one bit (the least significant bit). Measurements with Cambridge instruments confirmed that the voltage variation was ± 0.5 volts or ± 0.83% of rated voltage. It is also noted that the changes in the line current are within the ±1% of rated current. Small changes in the speed of the motor can be seen only during the first hour of the load tests, these were caused by the initial high rate of change of the machine temperature. At the end of the induction motor test, which takes four hours section 3.4, the test motor was stopped and the dc winding resistance measured using the electronic measuring and logging system section 4.3.3. Having taken all the readings the induction motor was driven externally by the dc machine with no supply for about one half hour until the outlet air temperature was just above the inlet value. This period of cooling was necessary in order to reduce the internal temperatures of the induction motor towards the value which they assumed at the end of the balance test. The balance test was then performed, during which the induction motor was disconnected from the supply and rotated by the DC machine at the same speed as during the preceding induction motor test. An alternative source of heat (main heater section 3.3) was used to provide the same temperature difference across the calorimeter as that measured at the end of the induction motor test. At the begining of the balance test the power input to the main heater was determined from a curve figure 4.11 which had been obtained from a series of a balance tests performed at different levels of power and which shows power input to the main heater against Δt. The power into the main

and the outlet temperature monitored using the closed loop system, similar to that shown in figure 4.6. As soon as the required temperature difference was obtained the closed loop system was switched off and the power into the main heater put under manual control to avoid time variation of the input power inherent in the use of the closed loop system. The power input to the main heater was recorded and it is this value which is equal to the total losses in the test machine, less the friction and windage losses , since these are provided by the driving DC machine during balance test. Constancy of the air flow rate and the room temperature are also taken into account during both parts of the test and discussed in detail in Chapter 3. The speed of the test machine during the balance test has to be maintained as it was at the first part of the calorimetric test, this is achieved by adjustment of the field voltage to the DC driving machine.

The tests carried out were no load tests at rated voltage and ±10% of the rated voltage, and load tests at rated current and ±10% of the rated current. The details of the tests and the design changes are given in the following section of this Chapter.

5.2 MACHINE PARAMETERS

The machine used in this project was a 4 pole aluminum framed,

TEFV, foot mounted cage induction motor, rated at 5.5kW, 3phase, 50Hz, frame size D132S manufactured by GEC Small Machine Limited. Two stators, a standard 415V, 50Hz single layer winding and a double layer winding, identified as S1 and S2 respectively were used and tested. S1 has a single layer concentric mesh, fully pitched winding with 45 turns per coil. S2 has a double layer lap winding with chorded coils of 48 turns per coil and a pitch of (7/9). The main objective of using the double layer chorded winding was to investigate the effect of the double layer winding on skew related losses.

5.2.1 STATOR SPECIFICATION

The two stators S1 and S2 have the following common features.

Core length	= 114.3 mm
Core output diameter	= 203.2 mm
Core bore diameter	= 127 mm
No of stator slots	= 36
Slot area	= 114.19mm^2
Type of lamination	= Newcor 1000-65,British Steel
Wire size (S1)	= 1 x 0.8 + 1 x 0.75(mm)
Wire size (S2)	= 1 x 0.8 + 1 x 0.75(mm)
No of poles	= 4
Insulation	= class F

Note : Stator core and slot dimensions are given in figure 5.1

5.2.2 CAGE ROTOR

Thirteen rotors identified as rotors No.1 to No.13 were used in this project, two of these rotors have straight rotor bars and the rest have skewed bars, The degree of skewing and the identification of the rotors are given below. Each rotor has one or more duplicates as shown.

Rotor identifications	skew	skew (SSP)
Rotors No.8 & 9	0.0 SSP	0.0
Rotors No.2 & 4 & 5	0.5 SSP	0.5
Rotors No.1 & 3 & 12 & 13	1.0 SSP	1.0
Rotors No.6 & 7	1.0 RSP	1.28
Rotors No.10 & 11	1.5 SSP	1.5

Key : SSP = Stator slot pitch RSP = Rotor slot pitch

The above rotors have the following common specification:

No of slots = 28

Rotor core length = 114.3 mm

Rotor outer diameter = 126.4 mm (nominal)

Rotor inner diameter = 83.24 mm

Types of slots = Boucherot

Rotor slot area =65.16 mm^2

No. of balance pips = 8

The dimensions of the rotor core laminations and the rotor slot are illustrated in figure 5.2.

5.3 CALORIMETRIC TESTS

All thirteen rotors were tested calorimetrically at no load and load with the single layer winding stator S1 and seven of them with the double layer winding stator S2, (section 5.6). The purpose of testing duplicate rotors was to check the variation in losses introduced by manufacturing tolerances. Six of these rotors No.8,4,12,6 and 10 having skew of 0,0.5,1,1.28,1.5 SSP. respectively were tested at three air gaps of approximately 0.24, 0.30, 0.36 mm for both no load and load conditions, of the others No. 1,2&3 were tested at two air gaps (since they had a nominal air gap of 0.3mm when received) whilst the duplicate rotors (9,5,7 and 11) were tested at ±20% of nominal air gap only. Rotor No. 13, which has the same skew as rotors Nos. 1,3 and 12, was considered as the "duplicate" for the 1 SSP rotors; towards the end of the test programme it too was tested at three air gaps to provide further information on variation between normally identical rotors.

GEC provided a number of scrap rotors which were used by the University workshop staff to familiarise themselves with turning to size. They also obtained and used the same grade of tungsten carbide tipped lathe tool and made a tailstock bearing housing to provide extra rigidity during turning. As a result of these tests it was agreed that better surface finishes (a smooth surface with no turning or chatter marks) were achieved if only one cut was taken per gap

change. The nature of the rotors and machining equipment available meant that the desired air gaps were not exactly achieved the errors being about 0.02mm, in addition the diameter of the "as delivered" rotors were not identical. Consequently the rotors were not tested at exactly the same air gaps. In order to compare losses with skew variation at a given air gap the losses at the three desired air gaps, nominal (0.3mm) and ± 20% of the nominal were determined by interpolation, figures 5.15, 5.16, 5.17.

5.4 NO LOAD TESTS

The no load tests were carried out at the rated voltage of 415V and ±10% of the rated voltage, the results obtained from all the thirteen rotors (Nos.1-13) with the single layer winding stator S1 being given in table 5.1. The total power input to the test machine was measured by three wattmeters and is designated W_o. It is the sum of stator I^2R, iron losses in the stator core and teeth, stray no load losses and the friction and the windage losses of both the test induction motor and the DC driving machine. This power less the friction and the windage losses of the two machines is the electromagnetic loss of the test machine and is referred to as W_1.It is this which is measured directly by the calorimetric test, thus the difference between W_o and W_1 for all the results is the friction and windage losses of the rotating parts. The absence of the friction and windage losses from W_1 (explained in Chapter 3) is an advantage

since they are variable with speed and time as an inspection of the results shows. Had they been included in the measured losses W_1, they would have caused complications in the analysis of the results. However one calorimetric test was performed with the dc machine uncoupled from the induction motor to determine the friction and the windage losses of the test machine. It was found to be 68W. This agrees well with the measurements made by GEC and D.Roberts [42] on a similar GEC machine (excitation test). This value may change slightly from one rotor to another because each rotor has its own set of bearings, which can have different friction losses. From the measured losses W_o and W_1 of all the tested rotors with the single layer winding stator S1, the total of the friction and windage losses of both induction motor and the dc machine have been calculated by subtracting W_1 from W_o and it was found that the total for both machines varies from 145W to 330W. In view of the low value of agreement between independent measurements it is more likely that the large variation is attributable to the dc machine which has bush bearings. However since the variation of friction and windage losses does not affect the accuracy of the calorimetric measuring method there is no need to discuss it further, except to note that the agreement between the independent measurements gives further confidence in the calorimetric measurement system. From the no load results of the tested rotors (No.1 to 13) with the single layer winding stator S1 presented in table 5.1, the sum of the iron losses plus stray no load losses has been calculated by subtracting the stator I^2R losses from W_1. This value is designated W_2 and together

with W_o, W_1, and I_o has been plotted against voltage in figures 5.3 to 5.14. The purpose of these curves is to see how these losses and the magnetising current change when the flux level of the induction motor varies by ±10% at different air gaps. All the rotors with one exception, were tested at these three voltages for each air gap. The one exception was rotor No.12 which was tested at three voltages at 0.22mm, whilst at the large air gaps of 0.30mm and 0.36mm it was only tested at 100% rated voltage. The losses at the other voltages have been estimated and marked by (*) in table 5.1. The estimation is made assuming that the slope of losses W_1 and W_2 (with voltage) are the same for the three air gaps. These estimated values will be used when comparison is made between no load losses at different skews. It has already been mentioned that the "as delivered" gaps varied and as a result of machining subsequent air gaps were not exactly the required values of 0.24, 0.30 and 0.36 mm. Figure 5.15 shows a selection of the losses of the measured gaps and it can be seen that a linear approximation to the curves is not unreasonable. The values of the losses at the desired gaps have been determined using linear interpolation and these are summarised in table 5.2 and plotted in figures 5.18,5.19 and 5.20.

Examination of figures 5.3 to 5.14 shows that the losses are non linear functions of voltage and that W_o,W_1 and I_o increase more rapidly with voltage than does W_2. In quantitive terms I_o increases by between 50% for a 10% increase in voltage whilst W_2 only increases

by between 30 to 40%. Since the difference between W_o and W_1 is the windage and the friction loss of the two machines we would expect these two curves to have a similar slope and the results confirm this. The rapid rise of I_o with voltage is an indication of the high saturation level of the machines; this rapid rise in I_o means that the stator I_o^2R losses increases extremely rapidly, hence the rapid divergence between W_1 and W_2.

The losses W_2 are dominated by iron loss and it is generally accepted that this has two components, namely eddy current and hysteresis losses. It is also generally agreed that the former is proportional to V^2 whilst for the latter the power index for its variation with voltage is variously quoted between 1.5 to 2.3 [15]. The overall variation of iron loss with voltage will depend upon the relative contributions of these two mechanisms to the total. Rather than trying to segregate them for the machines tested it is convenient to determine the way in which the losses W_2 vary with voltage, by assuming W_2 to be proportional to V^n ,

$$\text{i.e.} \quad W_2 = a V^n \qquad \text{.....(5.1)}$$

$$\text{i.e.} \quad \log W_2 = \log a + n \log V \qquad \text{.....(5.2)}$$

Equation 5.2 can be written as $y = b + nx$

Where: $y = \log W_2$, $b = \log a$, $x = \log V$

The method of least squares [43] has been used to determine the values of a and n for the W_2 values given in table 5.1. The results of this analysis are given in tables 5.3a and 5.3b

for rotor Nos.1 to 13 for the different air gaps and voltages. From the results obtained and the analysis made it can be concluded that the losses have increased significantly faster than would be suggested by a coefficient of 1.5 to 2.3 suggested by many authors [15][17][44] and the machine must be heavily saturated. The only pattern which can be seen in the a and n values is :

1- The maximum a corresponds to the minimum n and the minimum a corresponds to the maximum n.

2- As the air gap increases the skew for the minimum n (i.e. the least sensitive with voltage variation) increases from 0.5 SSP to 1.28 SSP.

The length of the air gap is another factor in determining the characteristic of the curves of W_o, W_1 and W_2 and the magnetising current I_o. Generally most of the rotors (Nos.1 - 13) tested with the single layer winding stator S1 have shown that the magnetic losses W_2 decreases with increasing air gap . The exceptions are rotor Nos 8,2 and 13. In case of rotor No.8 which has straight bars the losses W_2 were increased by the change to a gap of 0.36mm. Careful inspection of the rotor revealed that some of the slot bridges were reduced to a very thin layer of metal, such that the corresponding slots had almost broken through to the surface. It was thought that this could indicate an eccentric rotor cage and be the cause of extra losses due to increased permeance variations.

In case of rotor No.2 as the air gap increased from 0.3mm to 0.36mm the losses W_2 at rated voltage and 95% of the rated voltage decreased by small values, which were less than the measurement sensitivity. Although the losses at 110% of the rated voltage decreased by 29W, the small change at the other two voltages indicates that there must be other factors to be considered. Inspection of this rotor showed that the rotor surface was much smoother than the surface of the other rotors. In fact this rotor is the only one for which grinding was tried to obtain the right desired diameter and the air gap of 0.36mm. This grinding could have caused extra surface losses at this air gap.

In case of rotor No.13 which is skewed by one stator slot pitch, as the air gap increases from 0.30mm to 0.36mm the losses W_2 increased by 12W. This value is larger than the measurement sensitivity and must therefore be considered a genuine result, but no cause was evident. It was noted during inspection of this rotor that it was slightly tapered by 0.18mm at its 0.36mm gap diameter.

Skew angle	Rotor ID No.	Air Gap (mm)	Total losses (W_1) (W)			$W_2 = W_1 - 3I_o^2 R_1$ (W)		
			90%rv	100%rv	110%rv	90%rv	100%rv	110%rv
Zero	8	0.23	240	350	560	206	283	392
		0.30	240	340	550	198	255	347
		0.36	260	380	620	204	278	386
	9	0.23	250	850	560	217	286	391
0.5 SSP	2	0.30	215	320	565	172	237	361
		0.36	220	350	570	165	235	330
	4	0.22	280	390	610	248	327	441
		0.29	260	360	580	219	280	380
		0.37	240	345	580	181	239	332
	5	0.22	280	400	610	248	337	443
1.0 SSP	1	0.29	235	360	585	189	270	363
		0.32	235	320	545	188	230	292
	3	0.30	260	380	560	217	303	368
		0.34	230	330	530	180	240	315
	12	0.22	260	350	560	230	290	395
		0.30	260*	350	560*	212*	267	364*
		0.36	270*	360	575*	206*	260	354*
	13	0.22		360			297	
		0.30		360			278	
		0.36		390			290	
1.0 RSP	6	0.22	260	370	580	228	306	418
		0.30	240	340	560	195	253	353
		0.40	250	350	560	186	233	305
	7	0.22	255	370	585	223	308	416
1.5 SSP	10	0.23	250	360	580	216	294	410
		0.30	250	350	570	205	270	370
		0.36	240	350	570	186	250	340
	11	0.23	260	360	590	226	293	412

SSP = Stator slot pitch RSP = Rotor slot pitch

Table (5.1) No load test results with single layer stator S1.

Skew Angle	Rotor ID No.	Air Gap mm	Total losses (W_1) Watts			$W_2 = W_1 - 3I_o^2R_1$ Watts		
			90%rv	100%rv	110%rv	90%rv	100%rv	110%rv
0.0	8	0.24	240	350	548	204	280	384
		0.30	240	340	550	198	255	347
		0.36	260	380	620	204	278	386
0.5 SSP	4	0.24	273	382	602	240	315	404
		0.30	255	358	580	212	274	372
		0.36	242	348	580	186	245	238
1.0 SSP	12	0.24	260	350	560	224	285	388
		0.30	260*	350	560*	212*	267	364*
		0.36	270*	360	575*	206*	260	354*
1.0 RSP	6	0.24	254	362	574	214	292	400
		0.30	240	340	560	195	253	353
		0.36	240	345	560	190	238	324
1.5 SSP	10	0.24	250	360	580	214	292	404
		0.30	250	350	570	205	270	370
		0.36	240	350	570	186	250	340

SSP = Stator slot pitch . RSP = Rotor slot pitch
* See text.

Table (5.2) No load test results obtained by interpolation

Skew	Air Gap (mm)								
	0.22	0.23	0.29	0.30	0.32	0.34	0.36	0.37	0.40
0.0		3.201 2.927		2.788			3.172		
0.5	2.862 2.889		2.737	3.68			3.451	3.015	
1.0			3.252	2.666	2.188	2.786			
1.28	3.105 3.105			2.947				2.458	
1.5		3.187 2.98		2.935			3.00		

Table 5.3a Values of the index n with air gap and skew

Skew Angle	Air Gap (mm)								
	0.22	0.23	0.29	0.30	0.32	0.34	0.36	0.37	0.40
0.0		1.19 6.34		13.1			1.4		
0.5 SSP	10.65 9.14		19.57	0.006			3.13 0.21		
1.0 SSP			0.81	30.55	43.75	12.23			
1.28 SSP	3.96 2.29			5.02				8.75	
1.5 SSP		1.35 4.75		5.71					

Table 5.3b Values of variable a with air gap and skew

Loooking at the losses W_2 for one stator slot pitch skew produced by identical rotors Nos 1,3,12 and 13 at different air gaps, it can be seen that they vary by up to 30W from one rotor to another at the same air gap (table 5.1). Although rotors 12 and 13 at the air gaps of 0.22mm and 0.30mm have very similar results, their losses change in a different way as the air gap increases to 0.36mm.

Rotor No.1 (at the air gap of 0.29mm) has lower losses than that of rotor No.3 at the air gap of 0.30mm, and the same is repeated as their air gaps increase to 0.32mm and 0.34mm respectively, except at 90% rated voltage at which the loss of rotor No.1 is 8W higher than that of rotor No.3. At the air gap of 0.30mm, the losses W_2 of

rotor No.3 are higher than the losses of rotors Nos.12 and 13, but as the air gap of rotor No.3 increases to 0.34mm the losses are reduced from 303W to 240W, while the losses of rotor No.12 and No.13 not reduced as much for the same air gap increase and they vary in a different way.

These differences between the values of losses W_2 produced by identical rotors are thought to be due to manufacturing tolerances and imperfections which may affect the stray losses produced by these rotors. Although not suggested as the sole and direct cause of these differences it is worth noting that when the end rings were machined off rotors Nos.2&8 and the end laminations removed, aluminium flash had leaked during rotor diecast between the laminations from the slot sections, figure 5.21. However inspection of duplicate results for the rotors with skews of 0,0.5,1.28,1.5 SSP shows that at the "as delivered" air gaps of 0.24mm, they are remarkably similar. The differences between rotors are shown in the table below.

Rotor pairs	Rated voltage			Skew SSP	Air gap mm
	95%rv	100%rv	110%rv		
8 & 9	+10	0	0	0	0.23
4 & 5	0	+10	0	0.5	0.22
12 & 13		+10		1.0	0.22
6 & 7	-5	0	+5	1.28	0.22
10 & 11	+10	0	+10	1.5	0.23

Table 5.4 The difference between the losses of the duplicate rotors(values stated in the table are in watts)

Since it is estimated that the measurement accuracy is ± 9.4W the difference can be said to be negligible, which is itself a comment on the manufacturing repeatability that can be achieved.

As the air gap increases the no load current I_o, which is almost the magnetising current, increases as one would expect and thus it follows that the stator I^2R losses will also increase. The magnetic losses W_2, obtained by subtracting the I^2R losses from W_1, however decrease with air gap with one exception, rotor No.8 about which comment has already been made (near opening of rotor slot bridge of 0.36mm air gap). Although each rotor produces a different change in loss with air gap there is a clear overall trend in the change as the voltage increases. Table 5.5 below shows the range of W_2 values at the two extreme gap values and it can be seen that there is a much larger change with gap at the higher voltage.

Air gap mm	Rated voltage		
	90%	100%	110%
0.24 down to 0.36	248/200 down to 205/181	327/283 down to 260/239	441/392 down to 355/332
change	-43/-19	-67/-44	-86/-60

Table (5.5) Range of variations in magnetic losse W_2 with gap

It is well known that part of the no load losses are stray losses which are produced by permeance variations of the main flux.

These losses are dependent on slotting, air gap configuration and the number of the slots [20]. Many of these loss are caused by high frequency eddy currents, they will vary with the square of the voltage. At small air gaps were the ratio of slot opening to air gap width is high the flux pulsation is also high and consequently the high frequency losses will be high[20]. While at large air gaps where the slot/air gap ratio is smaller the flux pulsation ratio is also smaller, hence the high frequency losses due to permeance variation will be reduced. The divergence between the curves of losses W_2 with voltage at different air gaps figures 5.8 to 5.14 agree with the argument.

The magnetic losses,W_2, for the three air gaps have been plotted against skew for the three test voltages in figures 5.18, 5.19, 5.20. Inspection of these curves shows that the maximum values of W_1 and W_2 occur at 0.5 SSP for the small air gap of 0.24mm, and that ignoring rotor No.8 (zero skew, 0.36mm gap) results the differences between the largest and the smallest values of W_2 are all less than 36W. Details of these differences are given in table 5.6. In view of the relatively small spread of values of W_2 it is difficult to discern significant pattern in the variation of W_2 with skew, indeed anticipating the conclusions slightly it is difficult to imagine that there is any major mechanism which could cause a change in losses with skew since the fundamental rotor current is almost zero on no load. It is therfore concluded that the experimental

results provide no evidence of a meaningful variation with skew of magnetic loss for no load condition.

voltage	W_2 (max)		W_2 (min)		W_2 (W)	Air gap
	(W)	Skew	(W)	Skew	(max)-(min)	mm
90%rv	240	0.5	204	zero	36	
100%rv	315	0.5	280	zero	35	0.24
110%rv	404	0.5	384	zero	20	
90%rv	212	0.5	195	1.28	17	
100%rv	274	0.5	253	1.28	21	0.30
110%rv	372	0.5	347	zero	25	
90%rv	205	1.0	186	0.5	19	
100%rv	260	1.0	238	1.28	22	0.36
110%rv	355	1.0	324	1.28	31	

Table 5.6 Variation of magnetic loss W_2 with skew

5.5 LOAD TESTS

The results obtained from testing the thirteen rotors Nos.1-13 with the single layer winding stator S1, at rated current and ±10% of the rated current are summarised in table 5.7. The total losses measured calorimetrically are refered to as W_1^- and this includes the stator and the rotor copper losses, the iron losses and the stray load losses. Subtraction of the stator copper losses from W_1^- yields W_2^- and these are plotted against current at different air gaps, figures 5.22 - 5.33. These curves show that the losses W_1^- and W_2^- increase with current and that generally the variation with current is almost linear, but the average slope of the W_1^- lines is higher than that of the W_2^- lines. This naturally follows since the difference between them is proportional to I^2 . It is also evident that the general effect of increasing the air gap is to reduce the losses, but rotor No.8 shows only a small change particularly between gaps of 0.30 and 0.36mm. It will be recalled that mention has already been made of the fact that the bridges across some rotor slots were reduced to very thin proportions after machining to the largest air gap.

Skew angle	Rot ID. No.	Air gap mm	Total losses W_1^-			Elec.mag.losses W_2^-		
			90%rc	100%rc	110%rc	90%rc	100%rc	110%rc
Zero	8	.23	1070	1330	1580	700	842	977
		.30	1000	1230	1480	615	730	878
		.36	950	1220	1480	590	735	873
	9	.23	1050	1320	1600	682	833	990
0.5 SSP	2	.30	965	1210	1510	580	730	918
		.36	915	1180	1440	540	690	840
	4	.22	1100	1390	1700	744	907	1093
		.29	1030	1220	1512	644	760	917
		.37	898	1150	1380	537	663	773
	5	.22	1100	1370	1650	744	893	1052
1.0 SSP	1	.29	1000	1300	1550	620	830	975
		.32	940	1195	1445	565	720	850
	3	.30	1015	1280	1620	632	804	1033
		.34	940	1145	1390	550	657	793
	12	.22	1100	1390	1750	750	915	1175
		.30	* 997	1260	*1586	* 638	778	*1000
		.36	* 950	1200	*1511	* 588	718	* 922
	13	.22		1400			919	
		.30		1260			775	
		.36		1280			778	
1.0 RSP	6	.22	1070	1340	1670	712	862	1050
		.30	930	1205	1446	585	728	856
		.40	880	1130	1360	504	650	775
	7	.22	1070	1340	1630	700	855	1020
1.5 SSP	10	.23	1100	1350	1640	720	862	1025
		.30	990	1240	1520	625	755	900
		.36	880	1130	1400	518	650	820
	11	.23	1125	1370	1650	758	885	1042

* see text

Tabl 5.7 Load tst results with stator S1

In table 5.7 some of the test results for rotor No.12 are marked by (*), which means that these values were estimated. At the smallest air gap of 0.22mm (as received) rotor No.12 was tested at three currents, while at the other two air gaps Of 0.30mm and 0.36mm it was tested at rated current only. The unmeasured values of losses at +10% of rated current have been estimated assuming that the losses at the air gaps of 0.30mm and 0.36mm vary with current in the same way as at the air gap of 0.22mm. Rotor No.13 which is a duplicate of rotors Nos.1, 3 and 12 was also tested at the three air gaps and at rated current only. Since the purpose of testing this rotor was only to check the variation of losses due to manufacturing tolerance, no estimation is made to find out the losses at $\mp$10% r.c. Comparing the losses of rotors Nos.9,5,13,7 and 11 with their "duplicates" at the smallest air gap "as received" and at the same load, yields the differences between them, as shown in table (5.8).

Rotor ID No.	Losses W_2^-			Skew SSP	Air gap mm
	90%rc	100%rc	110%rc		
8 & 9	+18	+9	-23	0.0 SSP	0.23
4 & 5	0	+14	+41	0.5 SSP	0.22
12 & 13	NA	-4	NA	1.0 SSP	0.22
6 & 7	+12	+7	+30	1.0 RSP	0.22
10 & 11	-38	-23	-17	1.5 SSP	0.23

SSP = Stator slot pitch RSP = Rotor slot pitch

rc = Rated current = 11.2 A NA = Not available

Table 5.8 Difference between the total losses of duplicate rotors

Table 5.8 shows that, in some cases the difference between the losses are larger than the accuracy of the measuring system. This is thought to be due to the differences in the rotor bar and interbar impedances of the tested rotors and other manufacturing imperfections, as observed in section 5.7.

The difference between the losses (W_2^-) of other identical rotors such as: rotors Nos.1 and 3 (which are skewed by one stator slot pitch) and their partners Nos.12 and 13, shown in table 5.7 can also be attributed to the same reason of manufacturing imperfections between rotors. From the results of the 13 rotors obtained with S1, table 5.7, the losses of the rotors Nos.8,4,12,6 and 10 having skews of 0,0.5,1,1.28 and 1.5 SSPs respectively were determined at the required air gaps of 0.24mm, 0.30mm, and 0.36mm by applying simple interpolation .

Exaample: If given W_1^- or W_2^- at 0.22mm and 0.29mm air gaps and required to find W_1^- or W_2^- at 0.24mm, then :

$$W_2^-(0.24\text{mm}) = W_2^-(0.22) - \left(\frac{W_2^-(0.22) - W_2^-(0.29)}{0.29 - 0.22}\right)(0.24 - 0.22)$$

By so doing the losses W_1^- and W_2^- for all the five rotors Nos.8,4,12,6 and 10 were determined, tabulated, tables 5.12a, 5.12b and plotted against skew, figures 5.34,5.35,5.36. Fig 5.35 shows the losses W_1^- and W_2^- against skew at 100% of the rated current and at three air gaps. Since the results are plotted against stator current

the stator I^2R at each current will be nearly the same for all the rotors (with small variations due to the stator temperature difference) and hence interest needs to be focussed on the W_2^- values. It can be seen from figure 5.35 that the losses W_2^- have the same pattern at the air gaps of 0.24mm and 0.30mm. The losses W_2^- tend to increase as the skew changes from zero to 0.5 SSP and then to one stator slot pitch and reach their maximum at one stator slot pitch. Subsequently the losses reduce, then increase at 1.5 SSP. This pattern is repeated at 90% and 110% of the rated current, figures 5.34, 5.36, with the range of the variation being more pronounced at 110% of the rated current. At the air gaps of 0.36mm some peculiar results were obtained.

It can be seen that at the zero skew (results obtained from rotor No.8) the losses did not decrease when the air gap was increased to 0.36mm, the losses staying nearly the same as at 0.30mm for rated current and at 110% Of the rated current. However at 90% of the rated current the losses have decreased by small amount. This could be due to the rotor slot opening which was described in the previous section. It is suggested that the result be treated with some scepticism, unfortunately time did not allow rotor No.9 to be machined to 0.30mm and 0.36mm air gaps and tested. It can also be seen that at the skew of 1.5 SSP (the results obtained from rotor No.10) the losses for 90% and 100% rated current at the air gaps of 0.36mm do not increase in the same way that 0.24mm and 0.30mm gap

results do, although the 110% current results follow the trends of the other two gaps results. Careful examination of the rotor revealed no unusual features (such as that noted for rotor No.8) and hence no simple explanation can be offered for 90% and 100% current results. From all the results obtained, particularly the graphs of losses at three air gaps and the three currents two interesting points can be observed. The first is that the maximum losses occur at the skew of one stator slot pitch and the minimum losses at one rotor slot pitch. Since the losses W_2^- include three main components of losses (iron losses, rotor I^2R losses and stray load losses) and each component has its own relationship with current and skew it is useful to segregate the losses into three components and study each one individually. It is recognised that the segregation of W_2^- into iron losses, rotor I^2R losses and stray load losses has restricted accuracy since it involves assumptions such as the constancy of iron losses from the no load to load condition, and this has to be born in mind when looking at the results achieved by the segregation. The latter is achieved numerically in the standard way using the total electrical input power, the stator current resistance, the slip and the calorimeter results W_2 and W_2^- for the no load and the load conditions. The results of the segregation at the three currents are given in tables 5.9,5.10 and 5.11. The iron losses are assumed to be the magnetic losses W_2 measured by the no load calorimeter test and since that has already been discussed in detail in (section 5.4) will not be considered here.

The second component of the load losses, the rotor I^2R loss has been calculated in each case by multiplying the power input to rotor (P_r) by slip (s), i.e

$$W_r = s\,(P_r) = s\,(P_i - I^2R - W_2)$$

Where : P_i = Power input to the induction motor

W_2 = Iron losses measured at no load

s = Slip

I = Stator load current

R = Stator winding resistance

P_r = Power input to the rotor

It can be seen from tables 5.9,5.10,5.11 that the rotor I^2R losses decrease with air gap increasing.

The third component of the losses is called stray load losses (section 2.4) which is designated W_s and calculated by subtracting the sum of the other two components from W_2^-. The stray load losses of all the thirteen rotors tested with the single layer winding stator (S1) calculated in this way are given in tables (5.9, 5.10, 5.11) It can be seen that they vary with air gap, load and with skew. W_s and W_r for five rotors No.8,4,12,6 and 10 having skews of 0, 0.5, 1, 1.28 and 1.5 SSP's respectively have been determined at the three air gaps (0.24, 0.30, 0.36mm) and the three current values were calculated in a similar way as that used to determine the values of W_2^-. The losses W_s together with W_2, W_2^- and W_r are summarised in

table 5.12b, W_s & W_r are plotted against skew as shown in figures 5.37 - 5.42.

Inspection of the curves of W_s with skew ,figures 5.37, 5.38 and 5.39 shows that at the air gaps of 0.24mm and 0.30mm the shape of the curves are similar at the three currents. The losses W_s tend to increase with skew and reach a maximum at one stator slot pitch. Subsequently the losses W_s decrease at one rotor slot pitch and increase again at 1.5 SSP. As the air gap increases to 0.36mm the shape of the W_s curves changes particularly for the zero and at 1.5 SSP skew. At 0.36mm air gap the losses W_s of the zero skew rotor at 90% r.c are 6W higher than those of the 0.5 SSP skew rotor, this difference increases with current and reachs 44W at 110% r.c. This increase at zero skew, derived from measurements on rotor No.8, is thought to be due to rotor slot opening which was discussed earlier in this section and in section 5.4 for the no load results.

It is not known why the two results at 0.36mm gap at 90% and 100%r.c do not follow the trend of the results at this gap. Generally the shape of the curves of W_s with skew figures 5.37 - 5.39 are shown to be similar to those of W_2^- with skew, this means that with the limit of the segregation method the variation of the losses W_2^- with skew and air gap are to a large extent dominated by the variation of the W_s. In order to determine the way in which the losses W_s vary with current at different air gaps and skew, it is

assumed that W_s is proportional to I , i.e

$$W_s = a (I^n) \quad \text{..... 5.3}$$

$$\log W_s = \log a + n \log I \quad \text{.....5.4}$$

The same method of least squares [43]which was used at no load for analysing the losses in terms of voltage, has been used here to determine values of a and n for the values of W_s given in table 5.12b. The results of the analysis are given in table 5.14 for rotors Nos. 8,4,12,6 and 10. From the results obtained it can be concluded that stray load losses W_s vary significantly with current. There is no correlation between values of a and n with skew and air gap, but n is maximum where a is minimum and vice versa. Figures 5.40 - 5.42 show the variation of rotor I^2R losses with skew at three air gaps and three currents. It can be seen that although the curves of W_r are not similar in shape to that of W_2^- & W_s there is one striking feature that they all reach a maximum at one stator slot pitch, although W_r at 90% r.c at the air gaps of 0.24mm and 0.30mm has high losses similar to that of 1 SSP at zero skew. In order to get an overall view of the relative magnitudes of W_s and W_r relative to the calorimetrically measured losses W_2^- table 5.13 has been produced by averaging the losses for all rotors at each of the three air gap values. The values of W_s & W_r are also given as percentage fraction of W_2^-. It can be seen that the percentage ratio of W_s relative to W_2^- increases with current and decreases with air gap. whilst the percentage ratio of W_r relative to W^-_2 increases with both current and air gap.

Skew	Rot. ID	Air Gap (mm)	P_i (W)	I^2R (W)	W_2 (W)	P_r (W)	s	W_r (W)	W_2^- (W)	W_s (W)	P_o (W)
		.23	6080	370	283	5427	.0364	197	700	220	4940
Zero	8	.30	5960	385	255	5330	.0333	177	615	183	4890
		.36	5660	360	278	5022	.0312	157	590	155	4640
	9	.23	6040	368	286	5386	.0343	185	682	211	4920
	2	.30	5895	385	237	5274	.0343	181	580	162	4860
0.5		.36	5750	375	235	5140	.0333	171	540	134	4765
SSP		.22	5965	356	327	5282	.0354	187	744	230	4795
	4	.29	5810	386	275	5149	.0328	169	644	200	4710
		.37	5580	361	239	4980	.0312	156	537	142	4612
	5	.22	5980	356	337	5287	.0354	187	744	220	4810
	1	.29	5835	380	270	5180	.0333	172	620	178	4765
		.32	5805	375	230	5200	.0323	168	565	167	4795
		.30	5920	383	303	5334	.0343	183	632	146	4835
1.0	3	.34	5890	390	240	5260	.0333	175	550	135	4880
SSP		.22	6893	350	290	6253	.0355	202	730	238	5743
	12	.30		359	267			173	638	198	
		.36		362	260			170	588	258	
		.22			297						
	13	.30			278						
		.36			290						
		.22	5860	358	306	5196	.0364	190	712	216	4720
1.0	6	.37	5720	345	253	5122	.0333	170	585	162	4720
RSP		.40	5620	376	233	5011	.0323	162	504	109	4670
	7	.22	5910	370	308	5232	.0364	191	700	201	4770
		.23	5900	380	294	5226	.0364	190	720	236	4730
1.5	10	.30	5760	365	270	5125	.0333	170	625	185	4700
		.36	5560	362	250	4948	.0312	155	518	113	4610
SSP											
	11	.23	5920	367	293	5260	.0364	192	758	273	4725

Table(5.9) Test results and segregated losses at 90% r.c

Skew	Rot. ID	Air Gap (mm)	P_i (W)	I^2R (W)	W_2 (W)	P_r (W)	s	W_r (W)	W_2 (W)	W_s (W)	P_o (W)
		.23	6920	488	283	6149	.0437	269	842	290	5520
Zero	8	.30	6770	500	255	6015	.0411	247	730	228	5470
		.36	6740	485	278	5980	.0406	243	735	214	5450
	9	.23	6940	488	286	6166	.0427	263	832	283	5550
	2	.30	6750	480	237	6033	.0427	258	730	235	5470
0.5		.36	6700	490	235	5975	.0416	249	690	206	5450
SSP		.22	6950	483	327	6140	.0438	269	907	311	5490
	4	.29	6760	460	275	6025	.0411	248	760	237	5470
		.37	6710	487	239	5948	.0406	241	663	183	5490
	5	.22	6870	477	337	6056	.0437	265	893	291	5430
	1	.29	6750	470	270	6010	.0427	257	830	303	5380
		.32	6670	475	230	5965	.0416	248	720	242	5405
		.30	6650	470	303	5871	.0411	242	804	260	5306
1.0	3	.34	6640	488	240	5912	.0406	240	657	177	5425
SSP		.22	6900	475	290	6135	.0468	287	915	338	5440
	12	.30	6760	482	267	6011	.0448	269	778	242	5430
		.36	6650	482	260	5908	.0448	265	718	193	5380
		.22	6890	481	297	6112	.0458	280	919	342	5420
	13	.30	6780	485	278	6017	.0458	276	775	221	5450
		.36	6700	502	290	5908	.0448	265	778	223	5350
		.22	6750	478	306	5966	.0458	273	862	283	5340
1.0	6	.37	6690	477	253	5960	.0427	254	728	221	5415
RSP		.40	6500	480	233	5787	.0406	235	650	182	5300
	7	.22	6780	485	308	5987I	.0458	274	855	273	5370
		.23	6760	488	294	5978	.0458	274	862	294	5340
1.5	10	.30	6690	485	270	5935	.0437	260	755	225	5380
		.36	6480	480	250	5750	.0406	234	650	166	5280
SSP	11	.23	6720	485	293	5942	.0458	277	885	320	5280

Table (5.10) Test resultsand segregated losses at 100% r.c

Skew	Rot. ID	Air Gap (mm)	P_i (W)	I^2R (W)	W_2 (W)	P_r (W)	s	W_r (W)	W_2^- (W)	W_s (W)	P_o (W)
		.23	7695	603	283	6808	.0510	347	977	347	6045
Zero	8	.30	7665	602	255	6803	.0510	347	878	276	6015
		.36	7500	607	278	6615	.0500	331	873	264	5950
	9	.23	7675	610	286	6779	.0510	346	990	358	6005
	2	.30	7552	592	237	6723	.0352	350	918	331	5972
0.5		.36	7488	600	235	6653	.0510	340	840	265	5978
SSP		.22	7600	608	327	6665	.0531	355	1092	410	5830
	4	.29	7500	595	275	6630	.0495	328	917	309	5918
		.37	7500	607	239	6654	.0489	326	773	208	6050
	5	.22	7625	598	337	6690	.0531	355	1052	360	5905
	1	.29	7500	575	270	6655	.0510	340	975	365	5880
		.32	7480	595	230	6655	.0500	333	850	287	5965
		.30	7525	587	303	6635	.0510	339	1033	391	5835
1.0	3	.34	7390	597	240	6553	.0500	328	793	225	5930
SSP		.22	7870	575	290	7005	.0640	451	1175	434	6050
	12	.30		585	267			422	1000	311	
		.36		555	260			415	922	247	
		.22			297						
	13	.30			278						
		.36			290						
		.22	7575	620	306	6649	.0562	374	1050	370	5835
1.0	6	.37	7425	590	253	6582	.0520	343	856	260	5909
RSP		.40	7300	585	233	6482	.0500	324	775	218	5870
	7	.22	7425	610	308	6512	.0541	353	1020	359	5725
		.23	7475	615	294	6566	.0550	362	1025	369	5765
1.5	10	.30	7375	620	270	6485	.0510	330	900	300	5785
		.36	7200	580	250	6370	.0500	318	820	252	5730
SSP	11	.23	7425	608	293	6524	.0541	353	1042	396	5705

Table (5.11) Test results and segregated losses at 110% r.c

Where:

$P_r = (P_i - I^2R - W_2)$, $W_r = s\,(P_r)$, $W_s = W_2 - W_2 - Wr$

$P_o = P_i - W_2 - I^2R - 70$ Assuming F&W (In.motor 70W)

P_i = Power input to the induction motor

W_2 = Iron losses (measured calorimetrically at no load)

W_2^- = Total losses - F&W losses (at load)

W_r = Rotor I^2R losses, s = Slip

I^2R = Stator winding copper loses, W_s = Stray load losses

Skew	Rot ID	Air Gap	(W_2) 100%	90% r.c $W1^-$	100% r.c $W1^-$	110% r.c $W1^-$
Zero	8	.24	280	1060	1320	1565
		.30	255	1000	1230	1480
		.36	278	950	1220	1480
0.5 SSP	4	.24	315	1070	1342	1632
		.30	274	1020	1210	1495
		.36	245	914	1150	1390
1.0 SSP	12	.24	285	1065	1350	1690
		.30	267	1020	1220	1535
		.36	260	950	1150	1450
1.0 RSP	6	.24	292	1060	1300	1605
		.30	253	930	1180	1446
		.36	238	900	1150	1380
1.5 SSP	10	.24	292	1085	1342	1625
		.30	270	990	1240	1520
		.36	250	880	1130	1400

Table 5.12a Load losses $W1^-$ calculated by interpolation at threee air gaps

Skew	Rot ID	Air Gap (mm)	(W_2) 100%	90% r.c $\bar{W}_2$	W_r	W_s	100%r.c $\bar{W}_2$	W_r	W_s	110% r.c $\bar{W}_2$	W_r	W_s
Zero	8	.24	280	688	195	215	826	266	281	963	347	337
		.30	255	615	177	183	730	247	228	878	347	276
		.36	278	590	157	155	735	243	214	873	331	264
0.5 SSP	4	.24	315	715	182	222	865	263	290	1043	347	381
		.30	274	631	168	193	746	247	230	900	328	296
		.36	245	550	158	149	677	242	190	791	327	220
1.0 SSP	12	.24	285	722	195	228	881	282	314	1132	443	404
		.30	267	638	173	198	778	269	242	1000	422	311
		.36	260	588	170	158	718	265	193	922	415	247
1.0 RSP	6	.24	292	680	185	202	828	268	267	1001	366	342
		.30	253	585	170	162	728	254	221	856	343	260
		.36	238	536	165	130	681	243	184	807	332	235
1.5 SSP	10	.24	292	705	187	229	847	272	284	1007	367	359
		.30	270	625	170	185	755	260	225	900	330	300
		.36	250	518	155	113	650	234	166	820	318	252

Table (5.12b) Segregated losses at three airgaps determined from the results presented in tables (5.9,5.10,5.11)

Air Gap	(W2) 100%	90% r.c $\bar{W}_2$	W_r	W_s	100% r.c $\bar{W}_2$	W_r	W_s	110% r.c $\bar{W}_2$	W_r	W_s
.24	293	702	189	219	849	270	287	1029	374	365
.30	264	619	172	184	747	255	229	907	354	289
.36	254	556	161	141	692	245	189	843	344	244
.24			26.9%	31.2%		31.8%	33.8%		36.3%	35.5%
.30			27.8%	29.7%		34.1%	30.6%		39.0%	31.8%
.36			28.9%	25.3%		35.4%	27.3%		40.8%	28.9%

Table(5.13) Average of losses from table 5.12b

Skew in SSP	G = 0.24mm		G = 0.30mm		G = 0.36mm	
	a	n	a	n	a	n
Zero	1.213	2.245	1.613	2.048	0.336	2.661
0.5	0.442	2.689	1.407	2.123	1.672	1.948
1.0	0.314	2.854	1.096	2.244	0.923	2.221
1.28	0.470	2.624	0.695	2.367	0.142	2.956
1.5	1.295	2.237	0.710	2.396	0.011	3.991

Table (5.14) Values of the constants (a) and (n) at different skew and air gaps.

5.6 DOUBLE LAYER WINDING STATOR

The effect of varying the stator mmf pattern upon the various losses was investigated by testing a limited number of rotors in the double layer winding stator,(S2), the details of this stator were given in (section 5.2.1). Seven rotors Nos.4,5,6,7,10,11 and 12 were used and each rotor was tested calorimetrically at no load and at load and at one air gap only, that being the largest 0.36mm since GEC did not make the stator S2 available until near the end of the work. The no load tests were conducted at rated voltage and the load tests at rated current. The results obtained for the seven rotors with stator S2, together with their corresponding results with stator S1, are summarised in table 5.15 and 5.16. The double layer winding stator S2 used in this project has a 7/9 pitch which is known to produce lower stator mmf space harmonics. The object of this set of

tests was to see whether the change in mmf pattern resulted in a reduction in the losses.

Table 5.15 shows that at no load the magnetising current with the single layer stator is higher than that of the double layer winding and consequently the I^2R losses produced by S1 are larger in all cases. It was expected that the magnetic losses W_2 produced by the single layer winding stator would be greater than those produced by the double layer winding stator S2. However in contrast S2 has produced higher losses with all the seven rotors. Similarly on load the losses $\bar{W}_2$, as defined earlier in this chapter are seen to be larger with the double layer winding stator S2. These unexpected results obtained for the double layer winding might be attributed to the differences between the two stator cores . Although the dimension of the two are exactly the same it is possible that the double layer stator core has higher losses than the single layer stator core due to manufacturing imperfections. Previous works in this field undertaken by GEC has shown that a variation of up about 90W in iron losses can be expected from identical stator cores of this size. Details of the dimensions of the stator core and the type of laminations used were given in (section 5.2.1).

Rotor ID No.	Air gap	Skew SSP	Single layer w'dg				Double layer w'dg				
			I_o	R_1	$I_o^2R_1$	W_2	I_o	R_2	$I_o^2R_2$	W_2	ΔW_2
4	.37	0.5	5.70	3.26	106	239	5.15	3.48	92	278	39
5	.22	0.5	4.46	3.16	63	337	3.98	3.59	57	363	26
12	.36	1.0	5.57	3.22	100	260	5.00	3.58	90	320	60
6	.40	1.28	5.95	3.29	117	233	5.33	3.58	102	298	65
7	.22	1.28	4.40	3.18	62	308	3.99	3.51	56	324	16
10	.36	1.5	5.57	3.22	100	250	5.04	3.54	90	310	60
11	.23	1.5	4.57	3.20	67	293	4.14	3.53	60	320	27

Table (5.15) Comparison between performances of S1 and S2. under no load condition.

Rotor ID No.	Air gap	Skew SSP	Single layer w'dg				Double layer w'dg				
			I	R_1	I^2R_1	W_2^-	I	R_2	I^2R_2	W_2^-	ΔW_2^-
4	.37	0.5	11.4	3.74	488	663	11.28	4.16	530	690	27
5	.22	0.5	11.3	3.75	477	893	11.33	4.42	567	983	90
12	.30	1.0	11.3	3.78	482	718	11.25	4.22	534	756	38
6	.40	1.28	11.3	3.74	480	650	11.28	4.17	530	690	40
7	.22	1.28	11.2	3.83	485	855	11.38	4.32	560	920	65
10	.36	1.5	11.3	3.73	477	635	11.38	4.20	544	726	73
11	.23	1.5	11.3	3.80	485	885	11.27	4.25	540	900	15

Table (5.16) Comparison between performances of S1 and S2. under load condition.

Where: I = load current W_2^- = load losses - F&W losses

R_1 = Stator winding resistance of the single layer stator S1

R_2 = Stator winding resistance of the double layer stator S2

5.7 MEASUREMENT OF THE BAR AND INTERBAR IMPEDANCES

The interbar and bar impedance of rotors Nos.2 and 8 were measured using the circuit shown in figure 4.15. The circuit used is similar to the circuit used in the previous works, [30][46], with some changes in connections, and the method of measurement is basically the same,(section 4.3.10).

Odock [30] made his measurements at different frequencies and found that as the frequency is changed the phase angle between bar end and bar end voltage and current did not change and hence the bar to bar impedance was entirely resistive. While others [32]found that the phase angle between voltage and current normally changed with frequency by five to ten degrees over a range of 500Hz and concluded that the bar and cross path impedance have resistance and reactive components and both components change with frequency. The contact resistance between bar and core are heavily dependent on the rotor manufacturing process, material, construction and category of the cage rotor, and could change from one rotor to another even of the same design. During the operation the contact resistance may vary with the rotor speed and centrifugal force and with the rotor temperature and the clearance between the rotor bars and the core is not the same as at standstill,. In this project the measurement of interbar and bar impedance are made at 50Hz only. Unfortunately the time did not allow to do more tests at different frequencies. The

results obtained from the measurement of the bar and interbar impedance are plotted in figures 5.43, 5.44 and 5.45. The last two figures show the relation between the measured voltage and current of adjacent bars of rotors Nos.2 and 8. It can be seen that the relationship are always linear. The values of the rotor interbar impedance can be determined from the slope of the lines. For rotor No.2 six sets of readings are plotted whilst for rotor No. 8 eight sets of readings are plotted showing the minimum and the maximum values of the interbar impedance of each rotor. From fig 5.44 it can be noticed that rotor No.2 which is skewed by 0.5 SSP.the values of the interbar impedance change from 0.463 mΩ to 0.833 mΩ, while for rotor No.8 fig 5.45 the interbar impedance vary from 0.1175 mΩ to 0.7375 mΩ , the ratio is more than 6:1. This means that the insulation between some of the rotor bars of rotor No.8 are much less than those of rotor No.2.

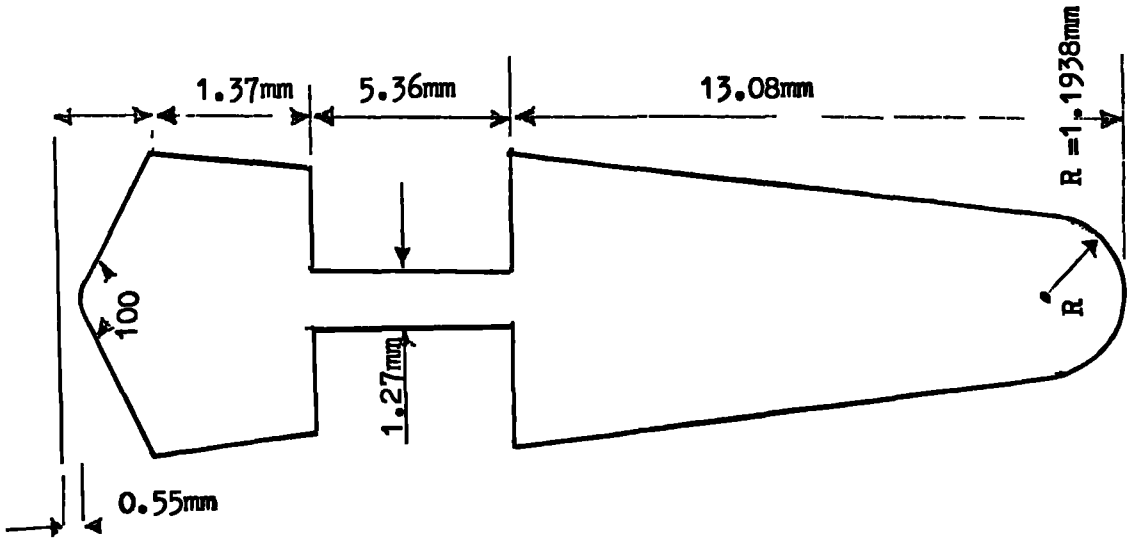

Fig 5.2 Rotor slot

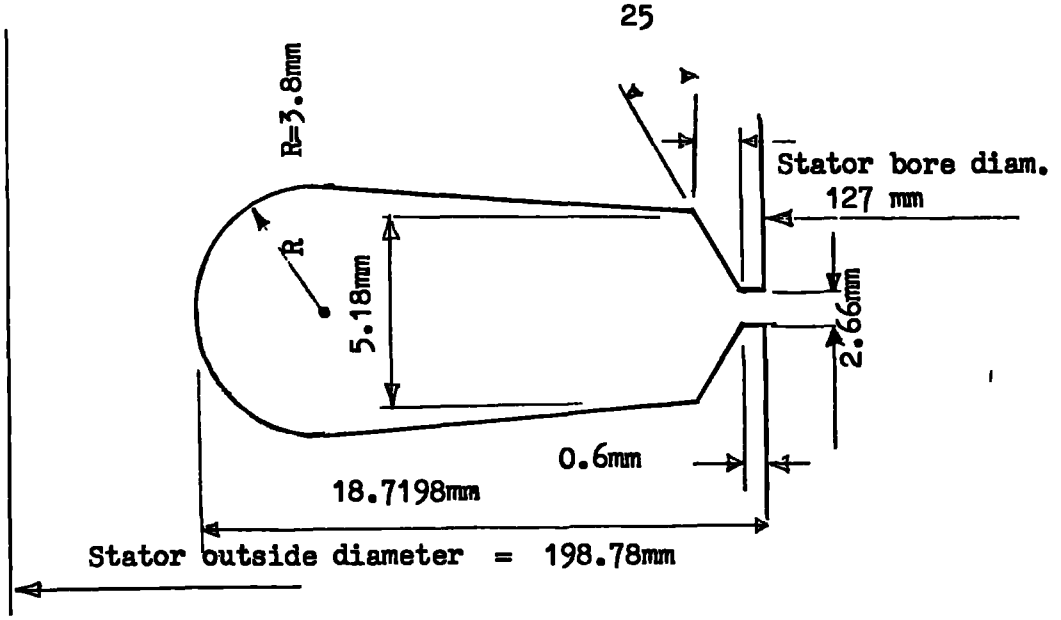

Fig 5.1 Stator slot

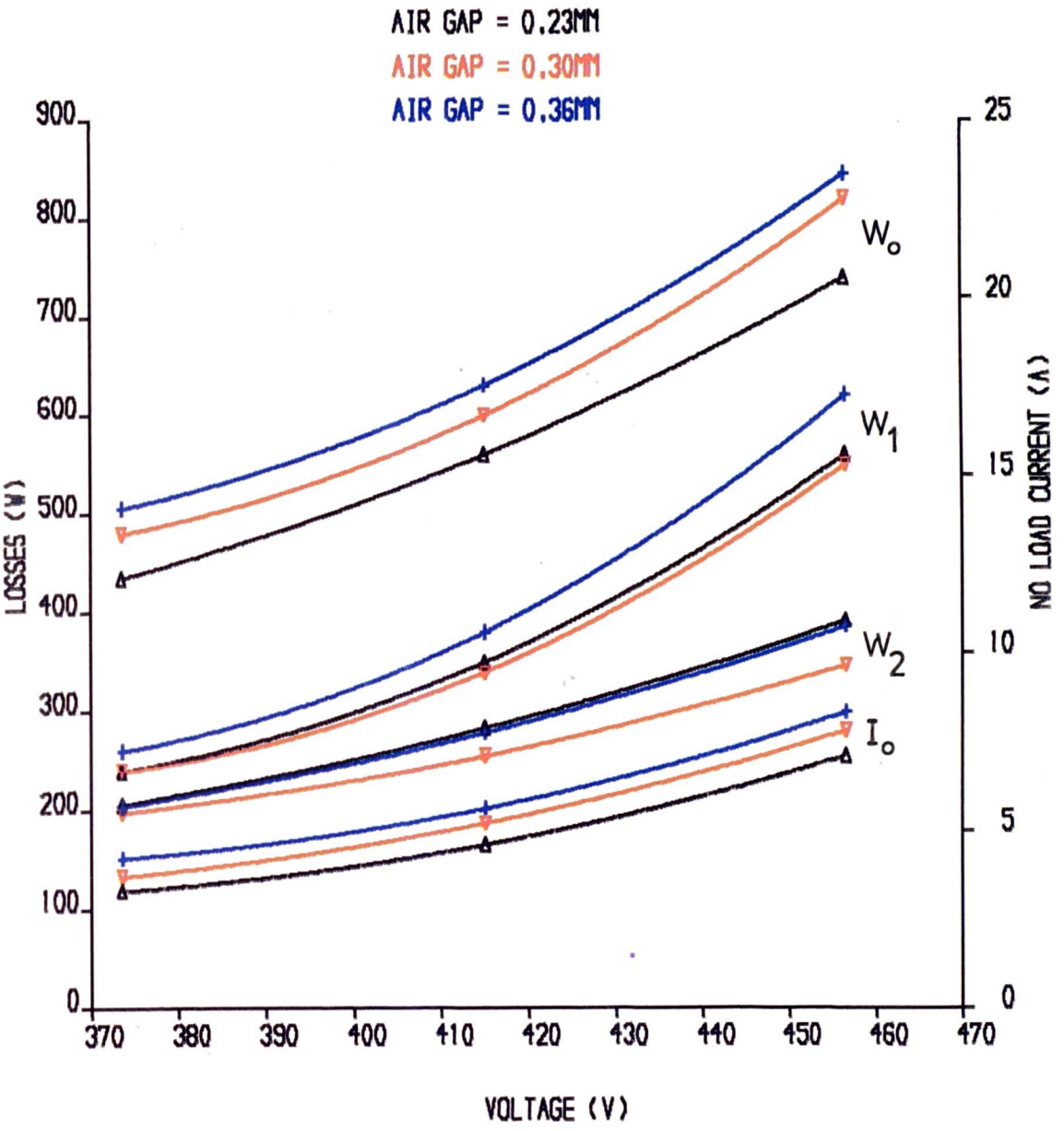

FIG. 5.3 .NO LOAD LOSSES. ROTOR NO.8. SKEW=0.0 SSP

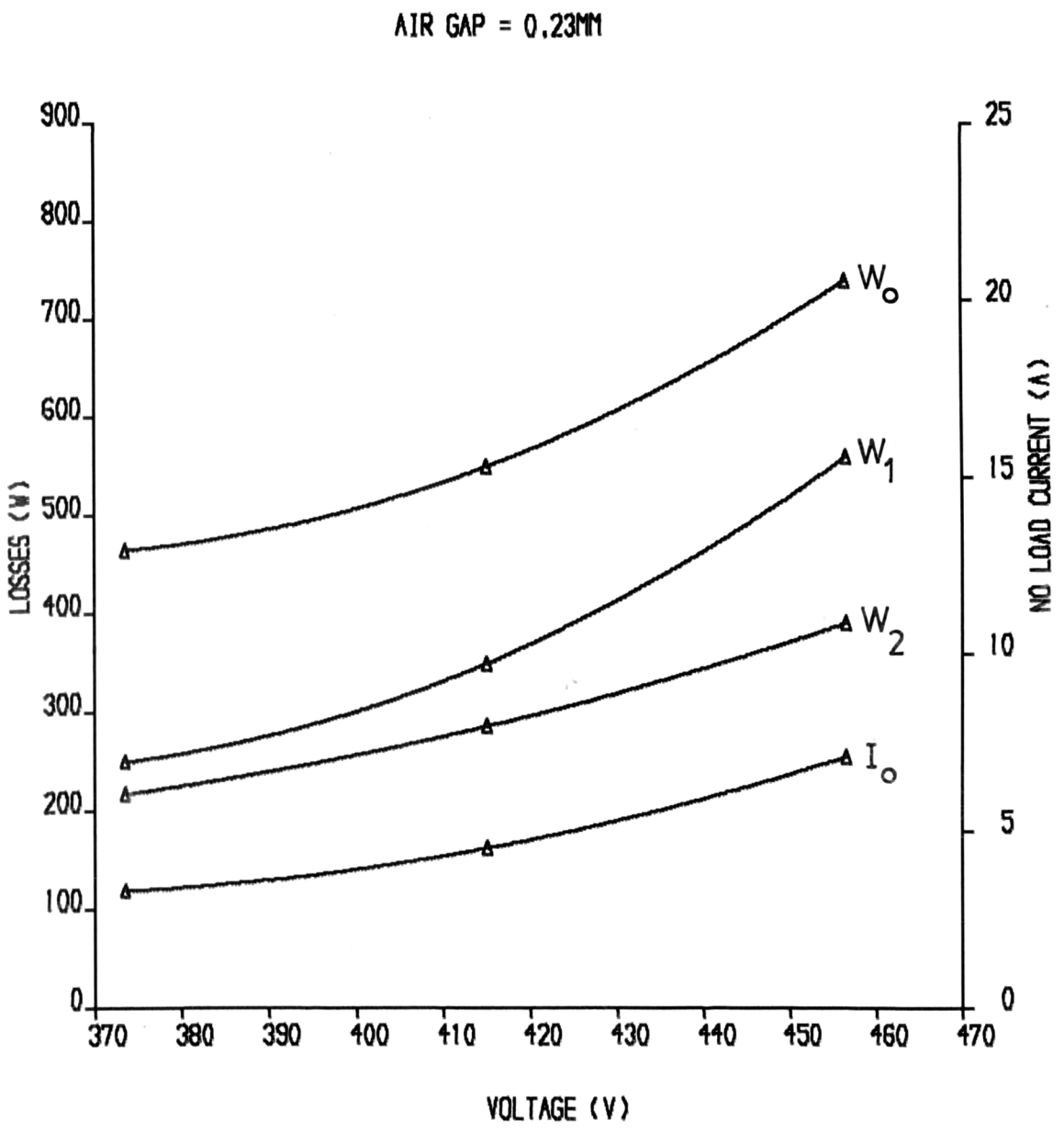

FIG. 5.4 ,NO LOAD LOSSES, ROTOR NO.9, SKEW=0.0 SSP

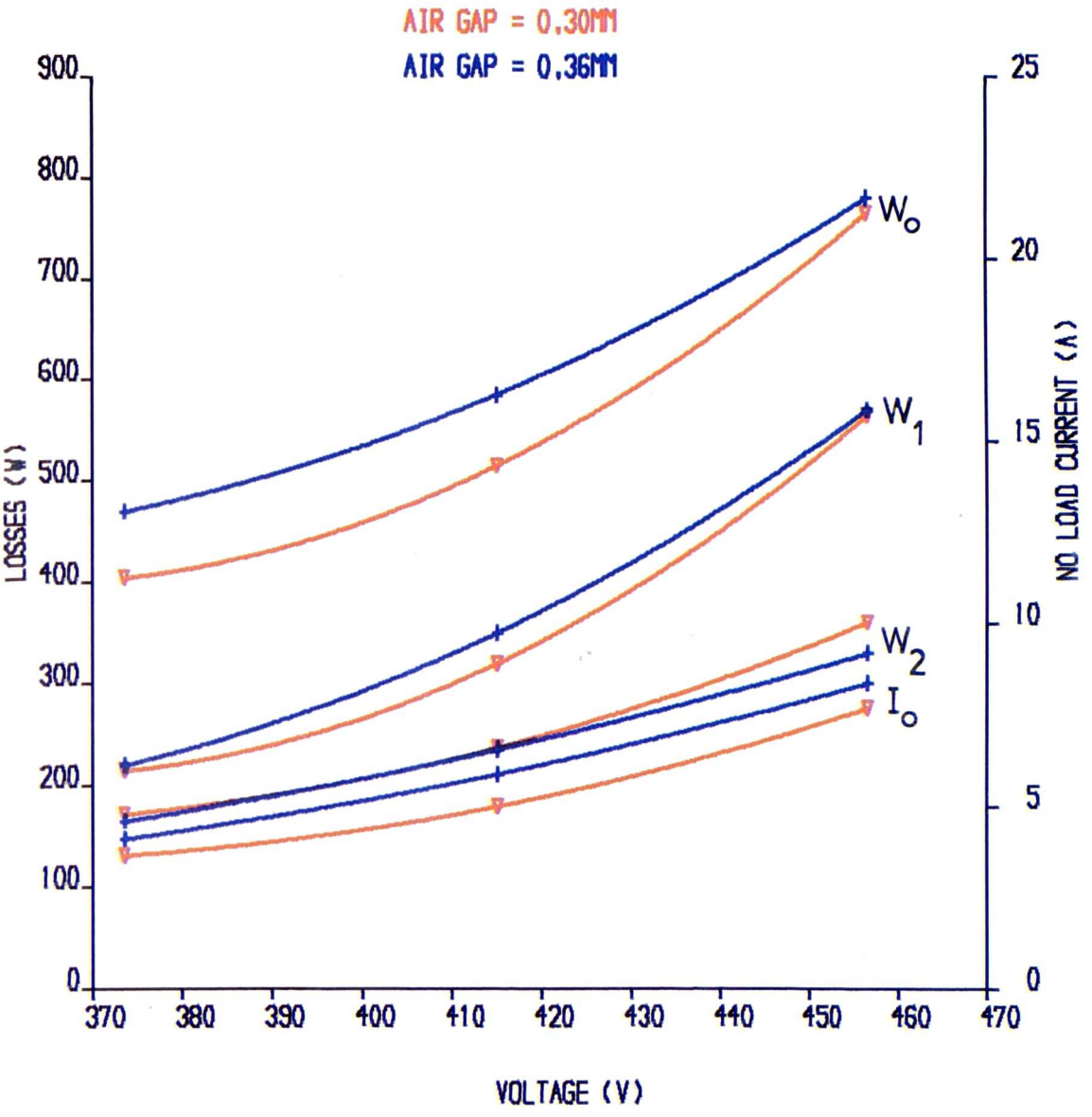

FIG. 5.5 .NO LOAD LOSSES. ROTOR NO.2. SKEW=0.5 SSP

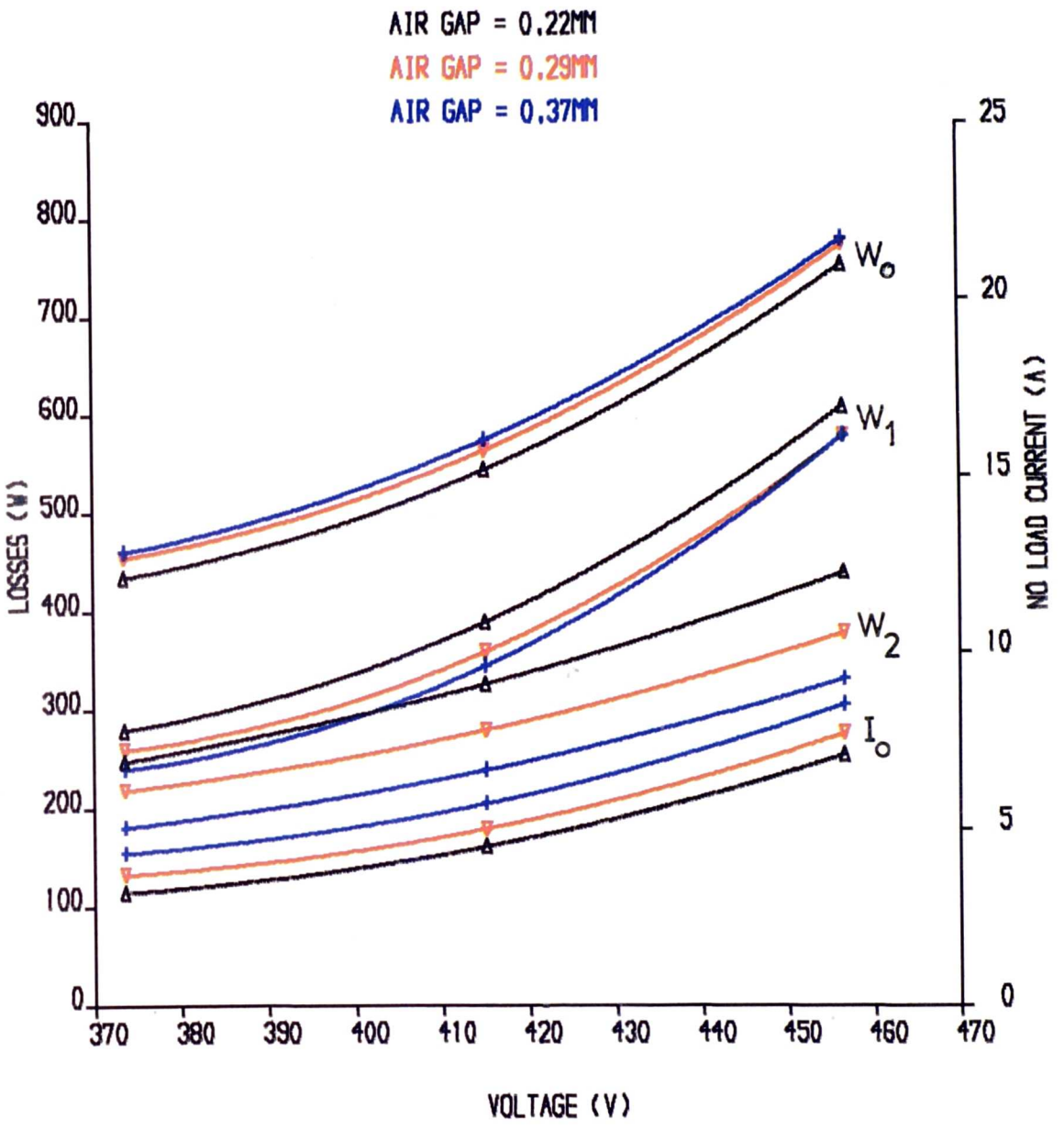

FIG. 5.6 ,NO LOAD LOSSES, ROTOR NO.4, SKEW=0.5 SSP

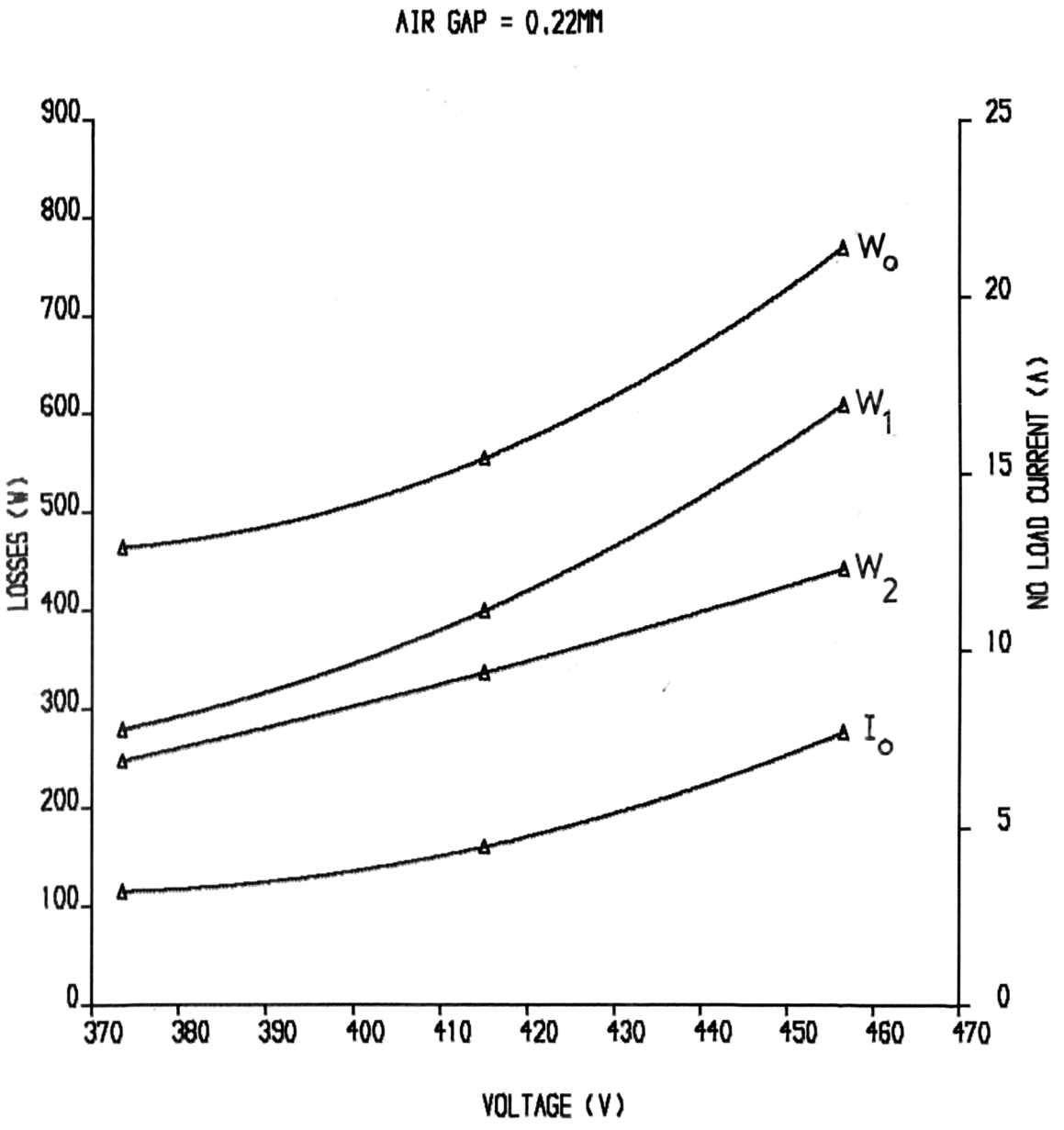

FIG. 5.7 .NO LOAD LOSSES. ROTOR NO.5. SKEW=0.5 SSP

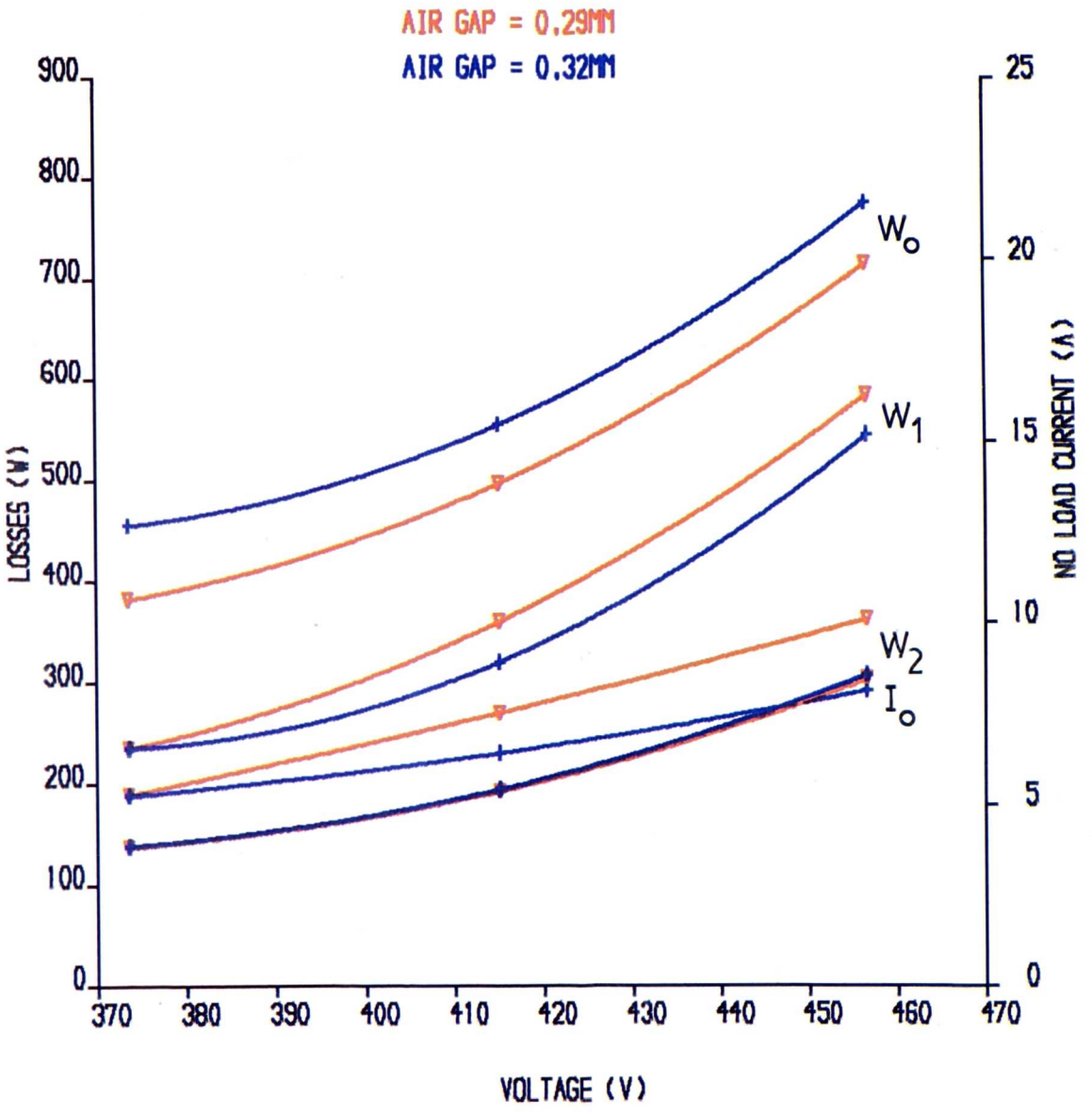

FIG. 5.8 ,NO LOAD LOSSES, ROTOR NO.1, SKEW=1.0 SSP

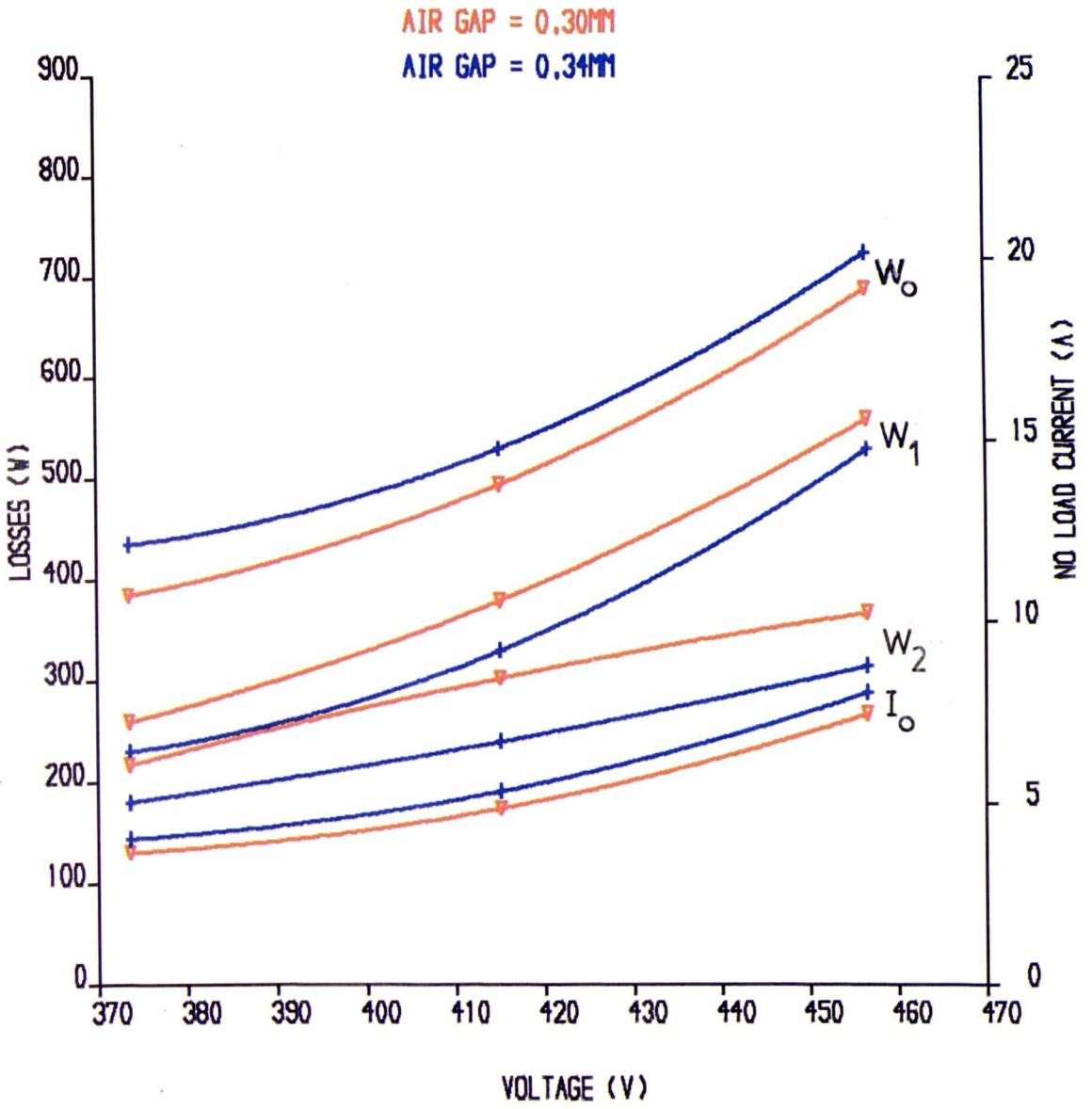

FIG. 5.9 .NO LOAD LOSSES. ROTOR NO.3. SKEW=1.0 SSP

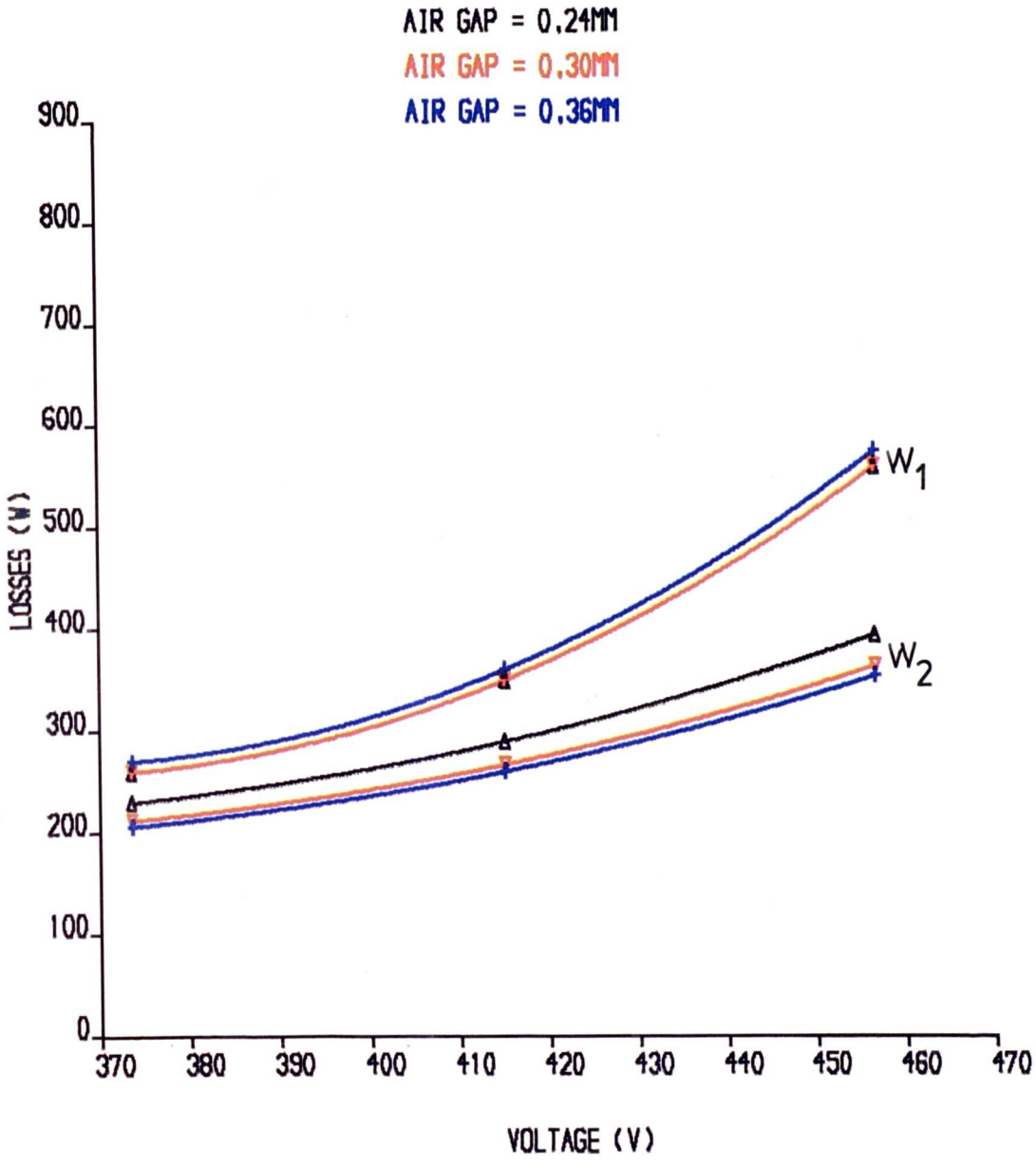

FIG. 5.10 ,NO LOAD LOSSES, ROTOR NO.12,SKEW=1.0 SSP

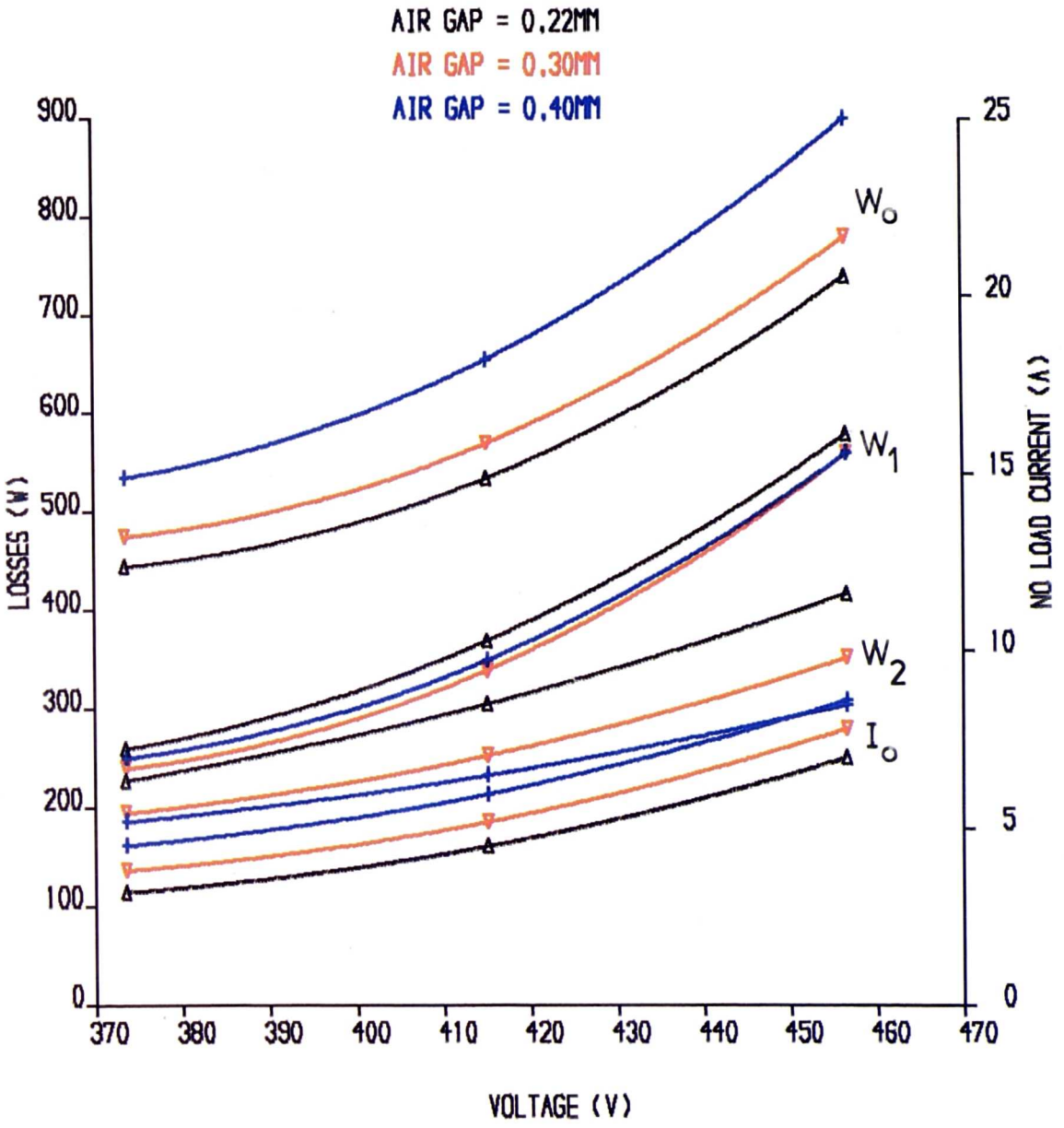

FIG. 5.11 ,NO LOAD LOSSES, ROTOR NO.6 ,SKEW=1.28 SSP

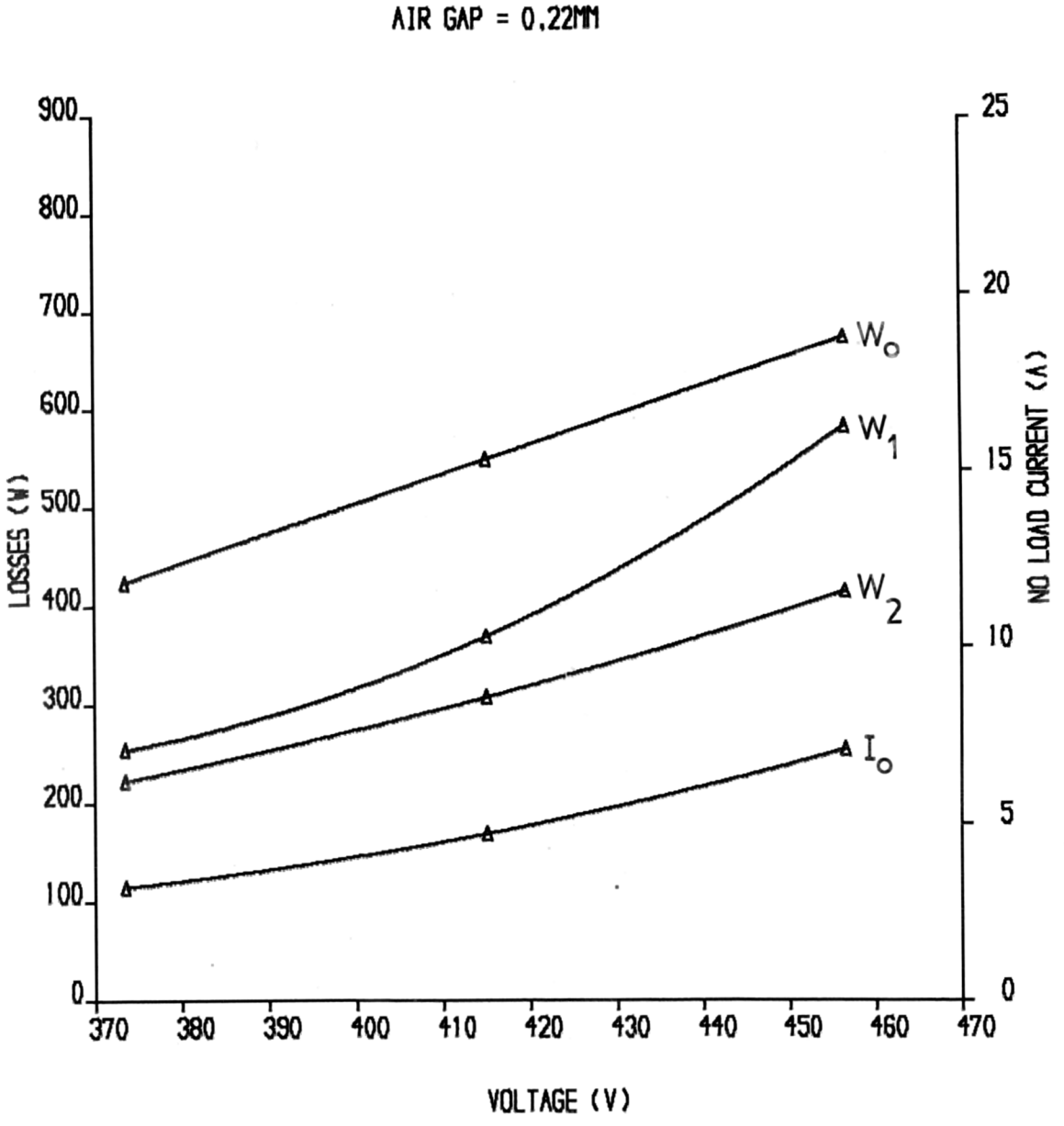

FIG. 5.12 ,NO LOAD LOSSES, ROTOR NO.7 ,SKEW=1.28 SSP

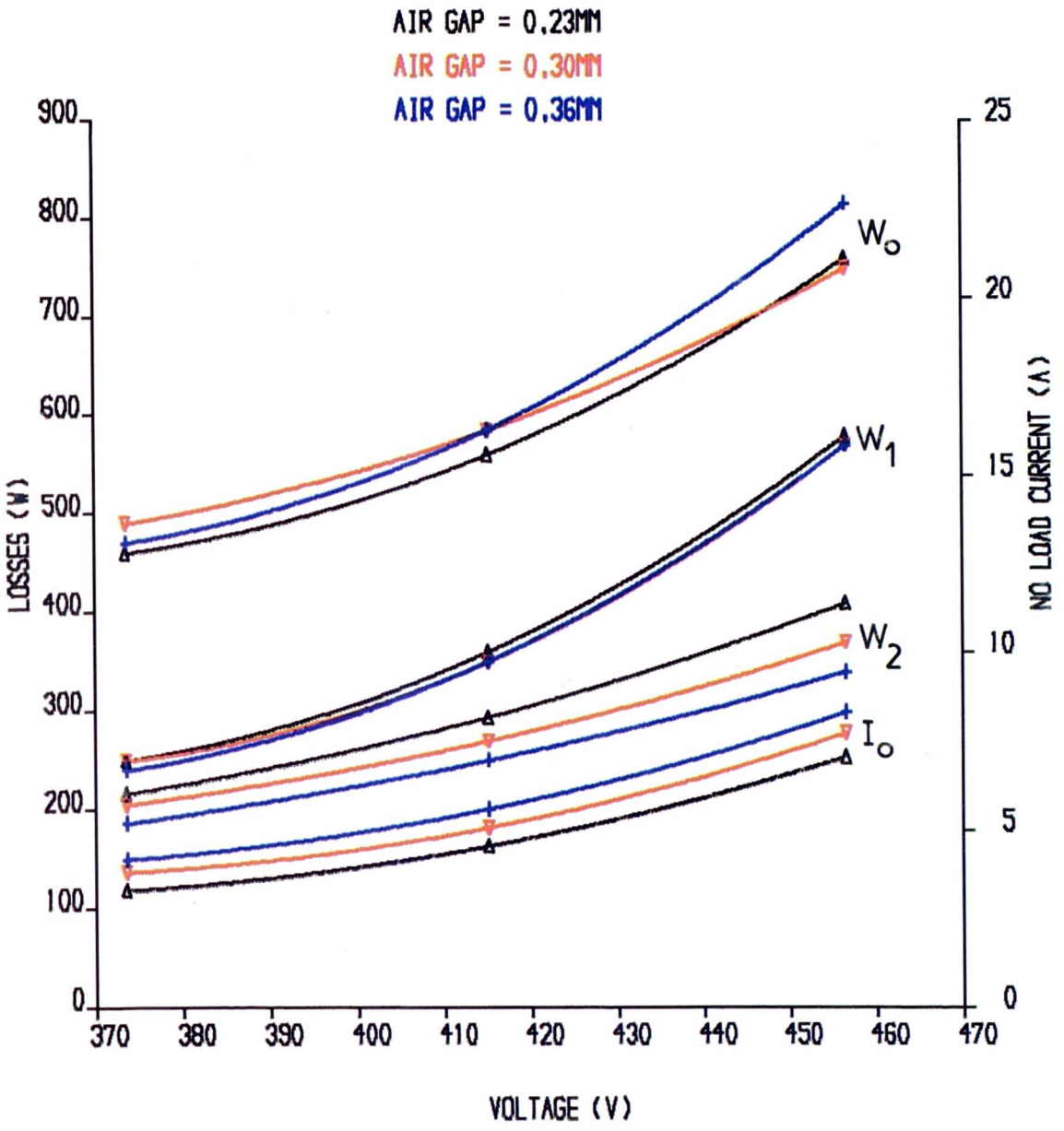

FIG. 5.13 ,NO LOAD LOSSES, ROTOR NO.10,SKEW=1.5 SSP

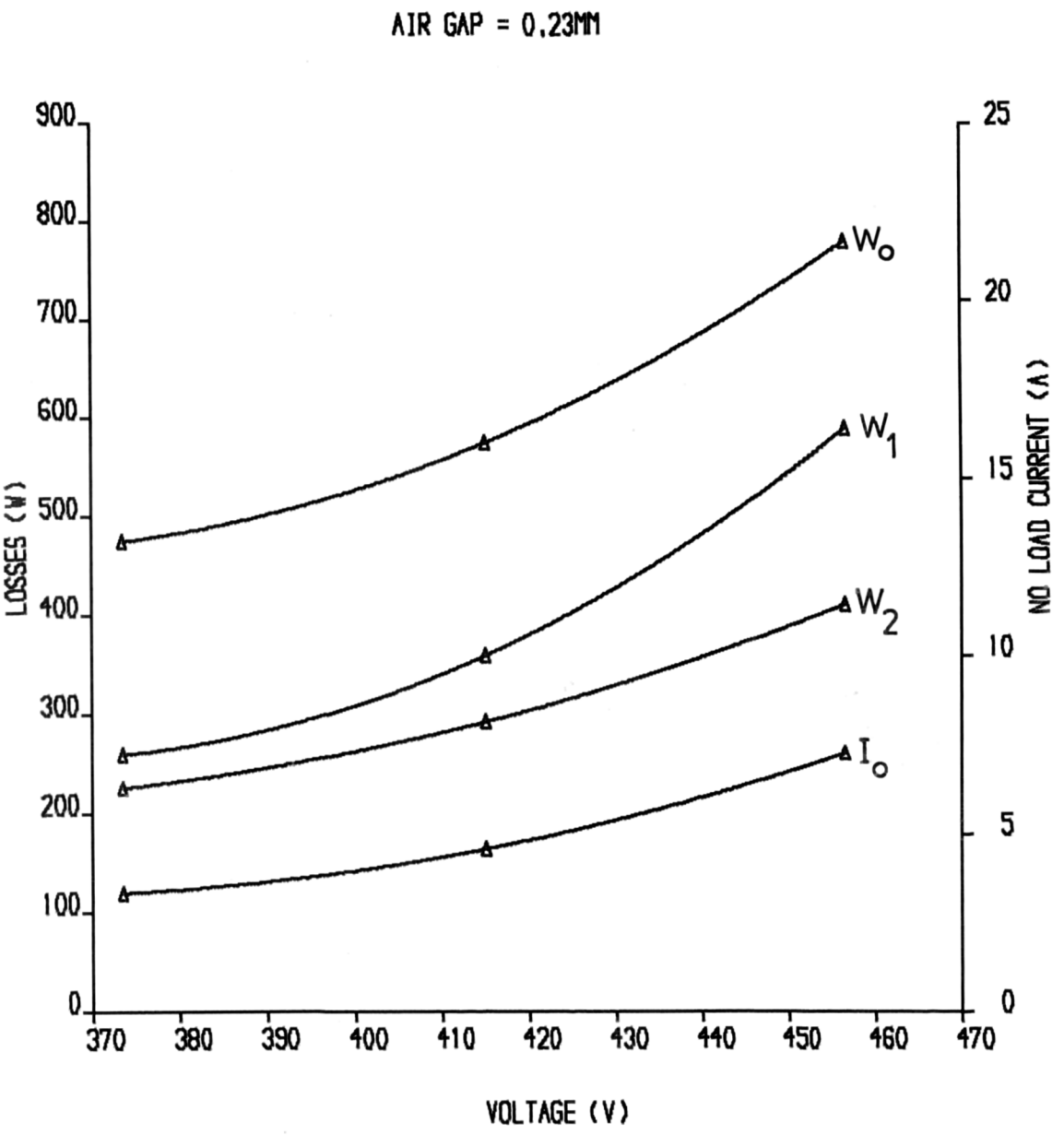

FIG. 5.14 ,NO LOAD LOSSES, ROTOR NO.11,SKEW=1.5 SSP

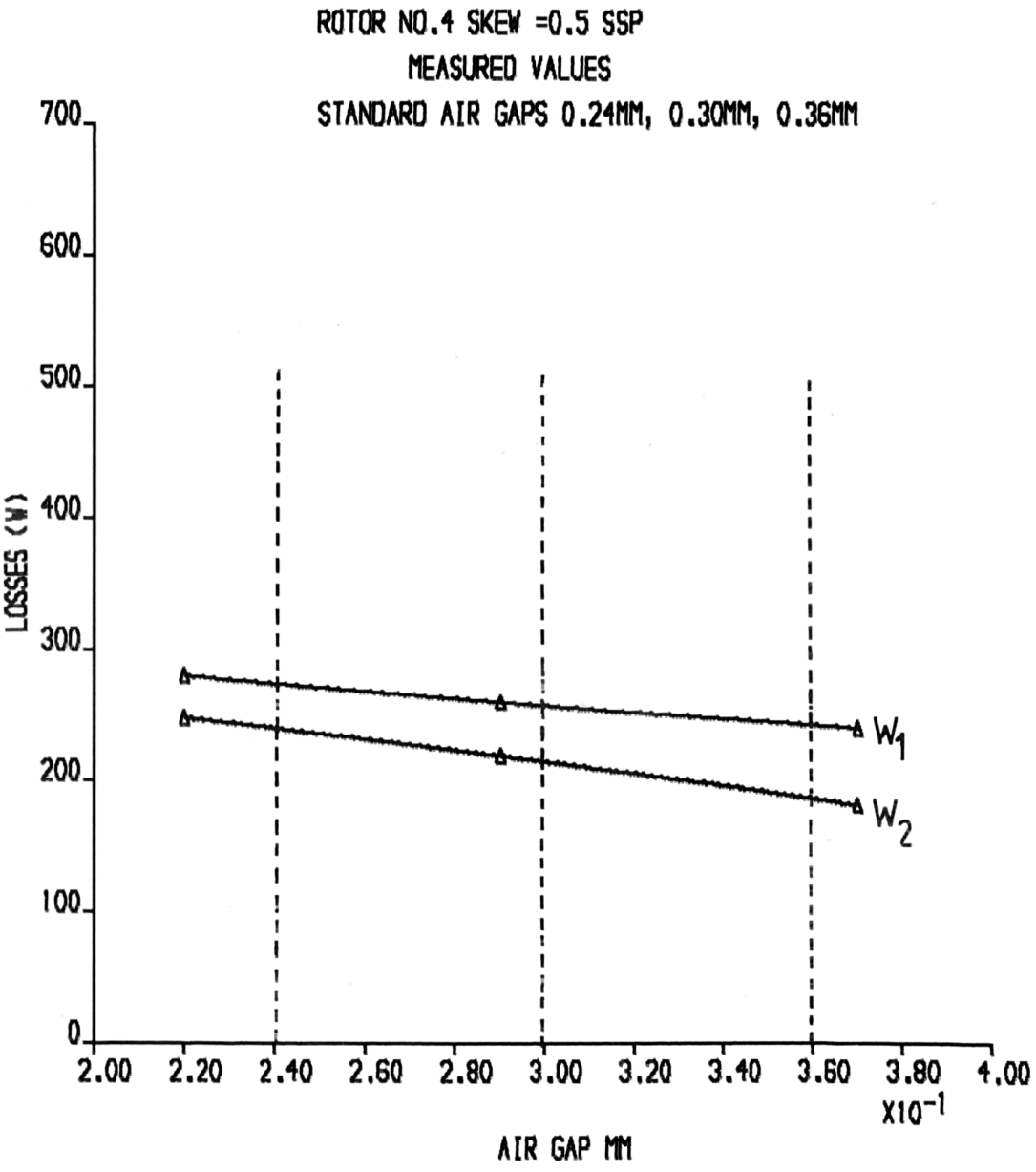

FIG. 5.15 .NO LOAD LOSSES AT 90% RATED VOLTAGE

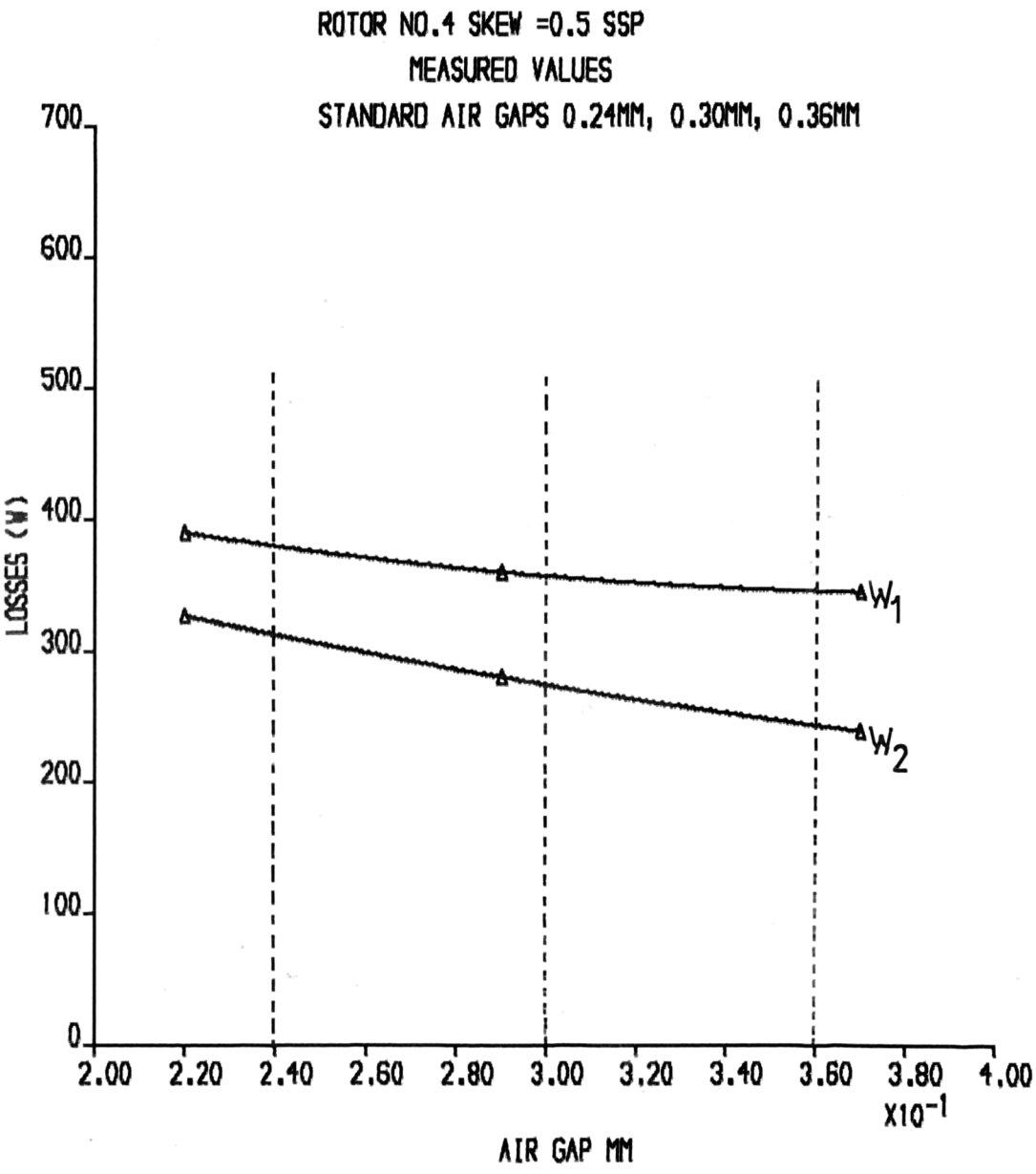

FIG. 5.16 ,NO LOAD LOSSES AT 100% RATED VOLTAGE

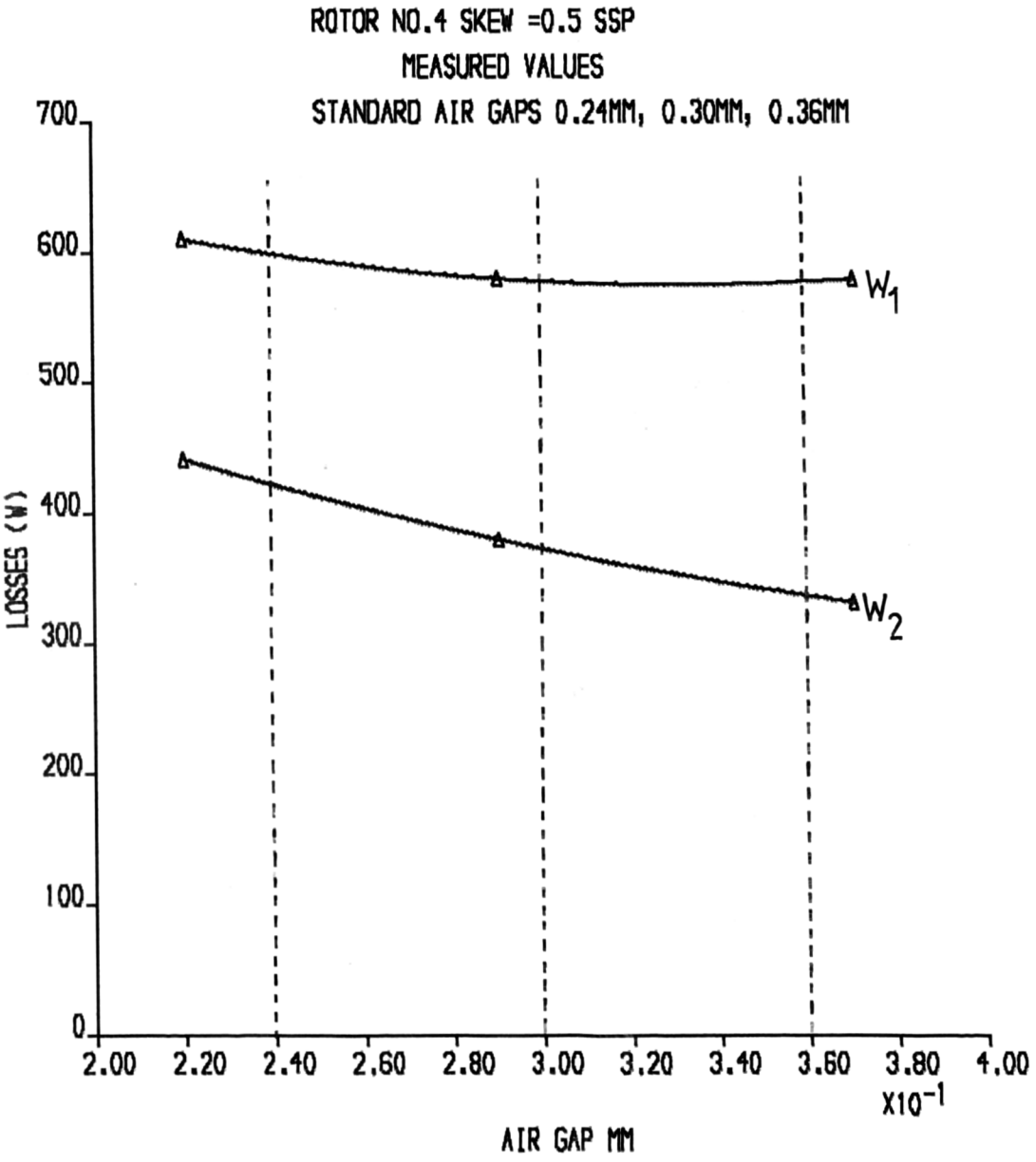

FIG. 5.17 .NO LOAD LOSSES AT 110% RATED VOLTAGE

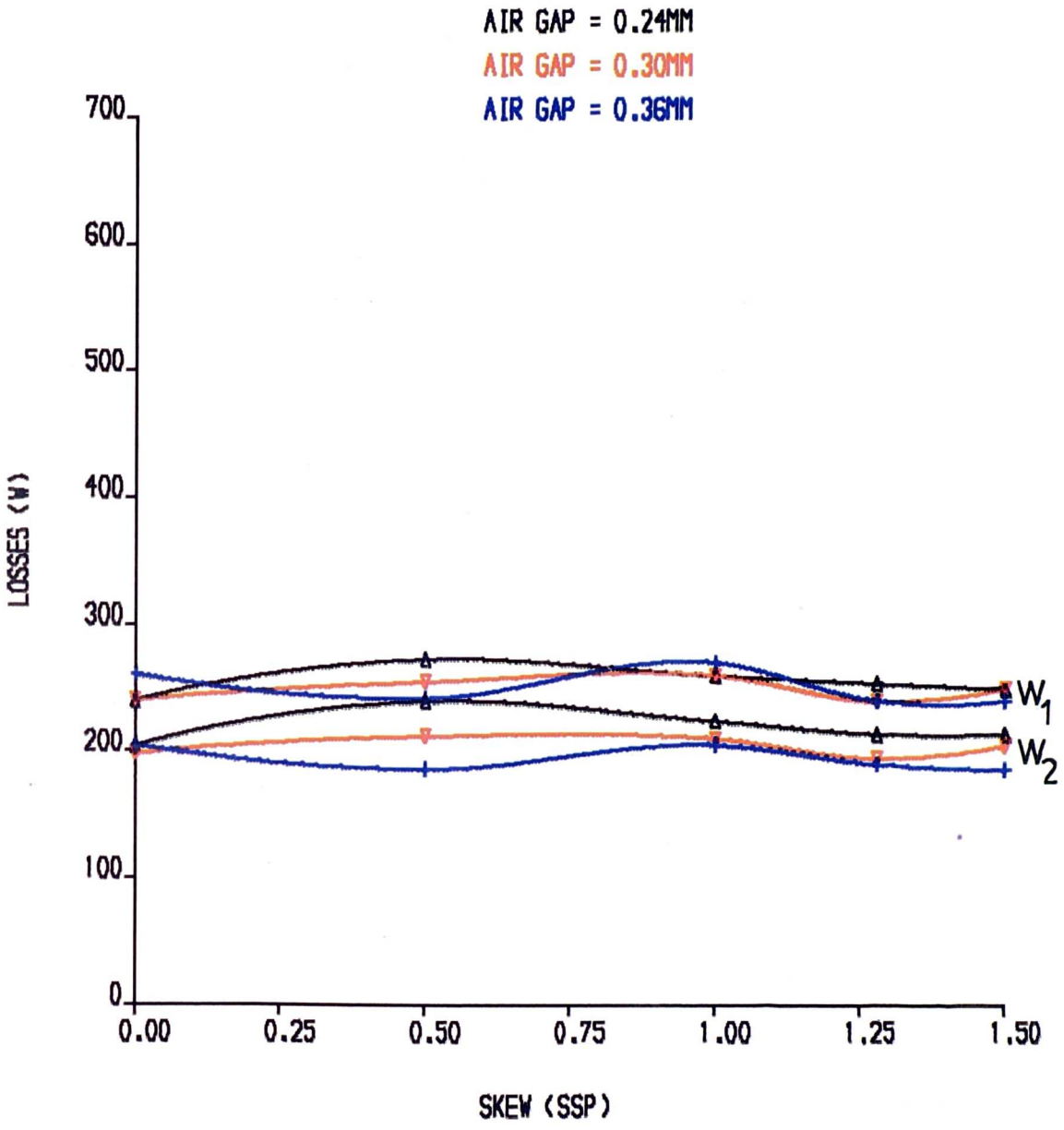

FIG. 5.18. NO LOAD LOSSES AT 90% RATED VOLTAGE

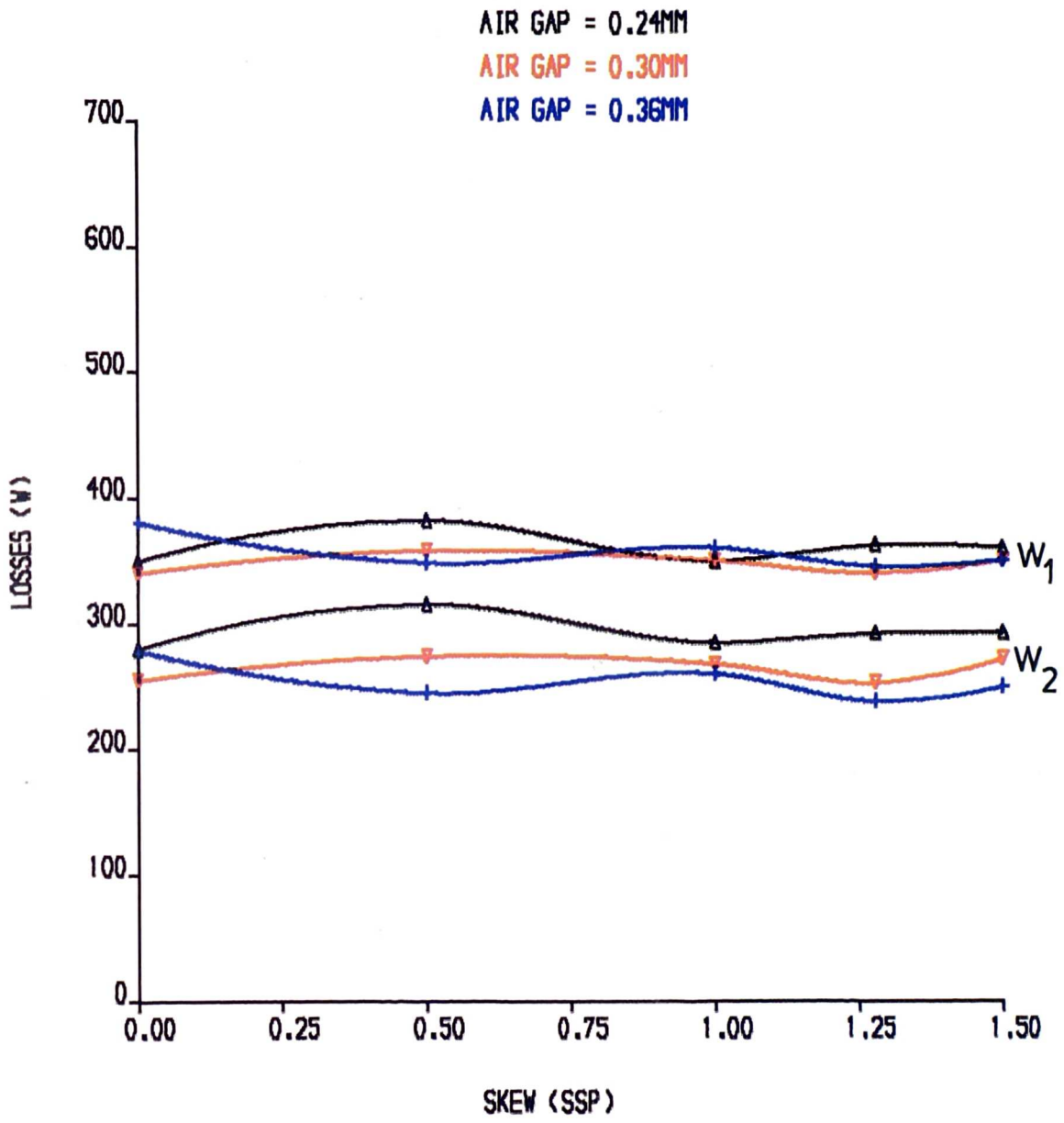

FIG. 5.19. NO LOAD LOSSES AT 100% RATED VOLTAGE

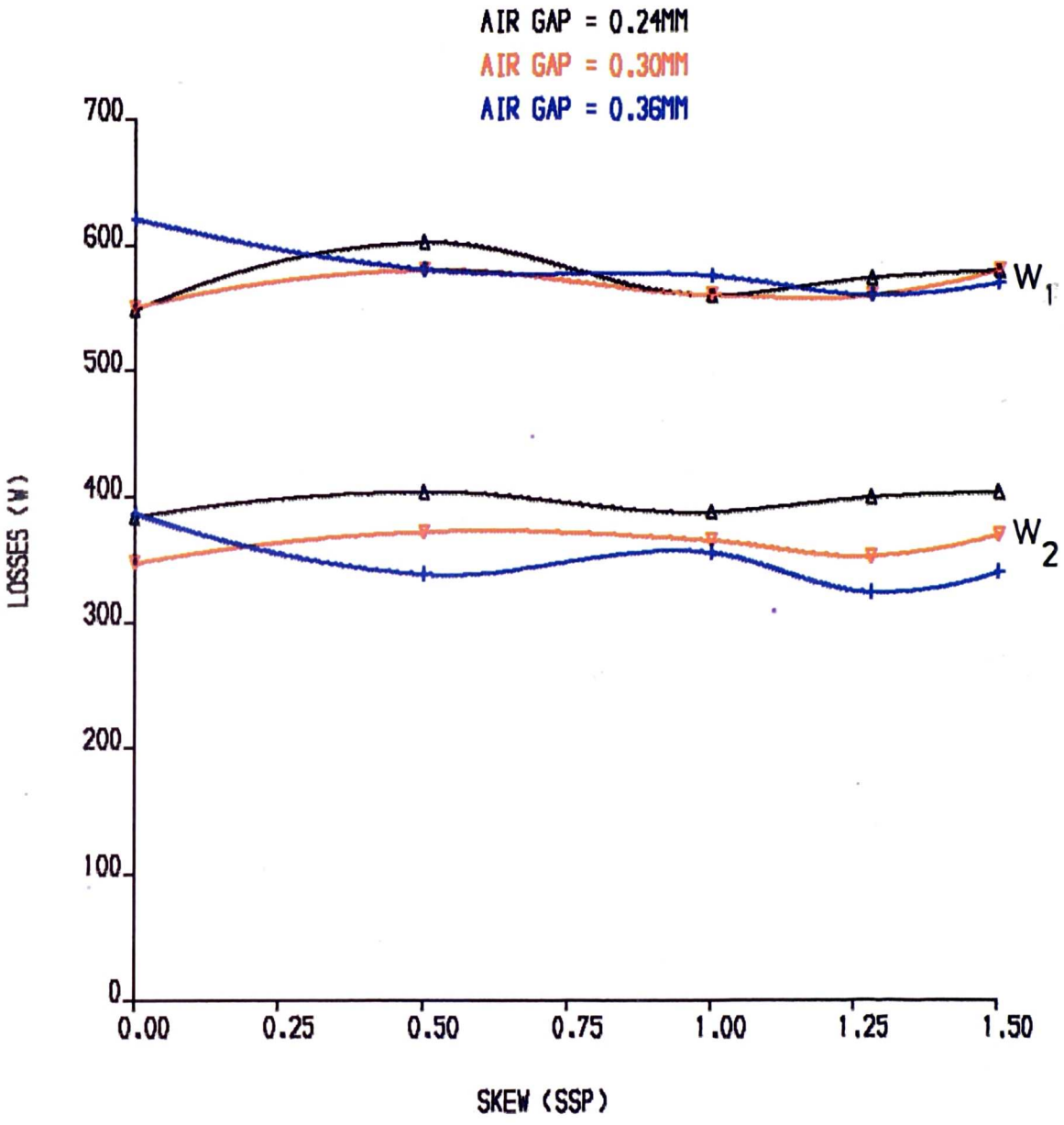

FIG. 5.20. NO LOAD LOSSES AT 110% RATED VOLTAGE

Figure 5.21 Rotor No.2 after removal of end rings and end laminations

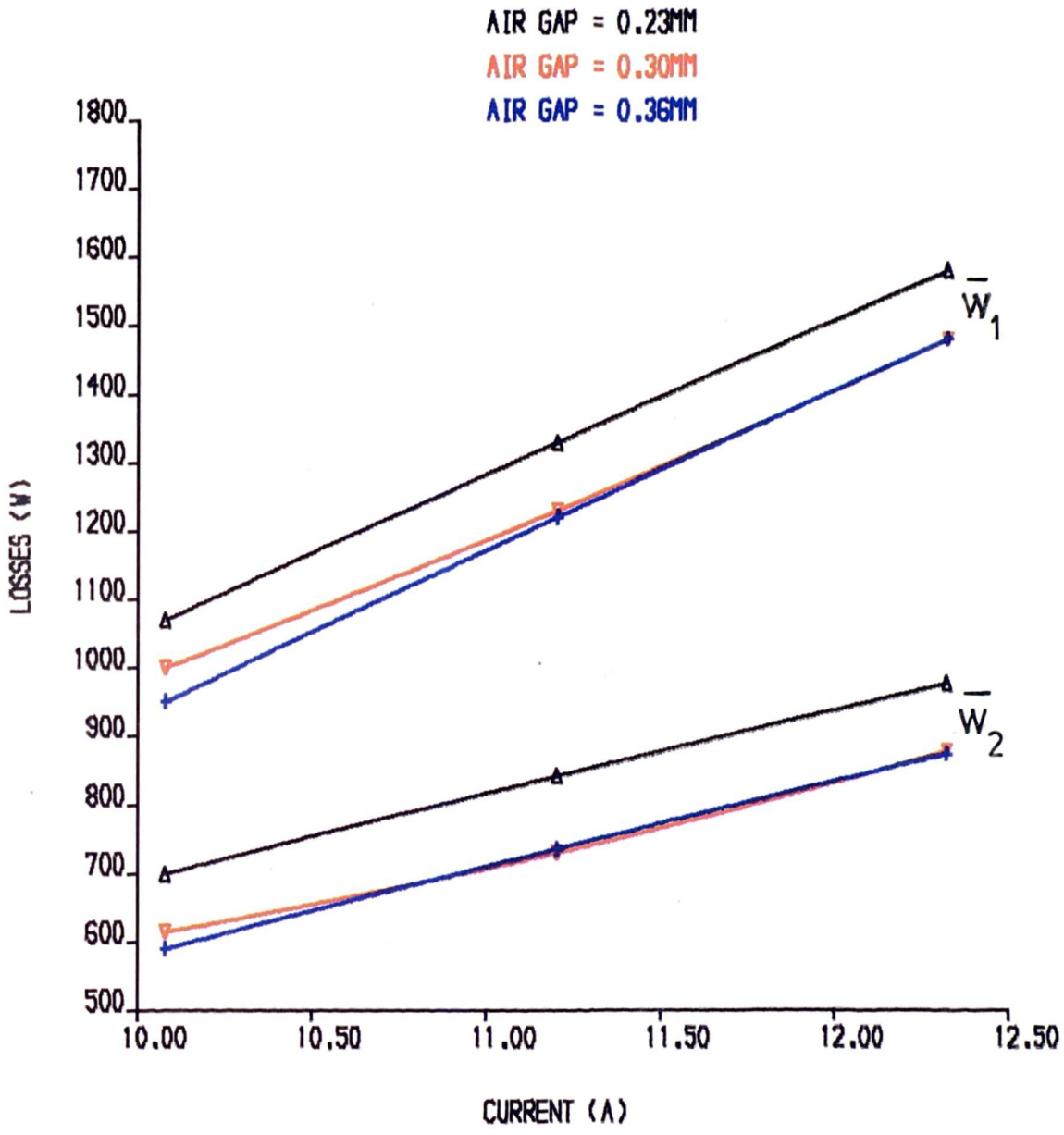

FIG. 5.22. LOAD LOSSES. ROTOR NO.8 .SKEW=0.0 SSP

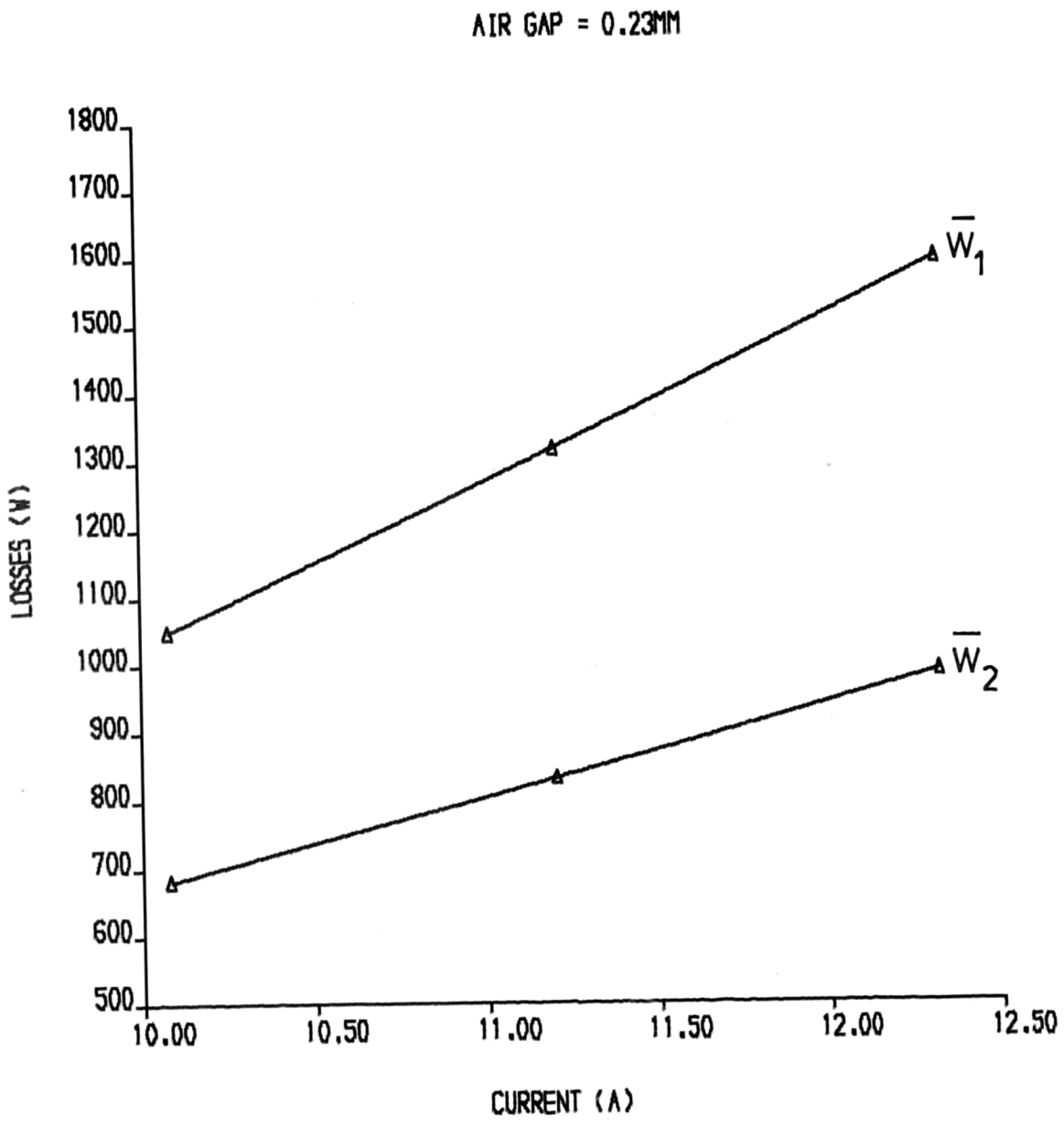

FIG. 5.23. LOAD LOSSES. ROTOR NO.9 .SKEW=0.0 SSP

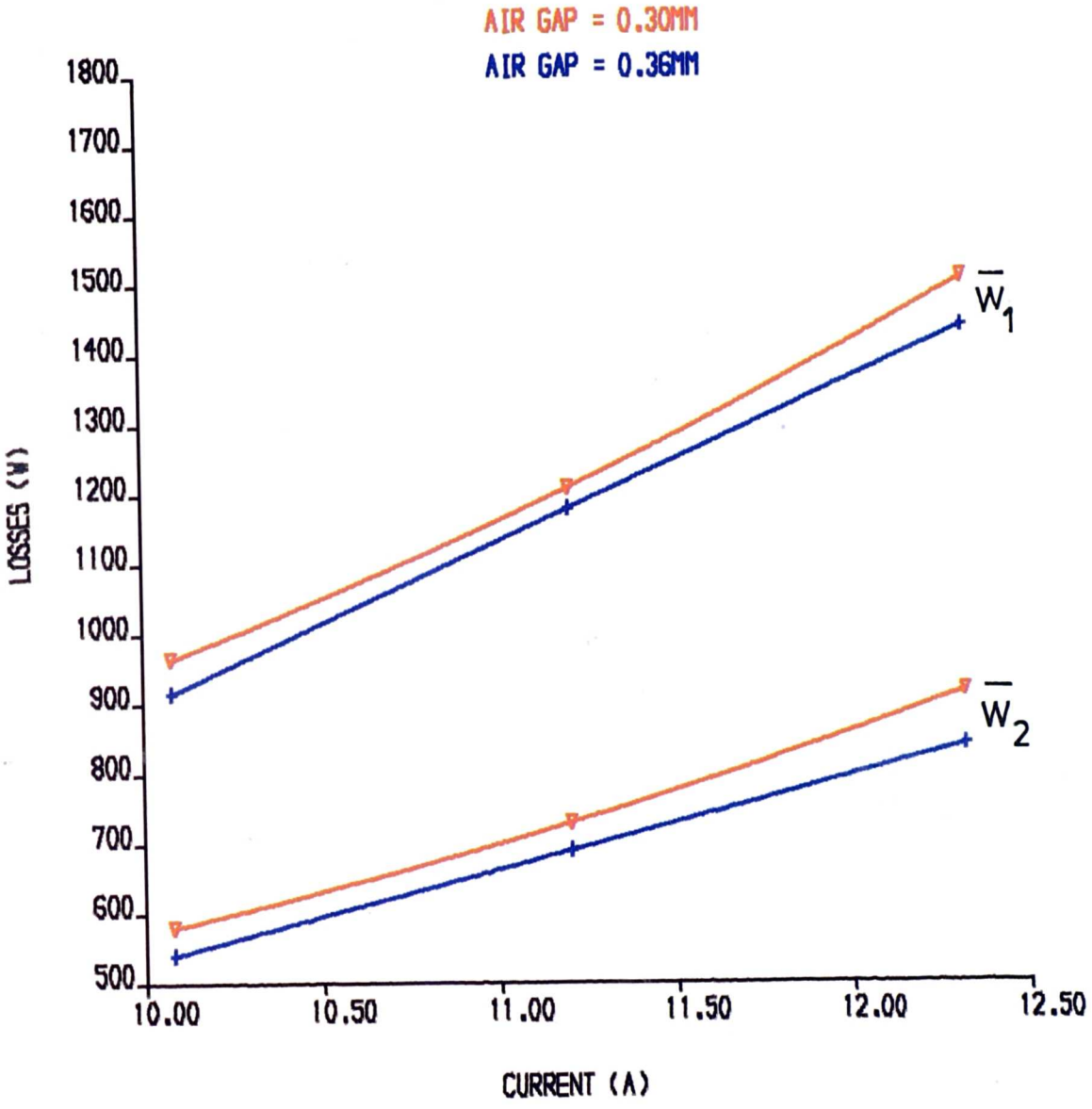

FIG. 5.24. LOAD LOSSES. ROTOR NO.2 .SKEW=0.5 SSP

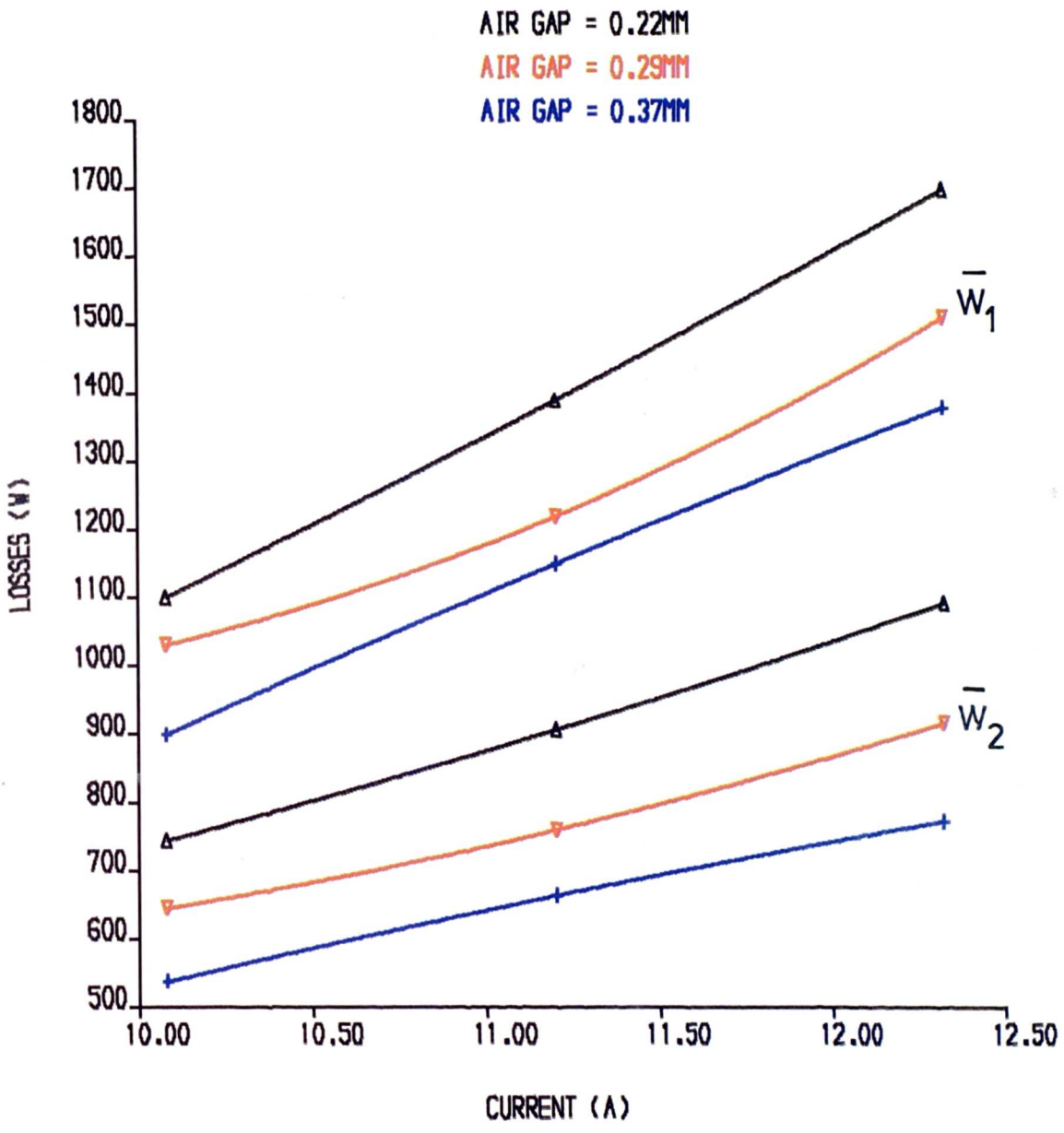

FIG. 5.25. LOAD LOSSES. ROTOR NO.4 .SKEW=0.5 SSP

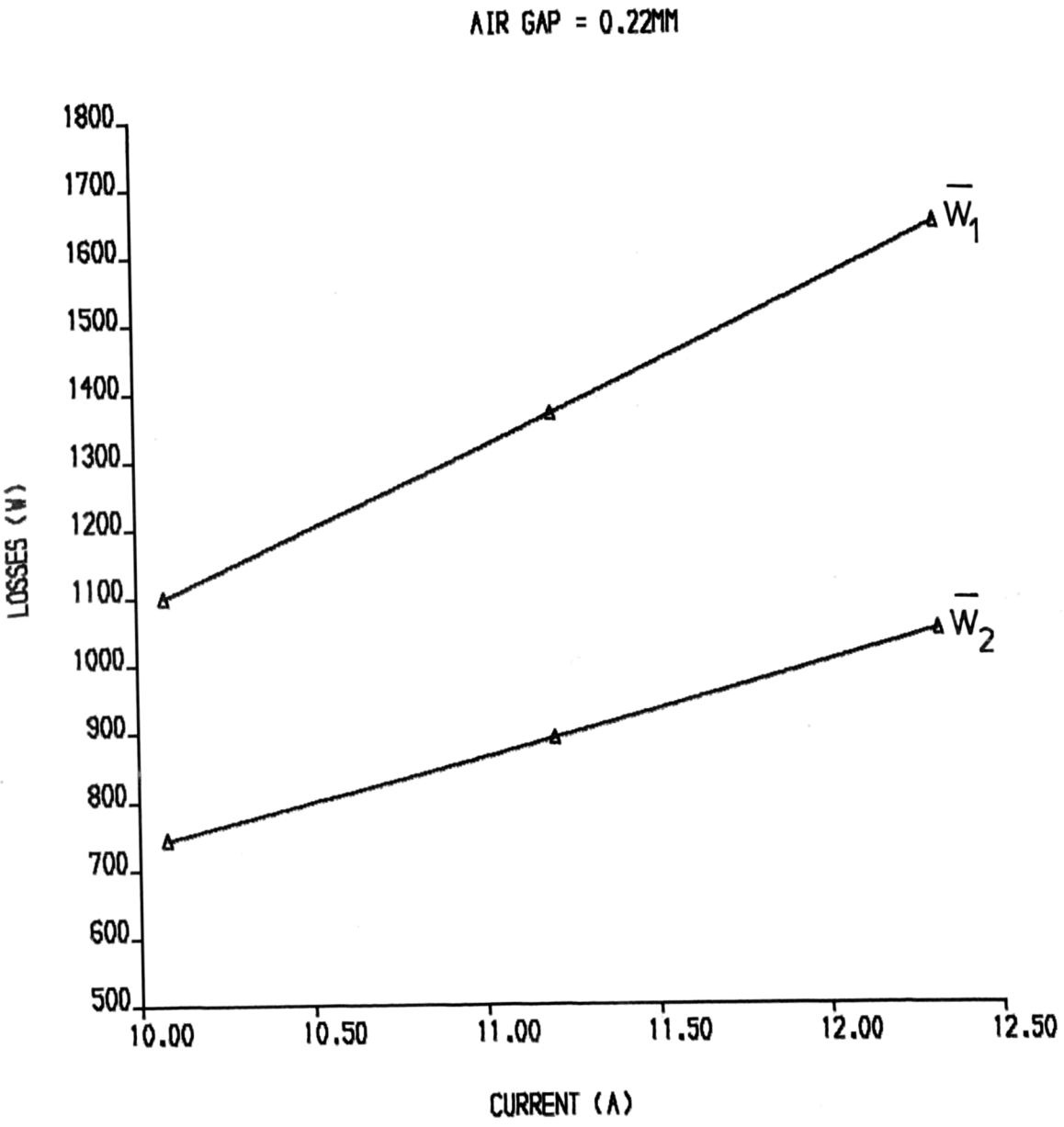

FIG. 5.26. LOAD LOSSES. ROTOR NO.5 .SKEW=0.5 SSP

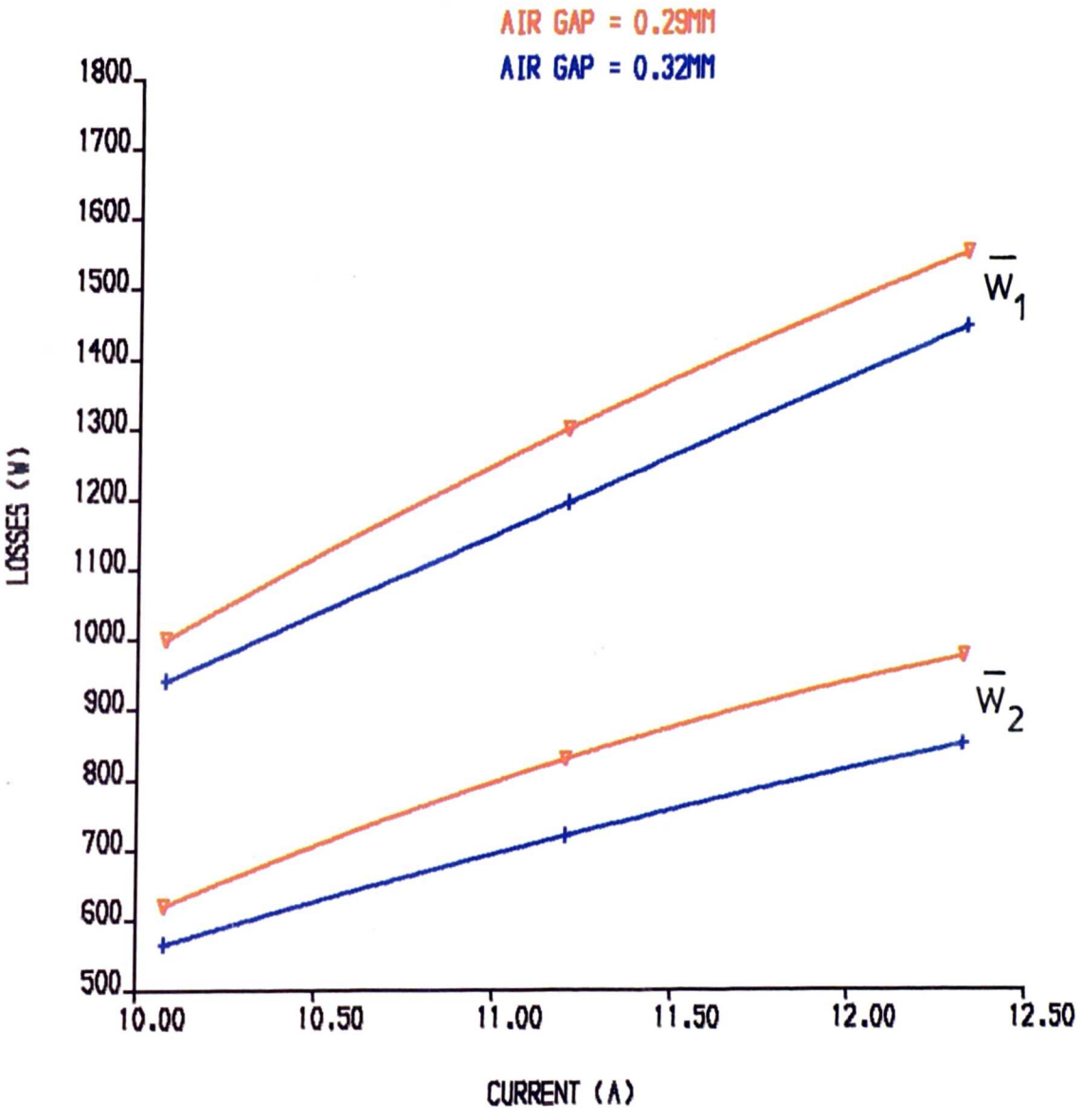

FIG. 5.27. LOAD LOSSES. ROTOR NO.1 .SKEW=1.0 SSP

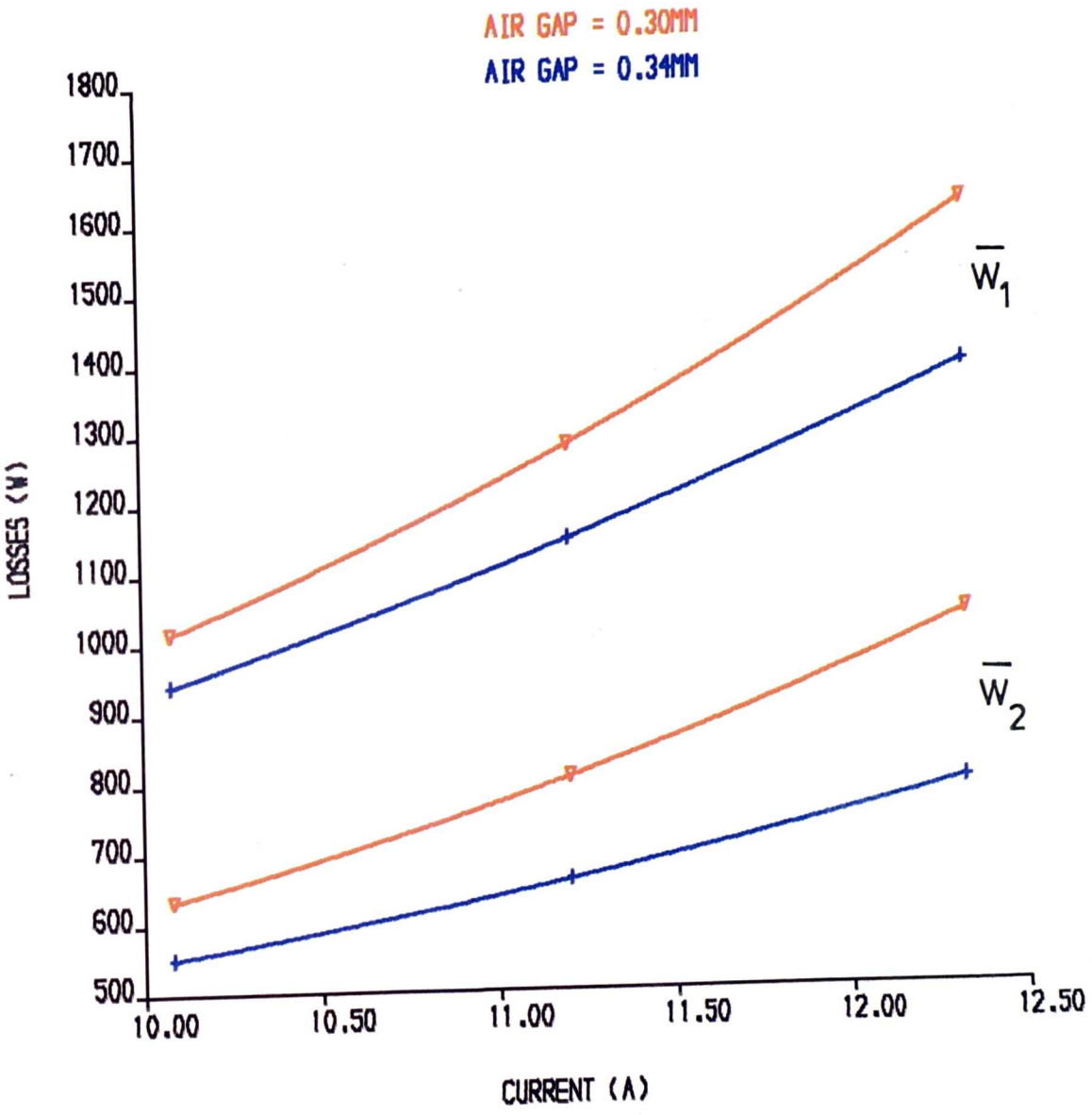

FIG. 5.28. LOAD LOSSES. ROTOR NO.3 .SKEW=1.0 SSP

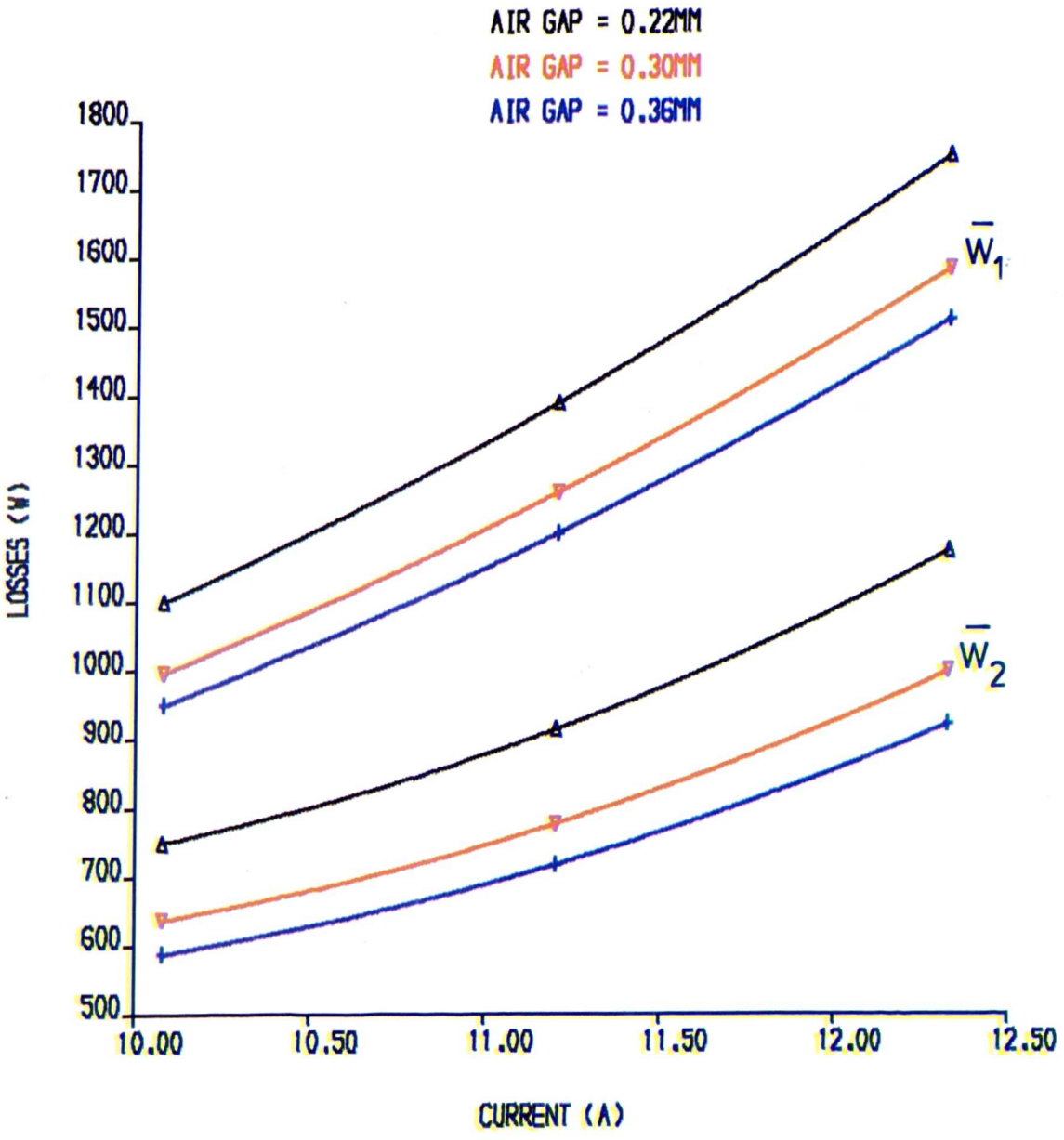

FIG. 5.29. LOAD LOSSES. ROTOR NO.12.SKEW=1.0 SSP

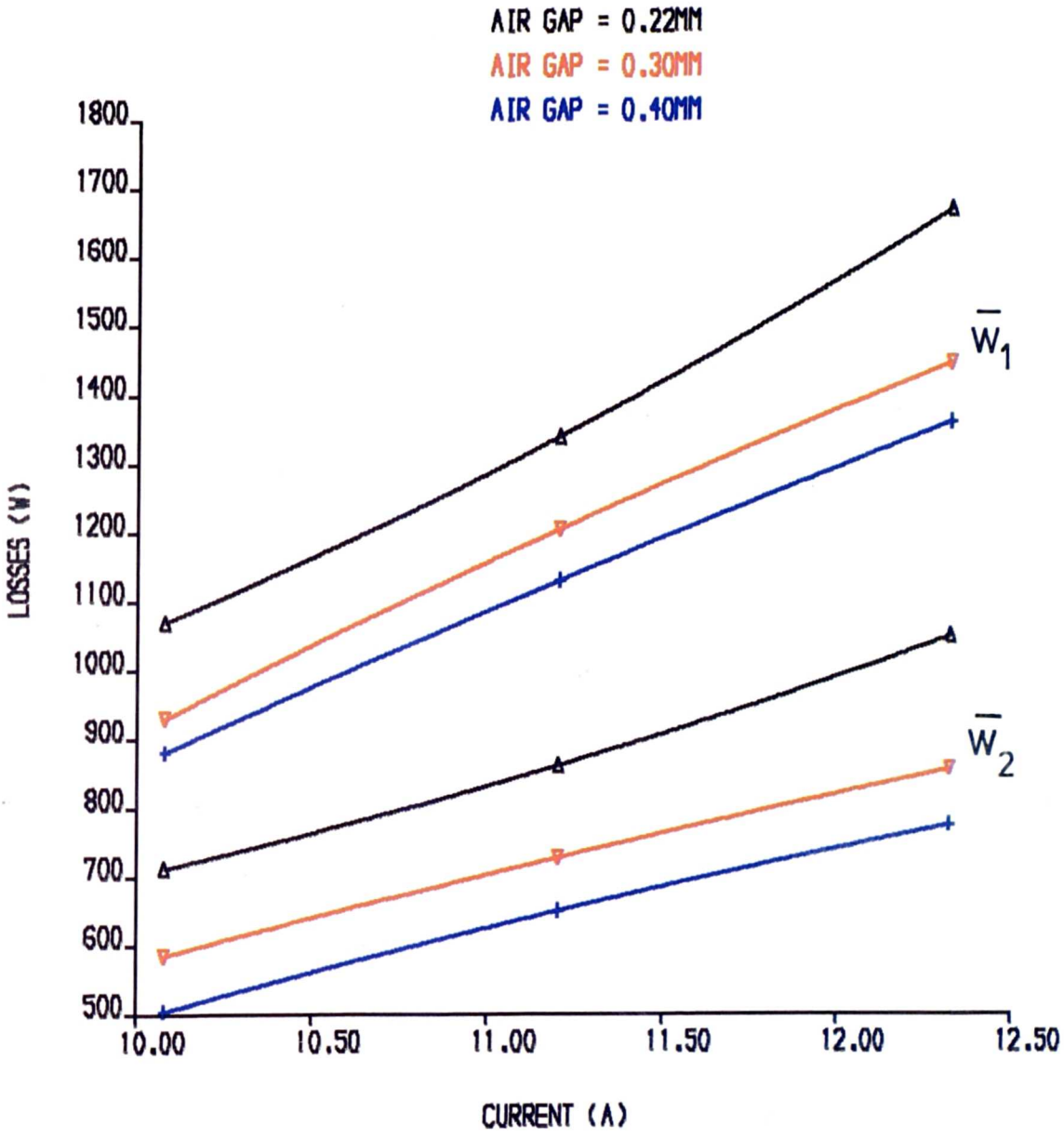

FIG. 5.30. LOAD LOSSES. ROTOR NO.6. SKEW=1.28 SSP

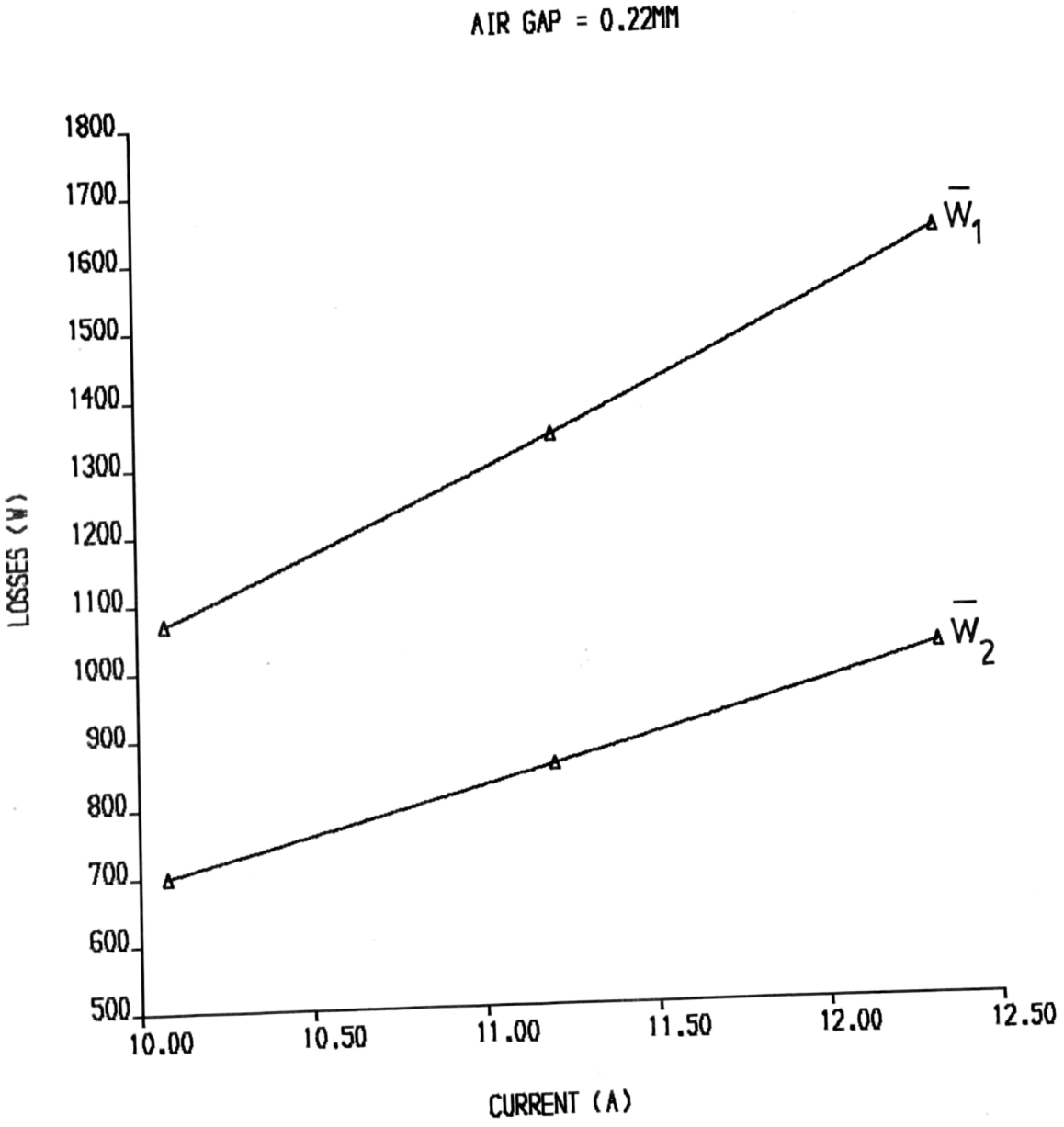

FIG. 5.31. LOAD LOSSES. ROTOR NO.7. SKEW=1.28 SSP

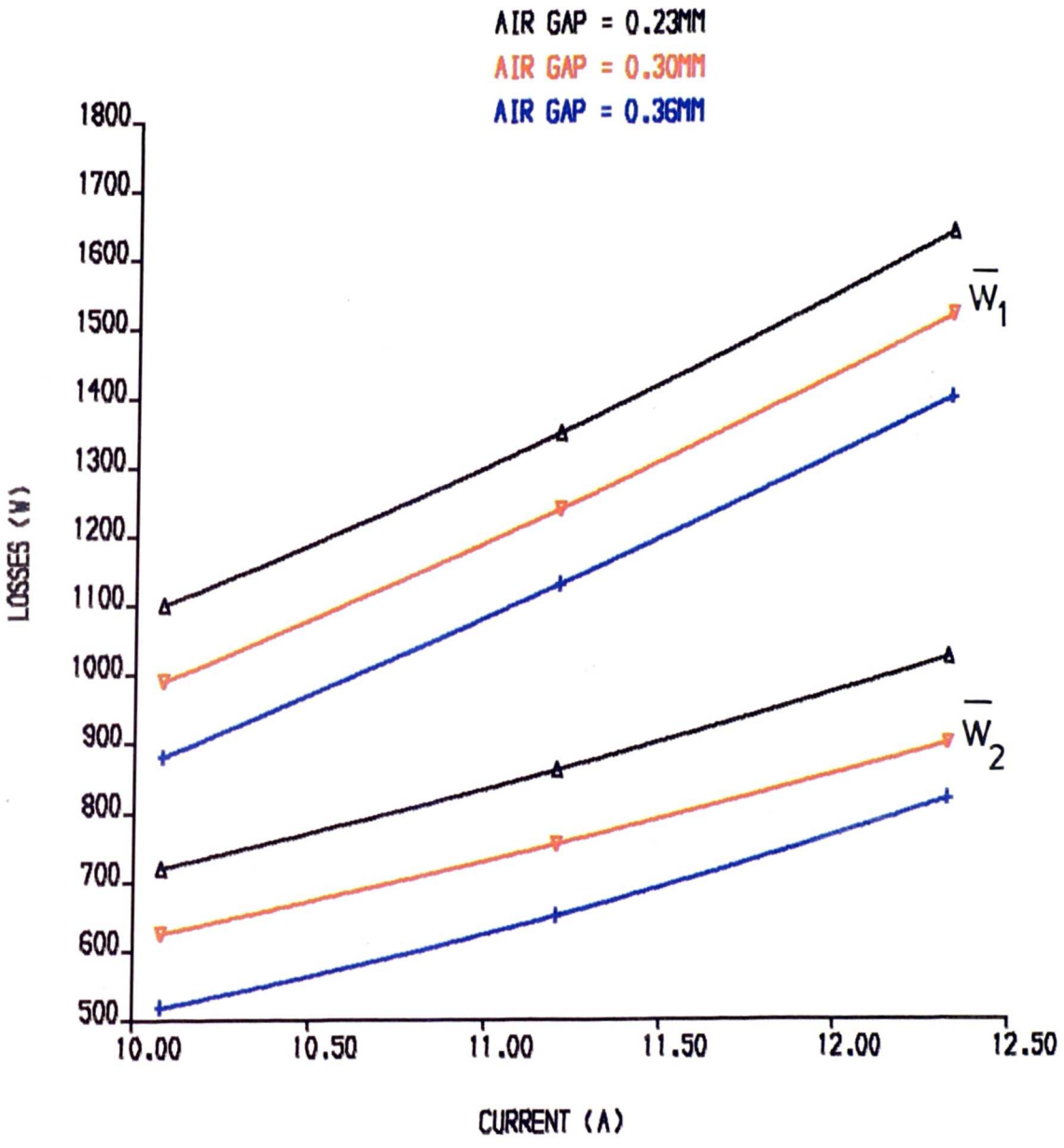

FIG. 5.32. LOAD LOSSES. ROTOR NO.10. SKEW=1.5 SSP

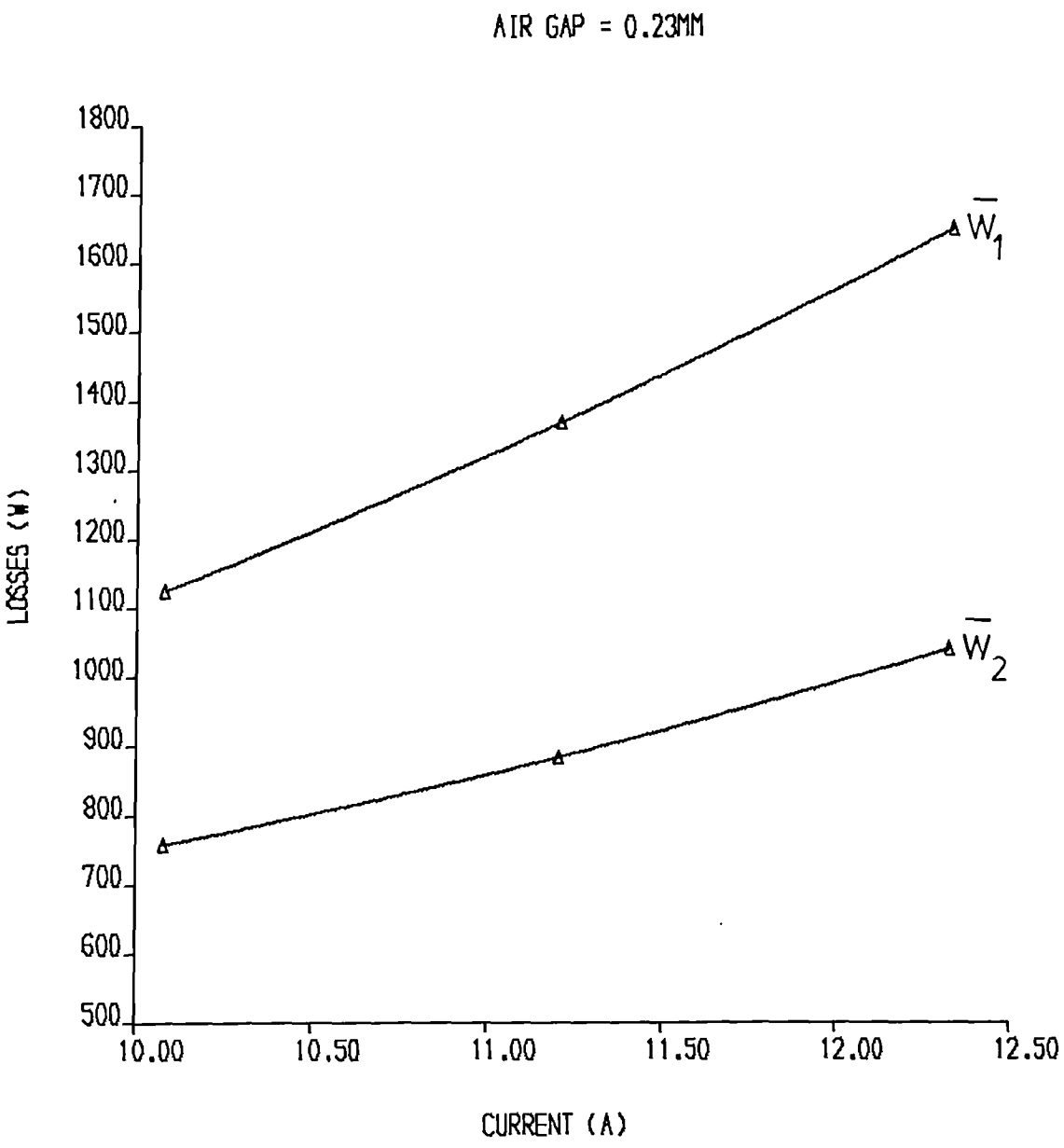

FIG. 5.33. LOAD LOSSES. ROTOR NO.11. SKEW=1.5 SSP

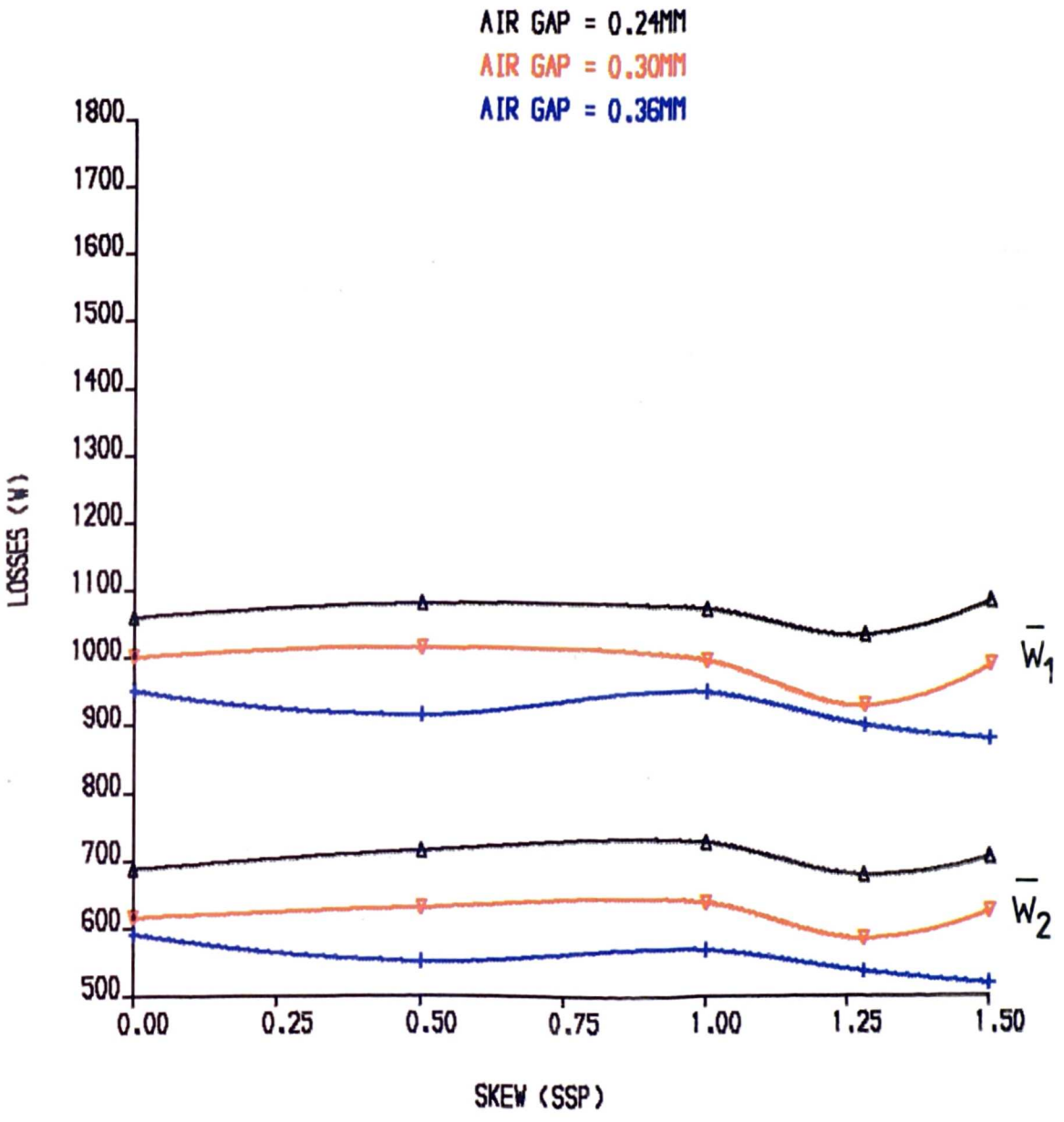

FIG. 5.34. LOAD LOSSES AT 90% RATED CURRENT

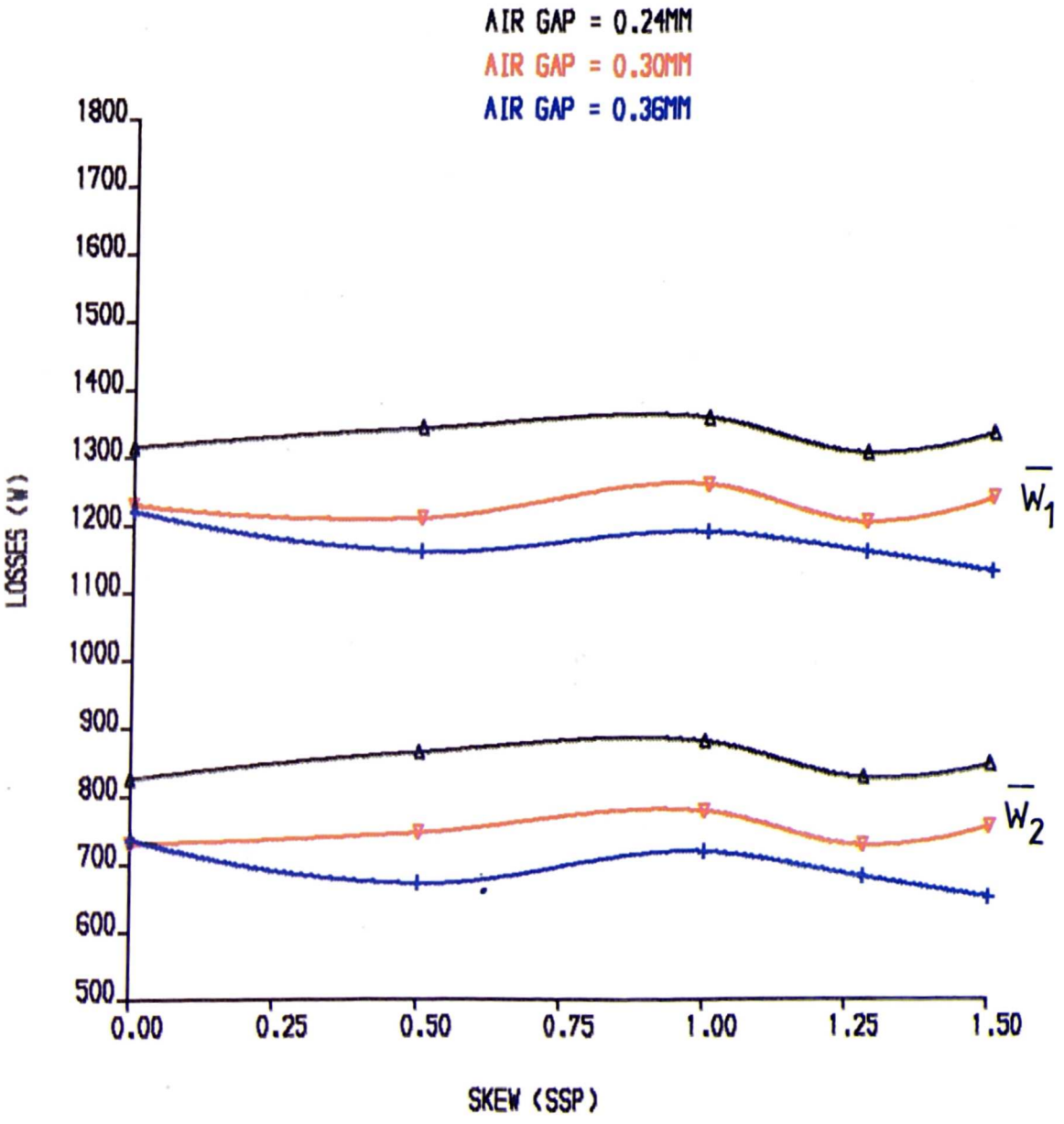

FIG. 5.35. LOAD LOSSES AT 100% RATED CURRENT

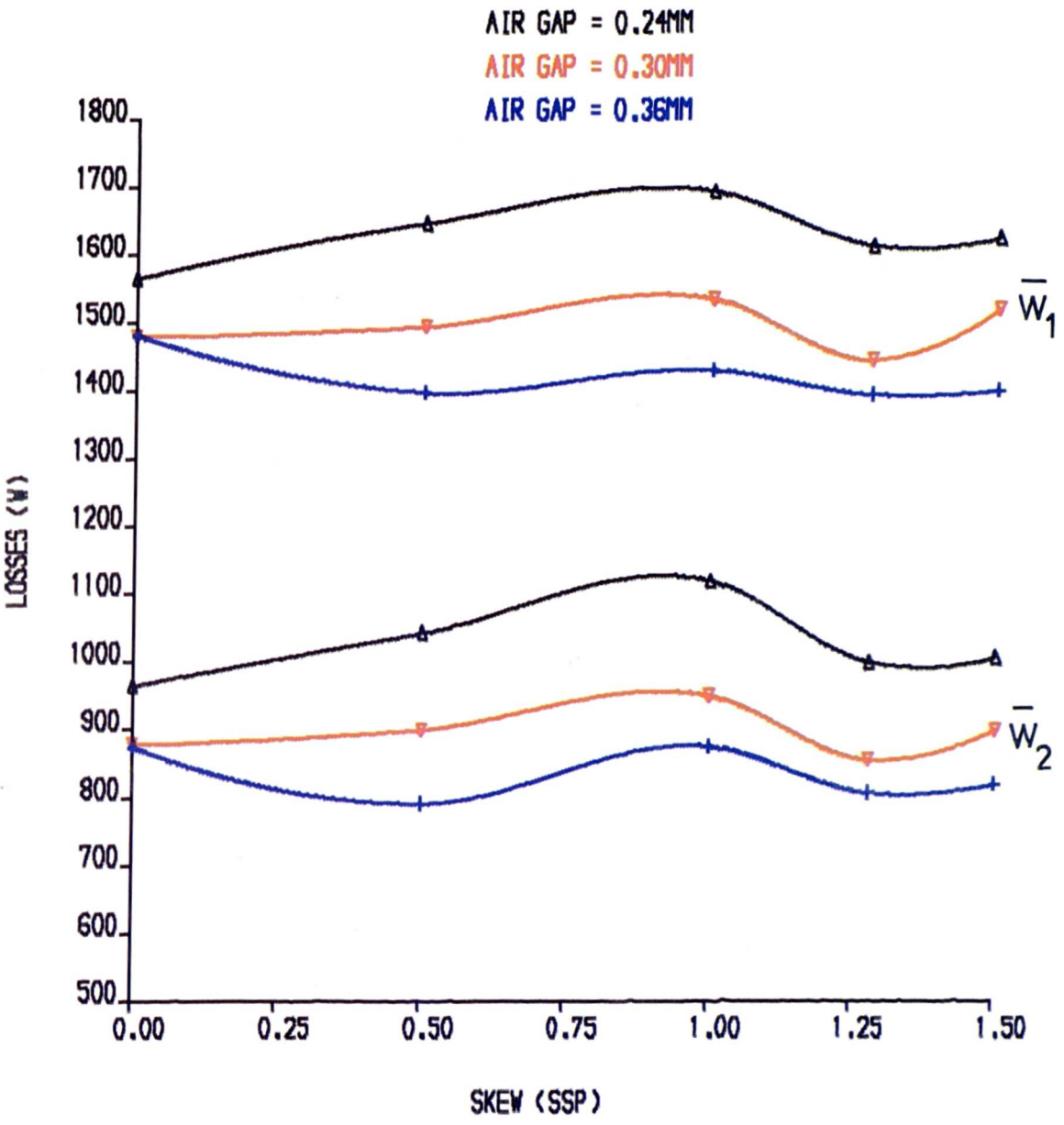

FIG. 5.36. LOAD LOSSES AT 110% RATED CURRENT

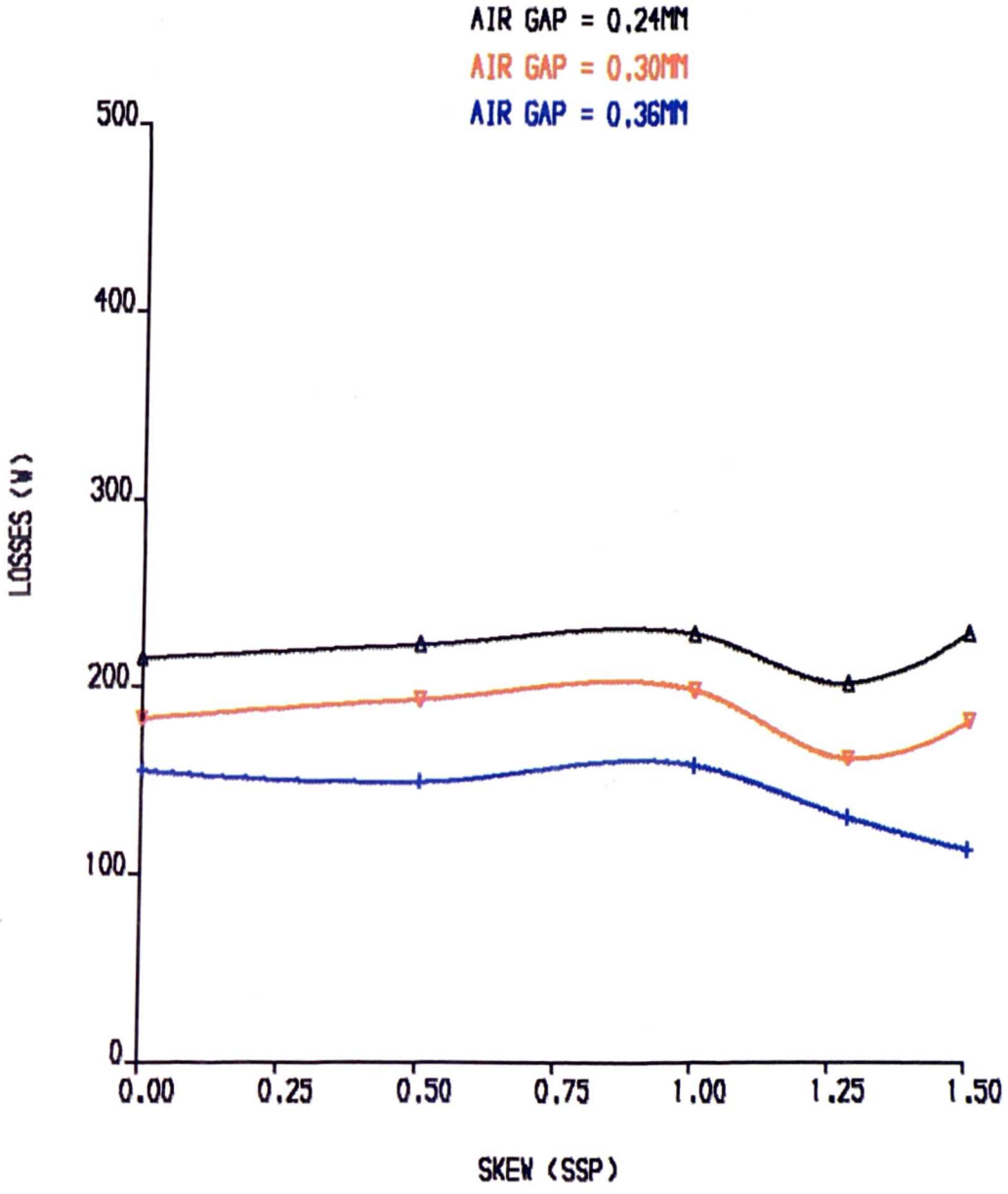

FIG. 5.37 STRAY LOSSES AT 90% RATED CURRENT

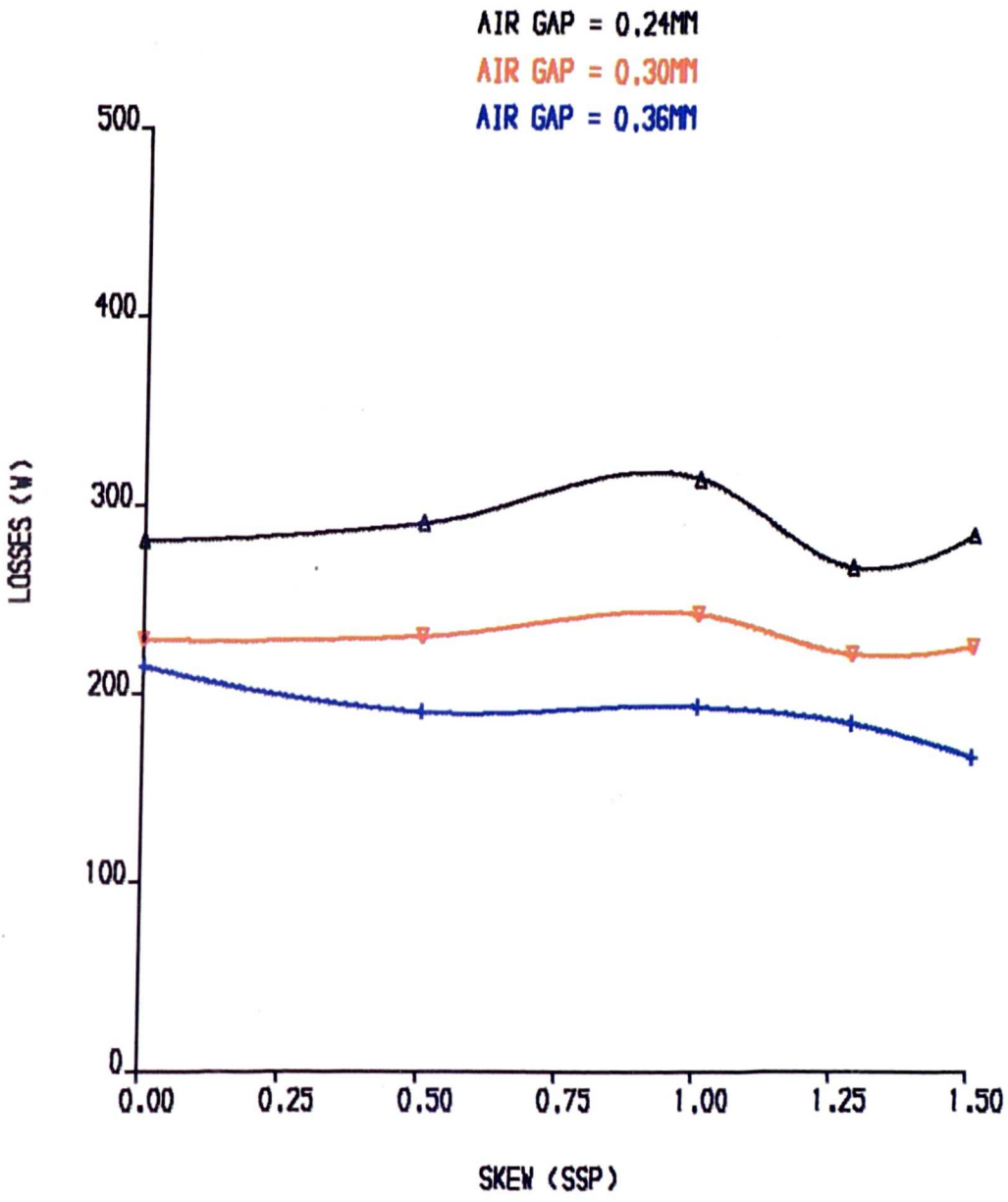

FIG. 5.38 STRAY LOSSES AT 100% RATED CURRENT

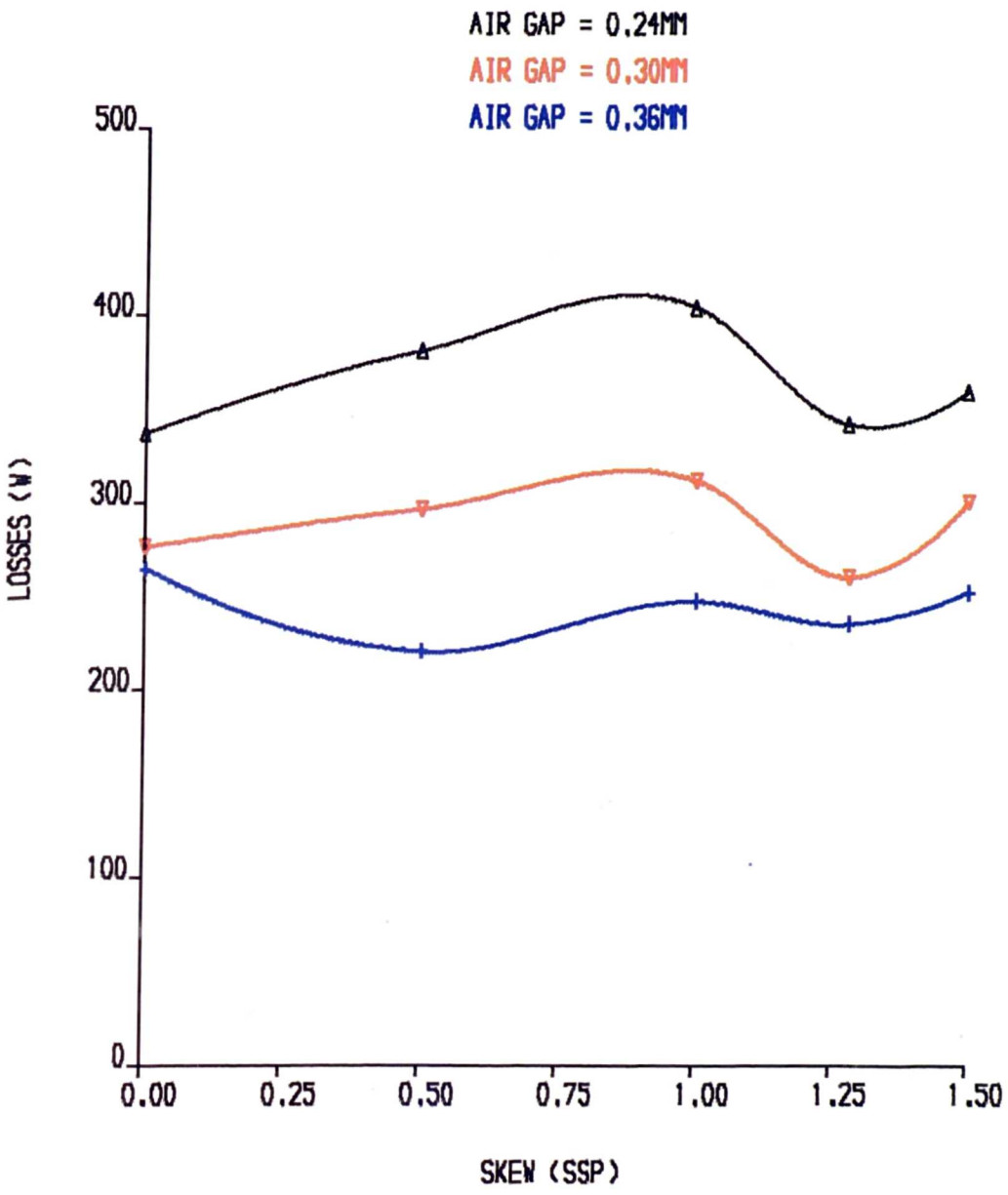

FIG. 5.39 STRAY LOSSES AT 110% RATED CURRENT

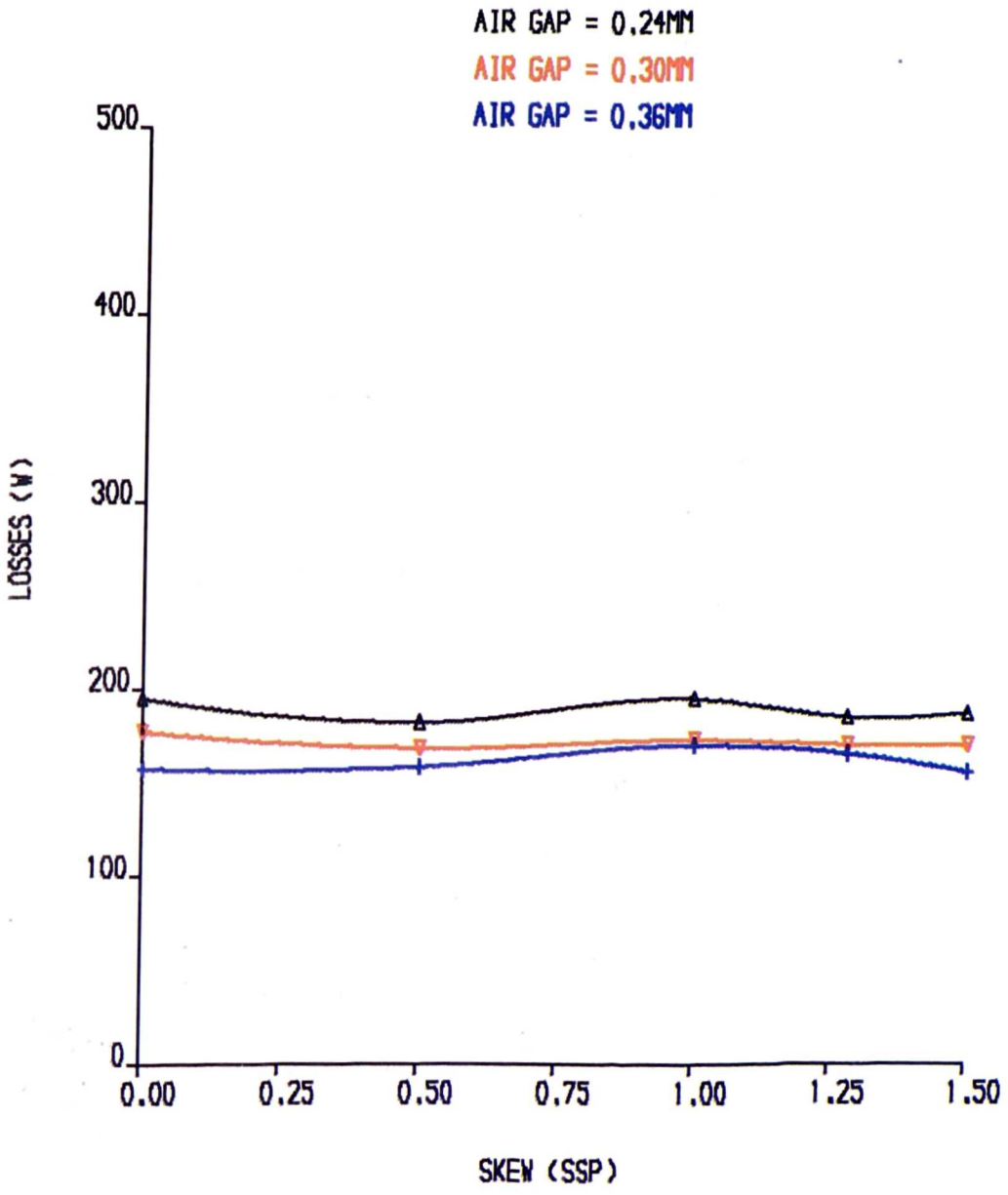

FIG. 5.40 ROTOR I^2R LOSSES AT 90% RATED CURRENT

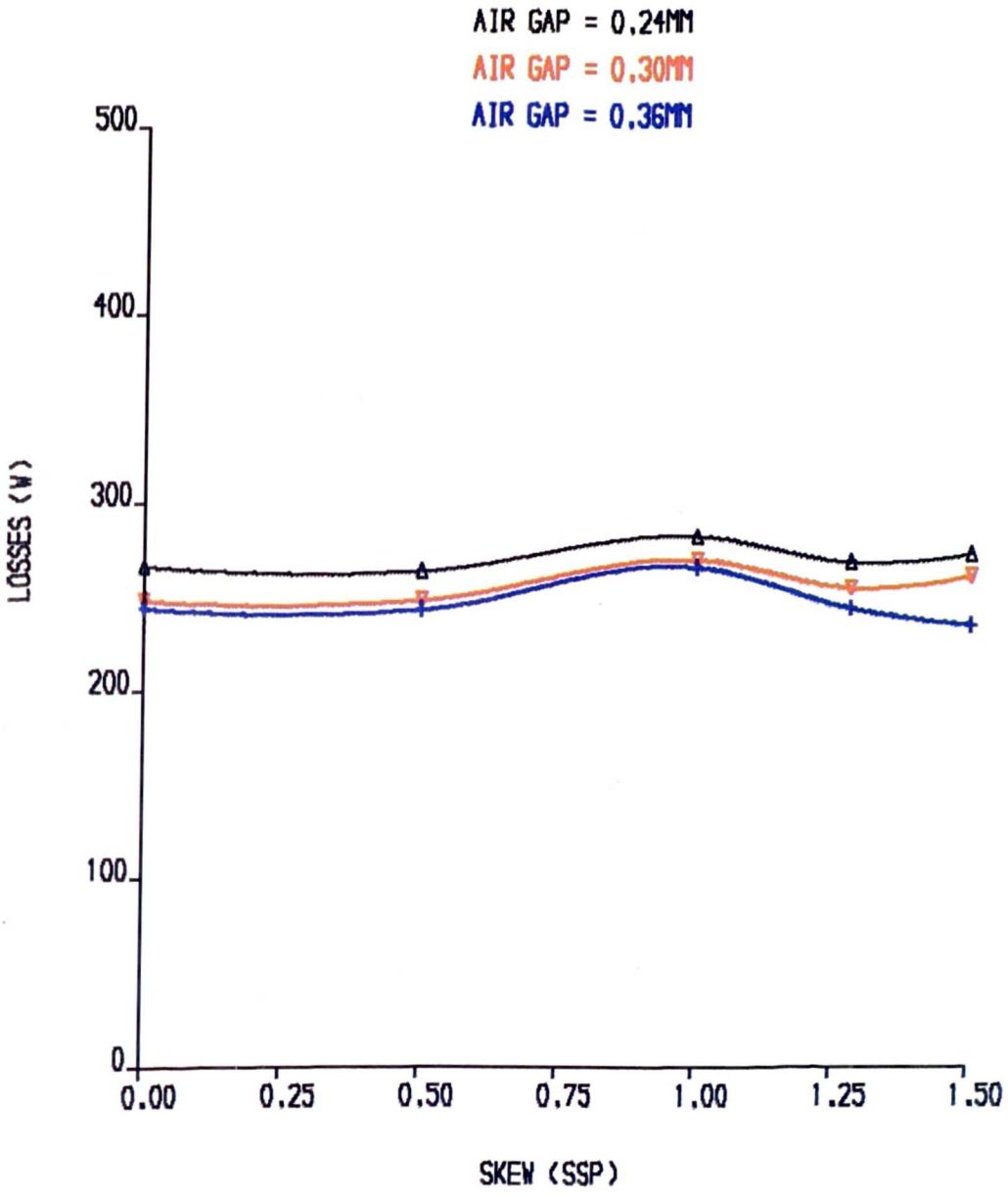

FIG. 5.41 ROTOR I^2R LOSSES AT 100% RATED CURRENT

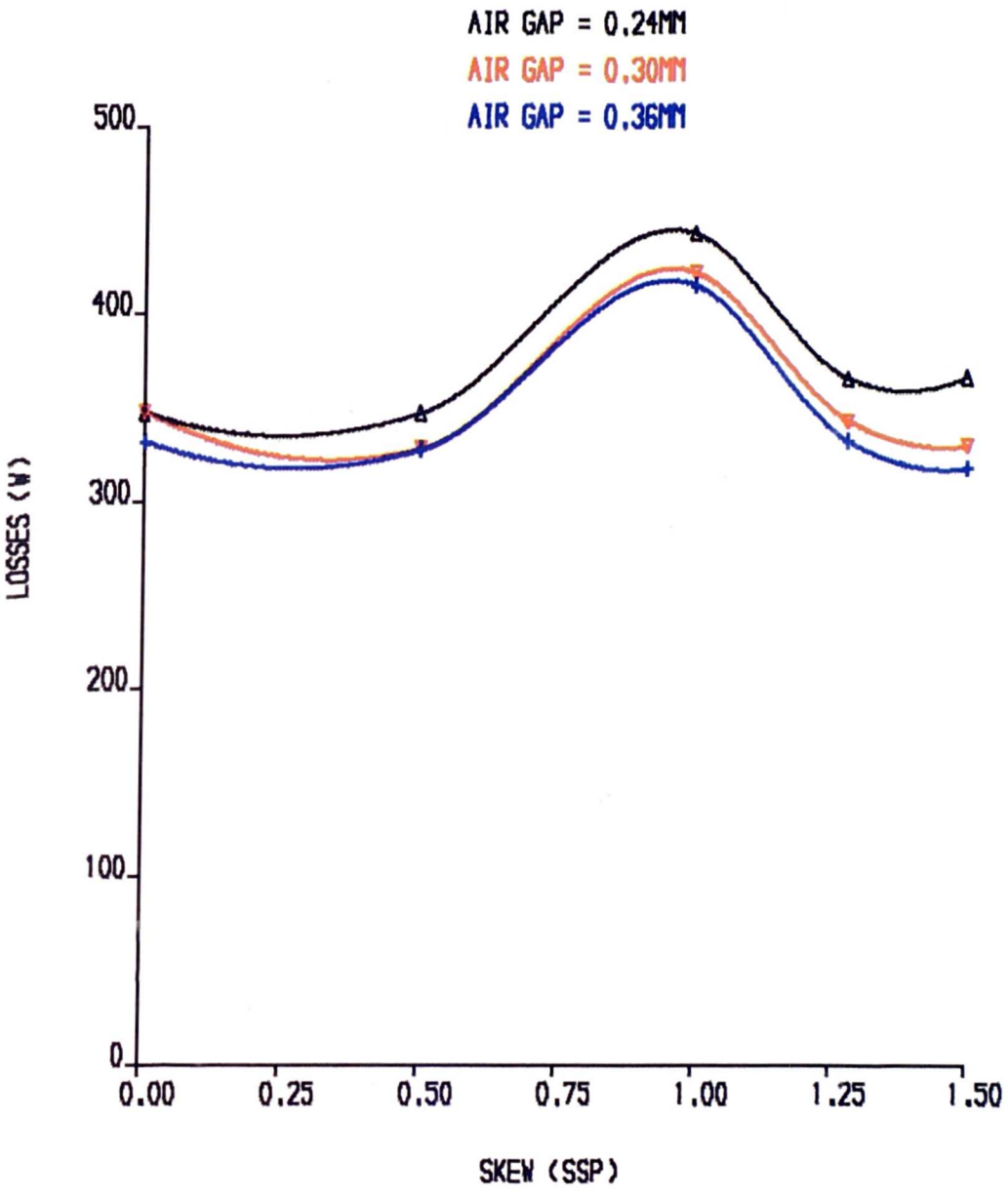

FIG. 5.42 ROTOR I^2R LOSSES AT 110% RATED CURRENT

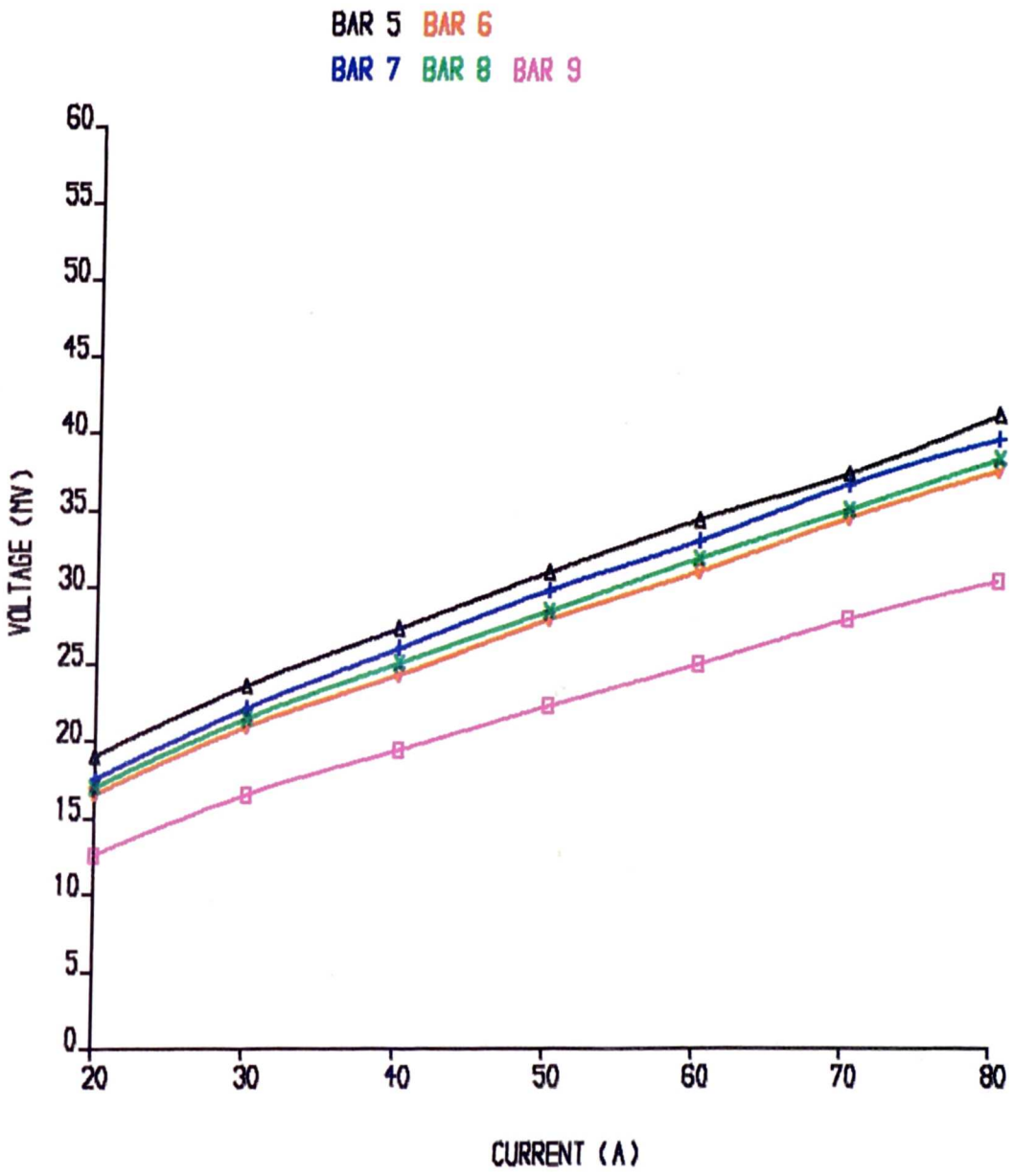

FIG. 5.43 . ROTORBAR IMPEDANCE. ROTOR NO.2.SKEW=0.5SP

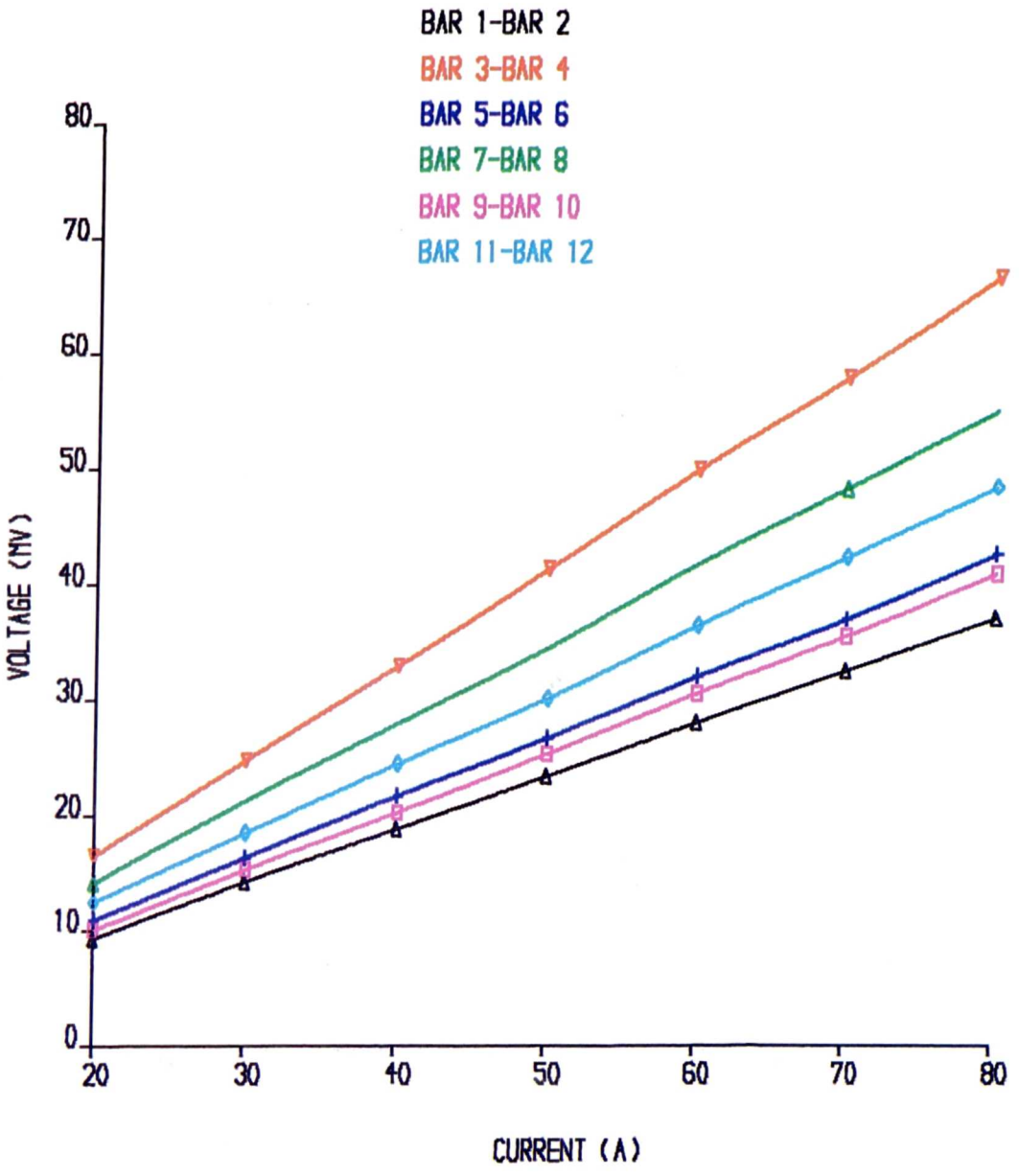

FIG.(5.44). INTERBAR IMPEDANCE. ROTOR NO.2.SKEW=0.5SP

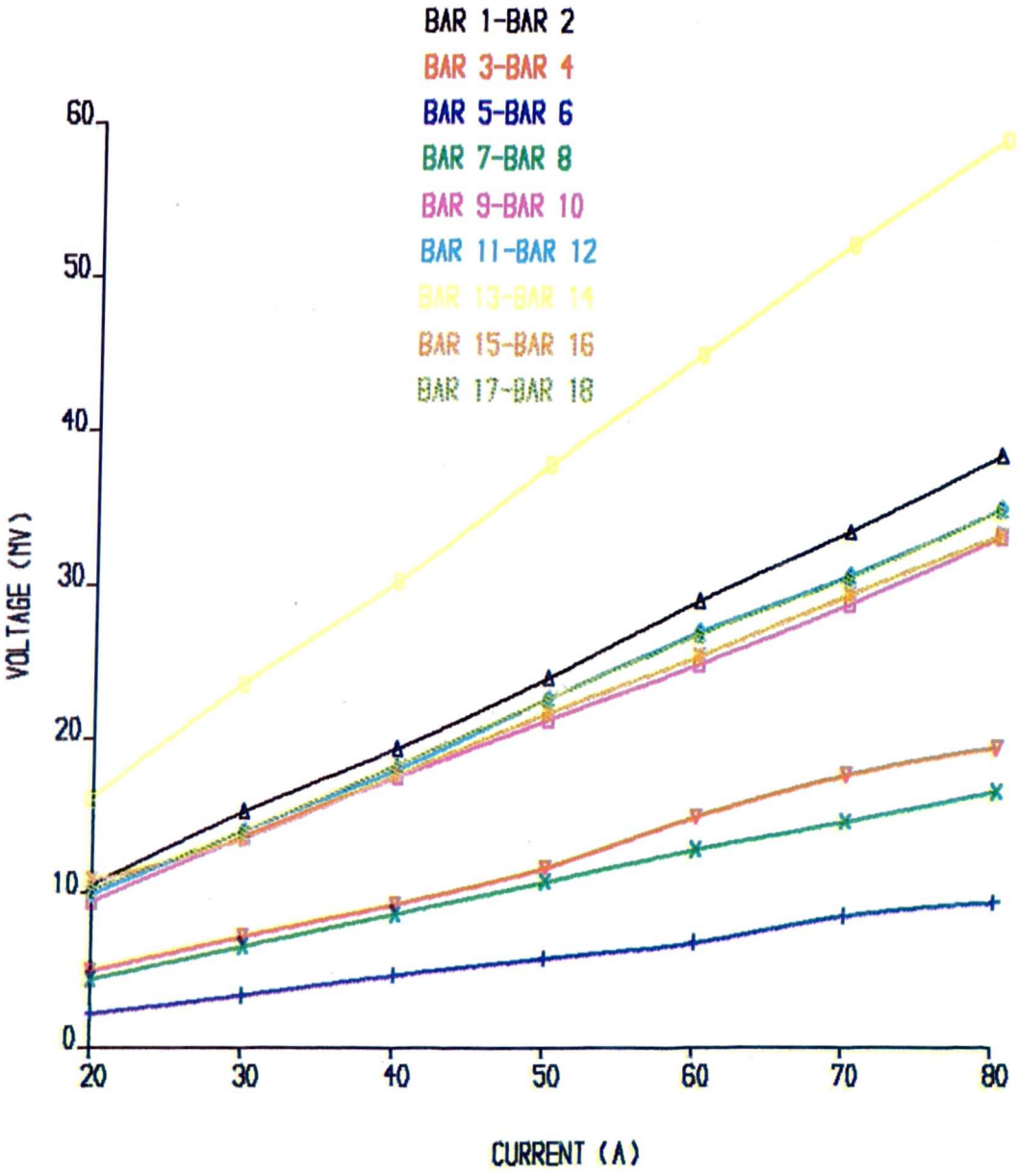

FIG.(5.45). INTERBAR IMPEDANCE. ROTOR NO.8.SKEW=0

CHAPTER SIX

ANALYSIS OF SKEWED INDUCTION MOTOR

INTRODUCTION

The vast majority of induction motors have skewed slots, usually on the rotor but sometimes on the stator. The main purpose of employing skew is the reduction of cogging torques [25], synchronous and asynchronous torques [17][26][27]. It is held by some that skewing leads to a reduction in magnetic noise [28]. Balancing these advantages, skewing has some undesirable effects; it causes changes in the magnetic field distribution and increases both the losses and the leakage reactance[28][29]. If the rotor bars are uninsulated the cross currents between bars increase, contributing to the increase in losses.

Small motors of up to 200KW are almost invariably skewed, but the amount of skew is arbitary, often one stator slot pitch is chosen by the manufacture. Whilst for large motors above 200KW, there is a greater variety, some manufacturers use skewing and whilst others do not.

The effect of skewing on motors performance have been studied previously by a number of workers. Binns [29] discussed the effect of skewing on the flux distribution in machines and showed that the

effect of skewing can be very significant and result in a poorer performance. In his study measurements of the axial variation in the air gap flux due to skewing of the rotor slots were made, revealing a nonuniformity in the fundamental flux, resulting in an axial force on the rotor, an increase in the harmonic fluxes and thus the losses.

Linkous [44] discussed the calculation of the leakage flux in skewed induction motors and analysed the fundamental flux. He has expressed the effect of skew in terms of the change in relative phase of the stator and rotor currents with axial position and concluded that skewing can cause the flux wave to vary significantly across the stack and the fundamental frequency iron losses are increased due to skewing.

Chalmers [6][35] also studied the effect of skewing on the magnetic field distribution in induction motors. His study is based on an ideal assumption that the fundamental m.m.f.s produced by the stator and rotor load currents of an unskewed induction motor are equal and opposite, and produce no additional flux in the air gap. Chalmers concluded that in a skewed motor the small phase displacement between the stator and rotor fundamental m.m.f.s at the ends of the motor produces an increase in the gap flux density, which increases with distance from the centre of the motor, he has called this extra flux skew leakage flux and the losses produced as skew leakage losses.

Alger [28] confined himself to a study of the effect of skewing on the leakage reactance and derived an equation relating the leakage reactance in terms of the degree of skewing and found that the increase in the leakage reactance is a function of the skew angle.

The result of skewing can be broadly described by three effects, namley:-

1 - an axial variation in the magnetising m.m.f due to change in phase between stator and rotor axial currents.

2 - the introduction of an axial component of m.m.f due to the peripheral component of current.

3 - a change in the variation of the gap reluctance caused by the "scissor" action introduced by *skewing*.

Skewing affects both fundamental and harmonic m.m.f's and the latter may be more dramatic. The effect of skewing on flux distribution is clearly very complex and has not yet been successfully tackled. A theoretical treatment of the whole problem is beyond this work, which has primarily been concerend with experimental problem of accurate loss measurement and application of the resultant method to the measurement of loss against skew. It is clear from the work of Binns [29] that there is an axial bunching of flux at one end of the machine even when attention is limited to the fundamental and there is the potential to increase the losses, particularly in the iron of the stator is being worked near

saturation . By inference if a theory based on the fundamental m.m.f and flux it does not produce the type of behaviour observed then clearly the harmonics must play an important role.

The changes in the magnetic field distribution causes a reduction in the mutual reactance and an increase in the leakage reactance. The value of these changes together with the change in the iron losses due to the phase displacement between the stator and rotor m.m.f's depend on the following parameters.

1- load current

2- skew angle

3- core length

The losses due to the cross currents between the rotor bars increase with skewing and the depend on the interbar impedances.

In this chapter the effect of skewing on the performance of induction motor is studied in terms of the fundamental field only. A model for a skewed motor is proposed and the effects of skewing on the changes on the leakage and mutual reactances together with the changes in the losses are discussed.

6.2 MODELLING THE SKEWED MOTOR

The analysis developed in this section is based on a model of the skewed motor which has a number of "sub motors" connected in mechanical parallel and electrical series. For the more frequent case of a skewed rotor device the stator is divided into a number of sub units, each of equal length adding to the complete motor and connected coaxially with corresponding slots connected in series so as to give completely axial currents. A similar number of rotors, all mounted on the same shaft and with corresponding slots in series and end rings at the outer ends is used to represent the rotor. Each rotor has axial slots, but is displaced from its neighbour by an angle such that the overall displacement from end to end corresponds to the skew of the original motor. Such a model can be analysed in circuit terms using methods such as the unified theory of machines [48]. However for brevity a simpler theory based on the similarity of the induction motor to the transformer is used here to derive an equivalent circuit for each sub-motor. A two motor model is developed first, followed by a three motor model to show the difference between the two cases . Then a general case is studied in which a skewed motor is represented by n motors, where n is any integer. The continuos skew of the original motor is thus represented by a "stair case" series of individual motors. The results of this simpler analysis can be shown to be the same as those of more rigorous analysis.

6.2.1 TWO MOTOR MODEL

Considering each sub-motor of the model as a transformer and showing only one phase for simplicity the two component model is shown in figure 6.1.

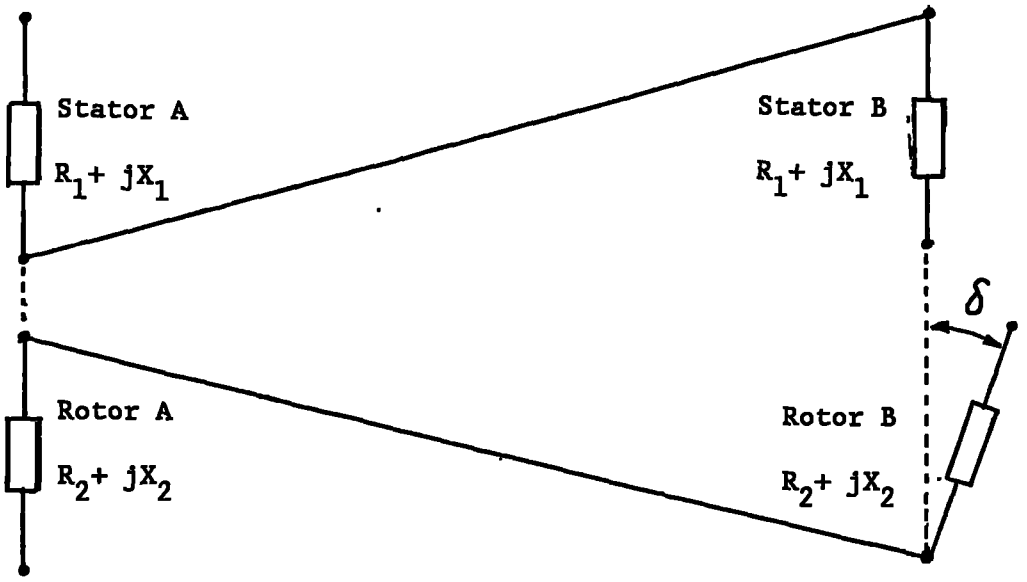

Fig 6.1 Two motor model showing displacement between the stator and rotor windings of the two motors A and B.

The stator of each sub-motor has a resistance R_1 and self inductive reactance X_1 whilst the corresponding values for the rotor are R_2 and X_2 respectively. The essential feature of the model is that the mutual reactances of the two sub-motors have the same magnitudes X_m but that the second sub motor is shifted in space with respect to the first by δ electrical degrees so that the voltage induced in stator B (on open circuit) by a current I_2 in the rotor is

shifted in phase by δ with respect to that in A. Thus for this condition the voltages induced in the two stators can be written as :

Stator A $\quad jX_m I_2$

Stator B $\quad jX_m I_2 e^{-j\delta}$

Whilst for a current I_1 in the stator and the rotors open circuited the voltages induced in the rotors are:

Rotor A $\quad jsX_m I_1$

Rotor B $\quad jsX_m I_1 e^{+j\delta}$

Where s is the slip in the normal way.

If the total skew of the machine to be modelled is α then the phase shift between the two rotors should be $\alpha/2$ as shown in figure 6.2.

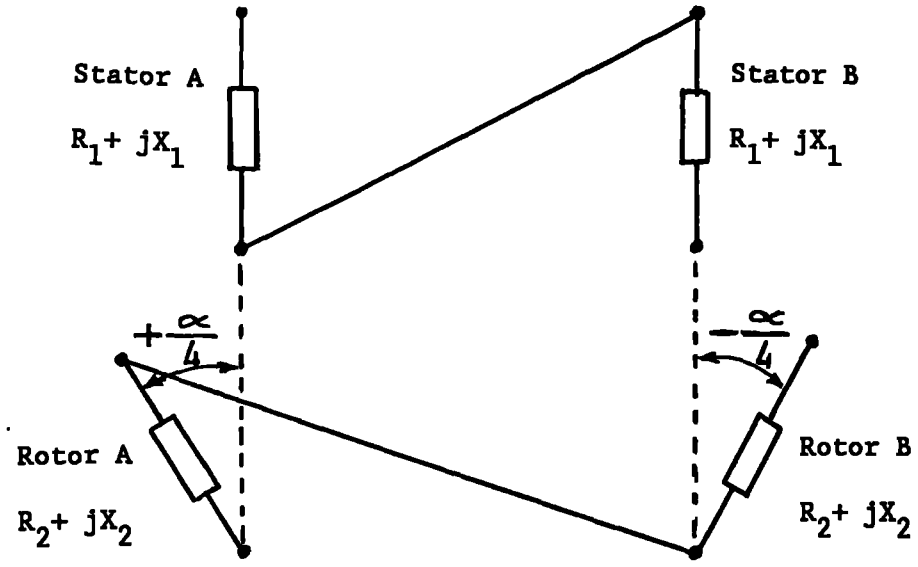

Fig 6.2 Phase shift between the two rotors A and B

For subsequent analysis it is convenient to take the reference for the phase shift in the centre of the machine yielding the induced voltages in the form:

Rotor to stator	$jX_m I_2 e^{+j\alpha/4}$	for A
	$jX_m I_2 e^{-j\alpha/4}$	for B
Stator to rotor	$jsX_m I_1 e^{-j\alpha/4}$	for A
	$jsX_m I_1 e^{+j\alpha/4}$	for B

Thus using conventional transformer ideas applied to induction motor the circuit equations can be written:

$$V_1A = I_1 (R_1 + jX_1) + (I_2 jX_m) \; e^{+j\alpha/4} \qquad .....6.1$$

$$V_1B = I_1 (R_1 + jX_1) + (I_2 jX_m) \; e^{-j\alpha/4} \qquad .....6.2$$

$$V_2A = jsX_m I_1 \; e^{-j\alpha/4} + (R_2 + jsX_2) I_2 \qquad .....6.3$$

$$V_2B = jsX_m I_1 \; e^{+j\alpha/4} + (R_2 + jsX_2) I_2 \qquad .....6.4$$

Where : V_1A and V_1B are the voltage acros stators A and B

and V_2A and V_2B are the voltage across rotors A and B

For the complete motor:

$$V_1 = V_1A + V_1B \qquad .....6.5$$

$$= 2I_1(X_1 + jX_1) + + jX_m \; I_2(e^{-j\alpha/4}) \qquad ..... .6.6$$

$$= 2I_1(R_1 + jX_1) + jX_m \; I_2(2\cos\alpha/4) \qquad .....6.7$$

$$\text{and } V_2 = 0 = V_2A + V_2B \qquad .....6.8$$

$$= 2jsX_m I_1 \cos\alpha/4 + 2(R_2 + jsX_2) I_2 \qquad .....6.9$$

dividing by s

$$0 = 2jX_m I_1 \cos\alpha/4 + 2(R_2/s + jX_2) I_2 \qquad .....6.10$$

Considering and rearranging the stator equation:

$$V_1 = 2(R_1 + jX_1 - jX_m + jX_m - jX_m \cos\alpha/4) I_1 + 2jX_m \cos\alpha/4 (I_1 + I_2) .....6.11$$

$$V_1 = 2[(R_1+j(x_1+X_m(1-\cos\alpha/4))]I_1$$
$$+2jX_m\cos\alpha/4(I_1+I_2) \quad \ldots\ldots\ldots 6.12$$

Where $x_1 = X_1 - X_m$ is the conventional leakage reactance (assuming unity turns ratio for simplicity)

The rotor equation can be similarly manipulated to yield:

$$0 = 2jX_m\cos\alpha/4(I_1+I_2) + 2(R_2/s+jx_2+X_m(1-\cos\alpha/4)I_2 \quad \ldots\ldots\ldots 6.13$$

Where $x_2 = X_2 - X_m$ is the rotor leakage reactance of the complete motor.

These equations for the stator and rotor of the complete motor can be represented by the equivalent circuit shown in figure 6.3. Similar manipulation of the equations for each sub motor yield equivalent circuits for the two sub motors shown in figure 6.4.

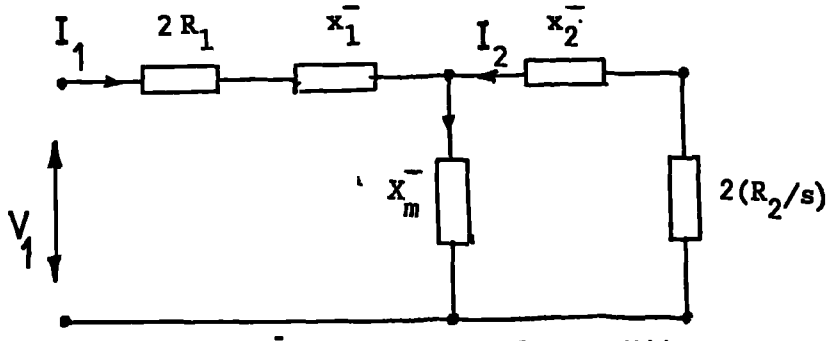

$$x_1^- = 2\ (x_1 + X_m(1-\cos\alpha/4))$$
$$x_2^- = 2\ (x_2 + X_m(1-\cos\alpha/4))$$
$$X_m^- = 2\ X_m\cos\alpha/4$$

Fig 6.3 Equivalent circuit of two machine model

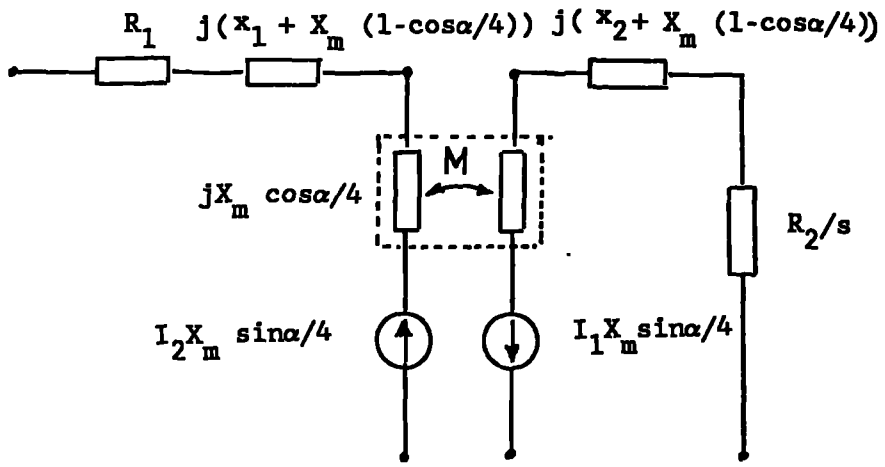

Fig 6.4 Equivalent circuit of one machine only

6.2.3 THREE MOTOR MODEL

In this model the skewed motor is represented by three motors instead of two, the first and the third rotors are displaced from their stators by (+α/3) and (-α/3),while the second rotor is in phase with its stator . Figure (6.5) shows the displacement between the three rotors A,B and C.

Applying the same rules as in case of the two machines model, the new parameters of the skewed motor represented by three machines are:

$$x_1^- = 3(x_1 + X_m) - X_m (1+2\cos\alpha/3) \quad \text{.....6.14}$$

$$x2^- = 3(x_2 + Xm) - X_m (1+2\cos\alpha/3) \quad \text{.....6.15}$$

$$Xm^- = (1+2\cos\alpha/3)X_m \quad \text{.....6.16}$$

Where: x_1, x_2, X_m are the parameters of one motor only and they are the same for the three motors.

And x_1^-, x_2^-, x_m^- are the equiv. cct. parameters of the complete motor(three motors)

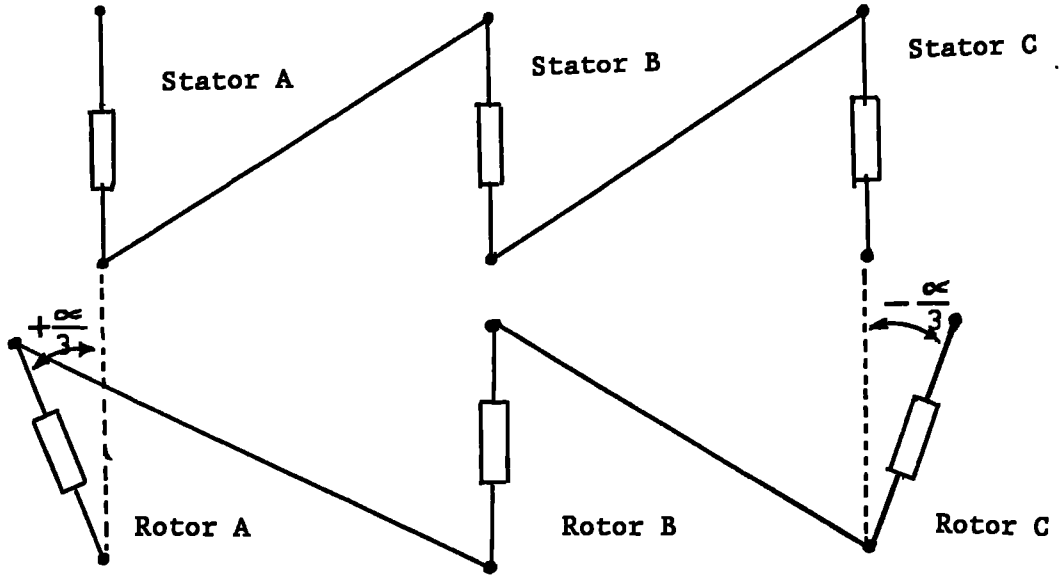

Fig 6.5 Three machine model

6.2.4 GENERAL EQUATIONS

From the two motor model and the three motor model general equations expressing the primary and the secondary leakage reactances and the magnetising reactance for a skewed motor represented by n motors are derived as shown below .The equivalent circuit of n sub

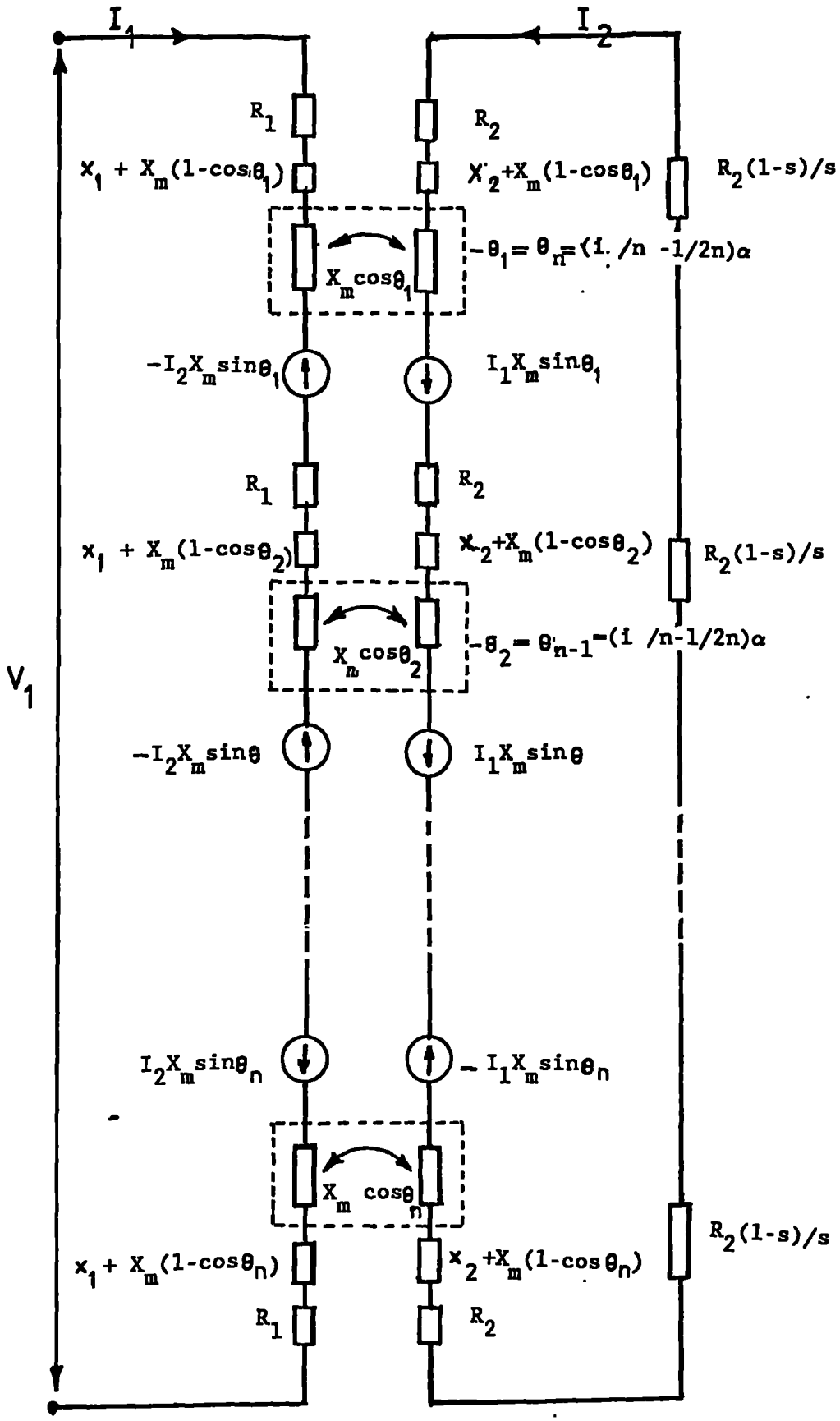

Figure 6.6 Equivalent circuit of n sub motors

motors representing a skewed motor and a stair case showing the phase displacement between the adjacent rotors are given in figures 6.6 and 6.7, n can be either odd or even.

For n = Odd number:

$$X_m = X_m \left(1 + 2 \sum_{i=1}^{i=(n-1)/2} \cos i\alpha/n\right) \qquad \text{.....6.17}$$

$$x_1 = nx_1 + X_m \left(n - 1 - 2\sum_{i=1}^{i=(n-1)/2} \cos i\alpha/n\right) \qquad \text{.....6.18}$$

$$x_1 = nx_2 + X_m \left(n - 1 - 2\sum_{i=1}^{i=(n-1)/2} \cos i\alpha/n\right) \qquad \text{.....6.19}$$

For n = Even number:

$$x_1 = n\,x_1 + n\,X_m \left(1 - 2/n \sum_{i=1}^{i=n/2} \cos\left(i\alpha/n - \alpha/2n\right)\right) \qquad \text{.....6.20}$$

$$x_2 = n\,x_2 + n\,X_m \left(1 - 2/n \sum_{i=1}^{i=n/2} \cos\left(i\alpha/n - \alpha/2n\right)\right) \qquad \text{.....6.21}$$

$$X_m = 2\,X_m \sum_{i=1}^{i=n/2} \cos(i\alpha/n - \alpha/2n) \qquad \text{.....6.22}$$

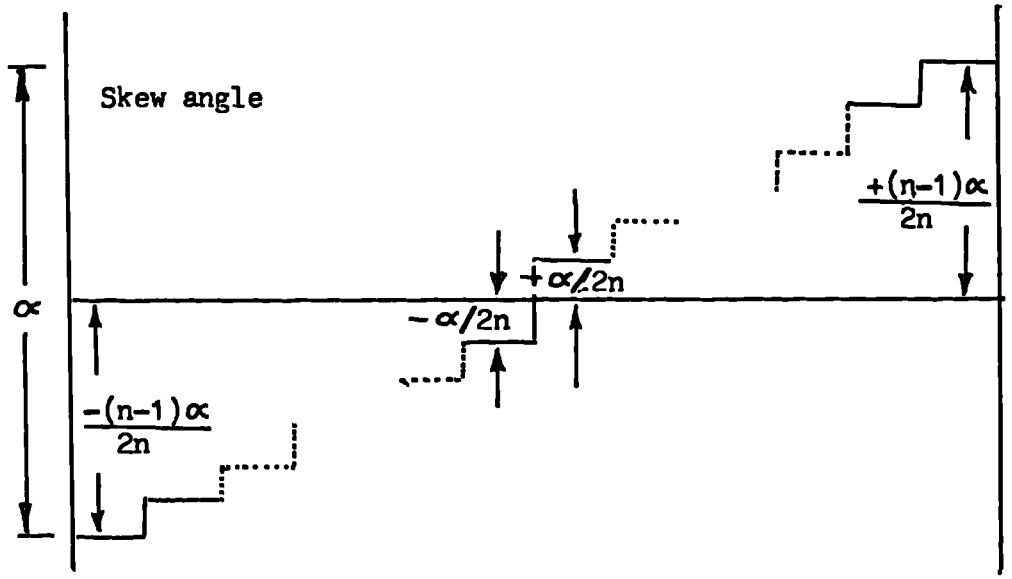

Fig 6.7 Staircase modelling of the phase displacement between the adjacent n sub rotors and the stators

The general equations obtained above have been applied for n = 1 to 10 and 20 motors, in each case the values of the total leakage reactance of the primary and the secondary circuits of the skewed motor represented by n motors have been calculated at α = 20 elect degree, as shown in table 6.1.Values of x_1, x_2 and X_m used in this calculation are determined from no load and locked rotor tests carried out on unskewed motor. (appendix A).

$x_1 = 7.51\Omega$ $x_2 = 10.14\Omega$ $X_m = 149\Omega$

n	X_m^-	x_1^-	x_2^-
2	148.43	8.07	10.7
3	148.33	8.18	10.81
4	148.29	8.21	10.84
5	148.27	8.23	10.86
6	148.26	8.24	10.87
7	148.26	8.25	10.88
8	148.25	8.25	10.88
9	148.25	8.26	10.89
10	148.25	8.26	10.89
20	148.25	8.26	10.89

Table(6.1) Equivalent circuit parameters of a skewed motor

In this model as mentioned before, n can be any integer above one, but it is very important to select the number of the sub-motors, in order to give the best representation of a skewed motor. For that purpose the values of the primary and the secondary leakage reactance together with the magnetising reactance given in table (6.1) have been plotted against the number of sub motors, n, used in the model as shown in figure.(6.8). It can be seen that the changes in the values of $\bar{x_1}$, $\bar{x_2}$ and $\bar{X_m}$ for n=1 to n=4 are significant, and above that number the changes are only marginal, but for n=10 to n=20 the changes are very small and can be neglected. For the sake of simplicity in calculations and modelling, the skewed motor is represented by 10 sub motors, and all the calculations for predicting the changes in leakage and magnetising reactances , in the air gap voltage and the losses in a skewed motor have been made for on that basis.

6.3 PERFORMANCE CALCULATION OF A SKEWED MOTOR

The equivalent circuit and the circuit parameters derived in (section 6.2.4) for a general case representing a skewed motor by 10 sub motors are used in this section to examine the performance of the skewed motor under no lod and load condition . Stator and rotor currents I_1 and I_2, iron losses W and rotor conductor losses, output power P_o and the torque T are determined as follows:

For n even (section 6.2.4)

$$x_1 = n\,x_1 + X_m\,(1-2/n\,\Sigma_{i-1}^{i-n/2}\cos\,(i\alpha/n - \alpha/n)) \quad \ldots\ldots\ldots 6.20$$

$$x_2 = n\,x_2 + X_m\,(1-2/n\,\Sigma_{i=1}^{i-n/2}\cos\,(i\alpha/n - \alpha/n)) \quad \ldots\ldots\ldots 6.21$$

$$X_m = 2\,X_m\,\Sigma_{i=1}^{i-n/2}\cos(i\alpha/n - \alpha/n) \quad \ldots\ldots\ldots 6.22$$

If the skewed motor, (n sub motors), are supplied from a sinusoidal supply V_1,

For a given S:

$$I_2 = \frac{V_1}{(a + b/s + j(c + d/s))} \quad \ldots\ldots\ldots 6.23$$

$$I_2 = \frac{V_1\,(a+b/s - j(c+d/s))}{(a+b/s) + (c + d/s)} \quad \ldots\ldots\ldots 6.24$$

$$\text{Re } I_2 = \frac{V_1(\,a + b/s)}{(a+b/s) + (c + d/s)} \quad \ldots\ldots\ldots 6.25$$

$$\text{Im } I_2 = \frac{-(c + d/s)\,V1}{(a+b/s) + (c+d/s)} \quad \ldots\ldots\ldots 6.26$$

Thus

$$[I_2] = \sqrt{((\text{Re } I_2)(\text{Re } I_2) + (\text{Im } I_2)(\text{Im } I_2))} \quad \ldots\ldots\ldots 6.27$$

And from equation 6.27 I_1 can be driven as:

$$I_1 = I_2\,(((1 + x_2/X_m) + R_2/sR_m) - j(R_2/sX_m - X_m/Rm)) \ldots\ldots 6.28$$

$$= I_2\,((e+f/s) + j(h-g/s) \quad \ldots\ldots\ldots 6.29$$

$$= ((e + f/s) + j(-g/s + h)(\text{Re } I_2 + j\text{Im } I_2)) \quad \ldots\ldots\ldots 6.30$$

$$\text{i.e. Re } I_1 = (e+f/s)\,(\text{Re } I_2) - (h-g/s)(\text{Im } I_2) \quad \ldots\ldots\ldots 6.31$$

$$\text{Im } I_1 = (h-g/s)\,(\text{Re}I_2\,) + (e+f/s)(\text{Im } I_2) \quad \ldots\ldots\ldots 6.32$$

And $[I_1] = \sqrt{(Re\ I_1 \times Re\ I_1 + Im\ I_1 \times Im\ I_1)}$ 6.33

Now the rotor conductor losses W_2, the output power Po and the output torque T can be derived as:

$W_2 = 3(I_2 \times I_2 \times R_2)$ 6.34

$P_o = 3(I_2 \times I_2 \times R_2\ (1-s)/s)$ 6.35

The change in the value of R_2 due to skewing of the rotor bars can be taken into consideration. Equation 2.8 derived in section 2.2.4.3 expressing the change in rotor resistance in terms of skew angle, is used here to calculate the value of the rotor resistance at each skew angle.

$\bar{R}_2 = R_2 + \Delta R_2$ 6.36

$\Delta R_2 = K_s R_2(1/\cos\alpha - 1)$ 6.37

where K_s is the ratio of the rotor bar resistance to the total rotor resistance, in this model it is taken as 0.9 (based on GEC design data), and R_2 is the rotor resistance at zero skew.

$T = P_o / (50 \times \pi (1-s))$ 6.38

Where:

$a = R_1 + R_1(X_2/X_m) - x_1(x_2/X_m)$

$b = R_2 + R1(R_2/R_m) + x_1(R_2/X_m)$

$c = x_1 + x_2 + x_1(x_2/X_m) + R_1(x_2/R_m)$

$d = x_1\ (R_2/R_m) - R_1(R_2/X_m)$

$e = 1 + x_2/X_m$

$f = R_2/R_m$

$$g = R_2/X_m$$

$$h = x_2/R_m$$

For n = even number, the air gap voltage across each motor is:

$$dE_{1i} = I_1\, jX_m/n \cos(i\alpha/n - \alpha/n) + I_2\, jX_m/n \cos(i\alpha/n - \alpha/n) + I_2\, X_m/n \ \mathrm{Sin}(i\alpha/n - \alpha/n) \quad \ldots\ldots\ldots\ldots 6.39$$

Assuming $Q = \alpha\,(i - n/2 - 1/2)$ 6.40

$$\mathrm{Re}\ dE_{1i} = -\mathrm{Im}\ I_1\,(X_m)\ \mathrm{Cos}\ Q/n + \mathrm{Im}\ I_2\,(X_m)\ \mathrm{Cos}\ Q/n + \mathrm{Re}\ I_2\,(Xm)\ \mathrm{Sin}\ Q/n \quad \ldots\ldots\ldots\ldots 6.41$$

$$\mathrm{Im}\ dE_{1i} = +\mathrm{Re}\ I_1\,(X_m)\ \mathrm{Cos}\ Q/n - \mathrm{Re}\ I_2\,(X_m)\ \mathrm{Cos}\ Q/n + \mathrm{Im}\ I2\ (Xm)\ \mathrm{Sin}\ Q/n \quad \ldots\ldots\ldots\ldots 6.42$$

Where : X_m is the mutual reactance of the original motor.

$$dE_1 = \sqrt{(\mathrm{Re}\ dE_1 \times \mathrm{Re}\ dE_1 + \mathrm{Im}\ dE_1 \times \mathrm{Im}\ dE_1)} \quad \ldots\ldots\ldots\ldots 6.43$$

The The voltage across the whole motor is given by :

$$E = \Sigma_1^n\, dE \quad \ldots\ldots\ldots\ldots 6.44$$

and the total iron loss for the whole motor is given by similar equation, $W = \Sigma_1^n\, dW$ 6.45

Where n = No. of sub motors

It is generally accepted that the iron loss can be represented by an exponential function of voltage, thus for a submotor:

$dW \alpha (dE)^k$, k varies from 2.18 to 3.45, section 5.4 ..... 6.46

i.e $dW_1/dW_2 = [\, dE_1/dE_2]^k$ 6.47

Now if dW_2 is taken as the loss in the no load case then:

$$dW_2 = W_o/n \quad \text{.....6.48}$$

and $$dE_2 = E_o/n \quad \text{.....6.49}$$

Where W_o and E_o are no load iron losses and voltage respectively.

Substituting equation 6.48 and 6.49 in 6.47 yields:

$$dW_1 = W_o/n \, [n \, dE_1/E_o]^k \quad \text{.....6.50}$$

But the total no load iron losses W_0 for the unskewed motor is:

$$W_o = 3 V^2 (1/R_m - (1/X_m + 1/R_m) R_1) \quad \text{.....6.51}$$

By substituting W_o from equqtion 6.51 in equation 6.50, iron losses dW in each sub motor can be determined . Then the total iron losses of a skewed motor represented by 10 motors can be found by adding the iron losses of the 10 sub motors.

Using the equations derived above, the leakage and magnetising reactances ,x_1^-, x_2^- and X_m^- of the skewed motor represented by 10 sub motors are calculated at different skew angles, from the measured equivalent circuit parameters for a zero skew machine (appendix A). These calculated values are given in table 6.2 and plotted against skew in figure 6.9.

It can be seen that the stator and rotor leakage reactances x_1^- and x_2^- are increased by skew in the same way, while the magnetising

reactance X_m^- decreases with skew. In a real machine the variation of the leakage and magnetising reactances are more complex than that seen from figure 6.9 due to the involvement of other factors, i.e the effect of harmonic fluxes, saturation, etc., and these parameters may not vary in this way.

Skew	x_1^-	x_2^-	X_m^-
0	7.51	10.14	149.0
10	7.70	10.33	148.8
20	8.26	10.89	148.3
25	8.68	11.31	147.8
30	9.19	11.82	147.3

Table 6.2 Variation of mutual and leakage reactances at different skew angle (in elect. angle) and for 10 series motors.

Iron losses at no load and at load are calculated at different skew angle together with the rotor conductor losses and plotted in figure 6.10 using the equations derived above. It can be seen that these losses increase with skew. As explained earlier, at the begining of this chapter, there are several factors playing roles in determining the losses and their variations with skew in cage motors. In this model the effect of the changes in the fundamental flux and the rotor conductor resistance on the losses are considered, whilst other changes due to the cross currents and harmonic fluxes are not.

Therefore the discrepency noticed between the predicted and measured results as far as the change in losses due to skewing is concerned are likely to be due to these other mechanisms.

The axial variation in the induced e.m.f in the winding of a skewed motor represented by 10 sub motors are presented in figure 6.11 at different skew angles . It can be observed that at zero skew the e.m.f is the same along the stator core as shown by a straight horizantal line, as the skew increases the e.m.f. tend to increase from the centre of the motor towards one end and decreases towards the other end showing the axial change in the magnetic field distribution of the skewed motor.

Although this analysis is limited to the fundamental flux, these not giving a complete picture of the changes in the performance of the motor due to skewing, it can be used as a basis and extended to a more comprehensive model in future to include the changes due to harmonic fluxes. However at this stage it can be considered as a useful tool for investigating the changes in the losses and leakage reactances attributable to the fundamental flux change.

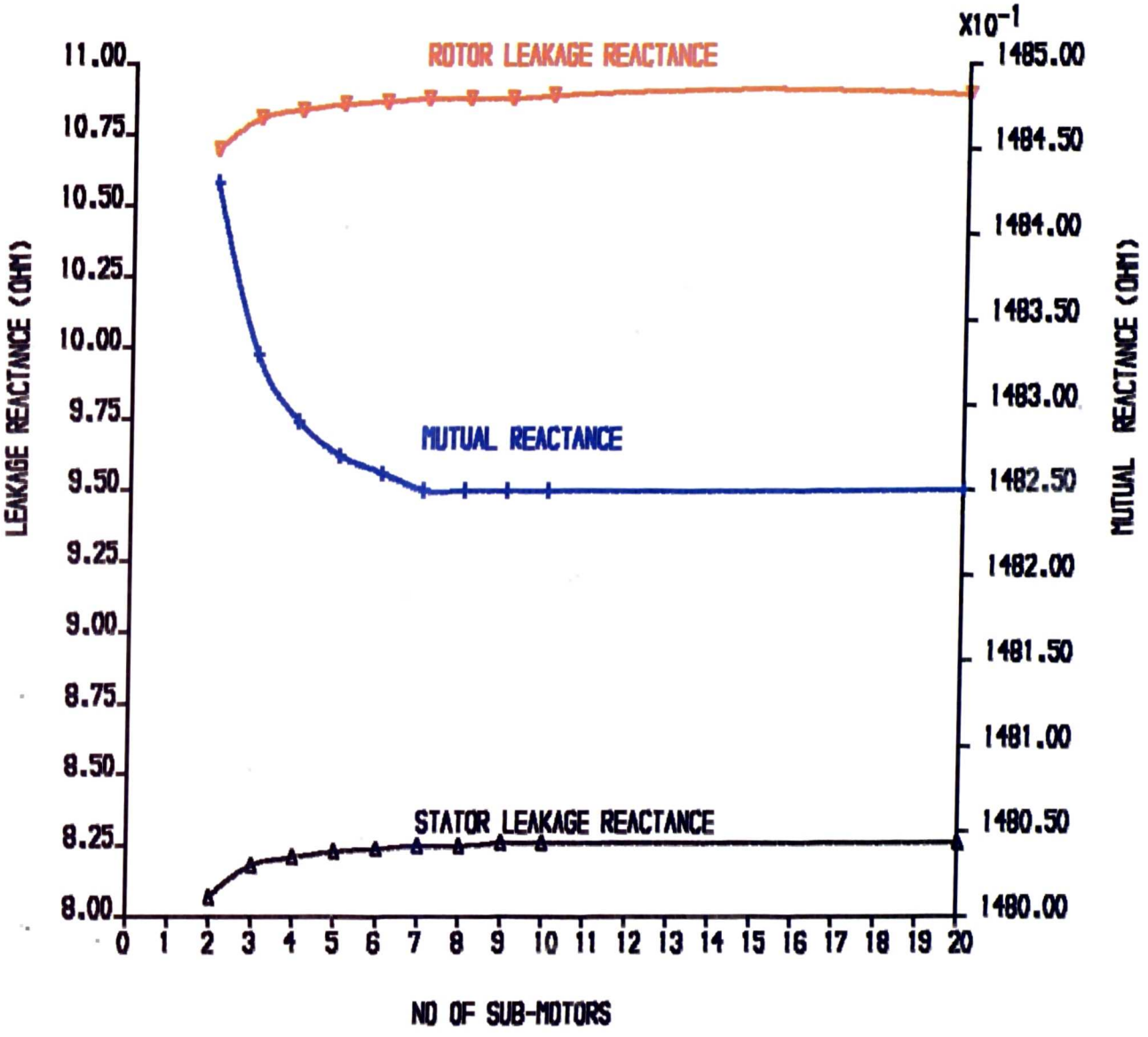

FIG. 6.8 .VARIATION OF MUTUAL AND LEAKAGE REACTANCE WITH NO. OF SUBMOTORS

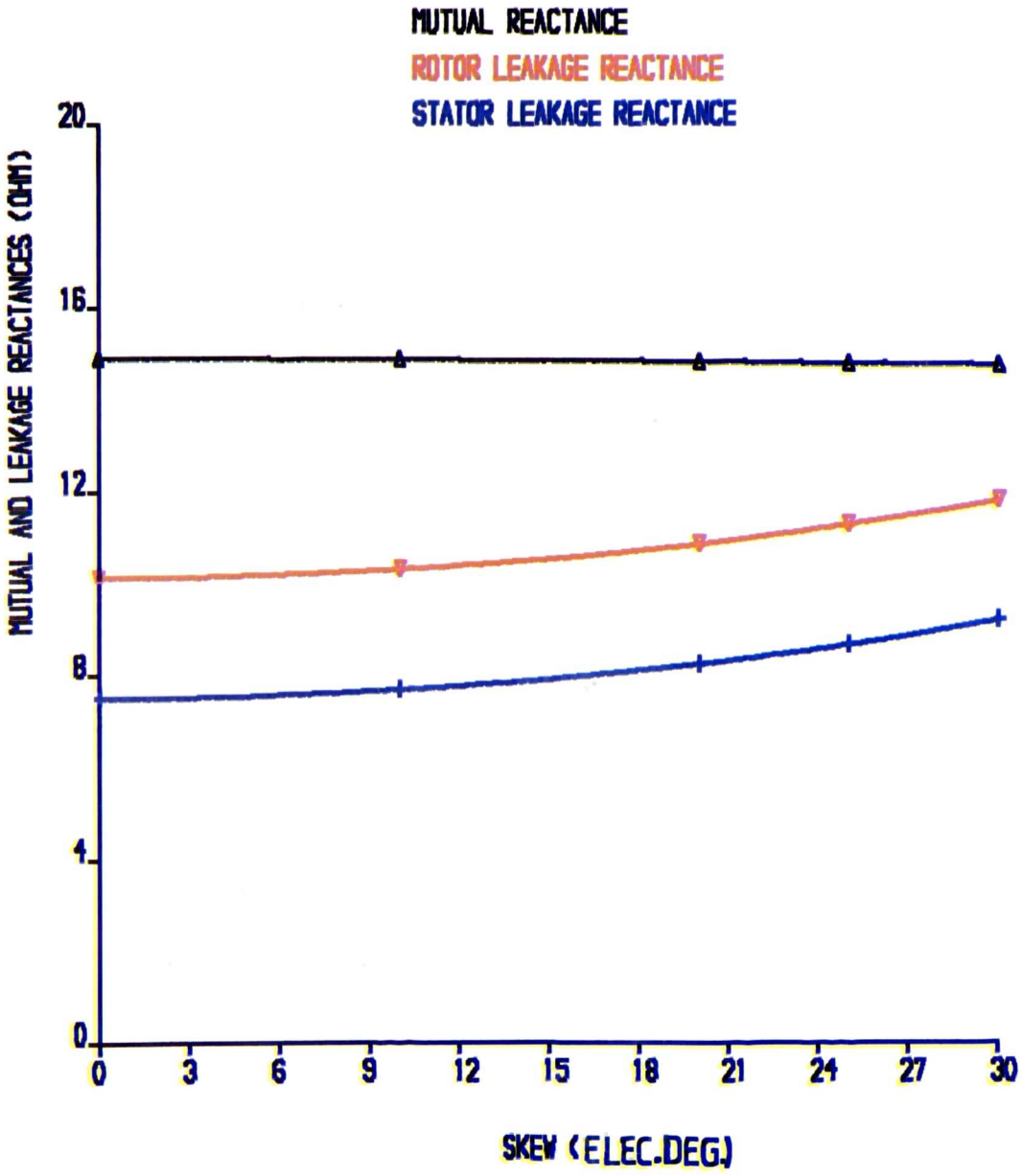

FIG. 6.9 .VARIATION OF MUTUAL AND LEAKAGE REACTANCE WITH SKEW

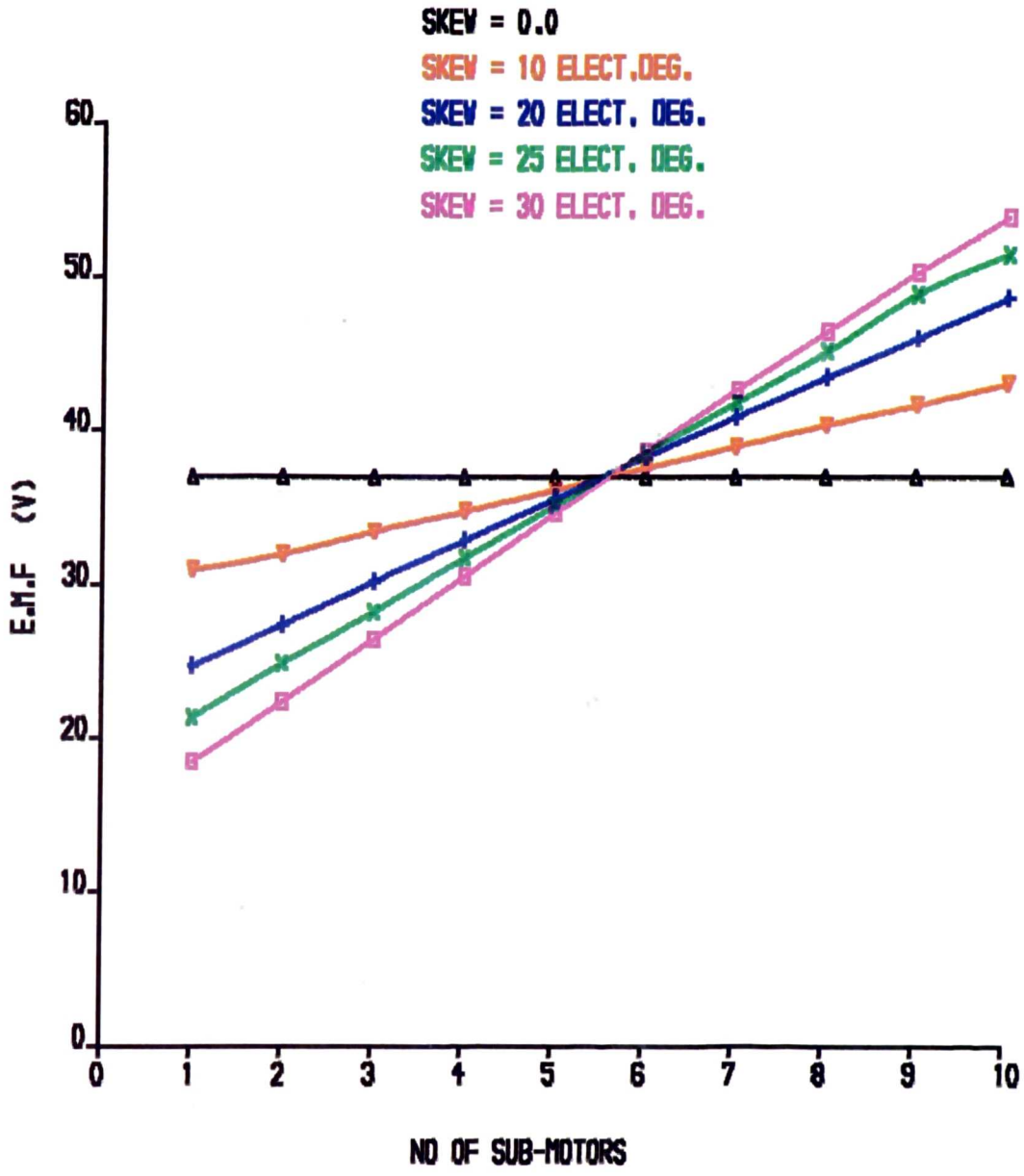

FIG. 6.11. VARIATION OF INDUCED E.M.F IN THE 10 SUBMOTORS WITH SKEW

CHAPTER SEVEN

SUMMARY AND CONCLUSIONS

7.1 THE CALORIMETER

The objectives of this project were to investigate the balance calorimetric method of loss measurement, specifically for small TEFV machines and to use the method to investigate the variation in the losses of a 5.5 kW cage induction motor with design parameters such as skew, air gap and winding configuration. To achieve these objectives a calorimeter system was built and used successfully for measuring total losses of the test motors. During the construction of the whole system several difficulties were encountered and given careful consideration. The shape and the size of the calorimeter was chosen in order to obtain a good heat transfer from the test motor to the air flow and adequate mixing of air inside the colorimeter. The calorimeter was built from panels made of insulating materials and jointed tightly to minimise the heat leakage. Air at a constant flow rate was forced through the calorimeter by means of a centrifugal fan mounted at the inlet of the air duct. A preheater was placed inside the air feed duct and operated under the control of a closed loop system to preheat the air to $20^{o}C$. The air ducting was insulated from the surrounding to reduce the thermal coupling between the inlet and outlet of the calorimeter. Inlet air cooling was provided and used at times when the ambient temperature was above

20°C. Monitoring of the air flow rate was achieved by using a water manometer to indicate the pressure difference across a choke plate placed inside the duct above the inlet chimney. The calorimeter was operated in a balance mode, with a resistive heater being used as the alternative heat source. This heater consisted of 4 elements in order to reduce its surface temperature and minimise heat radiation from its surface; appropriate additional insulation was provided in the vicinity of the heater. The inlet and oulet temperatures were measured by means of platinum resistance thermometers having a resolution of 0.1°C and placed inside the inlet and outlet chimneys.

Several tests were carried out in order to examine the repeatability of the test results. For these tests the induction motor was disconnected from the supply and driven externally at a constant speed. The main heater was used to provide heat. The tests were repeated on different days and at different times of the day and repeatable results were obtained. Then a series of results were obtained at different power inputs to the main heater yielding a set of input power against temperature difference pairs. These were plotted and used to determine the resolution of the system. The latter was found to be 9.4 W.

Accurate measurements of the total losses (less the friction and windage) at no load and load were were achieved. The absence of the

friction and windage losses from the measurements is an advantage since they are variable; had they been included in the measured losses, they would have caused complications in the analysis of the test results.

The thermal time constant of the test motor and the calorimeter were such that to achieve stable conditions the two parts of the test took 3 to 4 hours each. In order that the experiment could be left unattended a control system to provide constant supply voltage and load and a monitoring system to log the test condition and to check the constancy of the test parameters were provided. Experience over more than 232 calorimetric tests showed that both the system and the method are reliable for measuring total losses in small cage induction motors and this reality was confirmed through the accurcy of the results obtained.

7.2 NO LOAD CONDITION

It is known that on no load, only a very small rotor current is necessary to account for the friction and windage losses and the rotational iron losses due to stator slot openings . Therefore the flux level and its distribution is determined by the stator current and there is no bunching of the field to one end in a skewed motor. The no load iron losses should not therefore vary with rotor skew.

Since the rotor current is very small, other losses due to inter bar currents and the increased length of the skewed rotor bars are also very small and may be often negligible. Accordingly no changes are expected in the no load losses of cage induction motors due to skewing of the rotor bars. While other changes, i.e. in the flux level by increasing the supply voltage or in air gap width have significant effect on the no load losses.

It is generally accepted that the no load losses have four components, stator copper losses, iron losses at fundamental frequency, stray no load losses and the friction and windage losses. The latter, though of interest and significance to the machine designer, are not considered in this project, since an advantage of the measurement method is that they are specifically excluded. As the voltage changes the stator copper losses , iron losses at fundamental frequency and stray no load losses change, but the overall change of iron losses with voltage depends upon the relative contribution of the eddy current and hysteresis losses . While the former is proportional to the square of the voltage the latter depends on a co-efficient which is variously quoted between (1.5 to 2.3),[15].

The losses in the rotor due to the stator slot openings depend on the air gap width or (slot to air gap ratio). For small air gaps

the flux pulsation due to the stator slot openings penetrate deeply into the rotor teeth and produce losses in the rotor teeth and bars. While with large air gaps the flux pulsations penetrate less, and hence the losses are smaller. In induction motors, if the rotor slots are open they produce losses in the stator teeth in the same way as the stator slot opening does, but in small motors the rotor slots are usually closed, except in some cases when the rotors are over machined for larger air gaps.

Thirteen rotors with five different values of skew were tested at no load and at different air gaps and voltages. The results obtained provide no evidence of a meaningfull variation with skew, although some variatios with skew have been noticed, they are very small and within the accuracy of the measuring system.

The no load test results have shown that the magnetising current rises rapidly with voltage and the no load losses are non linear function of the voltage. The rapid rise in the magnetising current is an indication of the high saturation level in the machine when the voltage is increased to 110% of the rated value. Examination of the magnetic loss results revealed the power index of their variation with voltage to be in the range 2.2 to 3.4, significantly higher than the 1.5 to 2.3 [15]. The nature of the variation with voltage was in accordance with expectation, although the high rate of change with

voltage was surprising.

About half of the thirteen rotors were tested at three air gaps, namley nominal and nominal ± 20%, and in the majority of the cases the losses decreased as the air gap increased. The one or two exceptions to this rule being rotors which appeared to have surface problems such as machining marks or near breakthrough of the slots. This observed general decrease in losses with gap supports in a qualitative, if not quantitative, way the generally held views mentioned above.

Under certain circumstances, such as gap changes at lower voltage and with skew, the variations in the losses are relatively small especially on no load. In this project the calorimetric method has been used successfully to measure accurately the no load losses and to show their variations, without the calorimetric method it would have been very difficult to detect these variations by conventional methods of loss measerement.

It has to be concluded from the no load results that skewing has negligible effect on the no load losses, while the change of air gap and voltage have the expected effect and the accurate measurement of the losses and their variations with design changes is the best evidence one can give in favour of the calorimetric method.

7.3 LOAD CONDITION

In cage induction motors the total losses of the motor change very much with the load and the losses vary with skew and air gap. In a machine with skewed rotor bars, the progressive displacement of the stator and the rotor m.m.f's with axial position can produce a steady increase in air gap density from one end of the machine to the other as the load increases and this effect produces a load dependent axial force. Since the losses depend on B^x , the non-uniform distribution can result in extra loss. If the skewed rotor bars are uninsulated from the rotor laminations the difference in the voltage induced between the adjacent bars produces circulating currents which flow between the adjacent bars. These circulating currents produce another type of loss in the rotor which depends on the resistance between the rotor bars and rotor core [30][32].The degree of insulation varies from one rotor to another and between the bars of the same rotor due to imperfections in manufacturing the rotors . Measurements of the rotor bar and interbar impedances of two of the tested rotors demonstrate this point showing that there are significant differences between the values of interbar impedances of any rotor. Examination of the same two rotors after removing the end rings and some laminations revealed inter lamination aluminium flash bridging some of the bars possibly contributing to some of the random rotor to rotor loss varations noted. The relative changes in the length and the cross-sectional area of the rotor conductors due to skewing also cause changes in the rotor conductor losses . The

simple model designed in chapter six has shown that as the skew increases from zero to 1.5 SSP the rotor conductor losses increase by 27% .

It is known that in induction motors stray load losses increase with load but decrease with air gap. As the air gap width increases the penetration of the flux pulsation into the rotor and the losses produced are decreased

The thirteen rotors with different skews mentioned were tested at different air gaps and loads. The results obtained have shown that the measured losses (after subtracting the stator copper losses) changed with skew. In general, the load losses increased for skew changes from zero, through one half stator slot pitch to reach a maximum value at one stator slot pitch. Subsequently the losses reduces as the skew increased to one rotor slot pitch, but then increased again when the maximum skew tested (1.5 SSP) was used. Since the rotor bar and interbar impedances of the tested rotors (with different skew angles) are not exactly the same, the stray load losses are expected to be affected by factors other than skew. It is the combination of all the three factors mentioned which determine the stray load losses .

It can be concluded that load losses in the 5.5kW cage induction motor tested have a maximum value at a skew of one stator slot pitch. They appear to show a local minimum at a value of one rotor slot pitch subsequently rising again as the skew value increase. The effect of interbar impedance can be important, but is very difficult to identify.

It has been noticed from the no load and load results that bad surface machining, i.e: smooth rotor surface, rotor tappering, removing the bridges above the rotor bars and other industrial imperfections could cause extra losses in cage motors under both no load and load conditions.

Analytical results obtained from the model , in which the skewed motor is represented by a number of identical series machines have shown that the stator and rotor leakage reactances increase with skew whilst the magnetising reactance decreases. It has also shown that iron losses and rotor conductor losses are increased by skewing. However it was concluded from the absence of correlation between the measured and predicted values that the other mechanisms of loss generation are extremely important and that a full quantitative explanation of losses would have to include all such mechanisms.

7.4 SUGGESTIONS FOR FURTHER WORK

Having succeeded in building the calorimeter in the way discussed and using it to measure accurately the losses in induction motors with different designs , it is worth continuing to use the calorimeter method to determine the losses of cage motors with other design changes and using nonsinusoidal supply and inverters. This method is likely to be succesful in determining the effeciency of induction motors supplied by inverters if an accurate method is used for determining the output power, a test which is almost impossible to undertake by other conventional methods.

The present system can be modified to achieve greater accuracy and the following suggestions are made .

1 - The main heater could be enlarged to reduce further its surface temperature and the heat radiation, and the heater mounted closer to the test motor, to obtain a better heat transfer process.

2 - Mixing of the air within the calorimeter could be improved by careful attention to the aerodynamics of the structure.

3 - The calorimeter could be constructed in a way to allow for the easier replacement of the test motor, for example by opening only one of the panels instead of lifting up the calorimeter.

4 - The loss resolution improved by increased temperature resolution, but this would have to be accompanied by improved integration of the spacial temeratures in the outlet.

5 - The operation of the system from the start to the end of the calorimetric test could be automated, including all the measurements and control.

REFERENCES

[1] -IEEE Std 112 - 1984 (IEEE test procedure for polyphase inductionmotor and generator) pp 8 to 19.

[2] - Dell,A., Salvator,L., Savino, M. "A new test method for determination of induction motor effeciency", Trans. Power Apparatus and Systems, Vol. PAS - 103, No. 10, October 1984 pp 2961 to 2973.

[3] - Preston, T.W., Reece,A.B.J., Sangha, P.S."Induction motor analysis by time stepping technique ", IEEE Trans. Vol MAG- 24, No.1, Jan 1988 pp 471 to 474.

[4] - Design procedure for squirrel cage or slipring induction motors - GEC Electromotors Ltd.

[5] - British Standard Specifications 4999 Part 102 1987 "Methods for determining losses and efficiency from tests (Excluding machines for traction vehicles) pp 4 to 24.

[6] - Chalmers, B.J."Electromagnetic problems of AC machines" Chapman and Hall, 1965.

[7] - Bird, B.M."Measurement of stray load losses in squirrel cage induction motors" Proc. IEE, 1964, III,pp 1697 to 1705.

[8] - Morgan, T.H., Brown,W.E. ,Schumer, A.J."Reverse rotation test for determination of stray losses in induction machines" Trans. AIEE- 1939, 58, pp 319 to 322.

[9] - Morris, D.G.O, "Back to back test for induction machines:motorised coupling" Proc.IEE, Vol 114, No.8, August 1967,pp 1160 to 1161.

[10] - Buccianti, R., Gerlando, A.D., Spada,P.,"Applicability of the calorimetric method for measuring effeciency of low voltage synchronus motors" , L'ENERGIA ELECTRICA - No.5, 1986, pp196 to 208

[11] - IEC Publication 34- 2A, p 7 to 36, 1974

[12] - Schwarz, K.K."Survey of basic stray losses in squirrel cage induction motors" Proc.IEE, Vol.III, No.9, September 1964, pp 1565 to 1573.

[13] - Jimoh, A.A., Findaly, R.D., Poloujadoff, M."Stray losses in induction machines" Part 1,IEEE Trans., Power Apparatus and Systems"Vol.PAS 104,No 6, June 1985 pp 1500 1505.

[14] - Binns, K.J., Wood, A.W."The calorimetric measurement of the losses of induction motor" Third year project, University of Southampton.

[15] - Hammond, P."Electromagnetism for Engineers" Second Eddition,Pregmon press 1981.

[16] - Puchstein, A.F., Loyd, T.C." Alternating Current Machines" Chapman and Hall, 1936.

[17] - Liwischitz Garik, M."Alternating Current Machines" Second addition, April 1961, D.Van Nostrand Company, INC.

[18] - Spooner, T."Squirrel cage induction motor core losses" Jornal AIEE Jan 1925, PP32 TO 37.

[19] - Danburg, R.N., Acarnley, P.P., "Loss effects in machine windings subjected to high frequency excitation" Proceedings IEE conference on Electrical machine design and applications, London 1985.

[20] - Alger, P.L., Angst,G., Davies,E.J. "Stray load losses in polyphase induction machines" Trans. AIEE, June 1959, 78, Pt.IIIA, pp 349 to 355.

[21] - Chalmers,B.J. and Williamson,A.C.,"Stray losses in squirrel cage induction motors. Validity of reverse rotation test method " Proc. IEE, 1963, 110,pp 1773 to 1777.

[22] - Chalmers, B.J., Richardson, J."Investigation of high frequency no load losses in induction motors with open stator slots" Proc. IEE 113, 1966, pp 1597 to 1605.

[23] - Chalmers, B.J., Narain, Ch.K."High frequency no load losses of cage induction motors"IEEE Trans.PAS 89, 1970, pp1043 to 1049.

[24] - Tagen, F., Walezak, R."Experimental verification of stray losses in cage induction motors under no load, full load and reverse rotation test condition" Archiv fur Elektrotechnic,(Springer Verlag) 70, 1987, pp 255 to 263.

[25] - Binns, K.J., Dye, M." Effect of slot skew and iron saturation on cogging torques in induction machines" Proc. IEE, Vol. 117, No. 7, July 1970 pp 1249 to 1251.

[26] - Oberretl, K."13 rules to minimise stray load losses in induction motors" Bulletin Oerlinon Engineers Company, No. 389/390, pp 2 to 12.

[27] - Oberretl, K."The effect of parallel winding , delta connection, coil chording, slot opening and slot skew on torque of squrrel cage rotors" Electrotech,Z., 1965 A, 86,pp619 to 627.

[28] - Alger, P.L."Nature of induction motors" Gordon And

Research Science Publishers 1970.

[29] - Binns, K.J., Hindmarsh,R., Short, B.B." Effect of skewing slots on flux distribution in induction machines" Proc. IEE, Vol. 118, No. 3/4, March/Appril 1971 pp 543 to 549.

[30] - Odok, A.N."Stray load losses and stray totque in induction machines" Trans. AIEE, 1958, 77,Pt. III pp 43- 53.

[31] - Heller, B., Joki,A.L.,"Losses in squrrel cage motors due to rotor skew" Trans IEEE on Power Apparatus And Systems,Vol.PAS-90, No.2 March/April 1971 pp 556 to 562.

[32] - Waterson,D.G., Bagk,S., Diemoz,E. "Transfer of heat in electrical rotating machines, . Determination of rotor bar to bar crosspath impedance in cage induction motors " ERA Technology ,ERA report 88- 0351 issue 3, ERA Project 44-02-0213.

[33] - Waterson,D.G., Prescot,W., Bradford, M., Lockwood,M., Bagk,s."M.M.F and permeance harmonic torque and loss in cage induction motors. The effects of skew, bar to bar impedance and saturation" Proc. International Conf., Electrical Machines and. Drives, 1989 London.

[34] - Barton, T.H., Ahmad,V."The measurement of induction motor stray losses and its effect on performance" Proc. IEE, Sept.1957, 105C, pp69 to 75.

[35] - Chalmers, B.J." Skew leakage losses" ERA Project 44-02-0213 Therm, 29 March 1988.

[36] - Rawcliffe, G.H., Menon,A.M."A simple new test for harmonic frequency losses in AC machines" Proc. IEE, paper No. 1222 U, April 1959 , 99 part II, pp 145 to 150.

[37] - Heler,B., Hamata,V."Harmonic field effects in induction machines" Elsevier Scientific 1977).

[38] - Koch,C.J."Measurement of stray load losses in polyphase induction motors" Trans. AIEE 1932, 51, pp 756 to 760.

[39] - Ware, D.H."Measurement of stray load losses in induction machines" Trans. AIEE,1949,64,pp 194- 196

[40] -"MDS 85 User Manual" Intel Corporation 1978.

[41] -"SDK 85 Users Manual" Intel Corporation 1978.

[42] - Roberts, D." The application of induction motor thermal model to protection and other functions"Ph.D. Thesis, Liverpool University, Sept. 1986.

[43] - Hosking,R.J." First steps in numerical analysis" Edward Arnold 1985.

[44] - Linkos, C.E.,"Effect of skew on induction motor magnetic fields" , Trans. AIEE ,74, pt.III,pp 760- 765, August 1955.

[45] - Bulter, O.I., Birch, T.S." Comparison of alternative skew effect parameters of cage induction motors" Proc.IEE, Vol.118, No.7,July 1971.

[46] - Diemoz, E., Waterson D.G., "Determination of rotor bar to bar crosspath impedance in cage induction motors, ERA report, Sept. 1988.

[47] - SAY, M.G."Alternating current machine" Pitman, 1978.

[48] - Adkins, B., Harley, R.C."The general theory of alternating current machines" Chapman and Hall, 1976.

APPENDIX (A)

MONITORING SYSTEM

A monitoring system was designed built and used to check the constancy of the test parameters (current, voltages, power and slip) of the test motor during the induction motor test, which usually lasted four hours. The system was based on an INTEL SDK85 single board microprocessor development system, the detail of which is given in section 4.2.4. Readings of the three line currents, voltages, power and the slip of the motor taken during one of the induction motor tests carried out at 110% of the rated current using rotor No.10 which has a skew of 1.5 SSP and a nominal air gap of 0.3mm are plotted in figure A1. The circuit diagram of the system is illustrated in figure A2. This system was also used for the measurement of the stator winding resistance at the end of the induction motor tests, sectiom 4.3.3. A short sample set of the readings, taken during half hour of the test mentioned above, are given in table A1 as an example. The readings taken by the system were recorded in HEXADECIMAL, they have been converted to decimal values and shown in table A2.

Sequence of readings	IR (A)	IY (A)	IB (A)	VR (V)	VY (V)	VB (V)	PR (W)	PY (W)	PB (W)	SLIP
96D0	D4	DF	D0	E5	E5	E5	C3	D0	C3	38E
96E0	D3	DF	CF	E4	E5	E5	C3	D0	C2	38E
96F0	D4	DF	D0	E4	E5	E5	C4	CE	C4	38E
9700	D3	DF	D0	E4	E5	E5	C2	CF	C3	38E
9710	D3	DF	D0	E4	E6	E6	C2	CF	C3	38E
9720	D3	DF	D1	E4	E5	E5	C1	CE	C4	38E
9730	D3	E0	D1	E4	E5	E5	C2	CE	C3	38E
9740	D5	E1	D0	E4	E5	E5	C3	CE	C5	38D
9750	D5	E1	D2	E5	E5	E5	C4	D2	C3	38D
9760	D2	DF	D1	E5	E6	E6	C7	DF	C4	38D
9770	D4	DF	D0	E4	E5	E5	C2	D0	C4	38E
9780	D3	DF	D1	E3	E5	E5	C3	CF	C3	38E
9790	D5	DF	D1	E4	E5	E5	C3	CF	C4	38E
97A0	D4	E0	D1	E4	E5	E5	C4	CD	C6	38E
97B0	D4	DF	D3	E4	E5	E6	C4	D0	C4	38E

Table A1.Data logged in HEXADECIMAL during half hour of a test carried out on rotor No.10, at 110% rated current, skew = 1.5 SSP, air gap =0.3mm.

Sequence of readings	IR (A)	IY (A)	IB (A)	VR (V)	VY (V)	VB (V)	PR (W)	PY (W)	PB (W)	SLIP
2413	12.47	13.12	12.23	239.7	239.7	239.7	2925	3120	2925	.052
2414	12.41	13.12	12.17	238.6	239.7	239.7	2925	3120	2910	.052
2415	12.47	13.12	12.23	238.6	239.7	239.7	2940	3090	2940	.052
2416	12.41	13.12	12.23	238.6	239.7	239.7	2910	3105	2925	.052
2417	12.41	13.12	12.23	238.6	239.7	239.7	2895	3090	2940	.052
2418	12.41	13.06	12.29	238.6	240.7	240.7	2910	3090	2925	.052
2419	12.41	13.17	12.29	238.6	239.7	239.7	2925	3090	2940	.052
2420	12.53	13.24	12.23	238.6	239.7	239.7	2940	3105	2925	.053
2421	12.53	13.24	12.35	238.6	239.7	239.7	?955	3150	2940	.053
2422	12.35	13.12	12.22	239.7	239.7	239.7	2910	3120	2940	.053
2423	12.47	13.06	12.23	239.7	240.7	240.7	2925	3105	2925	.052
2424	12.41	13.12	12.29	238.6	239.7	239.7	2925	3105	2955	.052
2425	12.53	13.12	12.29	237.6	239.7	239.7	2940	3090	2940	.053
2426	12.47	13.24	12.29	238.6	239.7	239.7	2940	3120	2955	.052
2427	12.41	13.12	12.35	238.6	239.7	239.7	2940	3120	2955	.052

Table A2.Readings of the currents, voltages, power and slip during half hour of a test converted from HEXADECIMAL given in table A1.

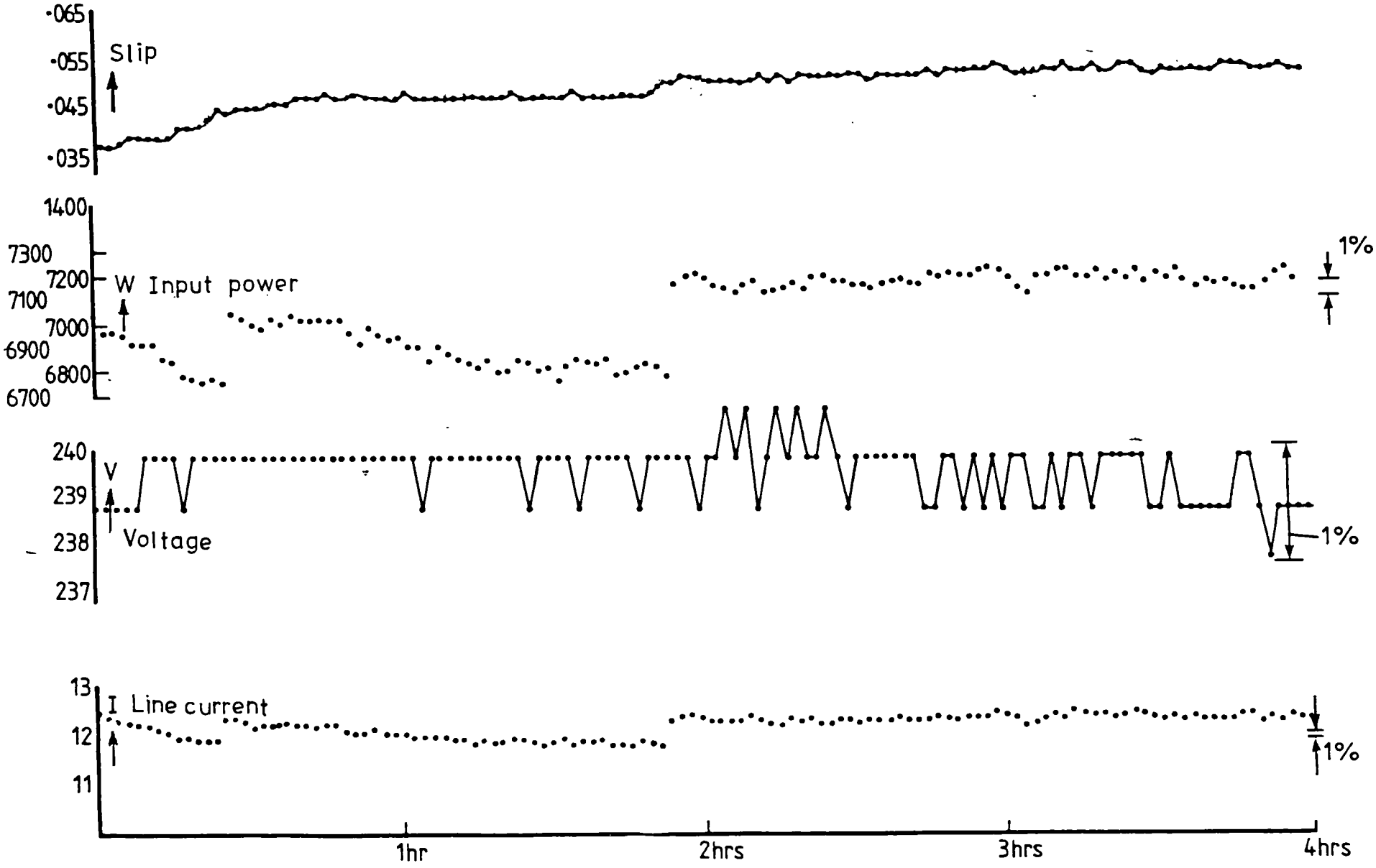

Figure A1 Readings of power input, voltage, line current and slip recorded by data logging system

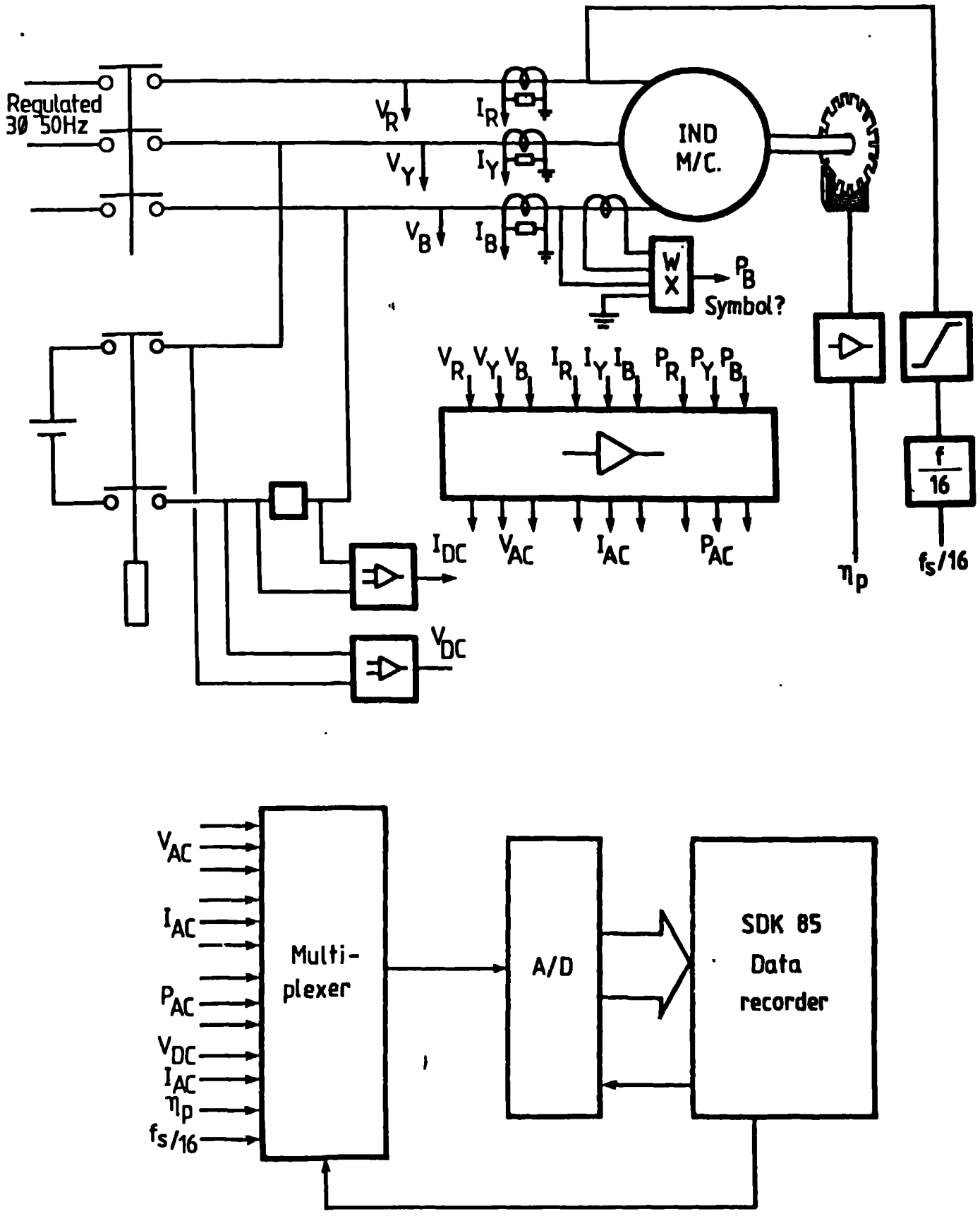

Figure A2 Data logging and stator dc resistance measuring circuits

APPENDIX B

DETERMINATION OF THE EQUIVALENT CIRCUIT PARAMETERS OF THE CAGE INDUCTION MOTOR, D 132S, 5.5kW, 4 POLE USED IN THIS PROJECT

Three tests (No load test, calorimetric test at no load and locked rotor test) were carried out to determine the equivalent circuit parameters of the tested motor using a single layer winding stator S1 and unskewed rotor (rotor No.8). In the no load test the motor was run inside the calorimeter enclosure at rated voltage and uncoupled mechanically from its load until it reached thermal equilibrium . At this point readings of the power input to the motor (P_i) the currents (I)and the voltages (V) were taken. As soon as the motor was stopped the value of the stator winding resistance (R_1) was measured.The readings taken were:

P_i = 441 W , V = 415 V, I = 4.57 A, R_1 = 3.08 Ω

This test was followed by a calorimetric test at no load during which the power input to the motor (P_{ic}) and the total no load losses (less the friction and windage losses) P_h were measured. The detail of the test is described in section 5.1. The measured values were as follows:

P_{ic} = 573 W , P_h = 373 W

Then a locked rotor test was carried out, during which, the test motor was locked mechanically and a voltage (V_L) sufficient to provide

a current (I_L) about the rated current of the motor was applied. The power input to the motor (P_L) and the stator winding resistance (R_{1L}) were measured.The measured values were:

P_L = 1027 W , V_L = 120 V, I_L = 7.36A (Phase current)

R_{1L} = 3.76Ω

From the no load results and the calorimetric no load results the values of the friction and windage losses ($P_{f\&w}$) of the test motor can be determined as follows:

The power input to the induction motor (P_{ic}) measured during the calorimetric test includes the friction and windage losses ($P_{F\&W}$) of the dc-driving motor in addition to the total no load losses of the induction motor (P_i) measured in the normal no load test.

Therefore the value of ($P_{F\&W}$) dc motor is:

$P_{F\&W} = P_{ic} - P_i$ = 573 - 441 = 132 W (from the measured results)

From the calorimetric results obtained, the sum of the friction and windage of the two motors can be determined by subtracting (P_h) from (P_{ic}) as follows:

($P_{F\&W}$)dc motor + ($P_{f\&w}$)induction motor = 573 - 373 = 200 W

Hence ($P_{f\&w}$)induction motor = 200 - 132 = 68 W

From the locked rotor test, the locked motor impedance and resistance Z_L and R_L can be found:

$Z_L = V_L / I_L$ = 120 / 7.36 = 16.3Ω

$R_L = P_L / 3\ I_L^2$ = 1027 / 3 (7.36) (7.36) = 6.31Ω

But R_{1L} (measured) = 3.76Ω

Therefore rotor resistance $R_2 = 6.31 - 3.76 = 2.55\ \Omega$

And rotor leakage reactance $X_L = (Z_L^2 - R_L^2)^{1/2} = 15.02\ \Omega$

Assuming that the stator and the rotor leakage reactances X_1 , X_2 are equal at standstill, hence :

$X_1 = X_2 = 15.02 / 2 = 7.51\ \Omega$

In order to determine the running performance of the motor from the equivalent ciruit parameters it is necessary to take into account the saturation effect and the skin effect . Here the saturation effect is assumed to be equal to 1.35 [17] and the skin effect is assumed to be unity (for simplicity).

Then the value of $X_2 = 1.35 \times (7.51) = 10.41\ \Omega$

From the no load test results obtained:

R_1 measured was $= 3.08\Omega$

$V = 415$, $I_1 = 4.57$ A

Therefore $Z_1 = ((7.51)^2 + (3.08)^2)^{1/2} = 8.117\Omega$

Hence the induced e.m.f $= 415 - 8.117 \times (4.57/\sqrt{3}) = 393.57$ V

Iron losses P_c of the induction motor can be found from the no-load losses results as :

$P_c = P_i - 3 * I_1^2 R_1 - P_{f\&w}$

By substituting the measured values in the equation above .

$P_c = 441 - 3 \times (4.57/\sqrt{3})^2 \times (3.08) - 68 = 308.6$ W

The main flux resistance $R_m = 3\ E^2/P_c$

$= 3 \times (393.57)^2 / 308.6 = 1505.8 = 1506\Omega$

The magnetising reactance $X_m = E / I = 393.571/(4.57/\sqrt{3}) = 149.16\Omega$.